SPORE GERMINATION IN THE RICE BLAST FUNGUS, *MAGNAPORTHE GRISEA*

Helen A. Atkinson

Thesis presented for the degree of
Doctor of Philosophy

University of Edinburgh
2001

FOR MY HUSBAND & MY PARENTS

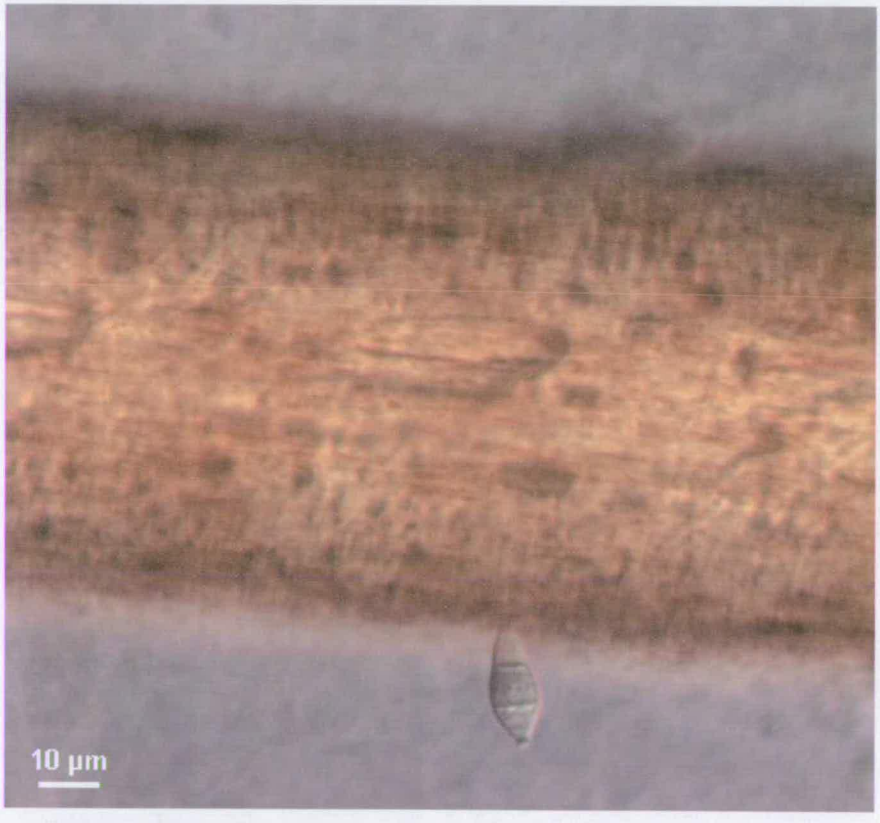

A *Magnaporthe grisea* conidium attached to a human hair by spore tip mucilage.

DECLARATION

The composition of this thesis and the work presented herein is my own, unless otherwise acknowledged in the text.

Helen A. Atkinson

ACKNOWLEDGEMENTS

I gratefully acknowledge the help that I have received, and in particular I would like to thank:

Nick Read, Alison Daniels and Jim Deacon for their guidance and support.

AgrEvo UK Limited and the BBSRC for funding the research presented in this thesis.

Everyone at Chesterford Park: especially, Alison Daniels for helping with the SEM analysis, and Alyson Platt and Caroline Rutherford for the technical help and advice concerning the experiments performed *in vivo*.

James Howes and Zeiss Microscopes for the technical advice and for lending me all that equipment!

All those at Daniel Rutherford, especially Janice Miller for being a patient listener and a kind friend, John Findlay for the valuable help and advice that he has given me over the years and for keeping me laughing, all the members of the Photo lab for performing miracles and always making the time, and Philip Smith, whose enthusiasm for all things scientific is quite simply infectious.

Everyone in the lab for helping to make learning fun!

My parents, my brother, Glenys, Brian and Angus for all their support, practical help and just for being there.

My husband, for everything.

ABSTRACT

Magnaporthe grisea infects rice plants via asexual spores called conidia. Germination involves the production of a germ tube from one of three conidial cells: the apical, middle and basal cells. Little is known about the process of spore germination in this or any other fungal plant pathogen, and this is the focus of the work presented here.

Spore germination was characterized using light microscopy and scanning electron microscopy both *in vivo* and *in vitro*. Conidia were shown to germinate via either a single or two slightly slower growing germ tubes. Germ tubes are characteristically produced in regions of the cell near to the substratum and also grow towards it. To examine the role of each of the three conidial cells for successful germination, individual conidial cells were selectively killed using a novel method. Isolated conidial cells were shown to be able to germinate and form appressoria. Evidence was obtained that the roles of the three cells differ and that communication occurs between conidial cells during germination and differentiation.

Organellar organization and dynamics were analysed in living and potentially pathogenic conidia throughout germination, using confocal microscopy and fluorescent stains. Each cell contains a single nucleus that changes position during germination but otherwise does not exhibit extensive movement. Mitochondria are primarily peripheral in the middle and basal cells and characteristically elongated in the germinating cell, from which they extend towards and into the growing germ tube. The vacuolar system was the most dynamic organelle examined. It is composed of spherical, globular and tubular elements that exhibit fusion and fission, and extend into and retract from the growing germ tube. During germination the compartments of the vacuolar system became progressively larger. The apical vesicle cluster was identified and characterized during germination. In addition, a range of dyes stained spots present at the periphery of the germ tube. These were shown to be extracellular, and produced at the germ tube tip. There was evidence that they exhibited esterase activity.

Confocal microscopy was used to analyse the process of endocytosis within conidia, germlings, and differentiated germlings. Evidence was obtained for the first time that the ungerminated and germinated spores of filamentous fungi undergo endocytosis. The first direct evidence for fluid-phase endocytosis occurring in a filamentous fungus was also obtained. The endocytic marker FM4-64 was used to characterize components of the vesicle-trafficking network during germination. It was demonstrated that spores exhibit endocytic internalization within two minutes of hydration, and there was evidence that the apical and basal cells exhibit a higher rate of endocytosis than the middle cell.

ABBREVIATIONS

A-cell	apical conidial cell
AVC	apical vesicle cluster
BCE	before current era
B-cell	basal conidial cell
CLSM	confocal laser scanning microscopy
CS	cover slip(s)
detCS	detergent-washed cover slip(s)
dH_2O	distilled water
DIC	differential interference contrast
ECM	extracellular matrix
EGT	emerging germ tube (stage of germination)
ER	endoplasmic reticulum
GT_1	germ tube 1 (stage of germination)
GT_2	germ tube 2 (stage of germination)
GT_3	germ tube 3 (stage of germination)
GTM	germ tube mucilage
LTSEM	low-temperature scanning electron microscopy
M-cell	middle conidial cell
MVB	multivesicular bodies
PS	peripheral spots
STM	spore tip mucilage
UNG	ungerminated stage of germination

TABLE OF CONTENTS

1. REVIEW OF THE LITERATURE

1.1 INTRODUCTION

1.1.1 Importance of fungal plant pathogens

Agriculture has been practised for at least 10 000 years (Diamond, 1997). With an increased dependence on the cultivation of land for the production of staple crops, there is a correlated increase in vulnerability to the damage caused by plant pathogens (Agrios, 1988). Many of the most aggressive plant pathogens are fungal and they are responsible for over seventy percent of all major crop diseases (Deacon, 1997). The effects of plant diseases can be devastating, causing starvation and malnutrition, death of people and their livestock, and sometimes mass migrations. Threophrastus (370–286 BCE) wrote about plant disease, and the Romans had a god of rust called Robigo to protect their cereal crops from disease. The old English words "blight" and "blasting" were commonly used to signify damage to crops and the terms "blasting" and "mildew" are referred to in the Old Testament (Ramsbottom, 1929; Agrios, 1988; Hudler, 1998).

Robert Hooke, an English contemporary of Anthony van Leeuwenhoek and the inventor of the compound light microscope, discovered that the rust on the underside of a Damask rose leaf had a discernible organized structure when viewed through the microscope. He likened this structure to a minute mushroom and presented a diagram of it in his *Micrographia* (Hooke, 1665). This is the earliest recorded microscopic examination of a filamentous fungal plant pathogen (Ramsbottom, 1929). Since this time the technique of microscopy has become increasingly refined and technically sophisticated, and in the last century this was demonstrated by the development of the electron and confocal microscopes. Recently, emphasis has been placed on the importance of microscopic examination of biological samples in their living state. Each technical advance is accompanied by advances in our biological understanding of subcellular structures and their organization. Thus, the technique of microscopy has evolved considerably over the centuries following Hooke's microscopic

examination of rust, and has been literally instrumental in furthering our understanding of fungal pathogens.

1.1.2 The rice blast disease

The filamentous ascomycete (Order: pyrenomycetes) fungus *Magnaporthe grisea* (T. T. Hebert) Barr (anamorph: *Pyricularia grisea*) parasitises over 50 grasses (Ou, 1985). Graminaceous hosts include barley, wheat, oats, and millet, but *M. grisea* is best known as the causal agent of the rice blast disease, hence its common name the "rice blast fungus". Primarily a disease of young rice plants, the fungus attacks all of the above-ground parts of the rice plant, producing lesions on all parts of the shoot but rarely on the leaf-sheath (Bonman, 1992). The most destructive symptom is "neck blast" or "rotten neck blast", in which the panicle base is infected. The physical appearance of lesions varies with environment, host resistance, host age and the stage of infection (Sadisvan *et al.*, 1965; Hashioka, 1965; Ou, 1980a, b). *M. grisea* exhibits very varied pathogenesis and exists in a mixture of pathogenic races (Ou, 1980b). This means that new resistant varieties of rice rarely remain so for more than a few years (Zhu *et al.*, 2000). It has been recently demonstrated in an unprecedentedly large-scale field trial in China, that the fungus spreads more slowly through mixed varieties of rice than through monocultures, which are conventionally planted (Zhu *et al.*, 2000).

There is archaeological evidence that rice was being cultivated in China by around 5000 BCE, and that the practice had spread to India by 2000 BCE and to Japan by 1000 BCE (Smith, 1995). Rice is currently a staple dietary constituent for nearly half the world's population including many third World countries (International Rice Research Institute, 1997). Rice blast was one of the earliest recognised plant diseases and is considered to be the principal disease of rice, occurring in all major rice growing regions of the world (Ou, 1980a,b). The rice blast fungus is responsible for major yield losses, and has been reported to account for losses of between 11–30% of the world's rice harvest, causing sporadic recurrent epidemics throughout South East Asia and South America (Baker *et al.*, 1997) and often dictates rice production practices (Kim, 1994; Shahjahan, 1994). Thus, *M. grisea* has enormous significance

for both economic and humanitarian reasons and is one of the most important pathogenic fungi in the world.

Magnaporthe grisea is generally considered to be a model system for plant pathology research (Valent, 1990; Valent & Chumley, 1991) and has been described as a "fascinating experimental system for assessing many aspects of the plant-microbe interactions that in themselves comprise an essential subdiscipline of modern science" (Smith, 1999).

Important advantages of *M. grisea* as an experimental system include:

- it is easily grown in culture,
- it is readily transformable and genetically manipulated,
- mutant isolation and analysis is simple,
- it exhibits both host species and host cultivar specificity,
- it has a rapid disease cycle.

1.2 THE FUNGAL SPORE

As sessile organisms, higher fungi may respond to adverse conditions in three main ways, (1) by growing out of it, (2) by producing a propagule that is dispersed, or (3) by producing a structure that can survive until conditions improve. The fungal spore is differentiated from the mycelium and specialised for reproduction, but also for survival and/or dispersal (Ingold, 1971; Smith & Berry, 1974).

Spores are produced by mitosis, meiosis, or mating (Table 1.1). Whilst mycelial hyphae display much phenotypic plasticity, the spore tends to be morphologically stable, but varies greatly between species with respect to size, colour, shape, and surface texture. Variation also occurs within an individual as one species may produce more than one spore type, e.g. *Neurospora crassa* produces macroconidia, microconidia and ascospores that differ in size, shape, colour, mode of dispersal, and mode of reproduction (Maheshwari, 1999). Thus, the types of spore and the

reproductive bodies that produce them are commonly used as phenotypic markers in taxonomic studies.

Origin	Examples	Type	Fungal groups
mitotic	zoospores sporangiospores conidia uredospores pycnidiospores	All dispersive	Chytridiomycota, Oomycota Zygomycota Ascomycota, Deuteromycota, Basidiomycota Basidiomycota Deuteromycota
meiotic	ascospores basidiospores	Resting Dispersive	Ascomycota Basidiomycota
mating	oospores zygospores teliospores	All resting	Oomycota Zygomycota Basidiomycota

Table 1.1: Main spore types in fungal plant pathogens (for further details see Agrios, 1988; Deacon, 1997).

There is a vast array of fungal spore shapes and sizes (Agrios, 1988). Spores can be thread-like, such as the 2 x 500 μm ascospores of *Cordyceps miltaris*; others can be branched, as in the aquatic hyphomycetes. However, the most common morphology is spherical or ovoid in the range of 5–50 μm (Ingold, 1971). Some spores are unicellular (e.g. conidia of *Aspergillus, Botrytis* and *Trichoderma* or the teliospores of *Ustilago maydis*), whilst others can be comprised of many cells (e.g. conidia of *Alternaria* and *Helminthosporium,* or the teliospores of *Puccinia graminis*). Colour and external architecture also varies between species. Many spores are colourless or white, but they can also be yellow, pink, purple, brown or black due to pigmentation, mainly within the spore cell wall, and in some cases due to pigmented cytoplasmic inclusions (Ingold, 1971). Whilst some spores have smooth walls (e.g. ascospores of *Sordaria*) many species display a distinctive pattern of surface ornamentation (e.g. the spine-like protrusions of *Erisyphe graminis,* or the ribbed surface pattern on ascospores in the genus *Neurospora* (Dutta *et al.*, 1981). These patterns frequently distinguish the taxon, and in some cases have been shown to aid the dispersal and attachment stages of infection (e.g. Rees & Jones, 1984). In addition, spores are sometimes flagellate (e.g. zoospores), possess a thin or thick cell wall, or have no cell

wall at all, as in the case of zoospores produced by members of the Mastigomycota. The mechanisms by which these variations arise have been considered in most detail for conidial fungi (Cole & Samson, 1979; Cole, 1981, 1986; 1990).

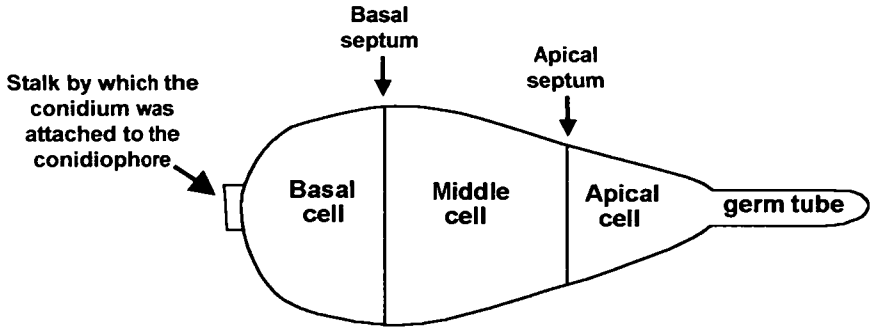

Figure 1.1: Conidial features and the terms used to define them.

M. grisea produces both sexual and asexual spores. Although sexual stages have been reported in the wild, reproduction is principally asexual (Leung & Taga, 1988; Valent *et al.*, 1991; Dobinson & Hamer, 1992; Shull & Hamer, 1994). Mature conidia of *M. grisea* are characteristically approximately 9 x 20 μm in size, non-motile, pear-shaped, and are typically comprised of three cells. These cells are morphologically different and may thus be referred to as apical, middle and basal cells (Fig. 1.1). The spore is grey/brown in colour and the cell wall has a unique reticulate pattern (Howard, 1994).

1.3 INFECTION CYCLE

The fungal plant pathogen infection cycle varies between different pathogens and host species. However, in general it is composed of the following stages: spore release and dissemination, spore attachment to the host, germination, penetration of the host, and infection of host tissues. These main stages of the infection cycle of *M. grisea* are shown in Figure 1.2 and are considered below with special reference to those events preceding and involved in spore germination.

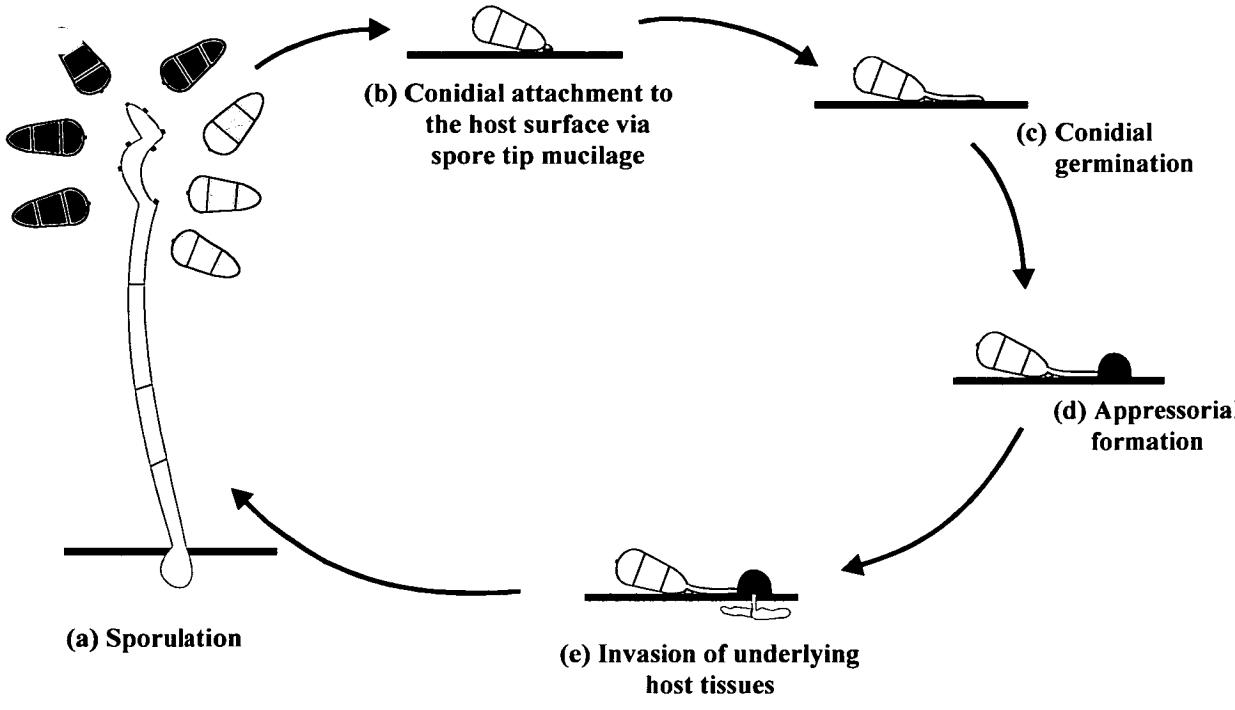

Figure 1.2: The infection cycle of *Magnaporthe grisea.*

1.3.1 Release and dissemination

In most fungal species, dispersal is primarily achieved by asexual spores, whilst sexual spores serve as dormant survival structures. However there are exceptions, the most pronounced being the Basidiomycota, which rarely produce asexual spores, and so the basidiospores also serve to disperse the fungus (Deacon, 1997), (Table 1.1). The structures that bear spores can be simple specialised spore-bearing hyphae such as the conidiophore of *M. grisea.* (Fig. 1.2a), or more elaborate multicellular structures such as the mushrooms of the Basidiomycota (Subramanian, 1968; Philips, 1981; Read, 1994). Some release spores actively, some passively, whilst in others the spores remain at their site of formation as survival structures. Fungal spores are principally spread by one or a combination of the following dispersal agents: air, water, insects, and other animals, including humans (Ingold, 1971).

Many fungi have adapted to airborne dispersal by either presenting the spores on tall conidiophores such that they may be easily lifted by the air currents or by evolving mechanisms that forcibly liberate the spore into the air current (Ingold, 1971). In some species spores clump together in the air, a feature that has been reported to

accelerate the dispersal time in *Erisyphe graminis* spores (Bainbridge & Stedman, 1979). The mechanism by which spores aggregate has been examined in *Uromyces* uredospores and has been attributed to a combination of the spiny cell wall ornamentation and the hydrophobicity of the entire spore surface (Clement *et al.*, 1994). Conidia of various fungi including *Neurospora crassa, Aspergillus nidulans* and *M. grisea* possess hydrophobin-encoded rodlet layers on their outer surfaces. Hydrophobins are small moderately hydrophobic proteins secreted by fungi and appear to be responsible for spore hydrophobicity. However, their precise role has not been determined and there may be other components that contribute to physicochemical properties of the rodlet layer, such as lipids and glycoproteins (Kershaw & Talbot, 1998; Girardin *et al.*, 1999). Spore rodlets have been proposed to be an adaptation for dispersal by air, to protect the spore from desiccation and function in part to aid adhesion to the hydrophobic host surface (Talbot *et al.*, 1993, 1996; Wessels 1996, 1997; Kershaw & Talbot, 1998).

The conidia of *M. grisea* are formed by holoblastic conidiogenesis on the tips of simple, rarely branched conidiophores to which they are attached by the basal cell via a small stalk (Subramanian, 1968; Leung & Shi, 1994). Under favourable conditions conidia are produced within 6–7 days after host inoculation (Fig. 1.2a). Conidiophores emerge from infected tissues through stomata, natural openings in the leaf surface or directly by eruption through the host cuticle (Howard & Valent, 1996). Cryo-scanning electron microscopy has shown that where conidiophore initials have forced their way through the epidermis and cuticle, an apparent tear can be seen, marked by the separation of wax crystals that characteristically coat the rice leaf (Howard, 1994). Spores are actively released upon bursting of the cell at the base of the conidium (Ingold, 1964). Spore release begins at around midnight reaching a peak between 2 am and 4 am (Bonman, 1992). Such "night patterns" of spore dispersal are unusual for conidia, being more typical of ascospores and basidiospores (Lacey, 1981). Each *M. grisea* conidiophore may bear 20 or more conidia resulting in an individual lesion producing 4000–6000 conidia per night for over 2 weeks (Ou, 1980a). This is not unusual; indeed *M. grisea* conidial production is low compared to

some fungal species (e.g. *Ganoderma applanatum*, 350 000 per second; Christensen, 1965). The magnitude of spore productivity has been attributed to the random nature of dispersal (Hudler, 1998). Conidia of *M. grisea* are released from the conidiophores by rain or dew and disseminated by air currents and gravity (Hashioka, 1965; Subramanian, 1968; Ou, 1980a). The maximum dispersal distance is the subject of some controversy, but conidia have been reported to travel up to 230 metres from the source (Teng, 1994). However, it is thought that most do not travel more than 2 metres (Ou, 1980a) but rice plants are usually grown within close proximity, increasing the likelihood that a spore will come into contact with a host surface (Fig. 1.2b). Thus, given favourable conditions for infection, the fungus will spread rapidly through a susceptible host population. The conidia are typical of spores that are primarily dispersed by air, which are often adapted to endure long periods of flight-time in the air: they are generally small and light, with thick pigmented cell walls (Ingold, 1971). There is no record of spores aggregating, although some clumping might occur via the spore tip mucilage (see Section 1.3.2) if spores come into contact.

1.3.2 Attachment to the host

Attachment to the host is a crucial stage in infection. The host surface is an inhospitable environment, adapted both chemically and physically to resist attack by pathogens (Smart, 1991). Of those few spores that encounter a host, only those that are able to remain in contact with the host surface will have a chance to infect the host tissues and thus survive to the next generation. The first components of a plant that a spore is likely to encounter are the waxes on the plant surface. These are comprised of a complex mixture of hydrophobic materials containing very long-chain aliphatic compounds (Kolattukudy, 1980; Kolattukudy *et al.*, 1995) and in some cases form an elaborate 3-dimensional architecture peculiar to that species. In several fungal species, spores have been demonstrated to sense the presence of the host surface and this is often evident by changes in the surface morphology of the spore: examples include the spine-like ornamentation of *E. graminis* which changes to globose bodies on contacting the host (Nielsen *et al.*, 2000) and the extracellular matrix network of *Uncinuliella australiana* conidia which moves towards the

substratum forming an adhesion pad (Mims *et al.*, 1995). In some cases it has been demonstrated that germination occurs at a higher rate when the spore population is attached to a substratum (Webster & Davey, 1984), whilst the pycnidiospores of *Phyllostica ampelicida* only germinate once they have attached to a substratum (Kuo & Hoch, 1996; Shaw *et al.*, 1998). Thus, the stage of attachment is generally considered to be the first step in establishment of successful infection (Mendgen & Deising, 1993; Kuo & Hoch, 1996).

Mucilage secretion by fungal spores is central to the process of attachment (Nicholson & Epstein, 1991; Braun & Howard, 1994). Attachment by adhesion can be either a passive or an active process (Kuo & Hoch 1996). Passive adhesion occurs when a spore sticks to a surface via pre-formed adhesive materials that are on or near the spore surface, or by mucilage expelled by the spore on hydration (e.g. *M. grisea*). Other types of spore actively release mucilage over a longer period of time, and this can involve a series of steps (Watanabe *et al.*, 2000). This is an energy-requiring process and might involve recognition of the surface (Nicholson & Epstein, 1991; Read *et al.*, 1992b; Neilson *et al.*, 2000). In addition to the extrusion of mucilage by the spore, other factors such as the chemical and physical properties of the host surface have also been demonstrated to influence the process of adhesion. Relative hydrophobicity can influence how aggressively a spore is able to adhere to a substratum (Hamer *et al.*, 1988; Terhune & Hoch, 1993; Clement *et al.*, 1994; Mercure *et al.*, 1994). Electrostatic charge might also influence spore adhesion (Jones & O'Shea, 1994). Fungal enzymes are also involved in some cases. The uredospores of *Uromyces viciae-fabae* have been demonstrated to produce serine esterases (including one with cutinase activity) that promote spore adhesion (Deising *et al.*, 1992, 1995). Cutinase and non-specific esterase activity has been localised within mucilage associated with spores of *E. graminis* (Nicholson & Moraes, 1980, Nicholson *et al.*, 1988; Pascholati *et al.*, 1992).

The process of attachment by *M. grisea* conidia has been thoroughly investigated *in vitro*. As a conidium reaches maturity, the wall of the apical cell ruptures releasing

spore tip mucilage (STM) from the periplasmic space (Fig. 1.2b). This mucilage has been reported to be visible on the tip of the apical cell in the form of a droplet, whilst the conidium is still attached to the conidiophore (Howard, 1994; Howard & Valent, 1996), although there is evidence that it is released upon hydration (Hamer *et al.*, 1988). Attachment occurs rapidly after encountering a surface, which is a common feature of many spores that attach via mucilage (Hamer *et al.*, 1988; Kuo & Hoch, 1996; Altre *et al.*, 1999). The rice leaf is coated by a waxy cuticle and is highly hydrophobic (Uchiyama & Okuyama, 1990; Talbot, 1995). The conidium is able to stick to this highly water repellent surface via STM, and there is evidence that this process of adhesion is more tenacious on a hydrophobic substratum (Hamer *et al.*, 1988). The presence of STM might be dependent upon a variety of factors such as strain, colony age, growth conditions, humidity and the technique used to isolate spores (Howard, 1994; Jelitto *et al.*, 1994; Howard & Valent, 1996). It has been proposed that hydrophobins (see Section 1.3.1) could play a role in adherence to hydrophobic substrata (Wessels, 1996, 1997). In *M. grisea* a gene (MPG1) that encodes a putative hydrophobin, is highly expressed during the pre-penetration stages of infection. There is evidence that MPG1 directs the synthesis of the conidial rodlet layer, and that *mpg1*$^{-1}$ mutants are less pathogenic. However, there was no evidence that conidia were compromised in their ability to adhere to the host rice leaf (Talbot *et al.*, 1993, 1996).

1.3.3 Germination

1.3.3.1 Dormancy and self-inhibition

All spores are initially dormant in that they do not synthesize new cellular material and have low metabolic rates (Smith & Berry, 1974). Many spores require favourable environmental conditions in order to germinate. These will vary between species, although water, oxygen and carbon dioxide are universally required for activating spore germination. Furthermore, factors such as temperature, pH, light and nutrient availability can also be important (Brown, 1922; Gottleib, 1950; Sussman, 1981; Van Laere *et al.*, 1987; Gold & Mendgen, 1991; d'Enfert, 1997). Those spores that do not germinate in these conditions are constitutively dormant and require to be activated

by some more specific requirement, e.g. a period of ageing referred to as post-maturation, heat shock, or chemical treatment (Smith & Berry, 1974; Deacon, 1997). Host surface chemical and physical characteristics can be important, e.g. flavonoids exuded from legume roots stimulate spore germination in a number of soilborne fungi (Bagga & Straney, 1999), and in *Colletotrichum gloeosporioides* surface wax from the host induces spore germination (Podila *et al.*, 1993, Perfect *et al.* 1999). In many fungal species, spores contain self-inhibitors that prevent germination within a dense population of spores. These inhibitors are small, often lipophilic in nature, and prevent germination unless they are leached away; which will only occur when the spore concentration is low and hence the diffusion gradient is towards the external medium (Macko, 1981).

1.3.3.2 Magnaporthe *spores exhibit exogenously imposed dormancy*

In the presence of water, germination of *M. grisea* conidia occurs rapidly either freely in liquid suspension or on a wide range of artificial substrata (Table 1.2). Thus germination appears to be independent of the substratum and of the process of attachment, and most research concerning the pre-penetration phase of infection by *M. grisea* has been conducted *in vitro* (Fig. 1.2b–d, Table 1.2). Optimal conditions for germination are achieved by maintaining a high relative humidity (92–96%), and a temperature of 25 °C with inhibition occurring at temperatures < 15 °C and > 30 °C, (Hashioka, 1965; Sadasivan *et al.*, 1965; Kim, 1994). Germination will occur in the dark and does not require external nutrients (Jellito *et al.*, 1994; Xiao *et al.*, 1994b). There is evidence that flavonoids produced by the host rice plant inhibit germination in *M. grisea* conidia (Padmavati *et al.*, 1997).

1.3.3.3 Emergence of the germ tube

The emergence of a germ tube can be regarded as the initiation of polarised growth and requires the synthesis of new plasma membrane and cell wall material. In many spore types the first morphological sign that germination has commenced is isotropic growth or swelling of the spore (e.g. the conidia of *A. niger* double in diameter to around 7 μm; Smith & Berry, 1974). In spores that do not undergo significant swelling such as the conidia of *M. grisea*, the emergence of the germ tube is the first morphological sign that germination has commenced.

Substratum	References
Rice leaves	Hashioka, 1972; Araki & Miyagi, 1977; Peng & Shishiyama, 1988; Chumley & Valent, 1990; Valent *et al.*, 1991; Sweigard *et al.*, 1992b; Jelitto *et al.*, 1994; Talbot *et al.*, 1996.
Rice leaf wax components (coated on glass or cellophane)	Weintraub *et al.*, 1958; Araki & Miyagi, 1977; Uchiyama *et al.*, 1979; Uchiyama & Okuyama, 1990; Hegde & Kolattukudy, 1997.
Glass	Uchiyama & Okuyama, 1990; Lee & Dean, 1993; Jelitto *et al.*, 1994; Gilbert *et al.*, 1996; Money & Howard, 1996.
Teflon™	Hamer *et al.*, 1988; Howard *et al.*, 1991a; Talbot *et al.*, 1993, 1996; Jelitto *et al.*, 1994; Beckerman *et al.*, 1997.
Cellophane	Araki & Miyagi, 1977; Hamer *et al* 1988; Bourett & Howard, 1990; Howard *et al.*, 1991a; Jelitto *et al.*, 1994.
Plastic	Howard & Ferrari, 1989; Xiao *et al.*, 1994b; Money & Howard, 1996; Adachi & Hamer, 1998; Dixon *et al.*, 1999.
Wax paper	Lee & Dean, 1993.
Polystyrene	Lee & Dean, 1993; Talbot *et al.*, 1993; Liu & Kolattukudy, 1999.
Polyethylene	Howard *et al.*, 1991a.
Mylar	Money & Howard, 1996.
Kevlar	Howard *et al.* 1991a.
Cellulose membrane	Howard & Ferrari, 1989; Bourett & Howard, 1992.
Gelbond (both hydrophobic and hydrophilic sides)	Lee & Dean, 1993; Xiao *et al.*, 1994b; Mitchell & Dean, 1995; Gilbert *et al.*, 1996; Liu & Dean, 1997; Adachi & Hamer, 1998; Dixon *et al.*, 1999.
Agarose	Weintraub *et al.*, 1958; Lee & Dean 1993; Xiao *et al.*, 1994b.
Liquid suspension (no substratum)	Lee & Dean, 1993; Jelitto *et al.*, 1994; Xiao *et al.*, 1994b; Gilbert *et al.*, 1996; Howard & Valent, 1996.

Table 1.2: Substrata upon which conidia of *M. grisea* have been germinated.

The germ tube must emerge through the cell wall, which is often thick and pigmented. Some fungal spores have predetermined areas from which the germ tube emerges. These are called germ pores, and they are regions in which the cell wall is thinner (Smith & Berry, 1974; Read & Beckett, 1996). Other mechanisms have been proposed in some fungal systems. For example, the chlamydospores of *Thielaviopsis*

have crease-like, electron transparent regions near the ends of the spore in the mature chlamydospore chain (Tsao & Tsao, 1970; Riggs & Mims, 2000). It has been postulated that these are part of two transversely located bands that run around the rim of each spore, and that they contain chitin that is degraded by soil microbes. The action of spore turgor pressure on the subsequently weakened region might result in the partial disjoining of the cell wall, allowing the emergence of a germ tube (Tsao & Tsao, 1970). In some species (e.g. *Alternaria cassiae*) the spores have no visible mechanism by which the germ tube emerges through the cell wall and apparently simply push their way out (Mims *et al.*, 1997).

Some types of spores characteristically produce a single germ tube (e.g. uredospores of *Puccinia graminis*; Read *et al.*, 1997) whilst others are multipolar, with typically more than one germ tube being produced (e.g. *Blumeria graminis*; Carver *et al.*, 1999). The conidia of *M. grisea* are reported to be able to germinate from one or more of the three conidial cells, but usually a single germ tube is produced from the tip region of the apical cell (Fig. 1.1, 1.2b) (Bourett & Howard, 1990; Jelitto *et al.* 1994). The cell wall is ruptured in the tip region of the apical cell as a result of the mechanism by which STM is released and so this region of the plasma membrane represents a prime site for the emergence of the germ tube. However, germ tubes may also emerge from other regions of the apical cell plasma membrane, and also from the other two cells in which the cell wall is intact (Fig. 1.1), (Hamer *et al.*, 1988).

1.3.3.4 Extracellular mucilage is associated with germ tubes

A range of fungi produce extracellular mucilage (ECM) that is associated with the germ tube (Braun & Howard, 1994; Jones *et al.*, 1995; Kuo & Hoch, 1995; Au *et al.*, 1996; Apoga & Jansson, 2000), and this is believed to be an essential pre-requisite to successful infection (Mendgen & Deising, 1993; Braun & Howard, 1994). It has been proposed that in *Uromyces appendiculatus,* extracellular proteins produced by the germ tube are involved in sensing the host surface topography (Epstein *et al.*, 1985), however these findings assume that only extracellular proteins are affected when an entire germling is exposed to a proteinase solution. ECM has been reported to be associated with both the germ tube and the appressorium of *M. grisea* (Bourett &

Howard, 1990; 1994; Xiao *et al.* 1994a; Jones *et al.*, 1995). As in the case of spore adhesion (Section 1.3.2), it has been proposed that hydrophobins could also be involved in the adhesion of germ tubes (Wessels, 1996, 1997). In *M. grisea,* there is evidence that in addition to directing the synthesis of the conidial rodlet layer, the MPG1 gene also encodes a putative hydrophobin that plays a role in the interaction between the germ tube/appressorium and hydrophobic surfaces (Talbot *et al.*, 1996).

1.3.3.5 Biochemical changes during germination

The transition from dormant to active growth is accompanied by profound structural and biochemical changes (d'Enfert, 1997). The emergence of the germ tube marks the initiation of polarised growth and is necessarily accompanied by the biosynthesis of nucleic acids, proteins, membrane systems, and cell wall material. During the early stages of germination many metabolic activities including respiration, and, RNA and protein synthesis commence (Brambl & Handschin 1976; Lovett, 1976; Brambl, 1981; Brambl *et al.*, 1987; Van Laere *et al.*, 1987; d'Enfert 1997). In *N. crassa* groups of genes involved in respiration, ribosome assembly, chromatin structure and amino acid biosynthesis (Sachs & Yonofsky, 1991), and in *A. nidulans* genes that encode ribosomal proteins, are all expressed at a higher level within germinating spores than in mycelia (d'Enfert 1997). Dormant asexual spores have been shown to contain a population of preserved, stable mRNA (Brambl *et al.*, 1978). Essential protein synthesis occurs early during spore activation and it has been suggested that this mRNA is responsible for this biosynthesis. Although this might be true for some species, in *N. crassa* it is not solely responsible, as inhibiting RNA synthesis blocks both protein synthesis and spore germination (Brambl *et al.*, 1987). Nuclear division and DNA synthesis during fungal spore germination have been studied in some detail in several species. A common feature is that the synthesis of DNA occurs after RNA and protein synthesis, and shortly before or after germ tube emergence (Brambl *et al.*, 1978).

1.3.3.6 Mobilization of carbon sources during germination

Lipid and carbohydrates can comprise a large percentage of the ungerminated spore (e.g. in *Neurospora tetrasperma* ~25% and 33% of the spore dry mass were found to be lipid and carbohydrate respectively; Lingappa & Sussman, 1959), and for those

spore types such as *M. grisea* conidia that are able to germinate in pure water, the mobilization of these internal carbon sources may allow germination to proceed in the absence of external nutrients (Gottleib, 1976). There is evidence that in *Neurospora* ascospores, the mobilization of stored carbon-sources such as lipids, carbohydrates or proteins does not occur within dormant spores, commencing immediately after activation (Lingappa & Sussman, 1959). Lipid mobilization during germination has been demonstrated in a number of species, and it is thought to be utilized for both generating energy and producing sugars for biosynthetic processes (Schadeck *et al.*, 1998). However, not all spore types are nutritionally independent in this way and the requirement for exogenous nutrients may vary within one taxonomic group (Blakeman, 1980; Garraway & Evans, 1984; Kolattukudy & Köller, 1983).

Trehalose and glycogen are the main carbohydrate reserves in fungi. Glycogen is synthesized during periods of active growth and degraded during the stationary phase or during the production of resting structures (Van Laere, 1995). There is evidence that in spores, glycogen is replaced by trehalose, a nonreducing disaccharide that is accumulated in a wide variety of organisms, including fungi, during periods of reduced growth (Elbein, 1974; Thevelein, 1988). It is thought to serve as a carbon source during germination as it is mobilized during this period by the enzyme trehalase, forming glucose (Thevelein, 1988). Genes have been isolated in both *A. nidulans* and *M. grisea,* that encode proteins with homology to the trehalase of *Saccharomyces cerevisiae*, providing evidence that trehalose is utilized as a carbon source (d'Enfert, 1997). In addition, trehalose may serve to protect the spore from environmental stress, such as exposure to heat, and has also been implicated in the control of osmotic pressure within spores. These features of trehalose could explain why it is more abundant in spores than glycogen (Van Laere, 1995).

1.3.3.7 Signalling during germination

The germ tubes of some species of rust exhibit directional growth, by growing at right angles to cell junctions or other host features, and there is evidence that other fungi also exhibit directional growth (Hoch & Staples, 1991; Read *et al.*, 1992b). The presence of ECM associated with germ tubes (see Section 1.3.3.4), and asymmetric

organization of the germ tube structure relative to the substratum could be important components of a topographical signalling system. Although both ECM and asymmetric organization have been reported in the germ tube of *M. grisea* there is no evidence of topographical signalling during germination and germ tube growth (Xiao *et al.*, 1994a,b; Howard & Valent, 1996).

There is evidence that a cyclic AMP-dependent protein kinase may play an important role in signal transduction during the germination of fungal spores (Van Laere, *et al.*, 1987; Bourret *et al.*, 1991; Yang & Dickman, 1999). In *A. nidulans,* a *ras* homologue called *Aras* has been shown to influence spore germination, and a model has been proposed in which "...particular levels of active A-RAS allow development to proceed to certain points while inhibiting further development" (Som & Kolaparthi, 1994). Since ras is linked with cAMP (cyclic AMP) synthesis, it is possible that the ras/cAMP/PKA pathway is involved in fungal spore germination (d'Enfert, 1997). However, germination of *Erisyphe* conidia is unaffected by the addition of exogenous cAMP or analogues of cAMP (Hall *et al.*, 1999). Although in *M. grisea* cAMP-dependent signalling has been demonstrated to be crucial to the process of differentiation, there is no evidence that it is involved in germination (Choi & Dean, 1997; Lee & Dean 1993; Mitchell & Dean, 1995; Dean *et al.*, 1996; Xu & Hamer, 1996; Xu *et al.*, 1997; Adachi & Hamer, 1998; Choi *et al.*, 1998; Hamer & Talbot, 1998; DeZwaan *et al.*, 1999; Shen *et al.*, 1999; Smith, 1999).

Polyamines are known to be essential for fungal growth, and although their precise role is still unclear, there is evidence that they might serve to reduce intracellular levels of cAMP (Tabor & Tabor, 1985; Choi, *et al.*, 1998). Fungal spores synthesize polyamines during the early stages of germination (Kim, 1971; Mennuci *et al.*, 1975; Stevens *et al.*, 1976; Calvo-Mendez *et al.*, 1987; Ruiz-Herrera & Calvo-Mendez, 1987; Khurana *et al.*, 1996; Choi *et al.*, 1998) and it is thought that this synthesis is achieved through the ornithine decarboxylase (ODC) pathway in fungi (Choi *et al.*, 1998). In many fungal species, specific inhibitors of polyamine biosynthesis restrict spore germination and germ tube growth (Tabor & Tabor, 1985; Ruiz-Herrera &

Calvo-Mendez, 1987; Rajam, 1993). The conidia of *M. grisea* contain high levels of polyamine just after the dispersal stage, which subsequently decreases during germination. However, the addition of external polyamines and inhibitors of polyamine biosynthesis do not affect conidial germination, but do impair differentiation (Choi, *et al.*, 1998).

There is some evidence that a Ca^{2+}/calmodulin signal transduction pathway could be important during the germination of fungal spores. In *M. grisea* there is evidence that calmodulin plays a role during differentiation, and that attachment to a substratum is required for the induction of the *cam* gene (Liu & Kolattakudy, 1999). In *A. nidulans* a Ca^{2+}/calmodulin-dependant kinase has been demonstrated to be important in controlling germination (Dayton *et al.*, 1997). In *P. ampelicida* external Ca^{2+} induced germination on non-inductive substrata (Shaw & Hoch, 1999), and in *Colletotrichum trifolii* there is evidence that germination is inhibited by calmodulin inhibitors and calcium channel blockers (Warwar & Dickman, 1996).

1.3.4 Differentiation and penetration

There is a vast array of mechanisms by which fungal pathogens may penetrate the underlying host tissue. Entry may be directly into the underlying epidermal cells, or indirectly through natural openings, such as stomata. Fungal structures that penetrate the host surface vary widely, and range from germ tubes to encysted zoospores and highly specialised piercing structures, including appressoria (Howard, 1997). The cytological and morphogenetic features of differentiation have been characterized in detail in *M. grisea* and much of our current understanding relating to appressorial formation is derived from this research (Howard & Valent, 1996; Howard, 1997).

In *M. grisea* after a period of growth, the germ tube differentiates to form an appressorium, initially swelling and bending at the apical region in a process referred to as 'hook formation'. A mitotic division takes place within the conidial cell from which the germ tube originates, and one of the two resultant nuclei migrates into the developing appressorium. A septum then forms between the germ tube and appressorium. During the final stages, the developing appressorium swells and becomes melanised (Bourett & Howard, 1990), to form a mature appressorium

(Fig. 1.2d): a unicellular, uninucleate, pigmented and highly turgid infection structure from which a slender (0.7 μm x 3.3 μm) infection peg (Fig. 1.2e) penetrates the underlying host cell wall (Bourett & Howard, 1990; Howard *et al.*, 1991a; Howard & Valent, 1996). A pore is formed on the appressorial substratum interface; the wall is extremely thin in this region, lacking melanin and chitin, and membrane cisternae and vesicles have been reported to accumulate around it (Bourett & Howard, 1990). A ring has been observed around the periphery of the pore, possibly serving to seal the pore to the substratum (Howard & Ferrari, 1989). The penetration peg cytoplasm is characterized by the absence of any recognisable organelles with the exception of a few apical vesicles. This has been referred to as a "zone-of-exclusion" and it has been hypothesised that actin, which is present, may play a role in its formation (Bourett & Howard, 1991, 1992; Howard & Valent, 1996).

In many fungal pathogens there is evidence that penetration involves enzymatic weakening of the cuticle by fungal enzymes such as cutinase (Jeffree, 1996; Hamer & Holden, 1997; Howard, 1997). A gene encoding cutinase has been isolated in *M. grisea*; however *cut*$^-$ mutants were found to be competent in pathogenesis and sporulation (Sweigard *et al.*, 1992a,b). *M. grisea* is able to penetrate synthetic surfaces made from polyethylene, Mylar (polyethylene terephthalate), and even Kevlar (*p*-phenylene terephthalamide), (Howard *et al.*, 1991a). Appressorial turgor has been estimated to exceed 8.0 MPa, making it one of the highest cell turgor pressures measured to date (Bechinger *et al.*, 1999; Money, 1999). The appressorium has been demonstrated to derive its invasive force solely from this turgor pressure (Howard *et al.*, 1991a; Money & Howard, 1996), which is achieved by accumulating osmolytes such as glycerol in the cytoplasm during germination and germ tube growth (de Jong *et al.*, 1997).

Appressoria of *M. grisea* possess a layer of melanin (~100 nm thick) just outside the plasma membrane (Howard & Valent, 1996). There is evidence in this and other pathogenic fungi that melanin plays a role in virulence (Woloshuk *et al.*, 1980, 1981; Wheeler & Bell, 1988; Wheeler & Greenblatt, 1988; Chumley & Valent, 1990). The appressoria of melanin-deficient *M. grisea* mutants *alb*$^-$, *buf*$^-$ and *rsy*$^-$ are unable to

penetrate artificial substrata and to infect intact host leaves, but are able to infect plants via leaf wounds (Howard & Ferrari, 1989; Chumley & Valent, 1990). They are also unable to generate the high turgor pressure estimated in the melanised appressoria of the wild-type and to accumulate glycerol. Thus, it has been suggested that melanin in the appressorial cell wall serves as a barrier to prevent glycerol from leaking out of the cell (Money & Howard, 1996; de Jong *et al.*, 1997; Money, 1999).

Topographical and chemical features of the host surface have been demonstrated to induce differentiation in many plant pathogen systems (Kaminskyj & Day, 1984; Hoch *et al.*, 1987; Hoch & Staples, 1991; Read *et al.*, 1992b, 1997; Kolattukudy *et al.*, 1995; Collins & Read, 1997). Physical and chemical features of the substratum such as relative hydrophobicity and host surface wax and its components have been demonstrated to influence differentiation in *M. grisea* (Uchiyama *et al.*, 1979; Uchiyama & Okuyama, 1990; Lee & Dean, 1993; Jelitto *et al.*, 1994; Xiao, *et al.*, 1994b; Gilbert *et al.*, 1996; Dean *et al.*, 1996; Hegde & Kolattukudy, 1997).

Recently, a gene (PTH11) has been implicated in host surface recognition by *M. grisea,* and it has been proposed that either hydrophobicity or cutin monomers alone are sufficient to induce differentiation (DeZwaan *et al.*, 1999).

1.3.5 Invasion of host tissues

In *M. grisea,* once the penetration peg has been produced by the appressorium and has successfully penetrated the plant cuticle and cell wall it enlarges to form a primary infection hypha, which in turn differentiates into a branched and bulbous secondary hypha, from which colonisation of the host tissue then takes place (Fig. 1.2e), (Heath *et al.*, 1990, 1992; Koga, 1994). Infection is rapid: 10% of the biomass of an infected plant can be composed of fungal material after just 72 hours post inoculation.

Hours post hydration	Conidial events during infection
0	Hydration, dispersal and contact with rice leaf surface. Adhesion by spore tip mucilage. Apical and basal cells generate high turgor pressure (1.3-1.4 MPa); middle cell is less turgid.
0.5–1.5	Turgor in all three cells falls (middle cell least turgid). Germination of one or more of the three cells. Germ tube elongation. Extracellular matrix associated with the germ tube. Apical cluster of cytoplasmic vesicles present in germ tube near the substratum.
2–4	Germ tube tip growth ceases. Hook formation. Mitotic division in cell from which germ tube originates. One nucleus migrates into developing appressorium. Septum forms between germ tube and appressorium. New outer wall layer forms over expanding appressorium. Appressorium cell wall thins in the pore region. Membrane cisternae and vesicles abundant in appressorium near substratum.
4–8	Melanisation of appressorium begins. Membrane cisternae and vesicles absent in appressorium. Appressorium pore becomes well defined.
16–24	Granular substance (possibly an adhesive) accumulates at appressorium substratum interface. Glycogen rosettes abundant in appressorium cytoplasm. Appressorial pore ring becomes visible.
24–31	Formation of appressorial pore wall overlay. Glycogen rosettes nearly absent in the cytoplasm of the appressorium. Penetration peg emergence from the appressorium. Actin present at penetration peg.
31–70	Formation of primary infection hyphae.
48	Development of bulbous secondary hyphae. Hyphae spread to adjacent epidermal cells.
72	Hyphae spread into mesophyll cells. Up to 10% of total plant biomass is fungal.
96–168	Lesions on rice leaves and conidiation.

Table 1.3: Summary of events during infection by *Magnaporthe grisea* with approximate timing. Note that most research concerning the pre-penetration phase of infection by *M. grisea* has been conducted *in vitro*. The information presented in this table is summarised from: Ou, 1980a; Bourett & Howard, 1990, 1994; Xiao *et al.* 1994a; Jones *et al.*, 1995; Talbot, 1995; Howard & Valent, 1996; Money & Howard, 1996.

Initially infection is of a biotrophic nature, ultimately becoming necrotrophic, which often results in the death of the host plant (Talbot, 1995). Lesions may form within 4 days after spore germination and conidia by 7 days (Ou, 1980a); and the cycle of infection then returns to the phase of release and dissemination (Fig. 1.2). In temperate regions where only one annual rice crop is grown, dissemination between host plants and between crops can not occur in a continuous cycle of infection, and in this case the fungus overwinters in crop residue and seeds, although the transfer of infection by seed is thought to be limited (Bonman, 1992).

The main events during differentiation and the subsequent infection stages in *M. grisea* have been summarised in Table 1.3.

1.4 FUNGAL SPORE ORGANELLES AND THEIR ORGANIZATION DURING GERMINATION

Tip growth, which is exhibited by fungal hyphae and germ tubes, is characterized by localised deposition of new plasma membrane and cell wall in the tip region, with concomitant cytoplasmic migration (Heath & Steinberg, 1999). The organelles within this cytoplasm are not, as it was once believed, simply dragged along by cytoplasmic flow, but instead exhibit independent motility. Organelle movement has been categorised as either organelle motility, or organelle positioning and is characterized by "rapid (1-10 μm/s), erratic (showing frequent stops and starts and moving variable distances each time), and bidirectional [movement]" (McKerracher & Heath, 1987). In contrast, the position of some organelles (e.g. nuclei and mitochondria) within the cytoplasm is often constant in relation to the hyphal tip, and they move at the same rate as the cytoplasm (McKerracher & Heath, 1986a,b, 1987). The cytoskeleton has been demonstrated to be intrinsic to organelle movement and positioning in filamentous fungi. Microtubules, microfilaments and their associated motor proteins have been identified in a range of filamentous fungi (Heath, 1995; Steinberg, 2000). In the germlings of *Uromyces appendiculatus*, microtubules and F-actin microfilaments were shown to be orientated along the longitudinal axis of the germ

tube, and to alter their organization in response to inductive substratal cues (Kwon *et al.*, 1991). Microtubules and kinesins/dynein have been shown to be important for nuclear, mitochondrial and vacuolar movement and/or position in a number of filamentous fungi (McKerracher & Heath, 1986a,b; Heath, 1995; Steinberg *et al.*, 1998; Wu *et al.*, 1998; Hyde *et al.*, 1999; Fischer, 1999; Seiler *et al.*, 1999). There is evidence that they play a role in vesicle transport but they might also be important in organelle movement and positioning (Oakley & Rinehart, 1985; Shepherd *et al.*, 1989; Heath, 1995; Steinberg, 1998, 2000; Torralba *et al.*, 1998; Fischer, 1999; Seiler, *et al.*, 1999). Furthermore, they may be central to the process of cytoplasmic migration and tip growth (McKerracher & Heath, 1987; Heath & Steinberg, 1999).

Fungal organelles exhibit considerable morphological variation, not only between species but also between individuals. In the latter case this can depend on the cell type, stage of cell development or location within a fungal hypha. However, even adjacent organelles can exhibit different morphologies, (e.g. the vacuolar system might have vesicular elements adjacent to tubular and larger spherical elements). Such morphological differences may reflect variation in a specific organelle's function or stage of development. These variables are important when analysing image data as different cell compartments can look very similar or very different. Ultrastructural data collected on organelle organization and morphology prior to the advent of freeze substitution techniques for TEM must be interpreted with caution because chemical fixation has been demonstrated to induce artefactual changes in morphology as it can take up to several minutes to arrest membrane flow (Howard & Aist, 1979; Howard, 1981; Hoch, 1986; Howard & O'Donnell 1987). For example, chemical fixation has been demonstrated to cause vesiculation of the vacuole in plantsa and fungal hyphae, and in the endosomal system of animal cells (Wilson *et al.*, 1990; Ashford, 1998).

1.4.1 Nuclei

The nucleus is surrounded by a double membrane and is commonly spherical to ovoid in shape, although its morphology is dependent on its stage in the nuclear cycle (Beakes, 1981; Beckett, 1981; Heath, 1981). Nuclear pores span the double

membrane, regulating the passage of macromolecules between the nuclear matrix and cytoplasm. These inner and outer membranes are continuous with one another, the former contains attached chromatin and the latter is studded with ribosomes and appears in places to be continuous with the endoplasmic reticulum (ER); indeed in animal and plant cells and in several fungal species it has been demonstrated that the rough ER and outer nuclear membrane are continuous (Beckett *et al.*, 1974; Stryer, 1988; Evans & Graham, 1989; Morré, 1990).

Most filamentous fungi are haploid, typically with small genomes of approximately 30 Mb (roughly 1% of the size of the average mammalian genome), and usually have nuclei of 1–3 μm in diameter, (Clutterbuck, 1995; Markham, 1995). The fungal hypha characteristically contains multiple nuclei within a common cytoplasm, and this might act to shield the mycelium from disadvantageous mutations within the haploid nuclear population. A small genome will be able to replicate quickly and perhaps is less prone to mutation, (Clutterbuck, 1995; Markham, 1995).

A nucleus is required in the proximity for most biosynthetic processes to occur and nuclei are able to move throughout the fungal cytoplasm, and sometimes over considerable distances (Markham, 1995; Suelmann *et al.*, 1997; Fischer, 1999). This makes the fungal hypha an excellent system in which to study nuclear migration, a process crucial to cytokinesis in eukaryotic cells, and several models for nuclear migration have been proposed (Fischer, 1999). Being small allows the nucleus to pass through small gaps such as septal pores or through the narrow bridges between anastomosed mycelia (Clutterbuck, 1995). Migration of the nucleus is often coupled with transient morphological changes, (e.g. nuclei passing through a septal pore may become characteristically dumbbell shaped), (Hunsley & Gooday, 1974; Markham, 1995).

In ungerminated spores, nuclei are commonly roughly spherical and often located centrally within each spore cell (e.g. Hawker & Abbot, 1963; Delvecchio, *et al.*, 1969; Gull & Trinci, 1971; Hoch & Staples, 1983; Mims *et al.*, 1988, 1997; Van

Dyke & Mims, 1991; Roberts *et al.*, 1996; Mollicone & Longcore, 1999). However, as in the mycelium, the nucleus displays morphological plasticity and this is especially noticeable when a nucleus migrates up a thin germ tube, requiring it to elongate (e.g. Hawker & Abbot, 1963; Van Dyke & Mims, 1991). Nuclear shape can apparently change passively, e.g. in ungerminated spores of *Colletotrichum truncatum*, the spherical shape of the nucleus is occasionally distorted by lipid bodies that press against it (Van Dyke & Mims, 1991).

The number of nuclei in ungerminated spores varies between species and sometimes, as in *N. crassa,* between conidia of the same species (Schmit & Brody, 1976). The number often increases during or just before germination (e.g. Van Dyke & Mims, 1991; Maheshwari, 1999). In the conidia of *M. grisea* each of the three cells contain a single identical nucleus (Ou, 1980b). During germination the nucleus within the germinated cell divides by mitosis, and one of the resultant nuclei migrates into the developing appressorium (Bourett & Howard, 1990), (see Table 1.3).

1.4.2 Mitochondria

Mitochondria are the sites of respiration and energy generation in eukaryotes. They possess a double membrane. The outer membrane contains transport systems by which the breakdown products of carbohydrates, proteins and lipids pass into the mitochondrion. The central matrix compartment contains all the enzymes associated with the final oxidation of these breakdown products and the inner membrane is in the form of highly folded cristae that contain the electron transport system essential to the production of ATP (Evans & Graham, 1989). Endosymbiotic in origin, mitochondria are able to synthesize many of the mitochondrial proteins and lipids required for their own function as they have retained their own ribosomes and some of their own DNA. Others are encoded by nuclear DNA and synthesized by ribosomes within the cytoplasm and transported into the mitochondria (Alberts *et al.*, 1989).

As in mammalian cells, the mitochondria of fungal cells are observed at higher densities where energy is required; for example they extend into the subapical region

of growing hyphal tips (Stryer, 1988; López-Franco & Bracker, 1996; Fischer-Parton *et al.*, 2000), and are present at high densities within maturing sporangia (Weber *et al.*, 1998) and adjacent to the flagella of zoospores (Lange & Olson, 1998). In *Mucor mucedo* mitochondrial activity has been demonstrated to be higher during sporangiospore formation than during germination or within the vegetative hyphae (Weber *et al.*, 1998). In the Oomycete *Phytophthora infestans* mitochondrial activity has been demonstrated to be very high within the vegetative hyphae (Pitt *et al.*, 1998). In Oomycetes and the Zygomycete *Basidiobolus ranarum*, the inner mitochondrial membrane is folded into a meshwork of tubes (Grove & Bracker, 1970; Weber *et al.*, 1998). However, in most fungi (like other eukaryotes), extensive folding of the inner membrane forms cristae, which are stacked more or less regularly across the width of the mitochondrion (Beckett *et al.*, 1974; Pitt *et al.*, 1998; Weber *et al.*, 1998). It has been suggested that the methods of fixation used might be responsible for some of the observed differences but this hypothesis remains untested to date (Weber *et al.*, 1998).

Mitochondrial morphology is highly variable within fungal hyphae. Ultrastructural studies have shown that the mitochondria in *M. grisea* are filamentous, as in all major fungal groups. Filamentous mitochondria are usually ~0.5 μm wide and up to 5 μm in length, with some folded or coiled mitochondria being as long as 25 μm (Roberson & Fuller, 1988; Bourett *et al.*, 1993; Markham, 1995; Lopez-Franco & Bracker, 1996; Bourett & Howard, 1996; Weber *et al.*, 1998). Rod-shaped and spherical mitochondria are often present towards the fungal hyphal tip (Beckett *et al.*, 1974; Markham, 1995; Fischer-Parton *et al.*, 2000). The filamentous morphology of mitochondria is probably an adaptation to hyphal growth, since mitochondria generally lie approximately parallel to the long axis of the hyphae (Markham, 1995). Mitochondria are often observed to be branched and given their filamentous nature, an individual mitochondrion can be simultaneously in contact with many different regions of a cell (Weber *et al.*, 1998). Indeed the cells of. *S. cerevisiae* typically contain only one highly branched mitochondrion (Hoffman & Avers, 1973).

In ungerminated spores mitochondria are often reported to be spherical (e.g. Gull & Trinci, 1971; Millicone & Longcore, 1999), or elongated (e.g. Mims *et al.*, 1988, 1997; Mollicone & Longcore, 1999). The number of mitochondria usually increases with the onset of germination, although in the conidia of *Botrytis cinerea* this was found to be only a minor increase when expressed as a percentage of the total cytoplasmic area (Gull & Trinci, 1971; Mims *et al.*, 1997). Mitochondria are often orientated in the direction of the longitudinal axis of the spore cells (e.g. Hoch & Staples, 1983; Roberts *et al.*, 1996), and after germination their morphology is commonly filamentous (e.g. Hawker & Abbot, 1963; Mims *et al.*, 1997), although in *Uromyces* mitochondria remain smooth and rounded (Hoch & Staples, 1983).

1.4.3 Vacuolar system

Once thought to be organelles that simply served to fill hyphae emptied of cytoplasm by the growing tip region, vacuoles are now acknowledged as having a number of important physiological roles in fungal cells. They are acidic organelles that bear many similarities to the mammalian lysosomal system (Klionsky *et al.*, 1990; Ashford, 1998). The principal roles of the fungal vacuole include storage, osmoregulation and the control of cytoplasmic composition (Ashford, 1998; see references therein). The finding that there are seven different mechanisms by which cellular components can be imported into the yeast vacuole could be indicative of the importance of the vacuole in cellular physiology (Klionsky, 1997).

In filamentous fungi the vacuolar system is composed of extensive networks of spherical and tubular elements that have been demonstrated in fungal hyphae to be interconnected over long cellular distances (Shepherd *et al.*, 1989, 1993; Rees *et al.*, 1994; Hyde & Ashford, 1997; Cole *et al.*, 1998; Ashford, 1998; Orlovich & Ashford, 1998). In mature hyphal regions vacuoles are primarily spherical but in younger hyphal regions the vacuole is composed of extensive networks of spherical and tubular elements (Hyde & Ashford, 1997; Cole *et al.*, 1998). The vacuolar network in living hyphae has been visualised using vital dyes and in unstained material, revealing its dynamic nature (Shepherd *et al.*, 1989, 1993; Rees *et al.*, 1994; Hyde & Ashford, 1997; Cole *et al.*, 1998). Ashford (1998) has described it as involving

"tubule tip extension and retraction, dilation and contraction, fusion of tubules with spherical vacuoles, movement of varicosities along tubules, and the reversible conversion of tubules into strings of interconnected vesicles". Similarly they have been described in several members of the Oomycetes, although interestingly they were found to differ from the tubular vacuolar system of the true fungi by being more frequently branched and less mobile (Allaway *et al.*, 1997). Although the vacuolar system of the budding yeast *S. cerevisiae* is primarily spherical, tubules were found to arise from vacuoles of mature cells and extend into developing buds (Weisman *et al.*, 1987; Weisman & Wickner, 1988).

The vacuolar system of fungal spores has been less well characterized. Ultrastructural studies have revealed that in several members of the Erisyphales (*Erisyphe pisi, E. cichoracearum*, and *E. graminis*) the vacuoles are typically located in the centre of the conidium (McKeen *et al.*, 1967; Martin & Gay, 1983; Roberts *et al.*, 1996). Elongated interconnected vacuoles have been identified in basidiospores of *Gymnosporangium juniper-virginianae* (Mims *et al.*, 1988). However, in ungerminated spores of *Alternaria cassiae* and *Uncinuliella australiana* the vacuoles are mostly spherical and do not change appreciably during germination (Mims *et al.*, 1997). In ungerminated spores of *C. truncatum* the vacuolar network was shown to consist of a mixed population of primarily spherical vacuoles with some elongated vacuoles that were occasionally observed to be branched. Just prior to germination vacuoles were generally smaller in size and present in greater numbers, although the germinating cell was never found to be highly vacuolated (Van Dyke & Mims, 1991). In nondifferentiated germlings of *Uromyces,* vacuoles are absent from the first 15–20 μm of germ tube tip. Numerous small (0.2–3μm) vacuoles are present behind this region, most of which are interconnected, beyond this region the vacuoles are larger and often in the form of cylindrical cisternae with slight constrictions spaced at regular intervals along their length (Hoch & Staples, 1983). Increased vacuolation is often reported after germination, (e.g. Gull & Trinci, 1971; Van Dyke & Mims, 1991) and vacuoles are often reported to contain inclusions (e.g. Hoch & Staples, 1983; Van Dyke & Mims, 1991; Roberts *et al.*, 1996).

Ultrastructural studies of *M. grisea* germlings have shown that different morphological vacuolar types exist within the continuous cytoplasm, without any apparent connection between the organelles (Bourett & Howard, 1994). The germ tube and adjacent conidial cytoplasm contains two types of vacuole: (1) irregularly sized and shaped with a heterogeneous matrix, often containing membrane bound inclusions, and (2) consisting of branched cisternae with a fairly homogenous, coarsely granular matrix. A third type of vacuole was identified in ungerminated conidial cells that comprised interconnected subspherical vacuoles with inclusion bodies. In addition, a larger vacuolar type characterized by branched cisternae was observed within the somatic hyphae.

1.4.4 Endomembrane system

The endomembrane system is considered to be "...the structural and developmental continuum of internal membranes that characterizes the cytoplasm of eukaryotic cells" (Morré, 1990), and in animals and plants includes the nuclear envelope, endoplasmic reticulum, Golgi cisternae, vacuoles and the plasma membrane, as well as various transfer vesicles (Morré, 1990; Satiat-Jeunemaitre *et al.*, 1996). In eukaryotes the endomembrane system is responsible for the processing, sorting and delivery of newly synthesized macromolecules which are destined for the lysomosomal/vacuolar system or for secretion at the cell surface, and for the internalization of molecules and membrane by endocytosis and their subsequent processing and targeted transport (Morré, 1990; Ashford, 1998; Fischer-Parton *et al.*, 2000). The endomembrane system of filamentous fungi has proven difficult to characterize both biochemically and structurally and is much less well understood than in animal and plant cells.

1.4.4.1 Endoplasmic reticulum

The endoplasmic reticulum (ER) is responsible for the synthesis of proteins and lipids. The rough ER bears ribosomes on the cytoplasmic face and is the site of membrane protein synthesis. The smooth ER is responsible for the synthesis of membrane lipids and the addition of core carbohydrate residues to produce glycoproteins (Evans & Graham, 1989).

In higher fungi the ER profile is typically of a sheet type and predominately concentrated in the subapical zone of growing hyphae and is often observed as being closely associated with the membranes of other organelles (Beckett *et al.*, 1974; Grove, 1978). In *M. grisea,* sheets of rough ER have been identified behind the hyphal tip and large amounts of rough ER were also observed to be present within the developing appressorium (Howard *et al.*, 1991b; Bourett & Howard, 1996). It was shown, using green fluorescent protein (GFP) targeted to ER in the hyphae of *A. nidulans*, that the ER is present in the form of a network that extends throughout the cell to within 1–2 μm of the hyphal tip (Fernández-Ábalos *et al.*, 1998). The ER can be specialised in different regions of the hypha or specialised cell types. For example, in Basidiomycetes, the ER sheets are often seen to be continuous with the parenthosome (the perforated cap that sits over the dolipore in a septum), and it is thought that the parenthosome is a differentiated form of ER (Gull, 1978). During the biotrophic phase of infection by *U. viciae-fabae*, the ER cisternae within the haustorial mother cell forms tubular ER which is more dilated than usual (called the tubular-vesicular complex), (Mendgen *et al.*, 1995).

Ungerminated spores characteristically have very little ER, sometimes appearing in electron micrographs as short membrane profiles (e.g. conidia of *Botrytis cinerea*; Gull & Trinci, 1971), fenestrated sheets (e.g. conidia of *Blumeria graminis* f.sp. *hordei;* Roberts *et al.*, 1996; Mollicone & Longcore, 1999) or as strands/tubules (e.g. chlamydospores of *Thielaviopsis*; Delvecchio *et al.*, 1969; Van Dyke & Mims, 1991), and usually scattered throughout the cytoplasm. However, this is not always the case; the ungerminated ascospores of *Neurospora* have extensive longitudinally orientated ER profiles associated with the plasma membrane, which have been correlated with the ribbed spore wall ornamentation of the genus (Dutta *et al.*, 1981). Once spore germination has begun, the density of ER usually increases and it often takes the form of sheets of single or parallel, flattened cisternae which are often associated with the nucleus (Gull & Trinci, 1971; Smith & Berry, 1974; Schmit & Brody, 1976; Hoch & Staples, 1983; Mollicone & Longcore, 1999). In *C. truncatum* more ER was observed within the germ tube than the conidium (Van Dyke & Mims, 1991). In

Uromyces, ER is present throughout the germ tube cytoplasm, but most prominently near the plasma membrane, with the exception of the region in contact with the substratum (Hoch & Staples, 1983).

1.4.4.2 Golgi equivalents

Animals, plants, and members of the Oomycota possess a Golgi apparatus with stacked cisternae (Grove & Bracker, 1970; Beckett *et al.*, 1974; Bracker *et al.*, 1996). It is responsible for the addition of terminal sugar groups to glycoproteins and glycolipids, processing (e.g. enzymatic modification of carbohydrates) and for assembling lipids and proteins into the correct conformation for incorporation into membranes or for secretion (Evans & Graham, 1989).

Most fungi do not possess a multi-cisternal, stacked Golgi apparatus and instead have individual smooth membrane cisternae that have been described as "Golgi equivalents" (Howard, 1981; Bourett & Howard, 1994, 1996; Grove & Bracker, 1970; Bracker *et al.*, 1996). In the hyphae of *M. grisea* and *Fusarium acuminatum*, two classes of Golgi equivalents have been identified on the basis of cisternal diameter: wide and narrow (Howard, 1981; Bourett & Howard, 1994, 1996; Satiat-Jeunemaitre *et al.*, 1996). They appear somewhat pleomorphic in nature, but both types are interpreted as a system of anastomosing tubules or fenestrated sheets, and are often arranged as hollow spheres or elongated cisternal structures that can ensheath a mitochondrion. Typically more than one type of these cisternae can be found within any one hyphal cell. There is also evidence that Golgi equivalents vary between species; in *F. oxysporum* three distinct populations have been identified, whilst in *S. cerevisiae* the cisternae consist of three functionally distinct subcompartments (Mendgen *et al.*, 1995).

In basidiospores of *G. juniper-virginianae* the Golgi equivalents are variously shaped segments of inflated cisternae and were reported to be similar to those found previously within hyphae (Mims *et al.*, 1988). Similar structures are present in the nondifferentiated germlings of *Uromyces* (Hoch & Staples, 1983) where the cisternae are also distributed throughout the germ tube, and are most abundant in the apical

15–20 μm of the germ tube. In the ungerminated conidia of *B. graminis* f.sp. *hordei*, Golgi equivalents appear as a circular arrangement of vesicles in cross section that were sometimes associated with ER (Roberts *et al.*, 1996).

1.4.5 Spitzenkörper and apical vesicle cluster

Growing hyphae of the higher fungi (Ascomycota, Basidiomycota and Deuteromycota) characteristically possess an apical apparatus known as the Spitzenkörper (Markham, 1995; Gow, 1995). The dynamic behaviour of the Spitzenkörper is intimately associated with the precise growth pattern of the hyphal apex (Bartnicki-Garcia *et al.*, 1995; López-Franco & Bracker, 1996). The Spitzenkörper is not an organelle because it is not bounded by a membrane. Rather it is a multicomponent organelle complex predominated by secretory vesicles that comprise what is commonly described as an "apical vesicle cluster" (AVC) (Grove & Bracker, 1970; López-Franco & Bracker, 1996). Several other components can be associated with the Spitzenkörper and these include a vesicle cloud, a differentiated core region, ribosomes, actin microfilaments and microtubules. The pattern formed by these components varies between genera and nine distinct Spitzenkörper patterns have been defined (López-Franco & Bracker, 1996).

When imaged by computer-enhanced, phase-contrast microscopy, the Spitzenkörper of *M. grisea* hyphae has a phase dark vesicle cluster with an eccentric light core orientated towards the apical pole (López-Franco & Bracker, 1996). In conidia of *M. grisea*, vesicles (ca. 80 nm) are distributed within the cytoplasm near to the region at which the new germ tube is emerging (Bourett *et al.*, 1993). An AVC of cytoplasmic vesicles has been reported to be asymmetrically localised near the substratum in the tips of growing germ tubes. This is different from the location of the Spitzenkörper of vegetative hyphae, which is more centrally located in the growing tip (Bourett & Howard, 1990; Fischer-Parton *et al.*, 2000). The dynamic behaviour of the germ tube AVC has not been studied in relation to its role in the germ tube growth pattern.

1.4.6 Other cellular components commonly observed in fungal spores

1.4.6.1 Multivesicular bodies

Multivesicular bodies (MVB) appear as a membrane-bound sac of vesicles and are often located just below the AVC. The role and precise nature of this cytoplasmic inclusion remains elusive. It has been proposed that the vesicles are chitosomes because the shell around the chitosome does not contain phospholipid (Grove, 1978; Bartnicki-Garcia *et al.*, 1979). Multivesicular bodies have been reported to contain acid phosphatases, and to fuse with larger vacuoles and so it has been proposed that they are part of the lysosomal system (Hoch & Staples, 1983). It has been suggested that they could be intimately involved with the endocytic compartments and perhaps serve in membrane receptor sorting (Ashford, 1998), (see Section 1.5). MVB are often observed within ungerminated spores (e.g. Van Dyke & Mims, 1991; Roberts *et al.*, 1996) and have been observed in the appressoria of *M. grisea* (Bourett & Howard, 1990). However, in conidia of *Botrytis cinerea*, MVBs were only present within germinating conidia and germ tubes but never in dormant conidia (Gull & Trinci, 1971).

1.4.6.2 Woronin bodies

Woronin bodies are only observed in filamentous fungi, and are characteristic of the Ascomycota and Deuteromycota (Markham, 1995). They appear in electron micrographs as an electron-dense proteinaceous lattice surrounded by a membrane. Commonly located near the septum, they are sometimes observed to block the septal pore; an observation that has led to the proposal that the function of Woronin bodies is to plug septal pores, and thus maintain spatial organization within the mycelium (Markham, 1995). Woronin bodies have been observed within spores, for example spores of *Alternaria cassiae* have been reported as having numerous Woronin bodies present near the septum, which sometimes appear to plug the septal pore (Mims *et al.*, 1997). Interestingly, Woronin bodies have been reported to bud from MVBs in a number of fungi (Roberts *et al.*, 1996). In *M. grisea* Woronin bodies have been identified near the septum in germinated conidia (Bourett *et al.*, 1993).

1.4.6.3 Storage compounds in fungal cells.

As discussed in Section 1.3.3.5, fungal spores mobilize lipids, carbohydrates and proteins during germination. Glycoproteins have been demonstrated to be present within the spore cytoplasm of a number of fungal species, and they appear in electron micrographs as electron-transparent "white spots" within the spore cytoplasm (Roberts *et al.*, 1996).

The lipid content of most spores is significantly higher than that of mycelia, ranging from 5–17% of their dry weight, although it could be as high as 35% in some species of rusts (Weete, 1981). Triacylglycerols are neutral and virtually insoluble in water. They coalesce in the cytoplasm, forming lipid droplets that have been observed within the cytoplasm of spores and in a number of species, including *M. grisea*, commonly appearing in the form of numerous droplets often distributed throughout the cell cytoplasm (Mims *et al.*, 1988; Money & Howard, 1996; Read & Beckett, 1996; Schadeck *et al.*, 1998; Ho *et al.*, 1999; Riggs & Mims, 2000). However, lipid can also be localised within the spore, as in *Botrytis cinerea,* in which they are situated around the periphery of the cell (see Buckley *et al.*, 1966), and sometimes, as in *Halosphaeria appendiculata* and the zoospores of *Rhyzophydium* lipid forms a central complex (Barr & Hadland-Hartmann, 1978; Hyde *et al.*, 1997). Microbodies and mitochondria are sometimes observed to be associated with lipid within the spore cytoplasm (Barr & Hadland-Hartmann, 1978; Mims *et al.*, 1988; Mims & Snetselaar, 1991). In some spores, however, lipid bodies have not been observed (e.g. *B. graminis* f.sp. *hordei*; Roberts *et al.*, 1996).

Once germination has commenced lipid bodies commonly dramatically reduce in density, or even disappear completely (Daly *et al.*, 1967; Delvecchio *et al.*, 1969; Shadeck *et al.*, 1998). However, as in nondifferentiated germlings of *Uromyces*, lipid bodies are present throughout the germ tube, but are more concentrated at some distance behind the growing tip, where they probably coalesce to form larger bodies (Hoch & Staples, 1983).

Glycogen has been reported to occupy a large proportion of spore volume, (e.g. it was estimated to comprise one half of the volume of *Erisyphe cichoracearum* conidia; McKeen *et al.*, 1967). At the ultrastructural level glycogen appears in the form of rosette-like structures or electron dense deposits within the cytoplasm and sometimes within vacuoles (e.g. Mims *et al.*, 1995; Read & Beckett, 1996). In *M. grisea*, glycogen has been reported to be bound by Concanavalin A within conidia; however the extent and distribution of this binding was not reported (Bourett *et al.*, 1993). Extensive carbohydrate reserves are formed within the cytoplasm of maturing basidiospores and ascospores (Sundberg, 1978; Mims *et al.*, 1995; Read & Beckett, 1996; Ho *et al., al.*, 1999). In several members of the Erisyphales *(E. pisi, E. cichoracearum,* and *E. graminis*), deposits interpreted as glycogen are typically localised in the centre of the conidium (McKeen *et al.*, 1967; Martin & Gay, 1983; Roberts *et al.*, 1996). There is also evidence that glycogen is present within the cytoplasm of the germ tubes of *Uromyces*, in which it was most abundant at some distance behind the growing tip in the same region as lipid droplets (Hoch & Staples, 1983).

1.5 THE PROCESS OF ENDOCYTOSIS

Cells must control the uptake of molecules from the external environment, and this is one of the principal roles of the plasma membrane (Evans & Graham, 1989). A major route by which macromolecules enter animal cells is via the endocytic pathway. Endocytosis is the process by which molecules outside the cell are internalized within endocytic vesicles which typically form from coated pits, which invaginate from the plasma membrane. There are two different types of endocytosis, distinguished on the basis of how the endocytosed molecule enters the vesicle: (1) *receptor-mediated endocytosis* in which the molecule is bound by specific or nonspecific receptors within the pit, and (2) *fluid-phase endocytosis* in which the molecule is passively internalized by the cell as part of the fluid trapped within the lumen of the vesicle (Ashford,1998).

The endocytic pathway in animals has been the subject of much research and is well understood in general terms and it appears that plant cells also possess a similar pathway (Watts & Marsh, 1992; Gruenberg & Maxfield, 1995; Hawes *et al.*, 1995; Mellman, 1996; Ashford, 1998; Blatt *et al.*, 1999). In animal cells, after the endocytic vesicle is released from the plasma membrane into the cytoplasm, it enters the lytic pathway. This is a complex system of functionally interrelated membranous compartments, ultimately terminating in the lysosome, which contains a wide range of hydrolytic enzymes. This pathway also interacts at different stages with the protein synthesis/secretory pathway, via the Golgi complex in particular (Evans & Graham, 1989; Ashford, 1998). There is uncertainty as to how material is transferred between the different compartments within this endosomal-lysosomal network, and to what extent these compartments are physically related (Watts & Marsh, 1992; Gruenberg & Maxfield, 1995; Mellman, 1996; Ashford, 1998). However, vesicles are believed to play a central role in this process and for so the entire pathway has been referred to as the "vesicle trafficking pathway" (Blatt *et al.*, 1999).

1.5.1 Endocytosis in filamentous fungi

On the basis of structural and biochemical analysis it now seems likely that fungal cells possess an analogous pathway to the lytic pathway of animal cells, in which the vacuolar network functions in a similar manner to the endosomal-lysosomal network. However, it has yet to be established whether endocytosis is a component of this pathway (Ashford, 1998). There is accumulating evidence for the existence of endocytosis within filamentous fungi (Hoffman & Mendgen, 1998; Ashford, 1998; Fischer-Parton, *et al.*, 2000; Read & Hickey, 2000; Wedlich-Sölder *et al.*, 2000).

Various methods have been utilized to investigate whether endocytosis occurs in fungal cells. In animal and plant cells clathrin-coated pits and vesicles play a major role in endocytosis (Coleman *et al.*, 1988; Hawes *et al.*, 1995; Mellman, 1996). Coated vesicles have been identified in fungi (Howard, 1981; Caesar-Ton That *et al.*, 1987; Bourett & Howard, 1991). One class of coated vesicles are the filasomes, which are microvesicles that are surrounded by an actin network (Howard, 1981). Filasomes are commonly located in the subapical region of the hyphae in association

with the plasma membrane and have been proposed as a candidate for endocytic vesicles (Ashford, 1998; Fischer-Parton *et al.*, 2000).

Endocytic vesicles may be labelled either by (1) labelling the vesicle lumen using a fluid-phase endocytic marker or (2) labelling the vesicle membrane with molecules that bind the membrane but are unable to cross it. These approaches enable components of the endocytic pathway to be identified by TEM or confocal microscopy and have been employed most successfully in animal cells (Ashford, 1998). Cole *et al.* (1997) were unable to demonstrate that endocytosis occurs within the hyphae of *Pisolithus tinctorius*, using a number of fluid-phase endocytic markers. In spite of this, the evidence that endocytosis occurs within filamentous fungi is increasing. The membrane dye FM4-64 has been used as an endocytic marker in animal systems (Betz *et al.*, 1996) and has been demonstrated to be internalized by hyphae in a range of filamentous fungi (Fischer-Parton *et al.*, 2000; Read & Hickey, 2000; Wedlich-Sölder *et al.*, 2000). Internalization of FM4-64 has been demonstrated to be an energy-dependant process in budding yeast and in some fungal cells and this finding is also consistent with endocytic uptake of this dye (Vida & Emr, 1995; Hoffman & Medgen, 1998; Wedlich-Sölder *et al.*, 2000). Fungal hyphae internalize FM4-64 rapidly and the distribution and timing of staining supports the hypothesis that the dye was internalized by endocytosis (Fischer-Parton *et al.*, 2000; Read & Hickey, 2000). Furthermore, the same distribution and timing of FM4-64 staining was observed in both yeast cells and the protoplasts of sporidia of *Ustilago maydis* (Vida & Emr, 1995; Wedlich-Sölder *et al.*, 2000).

Whilst there is evidence that the germ tubes of *Uromyces fabae*, *M. grisea*, *P. graminis* and *U. maydis* internalize the membrane label FM4-64 (Hoffman & Mendgen, 1998, Fischer-Parton *et al.*, 2000; Wedlich-Sölder *et al.*, 2000), the fungal spore itself has not yet been studied.

1.5.2 Possible roles of endocytosis in fungal cells

The accumulating evidence that endocytosis occurs within fungal hyphae has led to a proposed hypothetical model of the vesicle trafficking network in fungi (Fig. 1.3)

(Fischer-Parton *et al.*, 2000, Read & Hickey, 2000). The possible functions of endocytosis in fungal hyphae have also been reviewed (Ashford, 1998; Fischer-Parton *et al.*, 2000; Read & Hickey, 2000) and will be considered here.

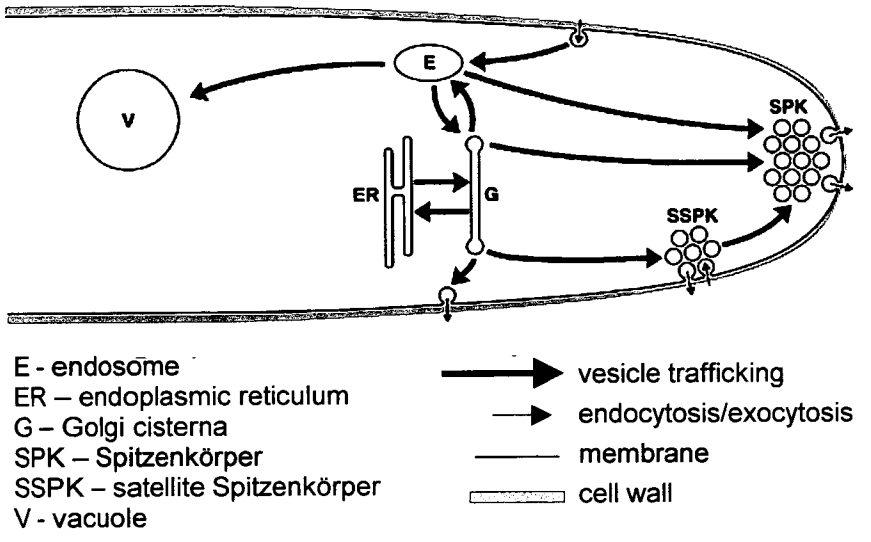

Figure 1.3: A hypothetical model of the organization of the vesicle trafficking network in a growing hypha based on the pattern of FM4-64 staining (reproduced from Fischer-Parton *et al.*, 2000).

1.5.2.1 Removal of excess plasma membrane

It has been estimated that in *N. crassa* at least 38,000 vesicles fuse with the hyphal tip per minute (Collinge & Trinci, 1974; Wessels, 1986). New membrane is added to the plasma membrane when secretory vesicles fuse with it and calculations for both fungal hyphae and pollen tubes suggest that there is an excess of new membrane delivered to the plasma membrane, relative to the amount of cell wall components required to maintain tip extension (Picton & Steer, 1983; Fischer-Parton *et al.*, 2000). Endocytosis is thought to be the best candidate for a membrane retrieval mechanism in both plants and fungi (Steer, 1988; Fischer-Parton *et al.*, 2000, Read & Hickey, 2000). In both *U. fabae* and *N. crassa*, initial internalization of the membrane label FM4-64 was observed to take place behind (ca. 5–15 μm) the hyphal tip (Hoffman & Mendgen, 1998; Fischer-Parton *et al.*, 2000). In fungal hyphae this region has been found to contain a high density of filasomes (Roberson, 1992) and in pollen tubes a high density of clathrin-coated pits and vesicles (Derksen *et al.*, 1995). Furthermore, the fungal vacuolar system has been proposed as the fungal equivalent to the

endosomal-lysosomal network of animal cells, and it is most active in the subapical region of the hyphae (Ashford, 1998). It has been suggested that membranous aggregates (termed plasmalemmasomes or lomasomes) found to be associated with the plasma membrane in chemically fixed fungal hyphae imaged by TEM might have been caused by the breakdown of an endocytic membrane retrieval system during the early stages of hyphal death (Read & Hickey, 2000). These results suggest that in both plant and fungal tip growing cells, a region of increased endocytic activity exists behind the growing tip, a finding that would be consistent with the recycling of excess plasma membrane by endocytosis.

It has also been proposed that recycled membrane might be delivered to the vacuolar system (Read & Hickey, 2000), and contributes to the large, primarily spherical vacuoles present within mature hyphal regions (Cole *et al.*, 1998; Hyde & Ashford, 1997).

1.5.2.2 Recycling of membrane protein and lipid

In order that the hyphal tip is equipped with the necessary proteins for growth (e.g. receptors, ion channels, enzymes), these proteins must be either synthesized *de novo* or recycled from older regions of the hyphal plasma membrane. Biosynthesis is a biochemically expensive process and so recycling proteins would seem to make energetic sense. Animal cells are known to recycle proteins, and even to store receptors within the lysosomal system prior to relocating them to the plasma membrane (e.g. Evans & Graham, 1989; Hein *et al.*, 1994; Mukherjee *et al.*, 1999). Although there is no direct evidence of membrane protein recycling within filamentous fungi, in budding yeast two of the three plasma membrane chitin synthetases are recycled via endocytosis (Chuang & Schekman, 1996; Ziman *et al.*, 1996, 1998; Holthius *et al.*, 1998).

The phospholipid composition of a membrane alters its physical characteristics (Ellar, 1978). For example, there is evidence that as the percentage of phosphatidyl choline in a membrane increases there is a related increase in membrane fluidity, and that changes in the concentration of this phospholipid in the plasma membrane could

be important in the control of mycelial morphology, and in particular in hyphal branching (Ellar, 1978; Bainbridge *et al.*, 1979; Markham *et al.*, 1993). Endocytosis is known to be responsible for lipid sorting in animal cells and might provide a mechanism by which membrane phospholipids can be removed, and so play a role in controlling the plasma membrane phospholipid composition and thus hyphal morphogenesis (Mukherjee *et al.*, 1999).

1.5.2.3 Transport of membrane proteins and lipids to the vacuole for degradation

The lipid and protein components of membranes are constantly degraded and synthesized (Evans & Graham, 1989). The half-life of cellular proteins and amino acids varies greatly, and can be very short (e.g. arginine ~2 min in the cytosol). Furthermore, oxidative damage to proteins occurs over time, and errors made during translation can result in the synthesis of defective proteins (Stryer, 1988). The fungal vacuole is considered to be the lytic compartment of the fungal cell (see section 1.4.3) and endocytosis might serve to transport proteins and lipids destined for degradation to the vacuole (Ashford, 1998). This is supported by findings that spherical vacuoles are ultimately stained by the membrane label FM4-64 in fungal hyphae and yeasts (Vida & Emr, 1995; Fischer-Parton *et al.*, 2000; Wedlich-Sölder *et al.*, 2000)

1.5.2.4 Uptake of molecules in fluid-phase endocytic vesicles

The uptake of molecules in the fluid-phase of endocytic vesicles is a non-specific process; the only limitations are that the molecule is able to pass through the cell wall to the plasma membrane and is small enough to be encompassed within an endocytic vesicle. Thus, factors such as size, charge and glycosylation are important (Gooday, 1995). It has been suggested that some nutrients are internalized by fluid-phase endocytosis in budding yeast (Dulic *et al.*, 1991). To date the only evidence that fluid-phase endocytosis occurs in filamentous fungi is reported for protoplasts of *U. maydis* sporidia which internalized Lucifer Yellow within the vacuolar system (Steinberg *et al.*, 1998). In hyphae of *P. tinctorius* no evidence of internalization of a number of fluid-phase markers was found (Cole *et al.*, 1997).

1.5.2.5 Uptake of signalling molecules involving receptor-mediated internalization of ligands

There is no evidence that filamentous fungi internalize specific molecules by receptor-mediated endocytosis. However, there is considerable evidence that yeast cells internalize molecules by endocytosis; the sex pheromone α-factor is internalized by yeast in a manner characteristic of endocytosis; furthermore, it was found that yeast mutants selected for their inability to accumulate the fluid-phase endocytic marker Lucifer Yellow, also did not accumulate the sex pheromone α-factor (Rieder *et al.*, 1996; Ashford, 1998). Filamentous fungi also produce pheromones and there are a number of examples in which they exhibit positive chemotropism towards pheromones (Bölker & Kahmann, 1993). Another possible role of receptor-mediated endocytosis is in the uptake of host signalling molecules by germlings and hyphae in host-pathogen interactions (Mendgen *et al.*, 1995; Read & Hickey, 2000).

1.6 INTRODUCTION TO THE RESEARCH DESCRIBEDIN THIS THESIS

Very little is known about the cell biology of spore germination in fungal plant pathogens. Most research on *M. grisea* has focused on the process of appressorium differentiation and the subsequent stages in the infection cycle. One of the main aims of this study was to characterize germination at the light microscope level and to investigate the role and relative importance of each conidial cell for successful conidial germination. This was partly achieved by developing a method in which individual conidial cells could be selectively killed by laser ablation, a technique that has not been previously used in fungal cells.

Most of the published information relating to organelle organization within fungal spores has been obtained from TEM studies and therefore not in live cells. Consequently, very little is known about organelle organization within live spores, and even less about organelle dynamics during germination. Another main aim of this study was therefore to characterize organellar organization and dynamics in live and potentially pathogenic conidia throughout germination. The analysis used confocal microscopy and vital fluorescent stains. To obtain biologically meaningful

results, the *in vitro* system used for confocal microscopy was optimised so that it mimicked the situation *in vivo* on the rice leaf as closely as possible.

Although there is growing evidence that fungal hyphae undergo endocytosis, fungal spores had not been previously investigated. *Magnaporthe grisea* presents an interesting system for such a study since the spores are able to germinate in pure dH_2O and there is no evidence that external host signals are required for either germination, or germ tube growth. The final main aim of this study was to analyse and characterize endocytosis within living conidia during germination. To facilitate this, a quantitative method was devised which enabled comparisons to be made of the rate of uptake of endocytic markers into conidia. The first evidence that spores of filamentous fungi undergo endocytosis is presented and in addition the first direct evidence that a filamentous fungus undergoes fluid-phase endocytosis was also obtained.

2. MATERIALS AND METHODS

2.1 PLANT AND FUNGAL GROWTH AND FUNGAL STORAGE

2.1.1 Fungal media

Oatmeal agar was made by heating 50 g of oat flakes (Scott's Porage Oats, A & R Scott, Cupar, Fife, Scotland) or oatmeal (Scottish Oatmeal, Hamlyns of Scotland, Grampian Oat Products, Banff, Scotland) in 400 ml of dH_2O in an oven at 70 °C for 1 h. The resultant broth was strained and the liquid was retained and made up to 1 litre with dH_2O. After adding 15 g of agar (Oxoid No. 3, Unipath Ltd., Basingstoke, Hampshire, UK) this was then autoclaved for 15 min at 121 °C. Plates were poured and then stored at 4 °C.

2.1.2 Fungal growth on agar

Magnaporthe grisea, strain 0-42 (supplied by Dr. Barbara Valent, DuPont Co., Wilmington, Del., USA) was inoculated onto oatmeal agar plates and grown at 24 °C under continuous light (fluorescent lamps; 45 $\mu mol.photon.m^{-2}.s^{-1}$).

2.1.3 Plant growth

Two varieties of rice were grown (M-210, California Co-operative Rice Research Foundation Inc., and Sasawishi, AgrEvo UK Ltd., Chesterford Park, Saffron Walden, Essex). Rice plants were planted in loam covered in Vermiculite and grown in a glasshouse (day and night temperatures of 25–30 °C and 20–25 °C respectively, and a relative humidity of 50–60%,) with additional overhead fluorescent lighting until reaching the second leaf stage.

Plants were moved to growth rooms during experiments in which they were inoculated with the fungus. Plants are routinely grown in the dark for the 24 h following inoculation at AgrEvo UK Ltd because this has been found to improve infection by the fungus (*pers. comm.*, C. Rutherford). Thus, immediately after inoculation the plants were placed in the dark for one day at 30 °C and thereafter

under a 16 h daylight cycle, with a maximum day temperature of 30 °C and a minimum night temperature of 22 °C. A high relative humidity (90–100%) was maintained throughout plant growth.

2.1.4 Producing fungal stock

Subculturing of *M. grisea* has been reported to have adverse effects on colony appearance, fertility and pathogenicity (Valent & Chumley, 1991). For this reason, enough fungal stock was produced at the start of the project for all subsequent experimental work.

Rice plants were inoculated with conidial suspension (see Sections 2.2, 2.3). Plants were grown as described in Section 2.1.3. After 5 days, lesions had formed on the rice leaves. Pieces of infected leaf tissue (2 mm^2) were sectioned by cutting parallel to the central leaf vein. Leaf sections adjacent to the edge of the lesion were surface sterilised by submergence in 2–3% w/v sodium hypochlorite dissolved in 10 % v/v aqueous Tween 20 (polyoxyethylenesorbitan monolaurate) for 10 min. Tweezers were used to agitate the sections and so prevent a protective air-leaf interface from forming. The leaf sections were then thoroughly washed in sterile dH_2O and each was then placed on either an oatmeal agar plate or on an autoclaved damp filter paper, which was placed on top of an oatmeal agar plate (Whatman No. 1, Whatman Int., Maidstone, UK). Petri dishes were left open for 30 min to allow the plate surface to dry and then closed. Cultures were grown under the conditions described in Section 2.1.2, until the mycelium had covered the plate. Filter paper samples were removed from the agar, left to dry for a further few days and then frozen in sealed Petri dishes (-20 °C). Agar-only samples were left until the agar had dried-out before freezing in the same way. Fragments of these samples were used as fungal inoculum stock.

2.1.5 Techniques to reduce or eliminate contamination

Bacterial contamination of fungal cultures was an intermittent problem, and was confirmed by staining with the membrane dye FM4-64 (method described in Sections 2.7–2.8). Antibiotics were not used because it was considered that they might also

influence spore growth and germination, thereby introducing an unknown variable into subsequent experiments. Two sources of contamination were isolated:

(1) Some of the fungal stock was contaminated by bacteria from the rice leaf. The technique employed to sterilise rice leaves was not consistently effective. These plates could be recovered by centrifuging (2,000 rpm for 2 min) spores scraped from the filter paper inoculum in 15 ml sterile dH_20 and discarding the supernatant. The spores were resuspended in sterile dH_20 and ca. 200 µl of this spore suspension was used to inoculate the oatmeal agar plate. Petri dishes were left open for 30 min to allow the plate surface to dry and then grown as described in 2.1.2.

(2) During the third year of the project all sources of porridge oats tested were found to be contaminated by a thermophilic member of the *Bacillus* genus. This was confirmed by Gram staining the oat extract liquid after autoclaving (as described in Heritage & Evans, 1996). Following this discovery, oats were sterilised before use by tyndallising the oat extract prior to the addition of agar. This was performed by either steaming (for 1 h) or autoclaving (as described in Section 2.1.1) the oat-extract liquid three times. The liquid was incubated at 30 °C for 24 h between each treatment.

2.2 METHOD OF HARVESTING SPORES

Conidia were harvested on either a small or large scale, depending on the amount of inoculum required. Spores were harvested on a small-scale from localised regions of the mycelium. This allowed young conidia to be selected for experimentation. Several methods were employed and they are listed below.

- *Eppendorf harvesting*: ca. 1 cm^2 of mycelium was scraped from the edge of a fungal culture with a sterile scalpel and added to 0.5 ml of sterile dH_20 in an Eppendorf tube. After brief agitation with a pipette tip, the liquid was used to inoculate the cover slip (CS). The average time of inoculation was 1 min post hydration. This method was used in experiments that required a number of replicates.

- *Float harvesting*: ca. 5 mm^2 of mycelium was scraped from the edge of a fungal culture and floated on a 50–100 µl droplet (on a CS) of sterile dH_20, or dye solution, depending on the experiment. After 1 min the piece of culture was removed. Inoculation time was the same as hydration time. This method was used for individual samples, and for harvesting spores in the presence of dye.

- *Dry harvesting*: a damp filter paper was placed in the Petri dish lid for 1 h preceding harvesting in order to increase humidity and the occurrence of STM. A glass CS was placed on the fungal colony, removed after 3 sec or longer and 50 µl of dH_2O was added to the CS. The inoculum was defined as the area immersed by H_2O.

Spores were harvested on a large scale using the entire culture by the two methods listed below.

- *Scrape harvesting*: an entire culture was harvested and conidia were suspended in a liquid suspension (ca. 2.5×10^5 conidia.ml^{-1}) as described by Jelitto *et al.* (1994). This method was used for population counts of percentage germination and differentiation. Average time of inoculation was 12 min post hydration.

- *Flood harvesting*: the fungal culture was flooded with 10 ml sterile dH_20 and gently rubbed with a glass rod. The resultant spore suspension was transferred by sterile pipette to a 15 or 30 ml polystyrene centrifuge tube, and the culture was rinsed with a further 10 ml of dH_20 that was then also transferred to the tube. The average time of inoculation was ca. 3 min and the technique was used where inoculation by spraying was performed (see Section 2.3). For smaller volumes of inoculum at a higher conidial density, the conidial suspension was centrifuged (2000 rpm for 2 min), and the spores were re-suspended in dH_2O to the required spore concentration. This technique was used in the *in vivo* pathogenicity test (Section 2.12.3).

2.3 METHODS FOR INOCULATING LEAVES AND ARTIFICIAL SUBSTRATA WITH CONIDIA

For most experiments performed *in vitro*, 50 or 100 µl droplets of conidial suspension were delivered by a Gilson pipette onto the substratum, or spores were inoculated by float harvesting (Section 2.2). Rice leaves (and detergent washed CS controls) were either inoculated with droplets of 10–30 µl delivered by a Gilson pipette, or sprayed with a Cub SLG gravity-feed HVLP (High Volume Low Pressure) gun (Bink Sames Corporation, USA).

2.4 CHEMICALS

Unless otherwise stated, chemicals were purchased either from Sigma Chemical Company (Sigma-Aldrich Company Ltd, Poole, Dorset, UK), or Aldrich Chemical Company (Gillingham, Dorset, UK). Dyes were either purchased from Molecular Probes, (Molecular Probes Inc., Eugene, Oregon, USA.) or Sigma Chemical Company.

2.5 IN VITRO SYSTEM

2.5.1 Incubation chambers

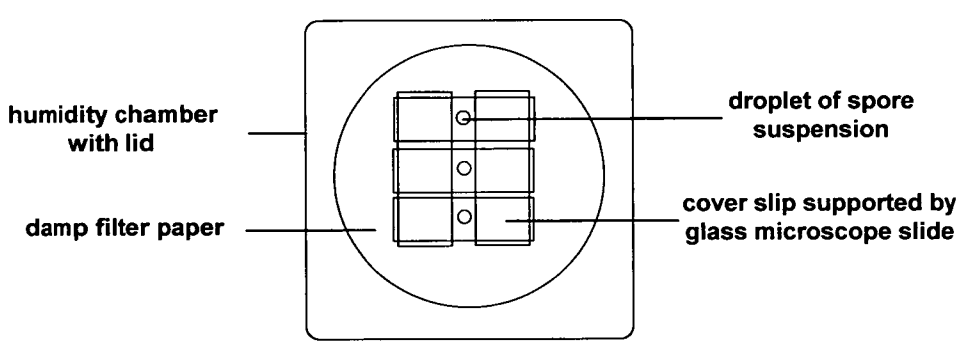

Figure 2.1: Conidia were inoculated onto glass cover slips that were supported by two glass microscope slides within a humidity chamber. The chamber had damp filter paper in the base, and was covered with a plastic lid. The same system was used for *in vivo* experiments, in which each glass cover slip was replaced by a rice leaf attached to a glass slide (Section 2.12).

Conidia were inoculated onto 22 x 64 mm glass CS (No. 1½ Chance Propper, Warley, UK) supported by slides placed on damp filter paper (Whatman No. 1) within plastic humidity chambers. Chambers were incubated in the dark (wrapped in black photographic bags) at 24 °C (Fig. 2.1).

2.5.2 Artificial substrata

Cover slip glass (no. 1½: Chance Propper, Warley, UK) and a thin Teflon™ film (polytetrafluoroethylene; as described by Hamer *et al.*, 1988; kindly provided by DuPont Co., Wilmington, Del., USA), were assessed as artificial substrata on which to germinate *M. grisea* conidia. The Teflon™ film was autoclaved prior to use. Cover slips (CS) were either untreated or cleaned by a variety of methods described below.

- *Untreated*: CS were used directly as supplied by the manufacturers.

- *Detergent-washed* (detCS): CS were separated and held in place by holders within a 3 litre plastic container into which tap water was fed by a mixer pipe at a high pressure. Hot (ca. 50 °C) tap water was used to wash the CS in 0.5 ml of Fairy Liquid detergent (Proctor & Gamble, Newcastle upon Tyne, UK), followed by continuous rinsing for at least 60 min in cold tap water. Finally the CS, were washed with 10 litres of sterile dH_2O.

- *Acid/Alkali-washed*: CS were left overnight in either 2M NaOH or chromium trioxide (5 g $NaCr_2$ dissolved in 100 ml of concentrated H_2SO_4, which produces an acidic solution of CrO_3) and then rinsed thoroughly in double distilled H_2O.

- *Heat-treated*: CS were wrapped in aluminium foil and heated in a muffle oven for 4–5 h at 400 °C.

- *Silanised*: CS were immersed in 5% Decon 90 (Decon Laboratories Ltd, E. Sussex, UK) overnight, thoroughly rinsed with sterile dH_2O, heat-treated (as above), immersed in Sigmacote (stock code SL2) for 10 min, immersed and agitated in absolute ethanol for 10 min, rinsed thoroughly in at least 10 litres of

sterile double-distilled H_2O, and stored in a pressurised desiccator for 1–2 days (re-pressurised once a day) before use.

2.5.3 *In vitro* system and microscopy

To examine fungal inocula on artificial substrata or on the leaf surface by light microscopy, samples were covered with a humidity chamber. For all live cell analysis there was no CS on top of the inoculum. The room temperature was set to 24 ± 1 °C, and the light on the microscope was set to a low intensity and turned on only when necessary. All experiments were performed in low-level light conditions.

2.6 LIGHT AND FLUORESCENCE MICROSCOPY

Objective	Type	DIC/phase	Numerical aperture	Manufacturer /microscope
x40 dry	Plan Apo	-	0.95	Nikon
x40 oil	"	Ph4 DM	1.0	"
x60 oil	"	"	1.4	"
x100 oil	"	"	1.4	"
x40 oil	"	DIC	1.0	Polyvar
x100 oil	"	DIC	1.32	"
x5	Plan-NEOFLUAR	Ph 2	0.15	Zeiss
x10	"	"	0.3	"
x20	"	"	0.5	"
x40	"	"	0.75	"
x40	water immersion	Ph 3/DIC	0.8	"
x63	(dipping)	Ph 3/DIC	0.9	"

Table 2.1: Microscope objectives used in this study. Microscope specifications are given in the text. Bright field, phase (ph) and differential interference contrast (DIC) optics were used.

Conventional light microscopy was performed using the following microscopes.

- Nikon Diaphot TMD inverted microscope.
- Zeiss Axiophot photomicroscope (Zeiss, Western Germany), with a Nikon 35 mm Camera or a CCD video camera (JVC model KY-F55B), which was used

to collect digital images with the KS300 software package (Imaging Associates, Zeiss).

- Zeiss Axioskop2 upright microscope with an Axiocam digital camera. Images were collected in Axiovision version 2.0.5.3 (Carl Zeiss Vision). This system was used with x40 and x63 water immersion objectives (Table 2.1) to analyse germination by differential interference contrast microscopy.

The objective lenses used on each system are shown in Table 2.1. High numerical aperture objectives were used for confocal microscopy and germ tube measurements in order to optimise the axial resolution and to reduce spherical aberration. Macro images were collected on a Zeiss Stereo-Zoom Stemi SV100 binocular microscope with an Olympus 35mm camera.

2.7 FLUORESCENT DYES

2.7.1 Preparation and storage

Details of fluorescent dyes used for confocal microscopy analysis, along with their loading parameters, are shown in Table 2.2 and Figure 2.2.

2.7.2 Dye loading

Unless otherwise specified, dyes were either added to the inoculum at a specific time after hydration, or in the case of float harvesting, the spores were inoculated in the presence of the dye. Times were recorded as min post hydration (this is the total time after which the spores were harvested), and min post dye (this is the total time of incubation in the dye). Note that the number of min post hydration and post dye were the same when spores were inoculated in the presence of the dye. Some dyes were left in solution throughout the experiment and others were washed out of the solution either by:

- completely immersing the CS in water,

- bleeding 5–7 ml of sterile dH_2O through the inoculum by capillary action using strips of tissue (especially useful when the sample must remain on the microscope stage, e.g. specific spores being studied).

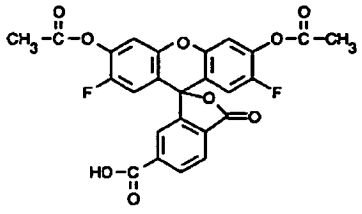

cDFFDA

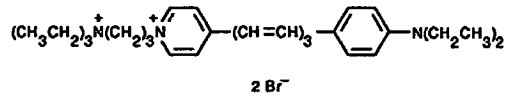

FM4-64

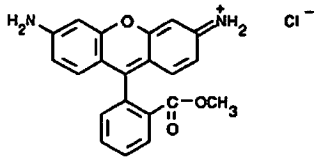

Rhodamine 123

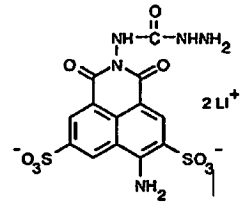

Lucifer Yellow CH

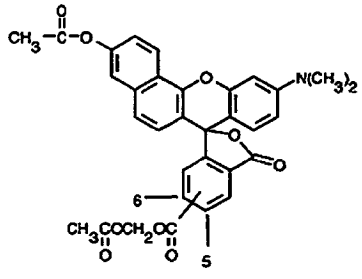

carboxy SNARF-1

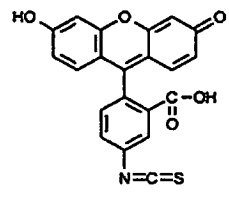

FITC

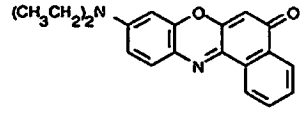

Nile Red

Figure 2.2: Structures of some of the dyes used in this study. Note that FITC was used conjugated to a 10 kDa dextran.

Dye selectivity	Dye	Cat. no.①	Molecular weight	Ex (nm)	Em (nm)λ	Excitation filter②	Stock conc. (mM)③	Stock solvent	Storage (°C)	Working conc. (μM)④,⑤
Vacuolar system	carboxy DFFDA	O-6151	496.38	492	517	BHS	10	DMSO	-70	7.5
	carboxy DCFDA	C-369/C-368	529.29	495	529	BHS	100	DMSO	"	5
	carboxy FDA	C-195	460.4	494	518	BHS	10	DMSO	"	3–10
	MDY-64⑥	Y-7536	384.48	456	505	BHS	10	DMSO	"	10–20
	FUN-1	F7030	528.84	508	550/600⑦	GHS	10	DMSO	"	5–10
	BCECF-AM ester	B-1150	~615	482	520	BHS	10	DMSO	- 20	10⑧
	Oregon Green AM ester	O-6807	1258	494	523	BHS	10	DMSO	-20	8–10⑧
	carboxy SNARF-1 AM	C-1272	567.55	488–530	580/640	GHS	0.2	DMSO	-20	2–5⑧
mitochondria	Rhodamine 123	R-302	380.83	507	529	GHS	10	Methanol	-70	7.5
	Rhodamine B, hexyl ester	R-648	627.18	556	578	GHS	1	DMSO	-70	0.1
	$DIOC_6$	D-3652*	572.53	484	501	BHS	10	Ethanol	-20	5
	DASPMI	D-288	366.24	475	605	BHS	10	DMF	-20	15–25
	Mitotracker™ Green FM	M-7514	671.88	490	516	BHS	1	DMSO	-70	0.1
nuclei	SYTO 11	S-7573	~ 400	508	527	GHS	5	DMSO	-20	1–10
	SYTO 12	S-7574	~ 300	499	522	BHS/GHS	5	DMSO	"	
	SYTO 13	S-7575	~ 400	488	509	BHS	5	DMSO	"	"
	SYTO 14	S-7576	~ 500	517	549	GHS	5	DMSO	"	"
	SYTO 16	S-7578	~450	488	518	BHS	1	DMSO	"	"
	Acridine Orange (base)	A-1301	301.82	500	526	BHS	10	H_2O	"	5–10
endocytic markers	FM4-64	T-3166	607.51	515	640	GHS	16.5	DMSO	-20	7.5
	Lucifer Yellow CH	L-453*	457.24	428	536	BHS	20 $mg.ml^{-1}$	H_2O	"	0.2 $mg.ml^{-1}$
	FITC-dextran	FD-10S*	10,000	494	519	BHS	20 $mg.ml^{-1}$	H_2O	"	4$mg.ml^{-1}$
lipids	Nile Red	N-1142	318.37	552	636	GHS	1 $mg.ml^{-1}$	DMSO	-20	0.6$\mu g.ml^{-1}$

① All dyes were purchased from Molecular Probes except those asterisked, which were from Sigma; ② BHS/GHS see Table 2.4; ③ all μM unless otherwise stated; ④ all mM unless otherwise stated; ⑤ all stock solutions were initially made into 250 μM aqueous substocks; ⑥ full name is Yeast vacuole membrane marker MDY-64; ⑦ 550nm (cytoplasm), 600 nm (vacuolar inclusions); ⑧ Some esters are relatively insoluble in H_2O and this can be overcome by preparing the working solution in 2% aqueous pleuronic detergent (Molecular Probes).

Table 2.2: Dyes assessed as vital stains for *M. grisea* conidia. Excitation wavelengths are quoted from the manufacturers' product information, but can vary with external conditions, in particular pH. Abbreviations: concentration (conc.); maximum excitation λ (ex); maximum emission λ (em).

2.7.3 Other staining procedures

2.7.3.1 Staining glycogen

The periodic acid-Schiff reaction (Pearse, 1985) was modified to allow samples to be imaged by confocal microscopy (*pers. comm.* C. Jeffree). Conidia were float-harvested in 50 µl of dH_20 on detCS. A range of sodium metaperiodate concentrations (0.1–10%w/v) were assessed over a range of incubation periods (5–60 min) and the best results were obtained when 5 ml of 10 % w/w sodium metaperiodate (10g of crystals heated at 70 °C in 100 ml water until they had completely dissolved) was bled through the inoculum by capillary action (using a piece of tissue) and samples were left for 45 min in the presence of the acid. The acid was then washed out of solution by capillary action using 5 ml of dH_20. The dye Lucifer Yellow CH was added at a concentration of 0.2 $mg.ml^{-1}$ and washed out after 5 min (Table 2.2). A CS was placed over the sample and the spores were imaged by confocal laser scanning microscopy using the "individual image" parameters (Section 2.8, Table 2.3).

Controls were conducted to determine whether (1) oxidation by 10% w/w sodium metaperiodate alone causes conidial cells to fluoresce, and (2) the fluorescence detected originated from Lucifer Yellow CH that was bound within the cells. The techniques used were as follows.

(1) Conidia were treated and imaged as above, but Lucifer Yellow CH was not added to the solution.

(2) Conidia were incubated in Lucifer Yellow CH without being oxidised by sodium metaperiodate. The dye will not enter intact cells and so in order to permeablise the spores (in the absence of the acid) the sample (on a detCS) was irradiated by the Nikon light microscope light (set to maximum) using a x40 Plan apo objective and with the field diaphragm aperture fully open. The dye Lucifer Yellow CH was added at a concentration of 0.2 $mg.ml^{-1}$ and washed out after 5 min. A CS was placed over the sample and the spores were imaged as described above.

2.7.3.2 *Staining lipid*

The lipophilic dyes FM4-64 and MDY-64 were added to conidia that had been desiccated either by the method described in Section 2.7.3.1 or by dry harvesting the conidia in the presence of the dye. The spores were desiccated in order that FM4-64 and MDY-64, which normally stain the plasma membrane (Betz *et al.*, 1996; Haugland, 1999), could directly enter the cytoplasm and stain the internal structures.

2.8 CONFOCAL MICROSCOPY

Conidia were analysed using a confocal laser scanning microscope (CLSM), a technique which offers several advantages over conventional optical microscopy, the most important being that images are free from out-of-focus blur (Sheppard & Shotton, 1997). The CLSM used was a Bio-Rad MRC-600 (described by Read *et al.*, 1992a) attached to a Nikon inverted microscope (Section 2.6) running COMOS, MPL and TCSM software (versions 7.0) supplied by Bio Rad (Hempel Hempstead, UK). Further image analysis was performed with Confocal Assistant (ver. 4.02), OPTIMAS (version 5.2; Optimas Corporation) and Paint Shop Pro (vers. 5.01; Jasc Software, Inc.).

Variable	Live-cell time-courses	Individual images
Laser power	1%	3%
Scan speed	1 sec/frame	3 sec/frame
Low signal enhance	-	ON
Photomultiplier gains	50–70%	50–70%
Black-level setting	10	10
Kalman filter*	1–2	4
Confocal aperture	20-33%♦	20–33%
Electronic zoom	3–4	3–4
optical sectioning	-	0.1–1 μm
objective (Plan Apo)	x40 dry	x40 dry or x60 oil

* averages successive scans

♦ equivalent to a pinhole of 3–5 on the Bio-Rad MRC-600

Table 2.3: Imaging parameters used on the confocal laser scanning microscope. See Table 2.1 for microscope objective details.

The confocal microscope used in this study was equipped with an 25 mW argon ion laser with both blue (488 nm) and green (514 nm) excitation filters (Table 2.4). The settings used varied depending on whether the conidia were being imaged as part of a time series or as an individual image (Table 2.3).

The range of Nikon objectives were used for confocal microscopy (Table 2.1). Live-cell time-courses were collected using the x40 dry or oil objectives in order to reduce the extent to which the sample was exposed to the confocal laser. For fine detail the x60 or x100 oil objectives proved to be best and they were used to collect individual images and short time-courses (Table 2.1). A rapid scan speed of 0.25 sec per frame with a laser power of 1% was used in order to focus and position the sample before collecting an image. Bright field images were also collected using the transmission device with the confocal aperture fully open.

2.8.1 Single and dual wavelength imaging

In most cases single channel fluorescence imaging was used, in which the loaded dye was excited with either blue (BHS) or green (GHS) fluorescence and the image was collected in channel 1 (see Table 2.4). Channel 2 was sometimes used to collect a simultaneous bright field image.

Filter set	Excitation filter (nm)	Dichroic reflector	Emission filter (nm)	Channel
Standard BHS	488	510 LP	515 LP	1
Standard GHS	514	540 LP	550 LP	1
A2	-	600 LP	600 LP	1
			540 ± 15 BF	2
SNARF*	-	610 LP	580 ± 15 BF	1
			640 ± 20 BF	2

* Custom-made for dual wavelength imaging of carboxy SNARF-1 during pH analysis

Table 2.4: Filter sets used for CSLM. All values are wavelengths in nanometers (nm). Abbreviations: BHS/GHS (Blue/Green excitation filter), LP (Long Pass filter), BF (Barrier filter).

Use of dual wavelength imaging allowed the simultaneous detection of two dyes loaded in to one spore. Both dyes were excited at the same wavelength and their emission spectra were separated by a filter block, enabling them to be collected in different channels (Table 2.4). The effectiveness of this technique was dependent on the differences in emission spectra of the dyes and how these relate to the available filter block used to separate the signal. This could be established by initially imaging each dye separately, and checking to see how much of the signal was confined to one channel.

2.8.2 Precautions taken to protect live cells during confocal analysis and experimental controls

To ensure that conidia and germlings were alive and unperturbed during data collection, a number of experiments were performed to examine the potentially cytotoxic effects of the fluorescent dyes used, the phototoxic effects of the confocal laser, and any possible effects caused by interactions between these two factors.

Cytotoxicity was assessed by comparing the mean percentage maximum germination and differentiation in the presence of a range of dyes and in the absence of dye. The dyes were applied at 5 min post hydration at a concentration of 10 μM. This concentration was selected because it was the maximum dye concentration used during analysis by confocal microscopy. The experiment was performed on Teflon™ in order to optimise differentiation and reduce experimental variation, which had previously been found to be greater on detCS. (see Table. 3.1, Section 3.2.2.1).

Germ tube growth rate was used as a measure of potential phototoxic effects caused by exposure to the laser during confocal analysis. Two experiments were performed. In the first, seven conidia (no dye) were imaged every 20 min from 20–180 min post hydration with CLSM live-cell time-course settings (see Table 2.3) with one scan per image (Kalman 1) and the GHS excitation filter. The second experiment was performed on germlings (with germ tubes of 2–20 μm in length) in the presence of the principal organelle dyes, at the concentrations used to collect organelle data (Table 2.2). The CLSM settings were as before but with two scans per image

(Kalman 2) and the appropriate excitation filter for each dye (Table 2.4). Images were collected either every 1 min or every 4 min. As before, the control (no dye) was excited by the BHS excitation filter block, which was chosen in preference to the GHS because excitation of <500 nm has been reported to be highly cytotoxic, making it the potentially more damaging of the two (Sheppard & Shotton, 1997).

2.8.3 Data extraction

CLSM images intended for extraction of fluorescence values were collected as median optical sections using the COMOS software. Photomultiplier gains were set such that autofluorescence from the spore was negligible (55–65% gain) and the fluorescence signal from the samples was between 11–255 grey scale units. The background fluorescence values were maintained at 10 ± 0.2 grey scale units per pixel. As a precaution, control (no dye) time-courses were collected for analysis during each experiment to ensure that conidial autofluorescence did not increase under different experimental conditions (e.g. in the presence of sodium azide). Direct comparisons between data were only made when the data had been collected using the same settings.

OPTIMAS v.4.0 image analysis software (Media Cybernetics) was used to extract fluorescence data from these images. Regions of interest were defined in each conidial cell from which data were extracted in the form of mean fluorescence per pixel (grey scale units). The region of interest was the largest possible rectangle that did not encompass the plasma membrane region. So that the values might be expressed as mean conidial fluorescence, they were converted to total fluorescence for each cell, the three cellular values were then summed and divided by the total number of pixels measured within the conidium, which effectively weighted fluorescence of each cell by its image area.

2.8.4 z-Series and 3-dimensional reconstruction of images

By collecting confocal images (x,y scans) through a series of successive focal planes (axial z-scan) a complete in-focus projection of the specimen along the z axis can be recorded. The distance between these z-series of images can be defined by the user

and in this study was 0.1–1.0 μm: most commonly 0.2–0.4 μm, however when a spore was at an extreme angle to the substratum the z-step was increased to avoid photobleaching of the dye. The axial and lateral resolution of the objectives used in this study have previously been calculated (with a 30% confocal aperture) to be 1.3 μm and 0.6 μm, and 0.8 μm and 0.4 μm for the x40 dry and x60 oil objective respectively (Parton *et al.*, 1997). Thus the physical overlap between optical sections can be calculated and the final set of images reconstructed as a 3-dimensional image. This was performed using the Confocal Assistant (version 4.02) software.

2.9 LOW-TEMPERATURE SCANNING ELECTRON MICROSCOPY

Conidia were flood harvested and inoculated onto rice leaves and detCS using a spray gun (Section 2.3). The inoculated samples were then prepared for low-temperature scanning electron microscopy (LTSEM) using the Polaron Cryopreparation system interfaced with a Philips XL30 FEGSEM scanning electron microscope (Multi Imaging Centre, Dep. of Anatomy, Cambridge University). Samples were mounted on customised LTSEM stubs using Tissue Tek O.C.T. compound (Miles Laboratories, Naperville, Illinois, USA) as a cryoadhesive. Sample mounting was performed as rapidly as possible (within 1 min) to minimise sample desiccation. The mounted sample was cryofixed by plunging it into sub-cooled nitrogen under dry nitrogen gas. Specimens were examined either fully frozen-hydrated, or partially freeze-dried after warming to -90 °C on the LTSEM cold stage. The sublimation of free H_2O was visually monitored at 2 kV before re-cooling and sputter-coating. Most material was sputter-coated with gold and examined below -170 °C at 5 kV. Digital images were captured using the MS Windows-compatible software supplied with the Philips XL30 SEM.

2.10 ASSESSMENT OF GERMINATION AND DIFFERENTIATION *IN VITRO*

Germination and differentiation were assessed on glass CS by light microscopy (Nikon; x40dry) between 0–24 h post hydration. The start of germination was taken

as the point at which the length of the emerging germ tube was more than half its width. At this point the conidial wall was deformed and the germ tube was clearly emerging. The percentage germination was the percentage of the spore population that had germinated ([no. of germlings/total number of spores]x100) and the percentage differentiation was the percentage of germlings that formed appressoria ([no. of differentiated conidia/total number of germlings]x100).

2.11 ASSESSMENT OF GERM TUBE GROWTH RATE

The rate of germ tube growth was assessed on detCS at 24.5 ± 1 °C in the dark. Germ tubes were measured at intervals of 5–15 min on the Nikon Light Microscope (x40 oil) with a Sony CCD camera linked to a frame grabber (DT55, Data translation Berkshire, UK) controlled by OPTIMAS (v.4.0) image analysis software (Media Cybernetics). A humidity chamber was placed over the CS and the microscope light was set to a low intensity and used as little as possible. Plan Apo objectives were used to minimise errors that might arise in length measurements due to spherical aberrations (Table 2.1). Germ tubes were measured between 0–3 h post hydration.

Data were extracted from the images using a Wacom Graphics tablet and pen (Wacom Co. Ltd, Japan). This was used in preference to a PC mouse, based on a comparison in which specific germ tubes were measured repeatedly showing that the data collected using the pen was more accurate and repeatable. A calibration image of the 100 μm micrometer grid was also used in this assessment.

2.12 *IN VIVO* EXPERIMENTS

2.12.1 Inoculating rice leaves with spore suspension

Due to their extremely hydrophobic surface and shape, rice leaves are difficult to inoculate. The surfactant Tween 20 is routinely used for large-scale fungal inoculation (*pers. comm.* C. Rutherford). It acts as a wetting agent and so makes it easier to inoculate the hydrophobic leaf. When leaves treated with 0.51 $\mu g.ml^{-1}$

Tween 20 (20% of the standard concentration) were examined by light microscopy the surface wax was observed to be disrupted. Tween 20 was therefore not used during the inoculation of rice leaves. In the absence of a wetting agent, rice leaves were very difficult to inoculate at a scale high enough to allow spore counts. Even when held horizontally with double-sided tape, droplets ran off the leaf surface down the central vein, picking up other droplets *en route.* It was found that the 50 µl inoculum drops used on artificial substratum were too large; their weight and size made them more liable to roll off. Smaller droplets were more likely to stay in position, and the volume was therefore reduced to 10–30 µl per droplet of inoculum. Various techniques were tried to increase the surface area of the rice leaf inoculated and the most successful was inoculation by spraying. It was important that the spray pressure was not too high and that the trajectory was such that the spores fell on the leaf, as otherwise the inoculum would bounce off the leaf, and knock off any droplets that had previously landed on it.

2.12.2 A time-course of spore germination and differentiation on the rice leaf

Rice leaves, stuck to glass slides with Scotch™ double-sided tape (Pressure sensitive Tape, 3M from Agar Scientific), and detCS (control) were spray inoculated (see Section 2.3) with conidia that were flood-harvested (5×10^5 spore.ml^{-1} prior to spray inoculation), (see Section 2.2). They were incubated at 24 °C in humidity chambers in the dark (Fig. 2.1). A range of concentrations (0.05–5 mg.ml^{-1}) of the dye, $DIOC_6$, was assessed in order to determine one at which germination was inhibited but in which the physical appearance of the spores was unaffected. This enabled the samples to be fixed by the dye, allowing more time for counting. A concentration of 0.5 mg.ml^{-1} was found to be the optimum of those tested; at higher concentrations the spores appeared granular and misshapen, whilst lower concentrations allowed some germ tube emergence to continue. At the post hydration time at which germination/appressorium count was required, the leaves and detCS were submerged in 0.5 mg.ml^{-1} $DIOC_6$ and a large CS was placed over the leaf. Each detCS control sample was stuck to a glass slide by water adherence, with another CS placed on top of the inoculum.

When examined by fluorescence microscopy using the Zeiss microscope (see Section 2.6) with blue fluorescence excitation, $DIOC_6$-stained spores and germ tubes were brightly fluorescent (green) against the less fluorescent rice leaf (red). Mature appressoria did not stain but were easily identifiable by their dark colour using standard light microscopy. The percentage germination and differentiation were therefore assessed using both fluorescence and bright field microscopy (Section 2.10). In each experiment 2–4 replicates were counted at each time point for both the rice leaf and detCS, except for the last time point (>21 h) for which 6–8 replicates were counted for both substrata. All the conidia present in each sample were counted (average of 101 ± 29 conidia per sample, n = 11,827). The experiment was performed twice.

2.12.3 An assessment of the relative pathogenicity of dye-loaded spores

Rice plants were grown under glass until the second leaf stage and then transferred to the growth rooms for inoculation (Section 2.1.3, Fig. 2.3A,B). Pots containing rice plants were placed in trays of water with the second leaves (still attached to the plant) held horizontally by double-sided sticky tape. Each second leaf was inoculated with 10–30 µl of inoculum (Fig. 2.3C). The different inoculum treatments are shown in Table 2.5. The dyes were added to the spore suspension prior to inoculating the rice leaves. All dyes were used at a final concentration of 10 µM because this was the maximum dye concentration used during analysis by confocal microscopy.

All the plants in an individual tray were treated with the same inoculum . The position and approximate size of each droplet was recorded. Each tray of plants was covered by a polythene hood to isolate each treatment, and to maintain a high humidity (Fig. 2.3D). Precautions were taken to ensure that all equipment was sterilised and free from alternative sources of inoculum.

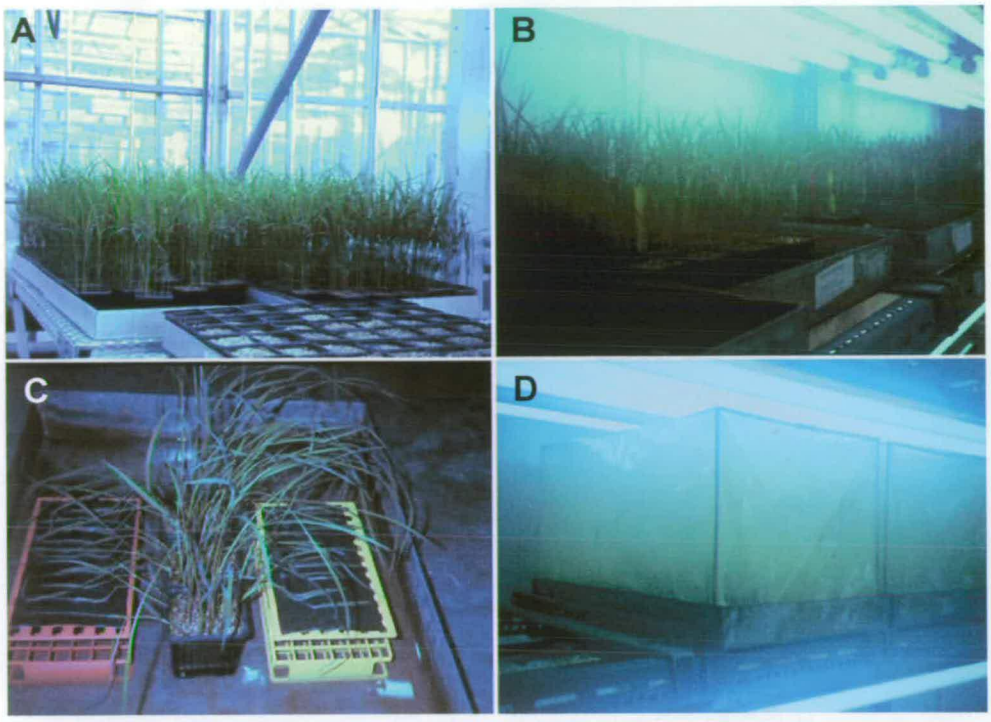

Figure 2.3: (**A**) Rice plants were grown under glass until the 2nd leaf stage, (**B**) Pots containing rice plants were placed in trays of water. (**C**) Second leaves were held horizontally by double-sided sticky tape and each leaf was inoculated with 10–30 µl of spore suspension, (**D**) a polythene hood was placed over the tray to isolate each treatment and to maintain a high humidity. After 5d lesions formed and these were assessed.

Treatment	Description
cDFFDA	vacuolar lumen dye
Rhodamine 123	mitochondrial dye
FM4-64	endocytic marker
MDY-64	vacuolar membrane dye
carboxySNARF-1	pH/vacuolar dye
spores only	control 1 (no dye)
water only	control 2 (no spores)

Table 2.5: Pathogenicity test inoculum treatments. Rice leaves were inoculated with *Magnaporthe grisea* conidia loaded with one of a range of dyes (10 µM). The following controls were included: (1) water only, and (2) conidial inoculum that had not been loaded with dye.

Five days after inoculation lesions formed and after 6 days these were scored as present or absent and images were captured using a Sony Digital photo camera (DKC-5000, 3 CCD) and collected using the Adobe Photoshop 4 software package. The leaves were also assessed microscopically (see Section 2.12.4). The experiment was performed once with rice variety M210 and twice with variety Sasawishi and at

conidial densities of 1, 2.5 and 4 x 10^3 conidia per ml. For each experiment one fungal culture was flood harvested to provide the inoculum for all treatments and replicates.

The percentage of each conidial population that internalized each dye (10 μM) was assessed. Conidia were imaged by confocal microscopy (Section 2.8). The signal was spit between the two channels: reflected light image in channel 2, and the fluorescence image in channel 1. A total of 4–11 samples (each of >500 spores) were counted for each dye.

2.12.4 Assessing fungal lesions and scoring infection

Leaves were detached from the plant and soaked for 1–2 days in a clearing solution (ethanol and dichloromethane were mixed in a 3:1 solution with 0.15 % trichloroacetic acid). This removed the pigmentation from the leaf tissue and allowed examination of stained fungal material within the leaf tissue. Three dyes were assessed as potential stains for internal fungal hyphae (Table 2.6).

Dye	Stock	Working Concentration
$DIOC_6$	5 $mg.ml^{-1}$ in methanol	1:10 in H_2O
Coomassie brilliant blue G	0.6 % in methanol + 15 % TCA	1:1 in H_2O
Aniline blue*	-	1:100 in H_2O

*soaked in 0.5M NaOH before addition of dye.

Table 2.6: Dyes assessed as potential stains for internal fungal hyphae in cleared rice leaves infected by *Magnaporthe grisea*. Leaves were incubated for 10 min in each case. Abbreviations: trichloroacetic acid (TCA).

Each dye was tested across a range of concentrations and times in solution. The most suitable concentrations are shown in Table 2.6, and these required that the rice leaf was incubated in the dye for 10 min. Samples were agitated in the dye in order to breakdown the air interfaces that existed between the hydrophobic leaf surface and the dye solution. This ensured that the dye came into contact with the fungal material. It was essential that samples were thoroughly washed between each stage, especially after incubation in the dye.

Lesions were scored on the Zeiss microscope (see Section 2.6) by assessing the presence of fungal hyphae within the leaf tissue and the production of conidiophores: both were assessed inside and outside of the lesion.

2.13 INHIBITOR EXPERIMENTS IN ENDOCYTOSIS STUDIES

2.13.1 Azide treatment

Conidia were Eppendorf-harvested, inoculated in 30–50 µl droplets onto detCS and covered by a humidity chamber. Sodium azide was added to the inoculum droplet by Gilson pipette, at the desired concentration from a 250 mM aqueous stock solution. After 2 min the dye solution was added by Gilson pipette and gently mixed into solution using the pipette tip. The volume of dye added depended on which dye was being used (Table 2.2). Where necessary, the dye was washed out with sodium azide solution at the same concentration as the inoculum, or with dH_2O. Washing was carried out as described in Section 2.7.2

2.13.2 Cooling treatment

Conidia were Eppendorf-harvested in 4 °C water and 50 µl droplets were inoculated in the refrigerator (4 °C) onto a detCS on a metal microscope stage plate and then covered by a humidity chamber. All of the above experimental components, and the dye solutions, water and pipettes used to wash dye out of the inoculum, were cooled in the refrigerator for at least 3 h before the experiment. To ensure that the dye was thoroughly diffused at this temperature, the stocks were diluted in dH_2O, and depending on the dye, volumes of 10–20 µl were added and gently mixed into solution using a Gilson tip. A hand held electronic thermometer with a thermocouple input (Thermospeed, type K thermocouple from Delta Ohm, Thermospeed, England) was used to ensure that the room temperature remained at 24 °C and the refrigerator remained at 4 °C.

2.14 A METHOD FOR SELECTIVELY KILLING CONIDIAL CELLS

A grid was drawn on the underside of a detCS with an indelible marker pen. Conidia were float harvested on 50 µl of dH_2O positioned over the grid. At 5 min post hydration, 2 µl of 0.5 $mg.ml^{-1}$ of the dead-cell stain propidium iodide (PI) was added and gently mixed into the inoculum.

Variable	A/B-cells	M-cell
objective	x40	x40
Excitation wavelength (nm)	488	488
Laser power	100 %	100 %
Scan speed	3 sec/frame	3 sec/frame
Kalman filter	4	5
Electronic zoom	60	60
Pixel area	80x80	90x90
Area (μm^2)	3.6	3.6

Table 2.7: Imaging conditions used to selectively kill conidial cells. At higher electronic zooms, the laser irradiates a smaller area of the specimen with the same laser power. Note that the area of the cell irradiated by the confocal laser is between ~ ¼ to ½ of the cellular area, depending on the cell type.

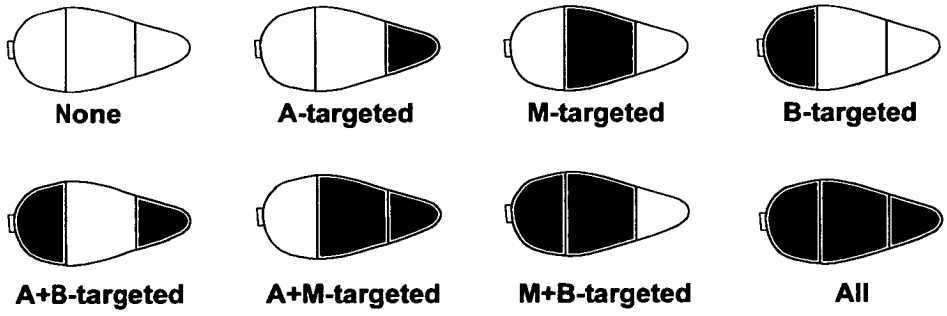

Figure 2.4: The different cell combinations targeted during experiments in which conidial cells were selectively killed.

Between 15–50 min post hydration, cells were selectively irradiated by the confocal microscope laser (see Section 2.8) using the settings shown in Table 2.7. A diagram was made at 30 min after irradiation to record which cells were dead in each spore and where these individual spores were in relation to one another and the grid. After

over 21 h the percentage and pattern of germination and differentiation were recorded for these spores and the cells were also reassessed for viability using the confocal microscope. Dead cells were identified by their fluorescence resulting from staining by PI.

All the possible conidial cell target combinations were attempted (Fig. 2.4) and where more than one cell was killed, a time interval of 5–10 min was allowed between killing cells in order to let the remaining live cells recover from the effects of the first laser irradiation.

3. CHARACTERIZATION OF SPORE GERMINATION

3.1 INTRODUCTION

There are many of factors known to influence the pre-penetration stage of infection in fungal pathogenic systems. Some are general, such as the availability of free water and a conducive temperature; others are more specific, such as the requirement for specific host topographies or components of host wax (Hoch *et al.*, 1987; Hoch & Staples, 1991; Read *et al.*, 1992b; Kolattukudy *et al.*, 1995; Collins & Read, 1997; Read *et al.*, 1997). The pre-penetration stage of infection in *M. grisea* requires free water and temperatures between 15–30 °C, with an optimum of 25 °C (Sadasivan *et al.*, 1963; Hashioka, 1965; Jelitto *et al.*, 1994; Kim, 1994; Teng, 1994), and a number of factors have been identified as being important, including the surface hydrophobicity and hardness, and components of leaf waxes; all of which appear important for the induction of germ tube differentiation (Uchiyama *et al.*, 1979; Uchiyama & Okuyama, 1990; Lee & Dean, 1993; Jelitto *et al.*, 1994; Xiao *et al.*, 1994a,b; Dean *et al.*, 1996; Gilbert *et al.*, 1996; Howard & Valent, 1996; Hegde & Kolattukudy, 1997). However, the full range of potential physical and chemical factors, and the possible interplay between them is currently poorly defined. Thus, in order to study the biology of germination in *M. grisea*, ideally the experimental substratum should be the rice leaf. However, this is a waxy, highly pigmented substratum and so must usually be chemically cleared to allow light microscopic analysis; a process that kills both the plant and the fungus. This approach is therefore unsuitable for studying living cells, making it necessary to use an artificial substratum.

In order that studies on *M. grisea* conidia germinated on artificial substrata provided biologically meaningful results, it was considered important that the characteristics of the pre-penetration stage of infection on the chosen substratum resembled those on the rice leaf as closely as possible. The **first aim** of the work described in this chapter

was therefore to characterize the processes of germination and differentiation, and by comparing their main features to identify a suitable artificial substratum for subsequent *in vitro* analysis by microscopy. The **second aim** was to analyse and characterize germination in more detail on the rice leaf and the chosen artificial substratum, and to compare the morphology and kinetics of spore germination *in vitro* with those *in vivo*.

In common with a number of other fungal pathogens, *M. grisea* produces three-celled spores, which are capable of producing multiple germ tubes (Ingold, 1971; Agrios, 1988). The **third aim** was to investigate the role and relative importance of each cell within the conidium for successful conidial germination. Communication between cells via intracellular signalling might be important in regulating germination from different cells and this was also examined. To address these questions, a technique was developed in which conidial cells were individually killed and the fate of the remaining live cells examined.

3.2 RESULTS

3.2.1 Timing of germination

Conidia were easily harvested and germination occurred freely on a range of substrata in the absence of nutrients in both distilled or double-distilled H_2O, approaching 100% within 3–4 h post hydration (95.8 ± 2.1%). A further slight increase in germination occurred after this time (rising to 98.2 ± 0.8%) and so maximum germination was assessed >21 h post hydration, at which time differentiation (i.e. the formation of an appressorium) also reached a maximum.

Conidia from older cultures exhibited a greater time lag before germination commenced; at 2 h post hydration >90% and <10% of conidia germinated when flood-harvested from 10 day and 26 day old cultures, respectively. Furthermore, it was considered that young conidia are most likely to be those that cause infection *in*

vivo under natural conditions. Thus, 10–14 day old cultures were used for all subsequent experimentation.

3.2.2 Selection of a suitable artificial substratum

Teflon™ and glass CS (cover slip/s) cleaned in various ways were assessed as suitable artificial substrata for microscopic analysis of germination (see Section 2.5.2). The rice leaf was included in these studies to provide a comparison with *in vivo* results (Section 2.12.).

3.2.2.1 The influence of artificial substrata on maximum germination and differentiation

Mean maximum germination and differentiation were assessed by light microscopy on a range of artificial substrata and on the rice leaf (Sections 2.10). Table 3.1 summarises the results. Germination is shown as the percentage of germinating spores, and differentiation is shown as the percentage of germinated spores that formed appressoria. The size of the spore population counted varied between samples and so weighted averages are given (Sokal & Rohlf, 1987).

	Germination		Differentiation		Total number	
Substratum	**mean %**	**SD**	**mean %**	**SD**	**spores**	**samples**
rice	99.0	1.59	91.2	3.56	1068	11
Teflon™	97.4	1.54	98.0	2.09	1137	8
untreated CS	97.5	2.08	92.7	4.21	5945	18
detergent-washed CS	97.8	1.44	59.7	13.49	4204	20
silanised CS	98.3	1.13	26.9	34.75	1770	5
NaOH-washed CS	98.1	1.12	15.8	5.84	2006	6
chromic acid-washed CS	95.9	5.39	6.7	12.75	2161	5
heat-treated CS	97.9	1.27	0.1	0.32	3691	10

Table 3.1: Mean maximum germination and differentiation on a range of substrata assessed after 21 h post hydration. Abbreviations: mean % (mean percentage), SD (standard deviation), CS (cover slip).

Mean maximum germination appeared not to be influenced by substratum (Table 3.1), being over 97% on all but chromic-acid washed CS, which had a large

standard deviation. Mean maximum differentiation varied considerably both within and between substrata. The mean maximum differentiation on Teflon™, untreated CS and rice leaves were all high (>90%) and on detCS (detergent-washed CS) it was ~30% lower. The mean maximum differentiation on Teflon™ was significantly higher than on rice leaves (Students two tailed t-test; $p = 0.001$, $n = 8, 11$) and untreated CS (Students two tailed t-test; $p = 0.0017$, $n = 8, 18$). Differentiation was low on silanised glass, chromic acid- and NaOH-washed CS and approached zero on heat-treated CS.

3.2.2.2 Other important attributes of the substrata

Other important factors when selecting a suitable substratum include the morphological appearance of the spores and germlings, the optical characteristics of the substratum (as it was to be used for light microscopy), the ease of preparation, consistency of substratum surface properties, and hence reproducibility of the percentage germination and differentiation obtained. These are considered below for each substratum and summarised in Table 3.2.

- The rice leaf is optically very poor and thus unsuitable for most analysis by light microscopy using transmitted light. Rice leaves can be cleared of pigmentation (Section 2.12.4) to improve their optical characteristics. However, this involves killing the leaf and the fungus, so the technique cannot be used for live cell analysis.

- Teflon™ is optically poor but easily prepared, with highly consistent surface properties and the maximum germination and differentiation data were found to be highly reproducible. Furthermore, the lengths of differentiated germ tubes were similar to those found on the rice leaf; this has been previously quantified by Jellito *et al.* (1994).

- On closer inspection, untreated CS were found to be highly variable with respect to their hydrophobicity owing to an oily coating which appeared to originate during the manufacturing process. Since this oily substance was of unknown composition, and varied considerably between batches of CS, untreated CS were

ruled out as a substratum for further experimental use. Note that those used in the analysis shown in Table 3.1 were chosen from a hydrophobic batch.

- Detergent washed CS were easily prepared and the surface was consistent with respect to hydrophobicity; they were observed to be less hydrophobic than the rice leaf but considerably more hydrophobic than heated CS. The lengths of differentiated germ tubes varied; sometimes being as short as those on the rice leaf, but often longer.

Substratum	Observations
rice leaf	optically poor
Teflon ™	optically poor
untreated CS	optically good; surface properties highly variable between batches due to oily coating of unknown composition.
detergent-washed CS	optically good; surface consistent with respect to hydrophobicity; differentiated germ tubes often longer than on rice leaf.
silanised CS	optically poor due to variation in the refractive index; very long differentiated and undifferentiated germ tubes; patchy surface
NaOH-washed CS	optically good; time consuming preparation.
chromic acid-washed CS	optically good; time consuming preparation.
heat treated CS	optically good, hydrophilic..

Table 3.2: Summary of important attributes of the artificial substrata tested, which were important when selecting suitable substrata for subsequent *in vitro* experiments. For further details see text. Abbreviations: CS (cover slip).

- CS silanised by treatment with Sigmacote, were highly hydrophobic and appeared to be more so than Teflon™. Differentiation was low and highly variable. The CS surface often appeared variable, with some regions that were highly inductive and other regions that were less inductive. Differentiated germ tubes were much longer than those observed on the rice leaf. The optical properties of silanised glass were poor because of variation in the refractive index resulting from inconsistencies in the thickness of silanised coating of the CS. It was decided that although

silanisation might be improved upon by refining the technique used, this substratum was unsuitable for the present studies as it resulted in the formation of abnormally long differentiated germ tubes.

- Acid and alkali-washed CS were less hydrophobic than detCS. The process of acid and alkali-washing was time-consuming and involved the use of chemicals which required extensive washing in order to remove any residues. The large standard deviation for germination on acid-treated CS (Table 3.1) might be due to insufficient washing of one or more CS. However, the mean maximum germination did not differ significantly from that on the rice leaf (Students two tailed t-test, $p = 0.15$, $n = 11, 6$). Although optically suitable, the mean maximum differentiation was low and thus both of these substrata were discounted.

- Heat treated CS were optically suitable for microscopy. However, the surface was highly hydrophilic and non-inductive, and thus produced very long germ tubes.

On the basis of the results shown in Tables 3.1 and 3.2, detCS were selected as the artificial substratum for further experimentation because of those substrata optically suitable for microscopy, detergent washed CS (detCS) were the most inductive for appressoria. Furthermore the surface properties of detCS were consistent, they were easily prepared and produced highly reproducible data. Teflon™ and heat treated CS were also used for specific experiments requiring a highly inductive or noninductive substratum respectively.

3.2.3 Time course of germination and differentiation

After selecting detCS as the artificial substratum for *in vitro* experiments, a more detailed comparison was made of the pre-penetration stage of infection on detCS compared to the rice leaf. The time-course of germination and differentiation was assessed on both detCS and rice leaves (Section 2.12.2). The experiment was repeated and the results were both quantitatively and qualitatively similar. Data from the first experiment are shown in Figure 3.1.

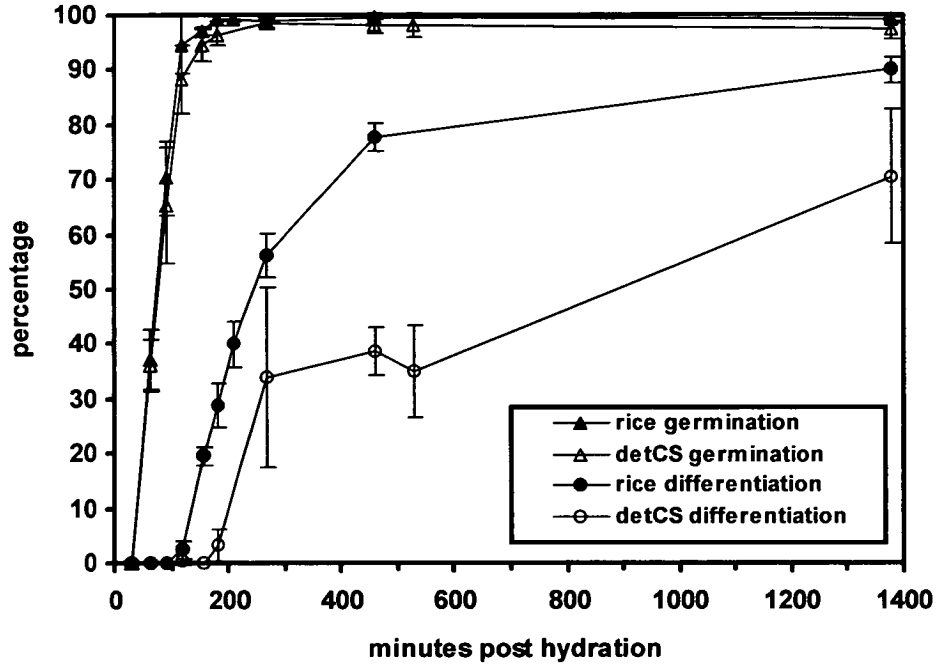

Figure 3.1: Time course of germination and differentiation on detCS and rice leaves. For both substrata 2–4 replicates were counted at each time point (or 6–8 at 1380 min post hydration) and the mean is plotted. Error bars are standard deviations.

There was no evidence that the rate and timing of germination on the detCS differed from those on the rice leaf; germination commenced after ~20 min and mean maximum percentage germination did not differ significantly (Students two tailed t-test, $p = 0.16$, $n = 14, 11$). Mean maximum differentiation on the rice leaf was ~30% higher and occurred ~50 min earlier than on detCS. Differentiated germ tubes were generally longer on the detCS than on the rice leaf; otherwise there were no other apparent morphological differences.

Germination approached its maximum by 3 h post hydration, and on detCS differentiation commences at ~3 h (Fig. 3.1). On this basis it was decided that 0–4 h post hydration would be the time period in which subsequent analysis of germination would be performed.

3.2.4 General features of germination observed using light microscopy

Conidia were imaged during germination using differential interference contrast (DIC) light microscopy (see Section 2.6). When float harvested on detCS, a large proportion of the spores initially attached to the substratum by A-cell spore tip mucilage (STM), and with time most of these spores settle into a more or less horizontal position. It was also found that when a detCS was inoculated with spore suspension and then completely immersed in water, a droplet reformed on the site of the conidial inoculum. This test was repeated using pure water instead of conidial inoculum, and it was found that the droplet did not reform, providing evidence that the conidia are able to retain water over the site of inoculation.

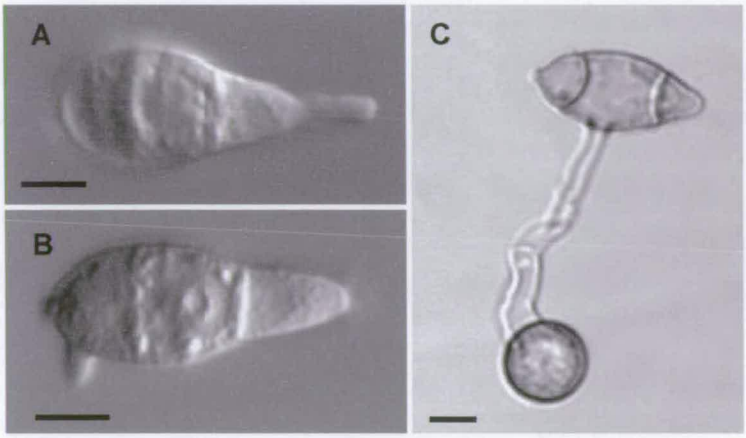

Figure 3.2: Two differential interference contrast (**A**, **B**) and a bright field image (**C**) of germlings on detCS showing (**A**) apical, and (**B**) basal cell germination. (**C**) The middle cell rarely germinates (<1%), and in this example the germ tube has differentiated. Note that the spore in (**C**) appears unusual in that the middle cell is large and has convex septa. The image in (**C**) was collected using the transmitted light device on the confocal microscope. Imaged at 70 min (**A**), 80 min (**B**) and 7 h (**C**) post hydration . x40 objectives used. Bars = 5 µm.

Each conidium is capable of germinating from all 3 cells, however <1% of the conidial population germinated from the M-cell (Fig. 3.2). Within the first 4 h post hydration conidia either produced 1 germ tube from the A- or B-cell, or 2 germ tubes sequentially. In the latter case, the germ tubes usually grew in roughly opposite directions (Fig. 3.3).

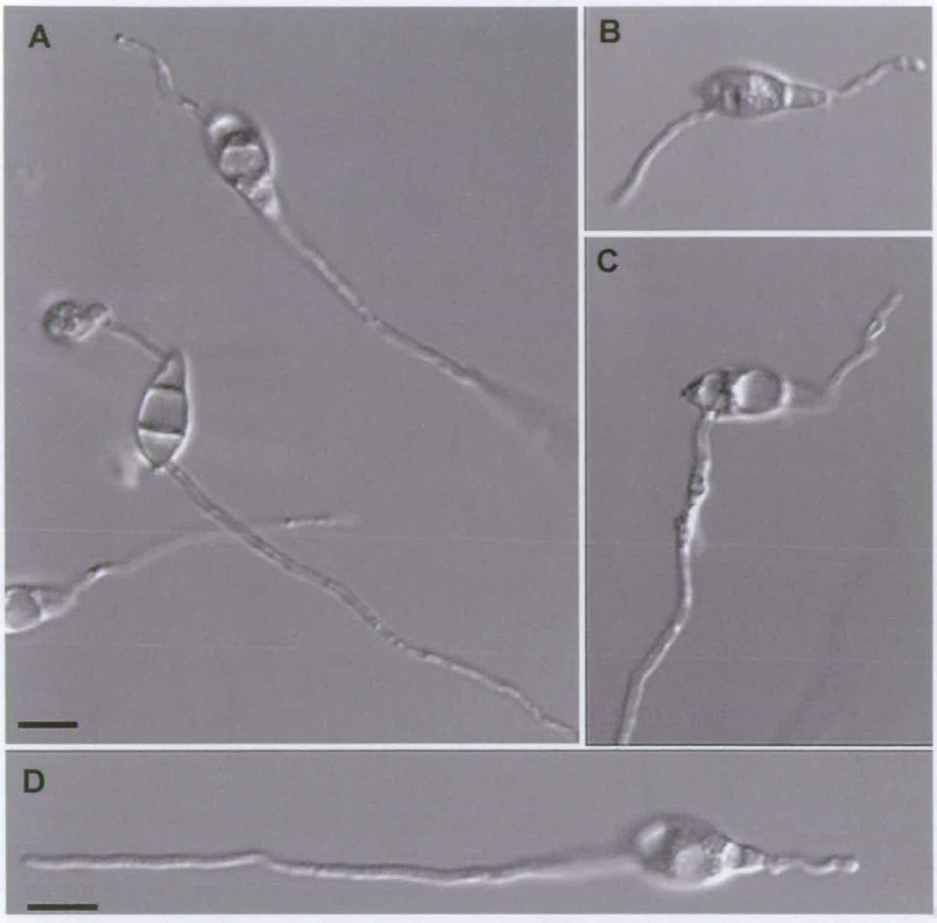

Figure 3.3: Differential interference contrast images of germlings on detCS at 24 h post hydration showing examples of germlings that have two germ tubes. Within the first 4 h post hydration conidia often produce 2 germ tubes, which usually grow in approximately opposite directions. x40 dipping objective used. Note that all bars = 10 µm, and that the bar in (**A**) also applies to (**B**) and (**C**).

Individual conidial cells are capable of producing >1 germ tube (Fig. 3.4). However on inductive substrata this only occurs in a very small percentage of the population during the first 24 h post hydration and has not been observed to occur during the first 6 h post hydration. If spores are incubated for >24 h, various other germination patterns emerge, especially on non-inductive substrata such as heat-treated CS.

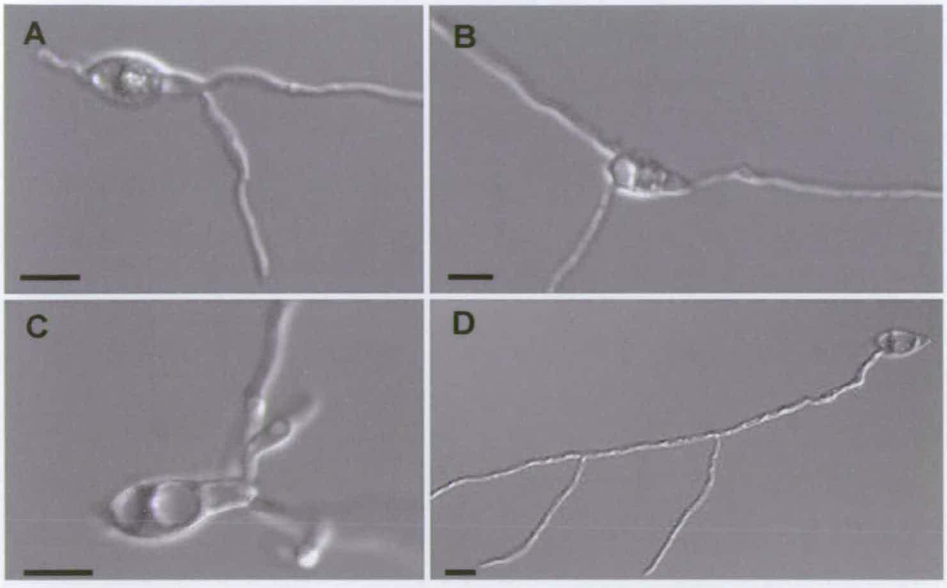

Figure 3.4: Differential interference contrast images of germlings on heat-treated CS after 24 h post hydration showing examples of conidial cell multipolarity (**A–C**) and germ tube branching (**D**). The most common multipolar germination pattern is where the conidium produces 2 germ tubes from either the apical (**A**) cell, or the basal cell (**B**). Less frequently, >2 germ tubes are produced from the apical or basal cell (**C**). Another common feature on non-inductive substrata is that germ tubes often grow to extended lengths and become branched (**D**). x40 dipping objective used. Bars = 10 µm.

3.2.5 Analysis of spore germination by low temperature scanning electron microscopy

Conidia were analysed by low temperature scanning electron microscopy (LTSEM) at various stages during germination on both detCS and rice leaves (Section 2.9). Representative images are shown below.

Problems were encountered when freezing conidia during LTSEM preparation. Prior to freezing, attempts were made to remove some of the free water in which the spores were suspended for inoculation. However, the spores were very sensitive to the absence of water, becoming desiccated and collapsing during partial freeze-drying (Fig. 3.5A cf. C). The best preserved spores were those that were associated with some ice since these appeared fully turgid (e.g. Fig. 3.8B). Partially freeze-dried spores often had strands or a broken film associated with them, the shape of which could have been influenced by the presence of extracellular matrix materials derived from spores or from fungal cultures from which they were harvested (Figs. 3.6, 3.9A,C,D).

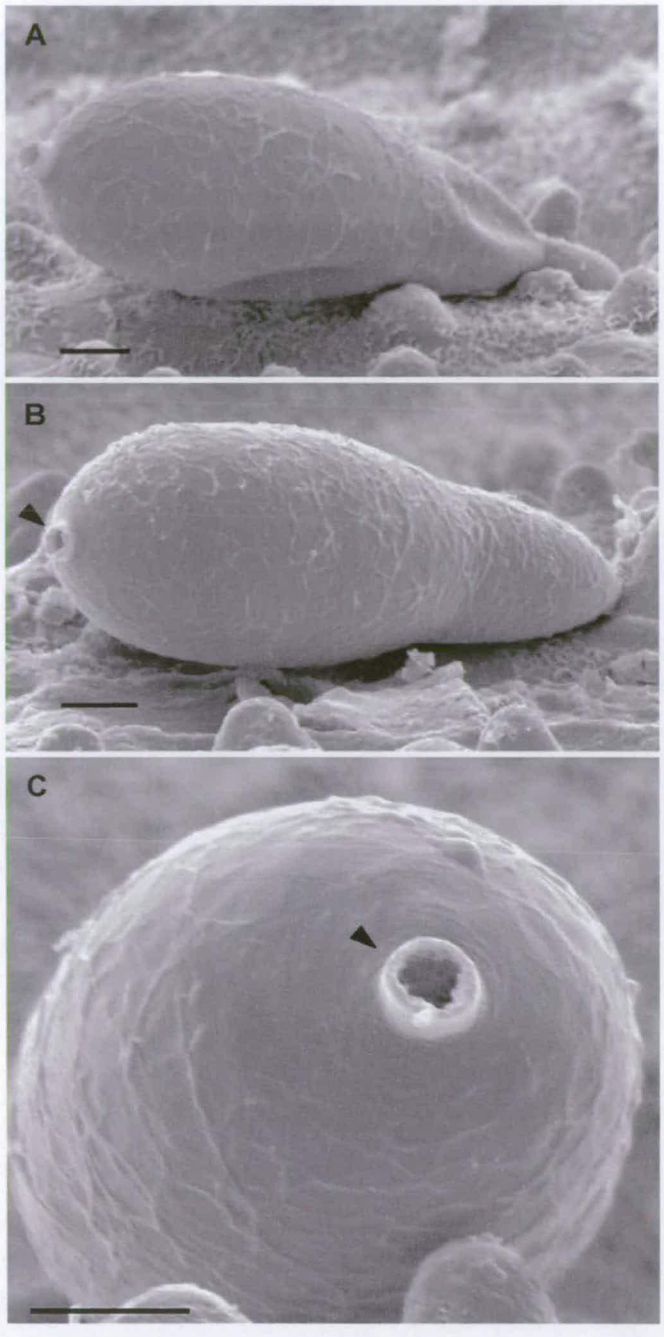

Figure 3.5: Scanning electron micrographs of (**A**) a collapsed germinated conidium on a rice leaf, (**B**) an ungerminated fully turgid conidium on a rice leaf displaying the characteristic reticulated surface pattern and stalk (▲), and (**C**) the base of a conidium, showing the hollow stalk (▲). 90 min post hydration. Partially freeze-dried. Bars = 2 μm.

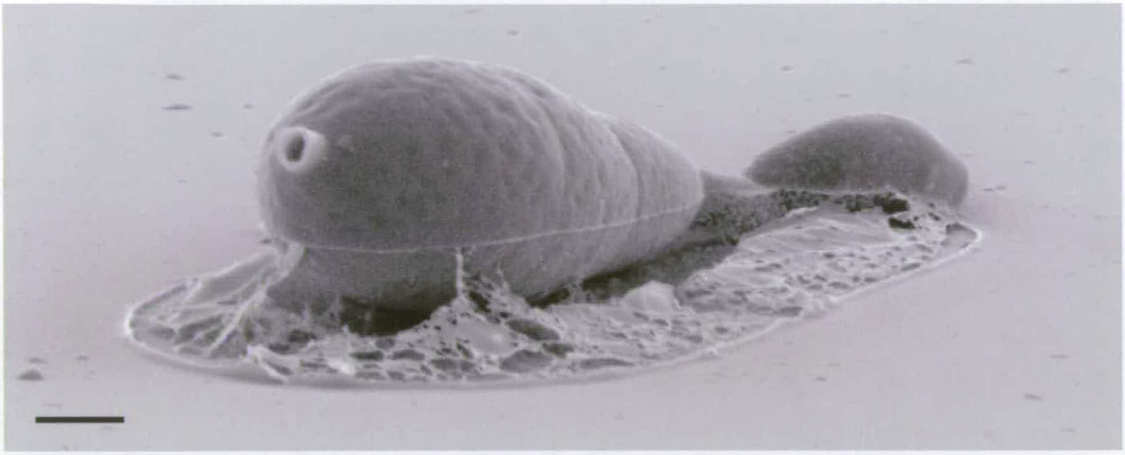

Figure 3.6: Scanning electron micrograph of a germling with a developing appressorium on a detCS after ice deposits were removed by etching. Note that a broken film surrounds the spore. The spore is fully turgid and has a smoother surface than conidia that were more extensively freeze dried. 5 h post hydration. Partially freeze-dried. Bar = 2 µm.

3.2.5.1 Morphology of the rice leaf

The rice leaf surface is undulating and often folded with parallel longitudinal rows of stomata (Fig. 3.7A). It also bears trichomes and papillae and the entire surface is covered by wax platelets (Fig. 3.7A–C). With the exception of the region of the stomatal complex, leaf papillae are numerous and dense (Fig. 3.7B), and so *M. grisea* spores are primarily in contact with the leaf via these leaf projections (e.g. Fig. 3.10A). However, even on detCS the underside of the spore is not completely appressed to the surface because of its curved shape (e.g. Fig. 3.10B).

3.2.5.2 Ungerminated conidia

It was found that droplets of spore suspension were sometimes retained on the leaf surface after freezing (Fig. 3.8A). Germlings were present on the surface of the droplet (Fig. 3.8 A,B). It is not clear whether the germlings were naturally present on the surface of the droplet *in vivo* or whether they represented germlings that had been dislodged from the rice leaf surface during preparation. However, the orientation of the spores in some regions of the droplet surface, in particular that of the germ tubes, was consistent with their having germinated in that position (Fig. 3.8B).

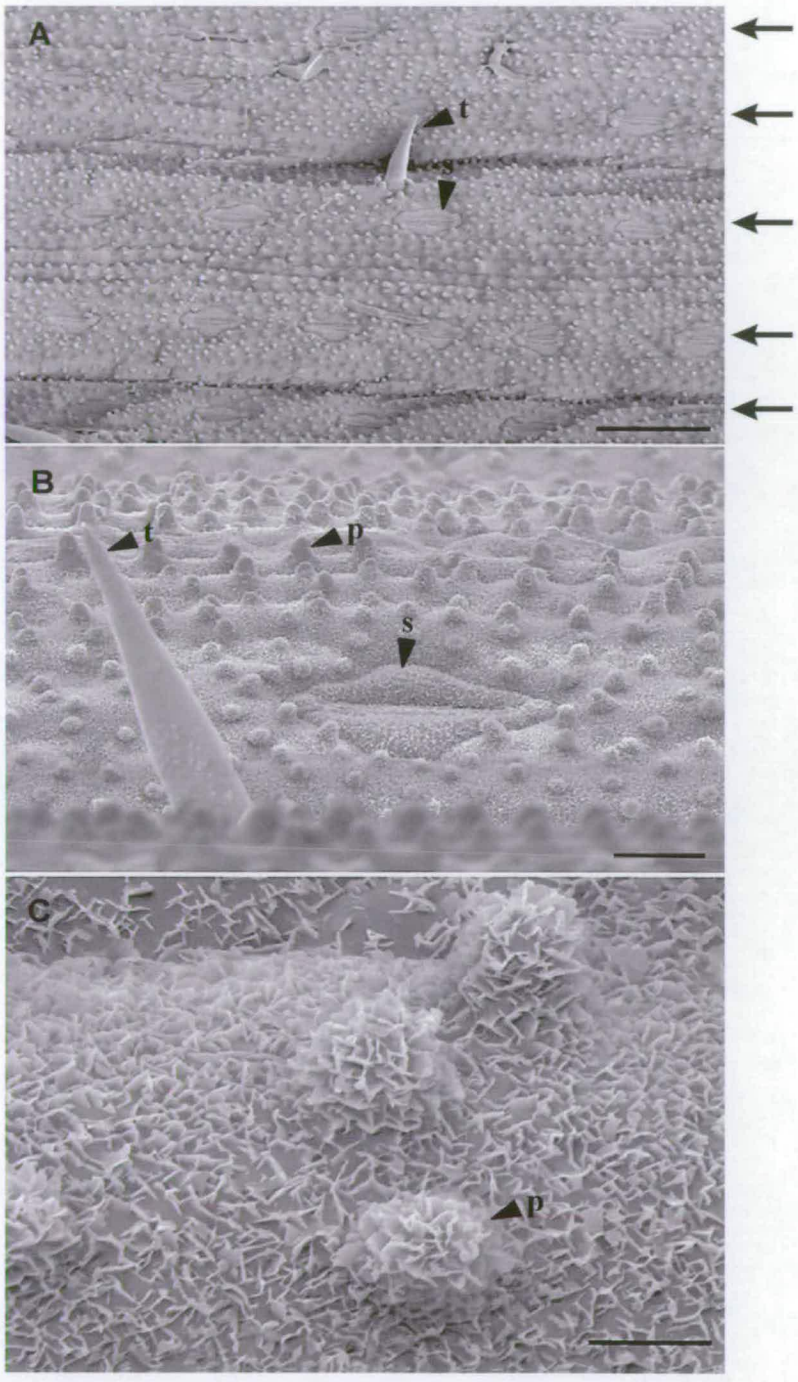

Figure 3.7: Scanning electron micrographs of the rice leaf surface at increasing magnifications (**A**–**C**). The stomatal complexes (**s**) form parallel longitudinal rows (→) and the leaf bears trichomes (**t**). The rice leaf is covered with papillae (**p**) (**A**–**C**), except for the regions occupied by the stomatal complexes (**B**). The leaf surface is covered by wax platelets (**C**). Partially freeze-dried. Bars = 50 µm (**A**), 10 µm (**B**) and 2 µm (**C**).

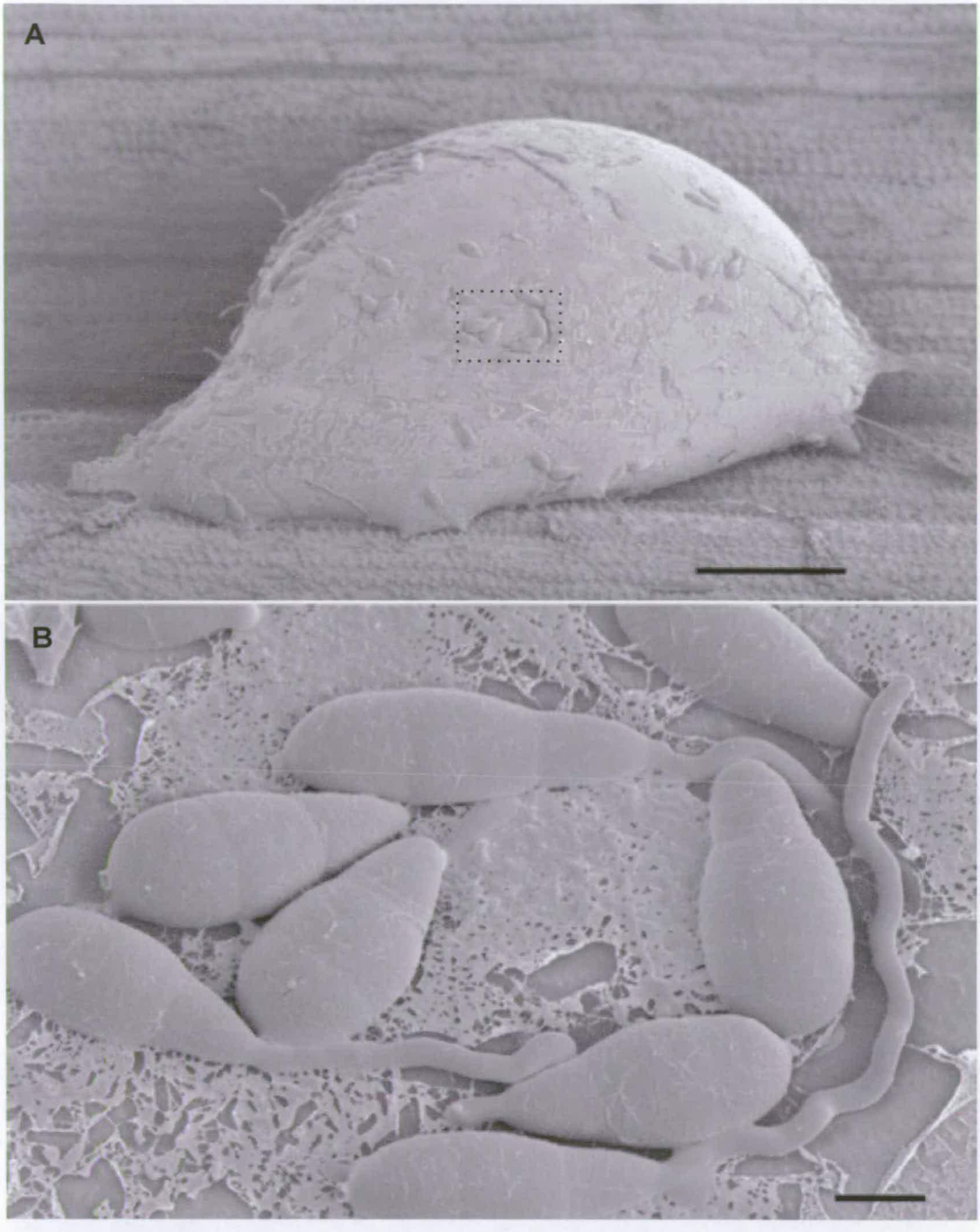

Figure 3.8: Scanning electron micrographs of (**A**) a droplet of frozen water containing germlings on the surface of a rice leaf, the dotted box surrounds the region of the droplet displayed in (**B**), in which germinated conidia are shown on the surface of the water droplet. Partially freeze-dried. 4 h post hydration. Bars = 100 μm (**A**) and, 5 μm (**B**).

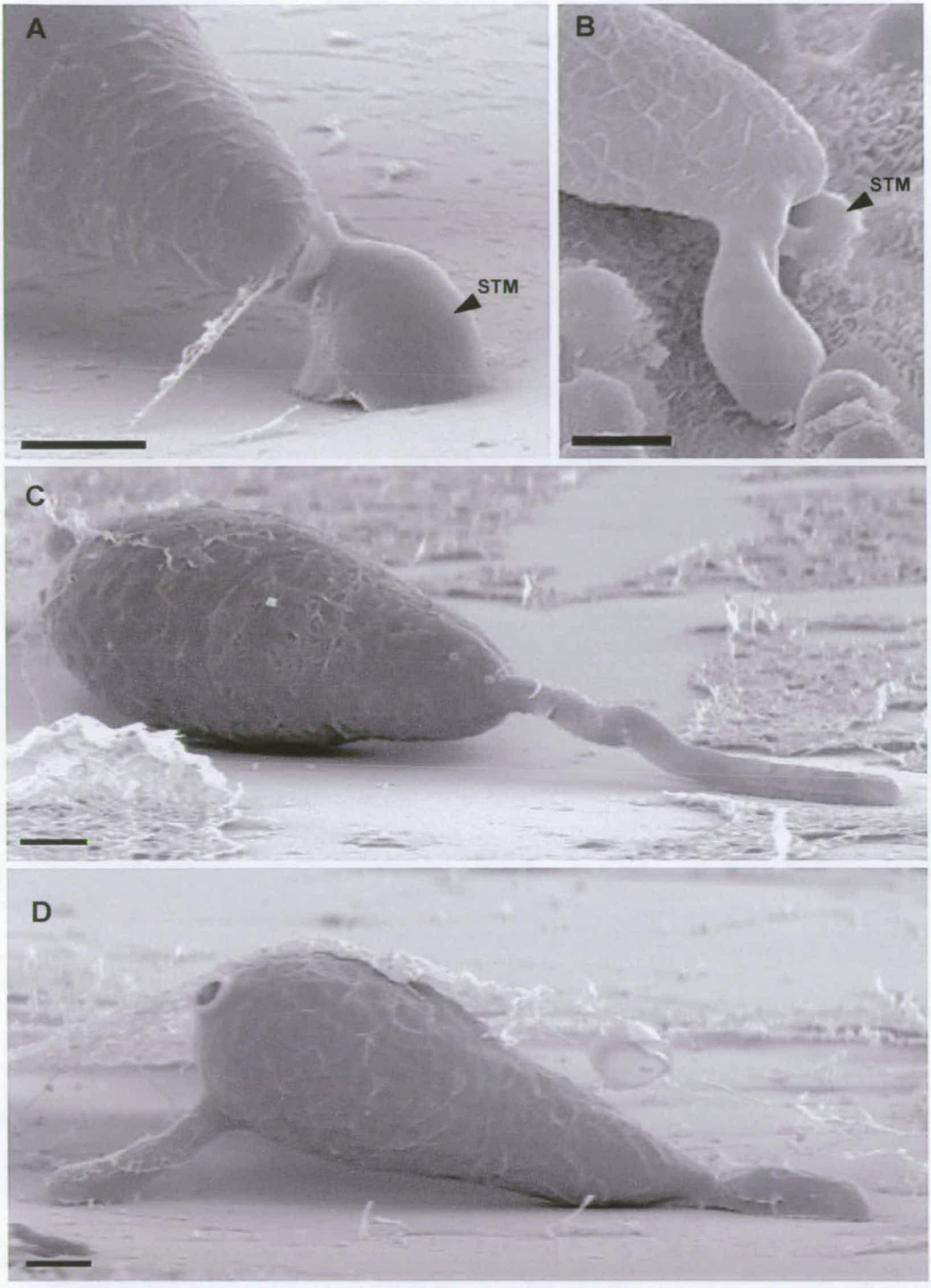

Figure 3.9: Scanning electron micrographs showing conidia attached via spore tip mucilage to, (**A**) a detCS, and (**B**) a rice leaf. Germ tubes typically arise in the region surrounding either (**C**) the tip of the apical cell, or (**D**) the stalk on B-cell. Germ tubes do not usually emerge from the underside of the conidium (**D**). Partially freeze-dried. 3 h (**A**, **C**, **D**) and 5 h (**B**) post hydration. Bars = 2μm.

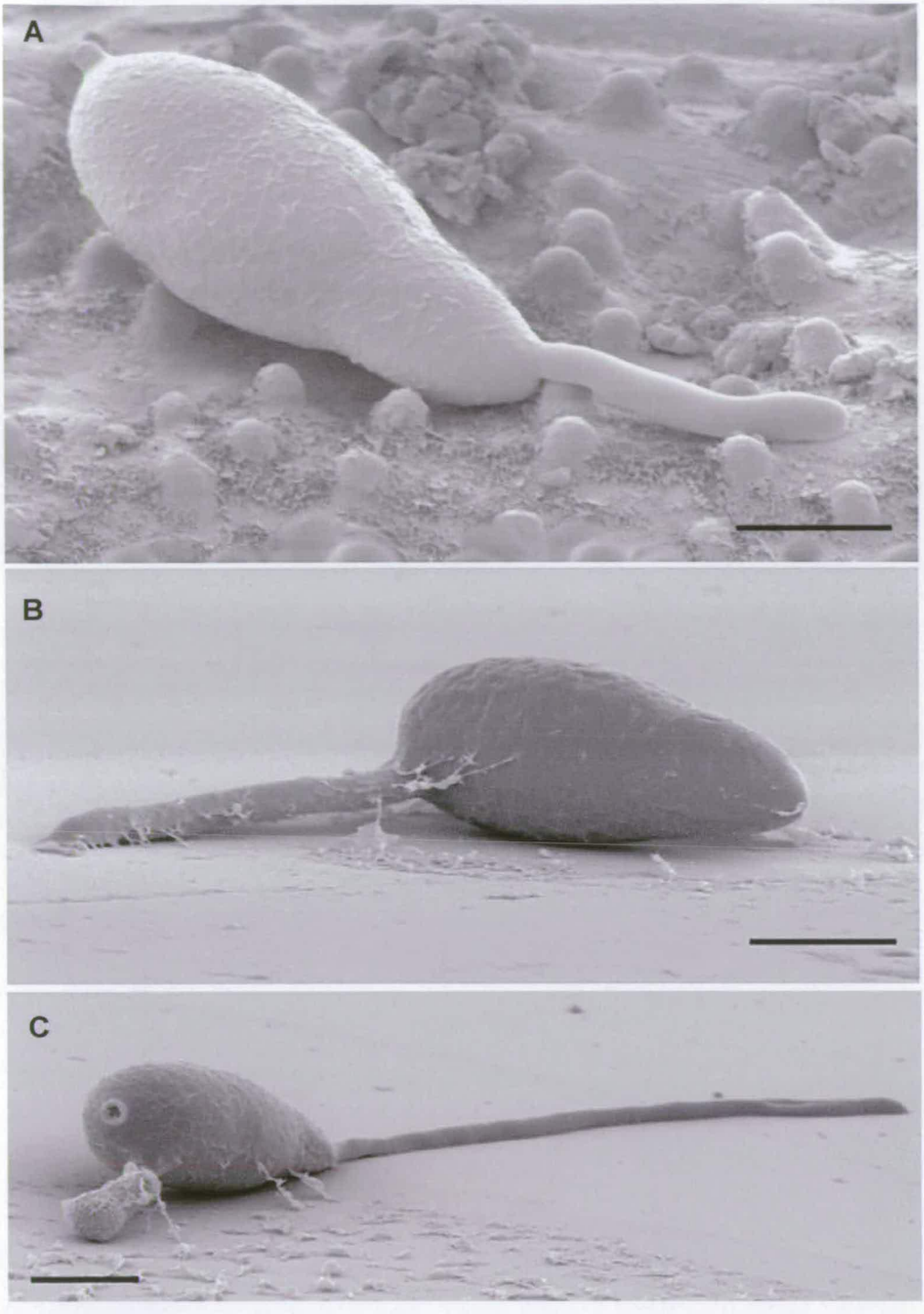

Figure 3.10: Scanning electron micrographs of (**A**) a germinated conidium supported by the rice leaf papillae. Note that the germ tube has emerged above a papilla, (**B–C**) germinated conidia on detCS showing that the underside of the spore is not appressed to the substratum. Note the mucilage associated with the germ tube (**B**) and the approximately straight orientation of the germ tube on the detCS. 4 h (**A**), 3 h (**B**, **C**) post hydration. Partially freeze-dried. Bars = 5 µm.

The conidial surface is characteristically reticulate (e.g. Fig 3.5). However, it was observed that those spores that appeared to be more turgid and thus more fully hydrated were smoother (e.g. Figs. 3.6, 3.8B). In all spores, the positions of the septa between the three cells were clearly discernible. The stalk that bore the conidium on the conidiophore was hollow (Fig. 3.5B,C). Spore tip mucilage associated with the A-cell often adhered the spore to the surface of both the rice leaf and detCS (Fig. 3.9A,B). Mucilage was also observed on occasions to be associated with the germ tube (e.g. Fig. 3.10B).

3.2.5.3 Germ tube emergence

Germ tubes were usually formed within a region around the A- and B-cell apices, and at some distance from the septum; the A-cell frequently germinated from its tip region (e.g. Figs. 3.8B, 3.9C, 3.10A), and the B-cell from a region adjacent to, and surrounding the stalk (e.g. Fig. 3.9D, 3.10B). Germ tubes emerging from both the A- and B-cells tended to emerge from the spore in regions closer to the substratum, rather than on the side of the spore opposite to the surface (e.g. Figs. 3.10, 3.11A,B). However, the latter was occasionally observed (Fig. 3.11C). Germ tubes generally emerged in regions that were not in immediate contact with a surface (e.g. Figs. 3.10A,B, 3.11A). Although the germ tubes of B-cells were occasionally observed to have emerged from the underside of the spore (Fig. 3.9D), it was unclear whether this region of the conidium had been in contact with the substratum at the time of germ tube emergence; conidia could be in contact with the substratum solely by the A-cell during this stage of germination (see Section 3.2.4).

3.2.5.4 Germ tube growth and differentiation

Having emerged from a region of the spore that is not in immediate contact with the surface, the germ tube usually grew towards it. The germ tube could grow for a considerable distance before making contact with the surface (e.g. Figs. 3.9C, 3.10B, 3.11A). Thus, during the first part of germ tube extension, it was not usually in contact with the substratum. Germ tubes that emerged on the side of the spore furthest from substratum tended to grow upwards, away from the substratum (Fig. 3.11C). Once the germ tube made contact with the surface, subsequent growth was maintained in contact with the substratum (e.g. Figs. 3.9C, 3.10A,B). The gaps

between the rice papillae are commonly 1.5–7 µm and are thus easily accessible to the narrow germ tubes (Figs. 3.10A, 3.11B). On detCS, the germ tubes tended to grow in a straighter orientation than on the rice leaf because on the latter their path was obstructed by leaf papillae (Figs. 3.10A, 3.11B). Typically, differentiated germ tubes were shorter on the rice leaf than on detCS. On the rice leaf, appressoria were observed to form between papillae and also near stomatal complexes. (Fig. 3.11D).

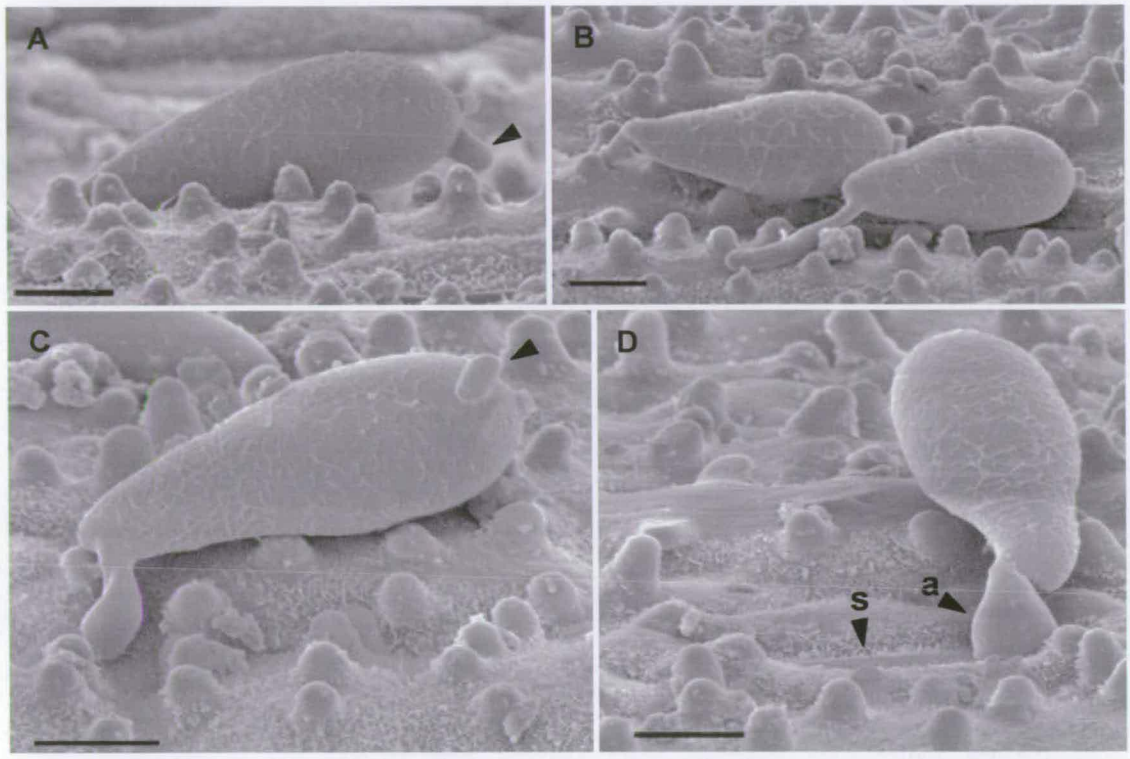

Figure 3.11: Scanning electron micrographs showing (**A**) a conidium that has germinated from the B-cell and the germ tube (▲) has grown through the air towards the substratum, (**B**) two germlings both of which have germinated from the apical cell, note that the germ tubes are growing between the leaf papillae, (**C**) a conidium that has germinated from both the apical and basal cells, note that the basal cell germ tube (▲) is unusual because it has emerged from the conidium on the side furthest from the substratum and then grown away from the substratum, and (**D**) a germling that has formed an appressorium (**a**) over a stomatal complex (**s**), note that the germ tube is very short. 90 min (**A**) and 5 h (**B–D**) post hydration. Partially freeze-dried. Bars = 5 µm

3.2.6 Analysis of infection by fluorescence and light microscopy

Three dyes ($DIOC_6$, Aniline blue, and Coomassie Brilliant Blue G) were assessed as potential stains of internal hyphae in cleared leaves (Section 2.12.4). In contrast to Aniline blue and Coomassie Brilliant Blue G, $DIOC_6$ did not penetrate the rice leaf tissue sufficiently to stain the internal structures. Coomassie Brilliant Blue G was

superior to Aniline blue for discriminating fungal hyphae from the leaf tissue. Rice leaves were inoculated with float-harvested *M. grisea* conidia and after 1, 2 and 5 days (Fig. 3.12A) the leaf lesions were either stained with $DIOC_6$ to observe fungal structures on the leaf surface, or cleared and stained with Coomassie Brilliant Blue G, primarily to observe fungal structures within the leaves. Both types of treated leaves were examined by fluorescence microscopy.

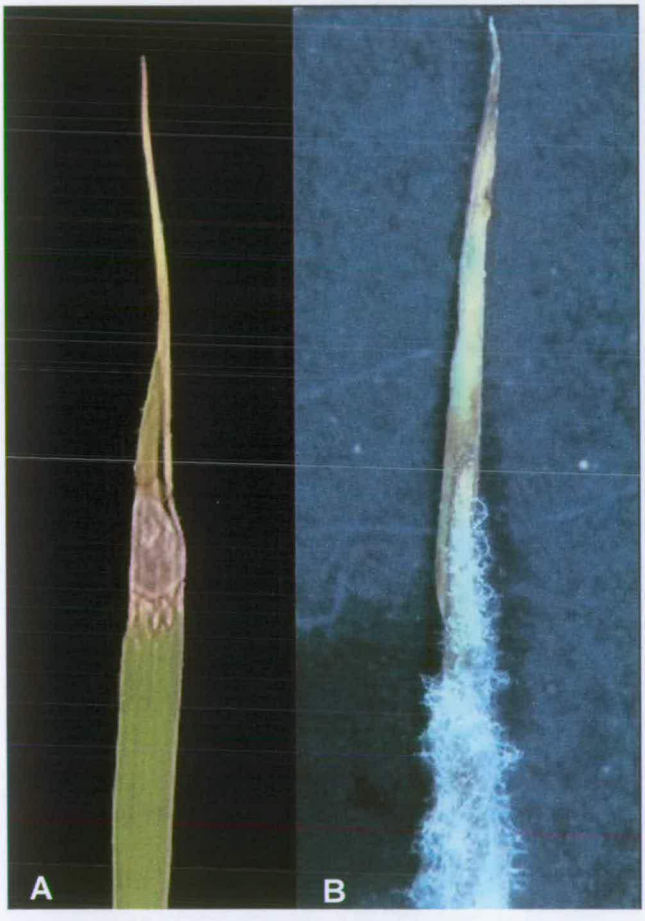

Figure 3.12: Photographs of rice leaves infected by *M. grisea*. (A) A lesion formed 5 days after inoculation with conidia. Note the brown necrotic edge around the lesion. (B) A leaf >14 days after inoculation covered in fungal hyphae bearing conidiophores.

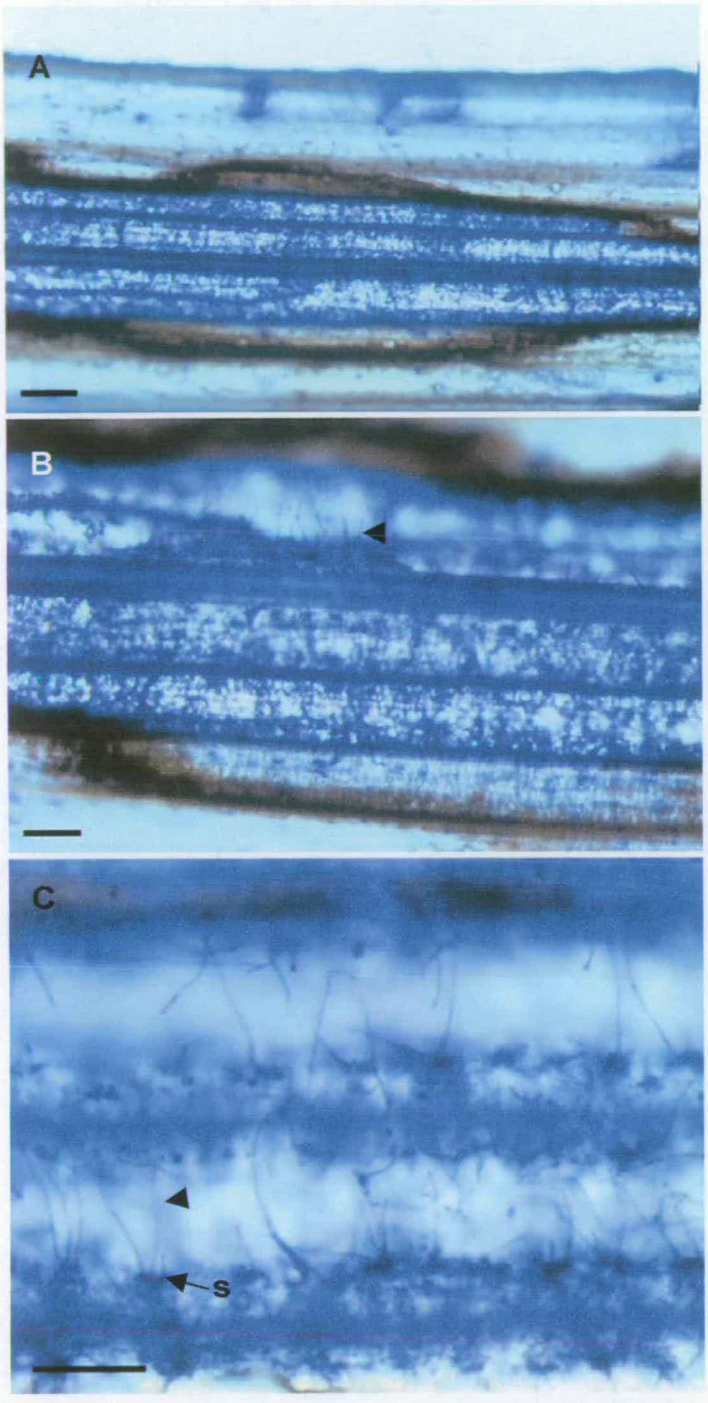

Figure 3.13: A lesion in a cleared rice leaf stained with Coomassie Brilliant Blue G at different magnifications. The lesion is surrounded by a brown edge (infected leaf tissue is blue due to the stained fungal material) and there is some staining beyond the edge of the lesion (**A**, **B**). Conidiophores and conidiophore initials (▲) characteristically emerge from the stomata (**s**) (**B**, **C**). Note that conidia are not present because they were dislodged during the process of clearing and staining of the leaf. Leaf cleared 5 days after inoculation. Bars = 200 µm (**A**) and 100 µm (**B**, **C**).

Coomassie Brilliant Blue G did not stain the leaf tissue, and only stained the fungal material. Fungal hyphae were therefore easily discriminated from the leaf tissue: the

more intensely stained areas contained denser fungal growth, making it possible to determine where and to what extent the fungus had invaded the leaf tissue (Fig. 3.13A).

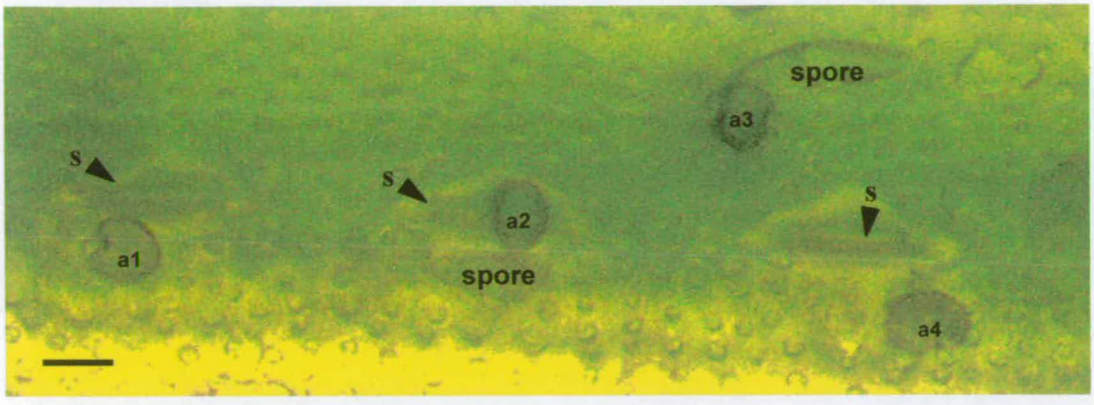

Figure 3.14: Differentiated germlings on rice leaves 1 day post inoculation. Note that appressoria are formed near (**a1**, **a3**, **a4**) or over (**a2**) the stomatal complex (**s**). Also note that the spore that produced appressorium (**a4**) is not within the field of view. Stained with $DIOC_6$ Imaged with a combination of fluorescence and transmitted light. Bar = 10 µm.

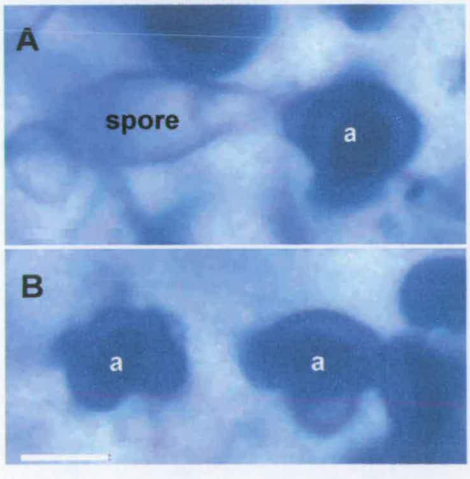

Figure 3.15: Examples of (**A**) a differentiated germling on the rice leaf, and (**B**) two appressoria (**a**) that are irregular in shape, note that this seemed to be determined by the surrounding leaf papillae on a rice leaf. Imaged 1 day post inoculation. Stained with Coomassie Brilliant Blue G-stained Bar = 5 µm.

The lesion edge was defined by a brown necrotic line, within which there was strong staining due to intense fungal growth (Figs. 3.12A, 3.13A,B). The external features of 1–2 day old lesions were examined. The central area of the lesion was comprised

of germ tubes, appressoria and hyphae, and some germ tubes appeared to have developed into vegetative hyphae rather than forming appressoria. Germ tubes also formed appressoria between papillae in positions that required direct penetration through the plant cuticle by the infection peg (Figs. 3.14, 3.15). Germ tubes were often observed to emerge on the side of the spore closest to a stoma (Fig. 3.14). There was evidence that germ tubes grew towards stomatal complexes and in some cases the germ tubes appeared to have directly penetrated the leaf via the stomatal aperture without forming an appressorium (data not shown). The appressoria on rice leaves were not characteristically smooth and round as observed on artificial substrata but were often irregular in shape (e.g. Fig. 3.2 cf. 3.15). This difference seemed to be determined by the surrounding leaf papillae.

Internal hyphae were assessed in older (5 day) lesions. They were primarily within the area bounded by the brown necrotic line, with some hyphae and conidiophores present beyond this region (Fig. 3.13A). Although most conidia had been dislodged from the conidiophores during the process of clearing the leaf of pigmentation, and during staining, conidiophores and conidiophore initials were clearly visible and primarily arose from the leaf in rows that corresponded directly to the line of stomata (Figs. 3.13C, 3.16A,B). Generally 1–3 conidiophores emerged from one stoma (Figs. 3.13C, 3.16B). The internal hyphae were often densely stained around the stomatal complex, as compared to the surrounding leaf tissue, and in such cases there was often evidence that the hyphae had grown towards the stoma through the leaf tissue (Fig. 3.16C). In older infected leaves (>14 d), conidiophores appeared to be produced all over the lesion from the mass of external fungal hyphae (Fig. 3.12B).

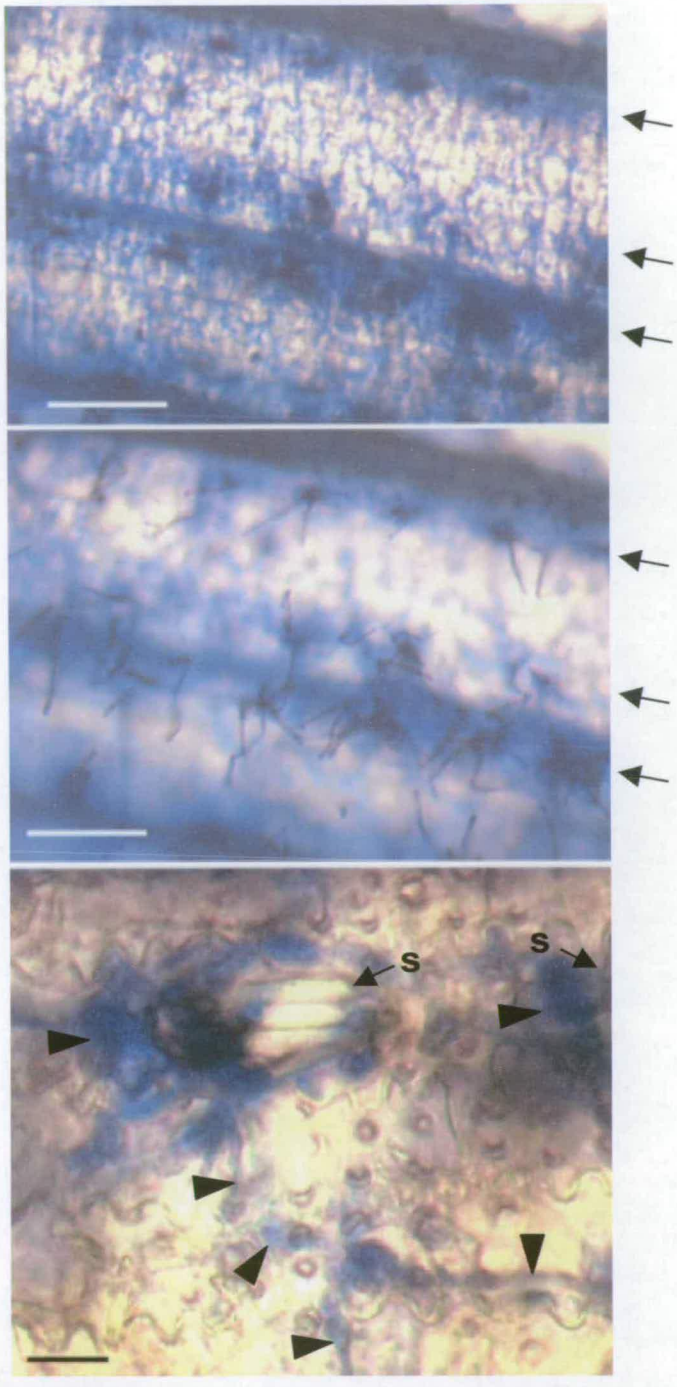

Figure 3.16: A lesion in a cleared rice leaf stained with Coomassie Brilliant Blue G at different magnifications. (**A**) and (**B**) show the same area of the same rice leaf, but at different focal planes. Note that the conidiophores/conidiophore initials emerge from the stoma, which form lines (→). (**C**) Internal hyphae (▲) are stained blue within the rice leaf showing that fungal growth is more dense around the stomatal complex (**s**) and that hyphae within the leaf tissue appear to have grown towards the stomatal complex. Leaf cleared 5 days after inoculation. Bars = 50 (**A** and **B**) and 10 μm (**C**).

3.2.7 Analysis of germ tube growth rate

During DIC and SEM imaging it was noted that either one or two conidial cells germinate during the first 3–4 h post hydration, and that when two germ tubes were produced there was a time lag between their emergence. During the first 3 h post hydration, spores can therefore be classified into two groups, (a) type α: those that produce only one germ tube (GT^{α}), and (b) type β: those that produce two germ tubes sequentially ($GT^{\beta 1}$ and $GT^{\beta 2}$). Because this occurs during the period selected in which to analyse germination in more detail (See Section 3.2.3), the timing of germ tube emergence and the rates of germ tube extension were analysed during the first 3 h post hydration (see Section 2.11).

Although approximately one third of the conidial population are of type β, the sample size for these spores is low because in order to minimise measurement errors spores had to be excluded from the analysis if it was not possible to measure both germ tubes accurately (e.g. if one germ tube grew at an extreme angle). Occasionally (<5%), newly emerged germ tubes were aborted, after which a second germ tube rapidly emerged from a different cell. As it was not possible to measure the growth rate of the $GT^{\beta 1}$, these germlings were not included in the analysis.

Growth was characterized for all germ tubes (GT^{α}, $GT^{\beta 1}$ and $GT^{\beta 2}$) by a period of linear increase during which the growth rate was at a maximum. The growth rate was measured during this period and an approximate time of germ tube emergence was estimated by extrapolation of the gradient through the x-axis. It should be noted that although not evident in the data, a slight time lag might be expected in the initial stage of germ tube emergence, and that this is not accounted for in the x-axis intersect calculation. The results are shown in Table 3.3.

The mean growth rate of GT^{α} was greater than that of both $GT^{\beta 1}$ (Students two-tailed t-test, $p = 0.005$, $n = 17, 9$) and $GT^{\beta 2}$ (Students two-tailed t-test, $p = 0.008$, $n = 17, 9$). There was no evidence to suggest that $GT^{\beta 1}$ and $GT^{\beta 2}$ grew at different rates (paired t-test, $p = 0.61$, $n = 9$), (Table 3.3).

Germ tube category	Growth rate ($\mu m.min^{-1}$)	Estimated emergence time (min post hydration)	n
GT^{α}	0.40 ± 0.04	78 ± 16	17
$GT^{\beta 1}$	0.33 ± 0.06	65 ± 14	9
$GT^{\beta 2}$	0.31 ± 0.08	154 ± 54	9

Table 3.3: Mean germ tube growth rates and calculated times of germ tube emergence for conidia which either produce only one germ tube (GT^{α}) or 2 germ tubes ($GT^{\beta 1}$ and $GT^{\beta 2}$) within the first 3 h post hydration. Abbrev. n (number of spores analysed).

All the spores analysed germinated from either the apical or basal cells. The cells from which the GT^{α} and $GT^{\beta 1}$ germ tubes emerged were compared in order to assess whether the observed difference in growth rate was attributable to a difference in the pattern of germination. Approximately 1/3 of the spores produced germ tubes from the B-cell and no detectable difference was found between GT^{α} and $GT^{\beta 1}$ when the ratio of A:B-cell germination was examined ($\chi^2 = 0.69$, $p = 0.40$, 1 d.f.).

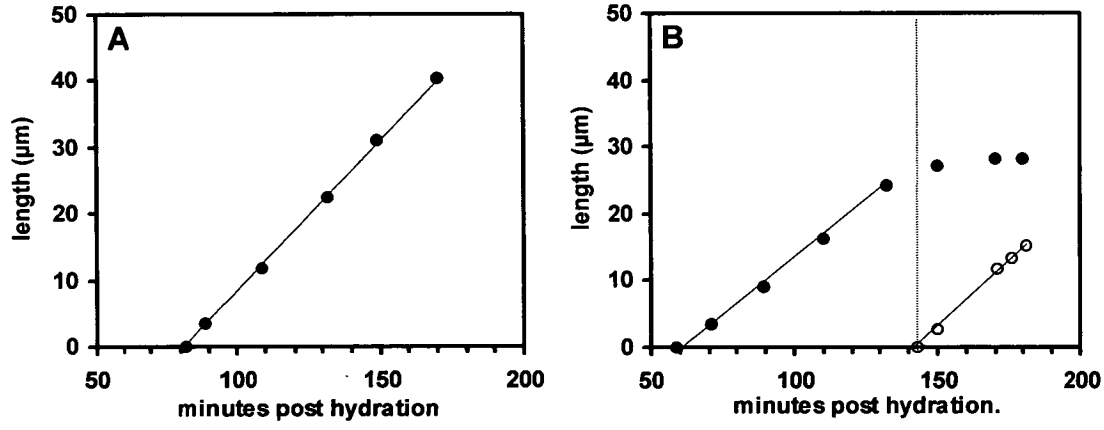

Figure 3.17: Germ tube growth on detCS. Each graph shows data for a single conidium and each data series represents a single germ tube. **(A)** Germ tubes produced by spores that only produce one germ tube (type α) often grow with a constant rate of extension during the first 3 h post hydration. **(B)** Some spores produce two germ tubes (type β) and the second germ tube ($GT^{\beta 2}$) commonly emerges either when the $GT^{\beta 1}$ growth rate begins to slow, or after it commences hook formation (and so extension slows).

There was considerable variation in the time of emergence within all three germ tube categories, the most variable being $GT^{\beta 2}$ which emerged after a mean time of 154 ± 54 min post hydration. The $GT^{\beta 1}$ category had a significantly earlier mean emergence time than that of the GT^{α} category (Students two-tailed t-test, n = 17, 9;

$p = 0.04$). The $GT^{\beta 2}$ category had a mean emergence time of 89 min later than the $GT^{\beta 1}$ (Students two-tailed t-test, $p = 0.0004$, $n = 9$) and 76 min later than the GT^{α} category (Students two-tailed t-test, $p = 0.0026$, $n = 9, 17$).

During the 3h observation period, the GT^{α} category, (1) began to differentiate (evidenced by swelling of the germ tube tip followed by hook formation) at 25 ± 1.1 μm ($n = 5$), (2) continued to grow at the same rate, reaching lengths of up to 50 μm after 3 h (varying depending on the exact time of germ tube emergence), (Fig. 3.17A), or (3) began to slow in growth rate. The $GT^{\beta 2}$ category were observed to emerge when the $GT^{\beta 1}$ was >10 μm in length (21 ± 9.7 μm, $n = 6$), and typically after the growth rate of $GT^{\beta 1}$ had slowed, or sometimes after $GT^{\beta 1}$ had begun to form an appressorium (Fig. 3.17B).

3.2.8 A method for selectively killing conidial cells

A technique to selectively kill conidial cells was developed utilising the confocal microscope laser (Section 2.14), and it proved possible to kill any single cell or a combination of cells within a conidium (Fig. 3.18).

Initial attempts to kill cells by laser irradiation alone gave highly variable results; irradiated cells often germinated, being non-fluorescent when the dead-cell stain propidium iodide (PI) was added after 21 h post hydration. When the experiment was repeated in the presence of PI from 5 min post hydration, irradiated cells were visibly dead, appearing granular and slightly pink when viewed by bright field light microscopy. These cells were never observed to germinate, even after 26 h post hydration, and those spores in which all 3 cells were killed in this manner never germinated. Thus, it was possible to use this physical change as a marker of cell death. This meant that that it was not necessary to irradiate the spore with the confocal laser again until the end of the experiment (>21 h post hydration), and that the remaining live cells were not directly exposed to the confocal laser until that time.

It was found that cells were killed most easily after long post hydration intervals and so conidial cells were irradiated after at least 15 min post hydration. It was also found that the A- and B-cells were easier to kill than the M-cell. For all cells, it was important that the septum was not exposed to irradiation as this resulted in the death of the neighbouring cell. Live non-targeted cells exhibited a low level of fluorescence when incubated in the presence of PI. The morphological appearance of live cells (those that were not targeted) did not differ from no-dye control spores, with the exception that when the adjacent cell had been targeted the septum was often convex, and that this effect was most noticeable when the M-cell was killed (Fig 3.18A).

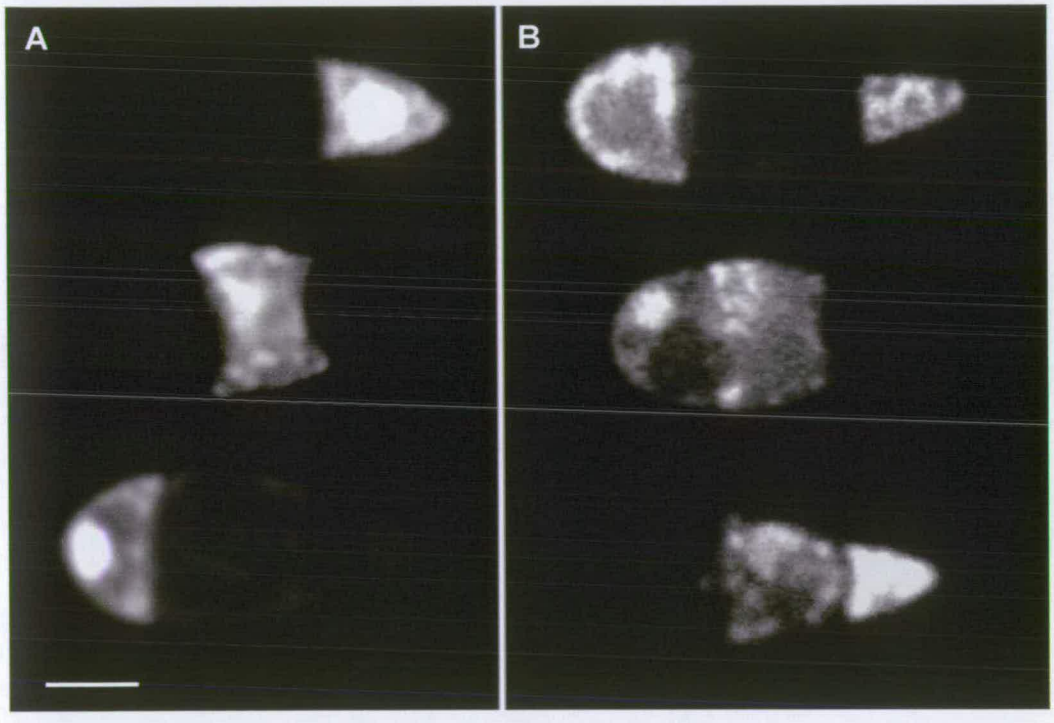

Figure 3.18: Confocal images of conidia in which either (**A**) single conidial cells, or (**B**) two conidial cells have been killed by the laser ablation method. The cells are stained with propidium iodide; the fluorescent cells are dead, and the nonfluorescent are alive. Note the convex shape of the septa when only the middle cell is killed (**A**). Images collected at 30–40 min after irradiation. x40 objective used. Bar = 5µm.

Cell death did not visibly occur immediately after irradiation. It was found that by increasing either the number of laser scans or the dye concentration, the target cell would die more rapidly. However, this also increased the likelihood that neighbouring (non-target) cells would die. Therefore, even with optimised dye and

A

		% germinated per germination pattern							number germinated	total no. spores	% germinated
		A-only	M-only	B-only	A & M	M & B	A & B	ALL			
	none	27	0	12	0	0	62	0	379	384	99
cells killed	A		0	100		0			10	10	100
	M	22		11			67		9	10	90
	B	100	0		0				14	15	93
	A+M			100					5	5	100
	M + B	100							4	5	80
	A + B		0						0	7	0

B

		% differentiated per differentiation pattern							number differentiated	total no. germlings	% differentiation
		A-only	M-only	B-only	A & M	M & B	A & B	ALL			
	none	69	0	31	0	0	1	0	353	379	93
cells killed	A		0	100		0			10	10	100
	M	50		25			25		8	9	89
	B	100	0		0				10	14	71
	A+M			100					4	5	80
	M + B	100							1	4	25
	A + B		0						0	7	0

Table 3.4: Percentage occurrence of (**A**) germination patterns and (**B**) differentiation patterns in spores subjected to cell-specific laser ablation. In (**A**) germination patterns for each laser ablation category ("cells killed") are given as percentages of the total number of spores in that category. In (**B**) the percentage differentiation values relates only to germinated spores. Note that it is possible for a spore to germinate from two cells, but to differentiate from only one; for example a spore may exhibit an "A+B" germination pattern and an "A-only" differentiation pattern.

laser conditions, cells sometimes did not die, took varying times to die, or non-targeted cells died. This variation was controlled for by scoring conidia for live/dead cells status at >30 min after irradiation: only those spores in which only the targeted cell had died were included in the analysis. Similarly, if any additional cells had died after >21 h post hydration, those spores were not included in the analysis. The success rate (i.e. the percentage of spores in which only the targeted cells were dead at 21 h post hydration) was <33% depending on which, and how cells were targeted. In this manner it proved possible to define how many cells were alive during the production of germ tube(s) and subsequent differentiation. Live cells had often internalized PI at a low level by this time but dead cells were easily distinguished by the intensity and general distribution of PI fluorescence.

Controls were performed either in the presence or absence of PI and in all cases maximum germination was >99% and maximum differentiation was >90%. There was no evidence that the presence of the dye affected the patterns of germination (A:B-cell germination) or that the germ tube growth rate was affected (0.33 ± 0.6 μm.min^{-1}, n = 5). The control data was therefore pooled (Table 3.4A,B).

3.2.8.1 Single cell targets

It was possible to kill any individual conidial cell (Fig. 3.18A, also see Fig. 2.4 in Section 2.14). Compared with the control data, there was no evidence that the percentage germination of the conidial population was affected by selectively killing any individual conidial cell (Fig. 3.19A, Tables 3.4A,B). Killing the B-cell resulted in 100% A-cell germination, and killing the A-cell resulted in 100% B-cell germination. The M-cell was not observed to germinate in this experiment and killing it did not appear to influence the ratio of A:B:A+B cell germination (Table 3.4A).

The frequency of cell differentiation in germinated conidia spores is shown in Table 3.4B. It should be noted that the data given relate to the differentiation pattern only. For example a spore germinated from both A- and B-cells (A+B) might only differentiate from the A-cell and thus be shown in the 'A-only' column of Table 3.4B.

The ratio of A:B:A+B differentiation in the control was 69:31:1 (Table 3.4B). When the A-cell was killed, 100% of germlings differentiated from the B-cell (Fig. 3.19A). When the B-cell was killed, 100% of the germlings differentiated from the A-cell (Fig. 3.19C). The largest change in the pattern of differentiation was observed when the M-cell was killed. The A+B pattern was 1 % in the control, and increased to 25 % (Fig. 3.19B).

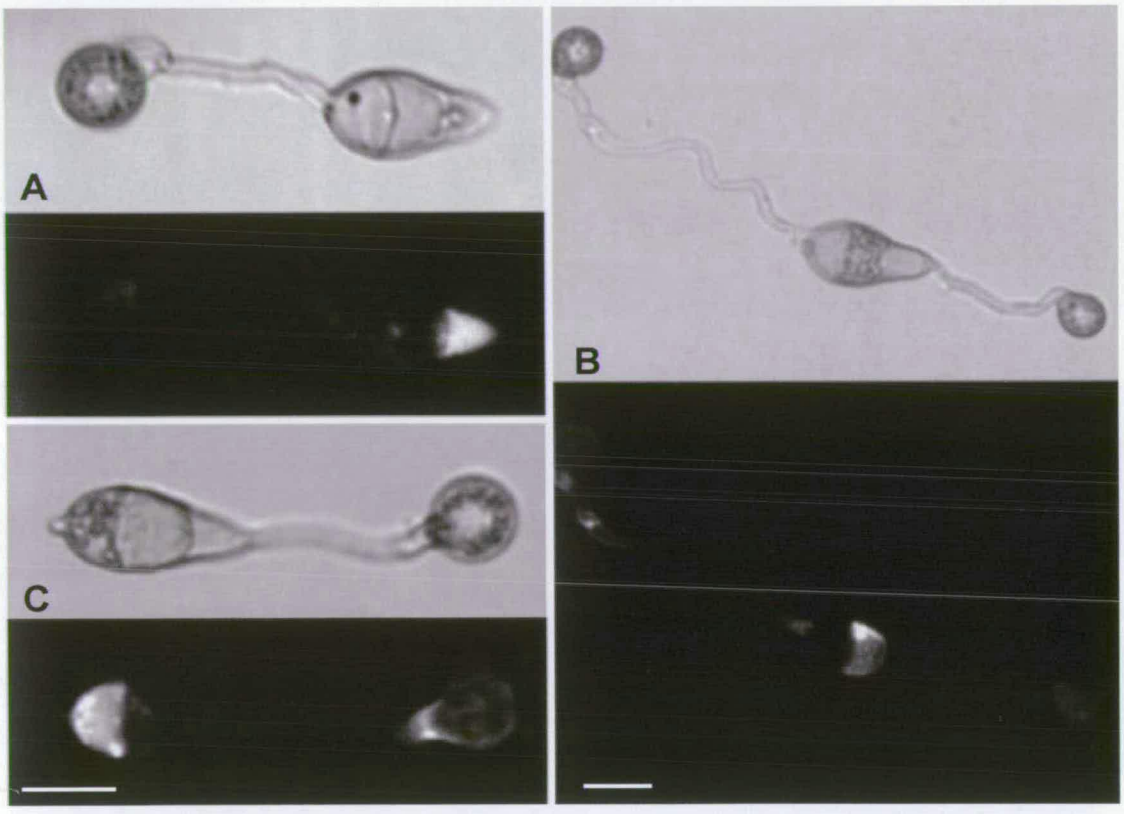

Figure 3.19: Confocal images of conidia after >21 h post hydration, in which either the (**A**) apical, (**B**) middle or (**C**) basal cell was killed between 15–30 min post hydration by laser ablation. Note that all conidia have formed appressoria. The cells are stained with propidium iodide; the brightly fluorescent cells are dead, and the nonfluorescent, and faintly fluorescent (e.g. appressoria) are alive. x40 objective used. Bars = 10 µm.

3.2.8.2 Double cell targets

Experiments were performed in which two cells within a single conidium were killed (see Fig. 3.18B, also see Fig 2.4 in Section 2.14). Killing two cells proved to be more difficult than killing a single cell, especially the A+B cell target. In such cases, all three conidial cells were often dead when assessed at either 30 min after irradiation, or over 21 h post hydration. This meant that during the study it was only possible to

collect small sample sizes for each cell category. The results are shown in Table 3.4A,B.

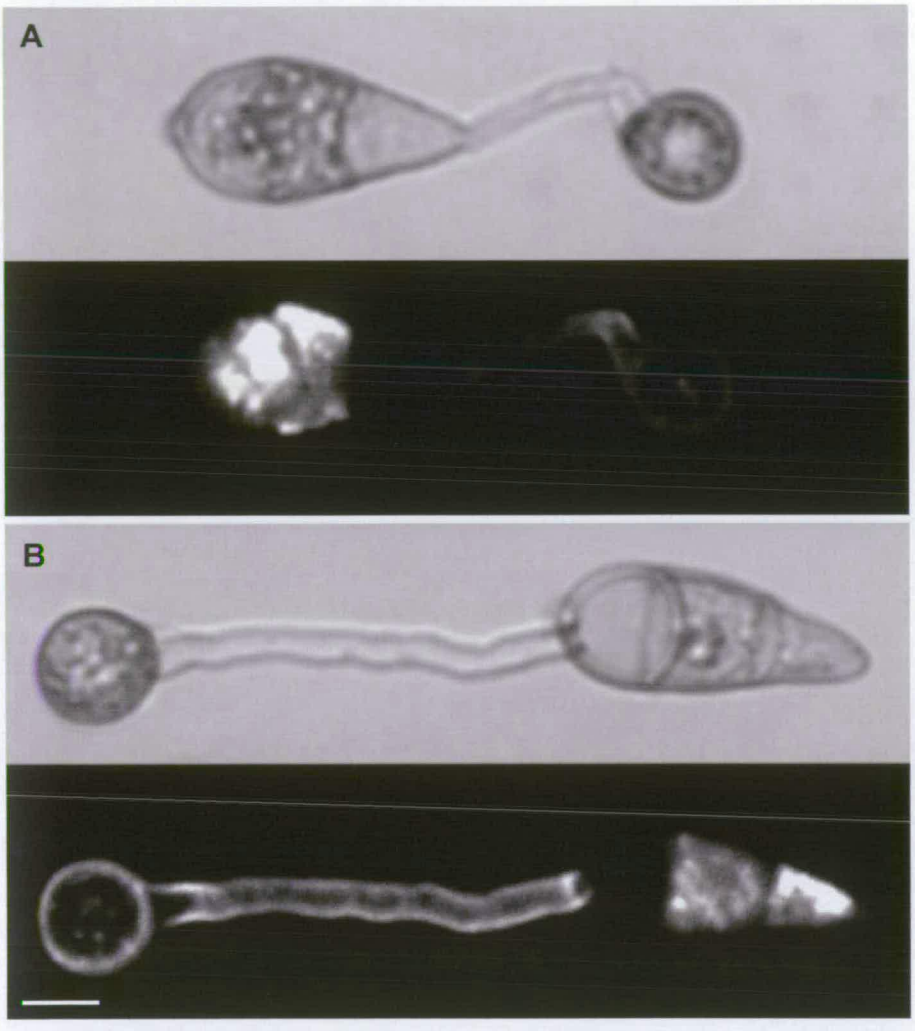

Figure 3.20: Confocal images of conidia after >21 h post hydration, in which either the middle and basal (**A**), or the apical and middle (**B**) cell were killed between 15–30 min post hydration by a laser ablation. In each case the remaining live conidial cell has germinated and formed an appressorium. The cells are stained with propidium iodide; the brightly fluorescent cells are dead, and the nonfluorescent, and faintly fluorescent (e.g. appressoria) are alive. x40 objective used. Bar = 5 µm.

There was no evidence that killing A+M or M+B cells attenuated the percentage germination of the spore population. However, killing A+B cells prevented germination, even though the M-cells looked healthy and were not stained by PI (Fig. 3.18B). It should be noted that there was no evidence that this treatment affected M-cell germination (Table 3.4A). It was possible for spores in which either the A+M or M+B cells were killed, to differentiate (Fig. 3.20), but there was some

evidence that A-cell germ tubes (M+B killed) were less able to differentiate than the B-cell (A+M killed) (Table 3.4B).

3.3 DISCUSSION

3.3.1 The influence of artificial substrata on germination and differentiation

The results described in this chapter indicate that germination in *M. grisea* is not dependent on the properties of the substratum. Flavanoids are produced by plants as both defence and survival compounds and there is evidence that they inhibit germination in *M. grisea* conidia (Padmavati *et al.*, 1997). However, there was no difference between the rice leaf and detCS with respect to the mean maximum, timing and rate of germination.

Hydrophobicity has been previously reported to influence differentiation in *M. grisea* and in general the data presented here provide further support for this hypothesis (Uchiyama & Okuyama, 1990; Lee & Dean, 1993; Jelitto *et al.*, 1994; Xiao, *et al.*, 1994b; Dean *et al.*, 1996; Gilbert *et al.*, 1996). Differentiation was high on the rice leaf and on Teflon™, both of which are highly hydrophobic; rice leaves are coated with a waxy cuticle (Fig. 3.7C) and have a contact angle of 170°, making their surface extremely hydrophobic, and Teflon™ has a contact angle of 90–130° making it hydrophobic but less so than the rice leaf (Talbot, 1995). Differentiation on detCS, which were observed to be less hydrophobic than the rice leaf, was ~1/3 of that on the rice leaf, and on heat-treated CS, which were the most hydrophilic substratum tested, differentiation was <1%.

Silanised glass is highly hydrophobic (Kuo & Hoch, 1996) and in this study the silanised CS appeared to be more hydrophobic than Teflon™. It was found that silanised CS were poor at inducing differentiation, producing long germ tubes compared to those observed on Teflon™ and the rice leaf (previously quantified; Jelitto *et al.*, 1994). This raises a question about the absolute degree of

hydrophobicity required for differentiation; and whether an artificial surface can be too hydrophobic. It has been proposed that either hydrophobicity or cutin monomers alone are sufficient to induce differentiation in *M. grisea* (Gilbert *et al.*, 1996; DeZwaan *et al.*, 1999). It is possible that the high rate of appressorium formation observed on the highly hydrophobic rice leaf is partly induced by components of the host surface, such as wax components (Kolattukudy, 1980). Alternatively, the fungus might be able to alter the physical properties of the rice leaf making it less hydrophobic. This could be via the production of extracellular enzymes, and although there is little evidence for the production of extracellular enzymes by *M. grisea*, a gene encoding cutinase has been isolated (Sweigard *et al.*, 1992a,b).

3.3.2 Detergent washed cover slips as a suitable artificial substratum for *in vitro* analysis of conidial germination

Detergent-washed CS were chosen as the substratum most suitable for subsequent studies on germination. Both maximum germination and the timing of germination on detCS are comparable to those on the rice leaf. Furthermore, the detCS are optically suitable for microscopy, consistent with respect to surface properties, and easily prepared. Maximum differentiation was attenuated and delayed on detCS compared to the rice leaf. Whether features of germination differ in germ tubes that are able to differentiate as compared to those that are not is unknown, but detCS are inductive and this means that at least a proportion of the conidia are able to differentiate.

Germling morphology was very similar on rice leaves and detCS. The main differences are that conidia and germ tubes associate more closely with the substratum on the detCS than on the rice leaf, and that on detCS germ tubes tend to be straighter; presumably because they do not have to navigate around the rice surface microtopography. Differentiated germ tubes were generally longer on detCS, which is consistent with previous findings (Jelitto *et al.*, 1994) and the appressoria tended to be more regular in shape on the detCS.

3.3.3 Are conidia able to germinate in the absence of a substratum?

Hanging drop experiments have demonstrated that *M. grisea* conidia do not require contact with a surface in order to germinate (see Table 1.2 for references). The droplets of inocula preserved here by LTSEM contained germlings on their surfaces, which provides further support for these findings; although it is possible that surface tension at the air/water interface could serve as a substratum, permitting germination. Lee & Dean (1993) reported that either a surface or nutrients were required for germination, but later studies reported that a surface was not a prerequisite (Gilbert *et al.*, 1996). The timing and rate of germination was not recorded by these authors. Weintraub *et al.* (1958) reported that maximum germination was unaffected but that the rate of germination was faster when spores were germinated on 1% agar containing rice waxes or liquid collected from leaf guttation, compared to 1% agar alone. It is possible that the lack of a hard substratum delays germination and that the presence of host chemicals (e.g. hydrophobic components) overrides this inhibition.

3.3.4 Do ungerminated conidia receive signals from the host?

Some spores of fungal pathogens respond to signals on making contact with a surface; e.g. *Uncinuliella australiana* forms an adhesion pad at the spore substratum interface (Mims *et al.*, 1995), and the reticulate network which ornaments the spores of *Erisyphe graminis* becomes globose and enzymes are produced (Kunoh *et al.*, 1988; Nicholson *et al.*, 1988). The region of the spore from which the germ tube emerges might be determined by perception of the host surface by the ungerminated spore. For example, in the conidia of *Botrytis squamosa* the germ tube emerges closest to the anticlinal wall junctions on both host leaves and leaf replicas, and uredospore germ tubes have been reported to commonly emerge from germ pores in close proximity to the leaf or artificial surface (Clark & Lorbeer, 1976; Wynn & Staples, 1981; Read *et al.*, 1992b). To date there is no evidence that the ungerminated conidia of *M. grisea* receive signals from the host; germination does not require a solid surface (see Section 3.3.3), and STM is not produced by conidia in response to making contact with the host surface (Hamer *et al.*, 1988; Howard, 1994). It has been proposed that mucilage produced by the conidia of *Blumeria graminis* serves to guide the germ tube to the substratum (Carver *et al.*, 1999). The conidia of *M. grisea* do not

produce germ tubes exclusively from the tip, so although STM might aid surface perception by a germ tube produced at the tip of the A-cell, this mechanism does not account for how other germ tubes locate the surface.

Although *M. grisea* conidia do not have germ pores, germ tubes do not emerge randomly. They were shown here to characteristically emerge from the region surrounding either the B-cell stalk or close to the A-cell tip, and therefore at some distance from the septum (Section 3.2.5.3). Furthermore, germ tubes generally emerged from the spore in a region that is not in direct contact with a solid surface, and rarely on the side of the conidium opposite to the substratum. This suggests that the conidium senses the presence of a surface, but how this is achieved is unknown, and the area of the spore in direct contact with the host can be small, as spores are most commonly supported by the leaf papillae.

3.3.5 Do germ tubes exhibit directional growth?

Although germination does not require a surface, the germ tube does sense the presence of a surface, as differentiation of the germ tube cannot occur in the absence of one (see Howard & Valent, 1996). Host signals such as surface hydrophobicity, leaf wax components and surface hardness are therefore important for the induction of germ tube differentiation but there is no evidence from the published literature that germ tubes of *M. grisea* exhibit directional growth (Howard & Valent, 1996).

In this study it was observed that having emerged from the conidium, the germ tube grew towards the substratum, during which period it was not in contact with the host surface, and thus unable to sense physical surface cues. The ability of a germ tube to locate the surface is important because the spore cannot infect the host without making contact. The mechanism by which the germ tube locates the host surface is unclear. It is unlikely to be gravitational as infection can occur on either side of the rice leaf, and furthermore, on occasions when a germ tube is produced on the conidial side furthest from the substratum, it is often observed to grow upwards into the solution. The germ tube appears to sense that it is in contact with the substratum because once it is, it generally remains closely associated with it. This is most

pronounced on the flat surface provided by the detCS (e.g. Fig. 3.10A). The characteristically flattened underside of germ tubes and the "nose-down" appearance of the germ tube tip with vesicles localised close to the substratum have been attributed to aiding surface signal perception (Bourett & Howard, 1990). The production of GTM and hydrophobins have been implicated in playing a role in enabling the germ tube to closely associate with the host surface (Xiao *et al.*, 1994a; Talbot *et al.*, 1996; Wessels, 1996, 1997)

The appressoria of *M. grisea* are able to penetrate the cuticle and cell wall of a rice leaf by mechanical force alone (Howard *et al.*, 1991a; Money & Howard, 1996). In the present *in vivo* study it was observed that penetration could occur directly (i.e. physically penetrating the surface into underlying epidermal cells). Thus it seems that the fungus can penetrate anywhere on the host surface equally well, and yet the lengths of differentiated germ tubes observed both here and previously (Jelitto *et al.*, 1994) were found to vary considerably. This might imply that inductive signals are not evenly distributed over the host surface. The question of whether germ tubes exhibit directional growth towards such signals remains unanswered for *M. grisea.* An interesting point in relation to the sensing of the surface signals by the germ tubes of *M. grisea* is that contact between the germ tube and rice leaf surface was often observed in this study to be intermittent due to the presence of wax platelets and papillae (Fig. 3.10A).

Members of the rust fungi are able to locate stomata and differentiate over them, and this is primarily achieved by sensing the topography of the leaf, and can also involve chemical signals (Read *et al.*, 1992b, 1997; Collins & Read, 1997). Some evidence was obtained that germ tubes often exhibited preferential growth towards stomatal complexes (Section 3.2.6). Indeed, the shortest differentiated germ tube observed by SEM analysis was that of a conidium which had attached to the leaf next to a stomatal complex, and produced an appressorium from a barely perceptible germ tube that had emerged on the side closest to the stomatal complex (see Fig 3.11D). These findings suggest that the germ tube receives some sort of signal from the

stomatal complex. Papillae density could serve as a topographical signal as these structures are absent in the region of the stomatal complex. Alternatively, chemical signals could be produced at the stomatal complex. *M. grisea* produces cutinase during infection (Sweigard *et al.*, 1992a,b), and the addition of cutin monomers has been found to induce differentiation (Gilbert *et al.*, 1996; DeZwaan *et al.*, 1999). There is evidence that cutin is exposed on the stomatal lip of broad bean and cowpea leaves (Collins, 1996) and if this were the case on the rice leaf the production of cutinase by *M. grisea* could release signalling molecules from the stoma. The finding that conidiophores primarily emerged from stomatal apertures, and that infection hyphae were often seen to grow in a direct path to the stoma also suggests that *M. grisea* exhibits directional growth (Section 3.2.6). It is possible that a chemical recognition system might be conserved between the different stages of infection.

If the response to cutin monomers, the production of cutinase and the apparent directional growth of the germ tubes observed here are related to the sensing of a stomatal complex by a germ tube, it would not have to represent an exclusive mode of entry into the host. Indeed, mutants unable to produce cutinase are not impaired in their ability to infect the host (Sweigard *et al.*, 1992b). Penetration directly through the stomatal aperture would be advantageous to the fungus because less energy would be required to infect the host, however, penetration in the region of a stomatal complex (but not directly through the aperture) could also be advantageous to the pathogen because the underlying host tissues are different in this region of the leaf and this could aid the subsequent stages of infection.

3.3.6 The requirement for free water for conidial germination

The conidia of *M. grisea* will not germinate in the absence of water and were here observed to collapse when free water was removed. Water is required to develop the extraordinary hydrostatic pressure required to penetrate the cuticle (Howard *et al.*, 1991a), and lesion number has been demonstrated to increase exponentially with increasing duration of free water on the leaf (Moss & Trevathan, 1987). When a droplet of pure water hits a hydrophobic surface it flattens until it reaches its maximum radius, and then retracts rapidly enough to be ejected from the surface

(Klein, 2000). To counteract this effect on the highly hydrophobic rice leaf surface, the conidia of *M. grisea* appear to be able to retain water around themselves.

Hydrophobins are likely candidates for such a mechanism, as they are able to make hydrophobic surfaces wettable (Wessels, 1997). Many fungi secrete them and spores of several species are covered by a hydrophobin-encoded rodlet layer, which has been suggested to play a role in adhesion to the host (Wessels, 1996). In *M. grisea* the MPG1 gene has been shown to encode a hydrophobin that is responsible for the hydrophobic rodlet layer on the conidium surface (Talbot *et al.*, 1996). The rodlets of *M. grisea* are small (~5–7 nm in length) compared to, for example, *Neurospora crassa* (~11–13 nm in length), and in general individual rodlets are believed to be too small to contribute individually to hydrophobicity (Wessels, 1997; Kershaw & Talbot, 1998). The role of the patterning in *M. grisea* is therefore unclear. The spores of *Uromyces viciae-fabae* are also hydrophobic, a property that might be due to surface lipids, hydrophobic proteins such as hydrophobins, or conformation of the spore surface (Clement *et al.*, 1993). Clement *et al.*, (1994) showed that these uredospores are able to retain water around themselves when incubated at 100% relative humidity, and that this occurs prior to the production of ECM. Thus, in addition to the potential roles in adhesion to the surface and perception of inductive surfaces, hydrophobins and perhaps the rodlet patterns they form on the spore surface, might serve to retain free water around the spore on the highly hydrophobic leaf surface.

It has recently been shown that by the addition of low concentrations of polymers to water, it is possible to prevent droplets from bouncing off hydrophobic surfaces by increasing their elongational elasticity (Bergeron *et al.*, 2000). An alternative mechanism by which a droplet might be retained on a hydrophobic surface is by the adherence of polymers to a solid surface, which produces a surface effect through adsorption (Klein, 2000). The conidia of *M. grisea* stick to surfaces very rapidly by STM, and this could have a similar effect. Furthermore, STM could contain polymers in a high enough concentration to act to increase the elongational elasticity of the

water in which the conidia are dispersed. Interestingly, spores of *Pyrenopeziza brassicae* have been reported to alter the surface tension of water (Rawlinson, 1979). Mucilage produced by spores has been assigned the role of adhesion by sticking to the surface physically; it is possible that mucilage serves an additional role involving the retention of water around the spore. The chemical composition of the STM of *M. grisea* has not been published and so this suggestion can only be speculative (Hamer *et al.*, 1988).

3.3.7 Germ tube growth rates before differentiation

Evidence was obtained here for two modes of germination, the conidium either produces one fast growing germ tube or two slightly slower growing germ tubes, produced sequentially (see Section 3.2.7). These differences in growth rate were detectable from the outset, suggesting that the mode of germination could be determined before the emergence of the germ tube.

The slower growth rate might be attributable to the limitation on internal conidial nutrient reserves, such that two faster growing germ tubes cannot be supported. Alternatively, spores that initially produce fast growing germ tubes are perhaps unable to support a further germ tube. The suggestion that internal conidial nutrient reserves could limit the number, and possibly growth rate, of germ tubes is supported by the finding that multiple germ tubes are produced in response to the addition of nutrients to the external medium (Howard, 1994).

In vitro conditions remain favourable for germination and differentiation throughout the pre-penetration stage of the infection cycle. In the natural situation there could be a limited time in which to infect the host, dictated by heat and relative humidity (e.g. spores produced during the night time peak will have a certain number of hours before the sun rises and begins to dry the rice leaves). There are advantages to both modes of germination; a single rapid growing germ tube has the advantage that it can cover large areas of the leaf surface in search of inductive conditions whilst conditions are favourable, whereas a spore which produces two germ tubes at different times, that usually grow in opposite directions (see Fig. 3.3), also optimises

its chance of finding inductive conditions, and by being staggered in time this includes finding optimal environmental conditions. Whether these two modes of germination reflect two true subpopulations with different genotypes, or the degree of phenotypic plasticity within a single conidial population, cannot be determined on the basis of the data reported here.

3.3.8 The requirement of three conidial cells for infection

Laser ablation is a technique in which pulsed ultra-violet irradiation is used to ablate the cell wall and expose the plasma membrane, without the application of degradative enzymes. It has thus been used in conjunction with patch clamping techniques in the study of ion channels in both plants and fungi (e.g. Henricksen *et al.*, 1995; Taylor & Brownlee, 1992; Taylor *et al.*, 1996; Roberts *et al.*, 1997). In this study a technique was developed that utilized laser ablation to selectively kill an entire conidial cell (Section 3.2.8).

An argon laser was used to ablate an entire conidial cell, and propidium iodide (PI) served both as a marker of cell death, and also served to reduce the extent of laser irradiation required to kill a cell. Propidium iodide is a dead-cell dye which stains nucleic acids and is likely to produce highly destructive free-radicals on irradiation. It is only internalized by damaged or dead cells in which the plasma membrane integrity is compromised (Oparka & Read, 1994). The most likely mechanism by which targeted cells died, is one in which laser irradiation stresses the cells sufficiently to allow the dye to enter and kill the cell. The finding that, with the settings used, laser irradiation alone was insufficient to kill a conidial cell suggests that conidia are very resistant during the ungerminated stage of the infection cycle. Conidia are melanised (Chumley & Valent, 1990), a property that might aid their survival under strong UV conditions in the field, and this could explain why they are resistant to electromagnetic radiation.

Targeting the M-cell had no effect on the ratio of A:B:A+B germinated conidia, suggesting that germination by one cell can occur independently of the other cells within the conidium. However, the finding that targeting the A- or B-cell resulted in

100% germination in the B- or A-cell respectively, suggests that communication exists between the conidial cells. The effect on differentiation of killing the M-cell is pronounced: the proportion of spores that differentiate from both the A- and B-cell increases from 1% to 25% (though the sample size was small for the latter). In other words, by removing the M-cell, communication between the two cells is broken down and apical-cell dominance partially overridden. As an appressorium is able to penetrate anywhere on the surface of the rice leaf (Howard *et al.*, 1991a; Money & Howard, 1996), only one is necessary for infection and by preventing other germ tubes from differentiating, the spores resources can then be used to support that appressorium.

Killing two cells was technically more difficult and this meant that the sample size was small. The difference between killing the M-cell only and the A+M or, M+B cells is not clear. However, targeting the A+B cells rendered an interesting result; even when it is the only remaining living cell, the M-cell did not germinate. In light microscope studies the M-cell was observed to germinate in <1% of the conidial population and thus a large sample would be required to ascertain whether killing the A+B cells has any effect on M-cell germination. However, the finding that the M-cell is not stimulated to germinate when isolated suggests that this cell has a different role to the other two conidial cells.

The finding that the A-cell and B-cells are each able to germinate and differentiate in isolation begs the question of why the fungus expends the energy required to produce a three-celled conidium if one cell is sufficient. It is possible that the production of STM is a highly energy-requiring process, making it more efficient to produce multicellular spores. It was observed in this study that germ tubes tend to grow in opposite directions and this provides a self-spacing mechanism; the germ tubes will grow over different regions of the host, increasing the likelihood that one will find inductive conditions and infect the host. However, the formation of an appressorium does not guarantee successful infection of the host. The appressorium must also be capable of generating sufficient turgor pressure to force an infection peg into the

underlying host tissues. Although the appressoria in this experiment were morphologically indistinguishable from those of untreated conidia, it is possible that they were not fully pathogenic. During germination and germ tube growth there is rapid synthesis of glycerol, an osmolyte required for the generation of appressorial turgor (de Jong *et al.*, 1997). Thus, a possible role of the M-cell is as a pool and generator of reserves required for differentiation, such as glycerol.

4. CONFOCAL MICROSCOPY OF ORGANELLE ORGANIZATION AND DYNAMICS DURING GERMINATION

4.1 INTRODUCTION

Our current understanding of fungal spore organelle morphology is heavily reliant on TEM studies, in which the cells are not alive (see Section 1.4). Little is known about the dynamic organization and morphology of organelles during germination. Furthermore, interpretation of TEM data is hampered by a lack of knowledge of the dynamic nature of the organelle in question. The best way to obtain an insight into the behaviour and morphology of organelles during germination is to analyse living cells and record the changes that occur within an individual cell. The **overall objective** of the research described in this chapter was to characterize the dynamic organization and morphology of organelles during germination in living cells.

The technique of confocal microscopy provides a suitable approach for live cell studies. It has a number of advantages, including (Czymmek *et al.*, 1994):

- images are free from out-of-focus blur and thus have a high spatial resolution,
- it is possible to obtain time-courses of living cells loaded with vital fluorescent dyes,
- optical sections can be collected through different planes of the sample and then reconstructed into a 3-dimensional projection of the image.

There is a wide range of single- and dual-wavelength fluorescent dyes available for use with the confocal microscope. In general, dye selectivity has been characterized within animal, plant and (in some cases) yeast cells (Haugland, 1999). Many are reported to be vital dyes (i.e. able to stain living cells without killing them). However, very little is known about the way in which these dyes behave within cells of filamentous fungi, and in particular within fungal spores. The **first aim** of this

study was to select the most suitable dyes for subsequent analysis of organelle organization and dynamics during germination.

Organelle morphology and dynamics might be altered in a stressed or dying cell. To ensure that cells are living and minimally perturbed during analysis by confocal microscopy, a number of factors must be examined including the influence of the dyes used to stain organelles (cytotoxicity), of exposure to the confocal laser (phototoxicity) and any possible effects caused by interactions between these two factors. The **second aim** of this study was to optimise dye concentrations and confocal imaging conditions, to minimise any stress caused to living conidial cells and germlings during the collection of organellar data.

Finally, in order that the results obtained *in vitro* are transferable to the *in vivo* situation, the conidia must be pathogenic. This requires that, in addition to germinating and differentiating, the conidium must ultimately be able to penetrate and infect the host. The **third aim** of this study was to assess whether pathogenicity is compromised in dye-loaded conidia.

4.2 RESULTS

4.2.1 Analysis of organelle organization and dynamics during germination using differential interference contrast light microscopy

The technique of differential interference contrast (DIC) light microscopy was used to image organelles within unstained conidia and germlings, and in particular to follow time-courses of germination of individual conidia. The best results were obtained using x40 and x63 dipping objectives (Table 2.1).

Figure 4.1: Differential interference contrast images of an individual conidium throughout germination. The numbers are min (**A**–**F**) and hours (**G**) post hydration. The spore germinates from the apical cell and that spore tip mucilage (STM) is clearly visible and remains intact throughout germination. The nucleus (n) is only visible in the apical cell. Note that by 14 h (**G**) post hydration the cells are vacuolated (v). Imaged using a x40 dipping objective. Bar = 5 µm.

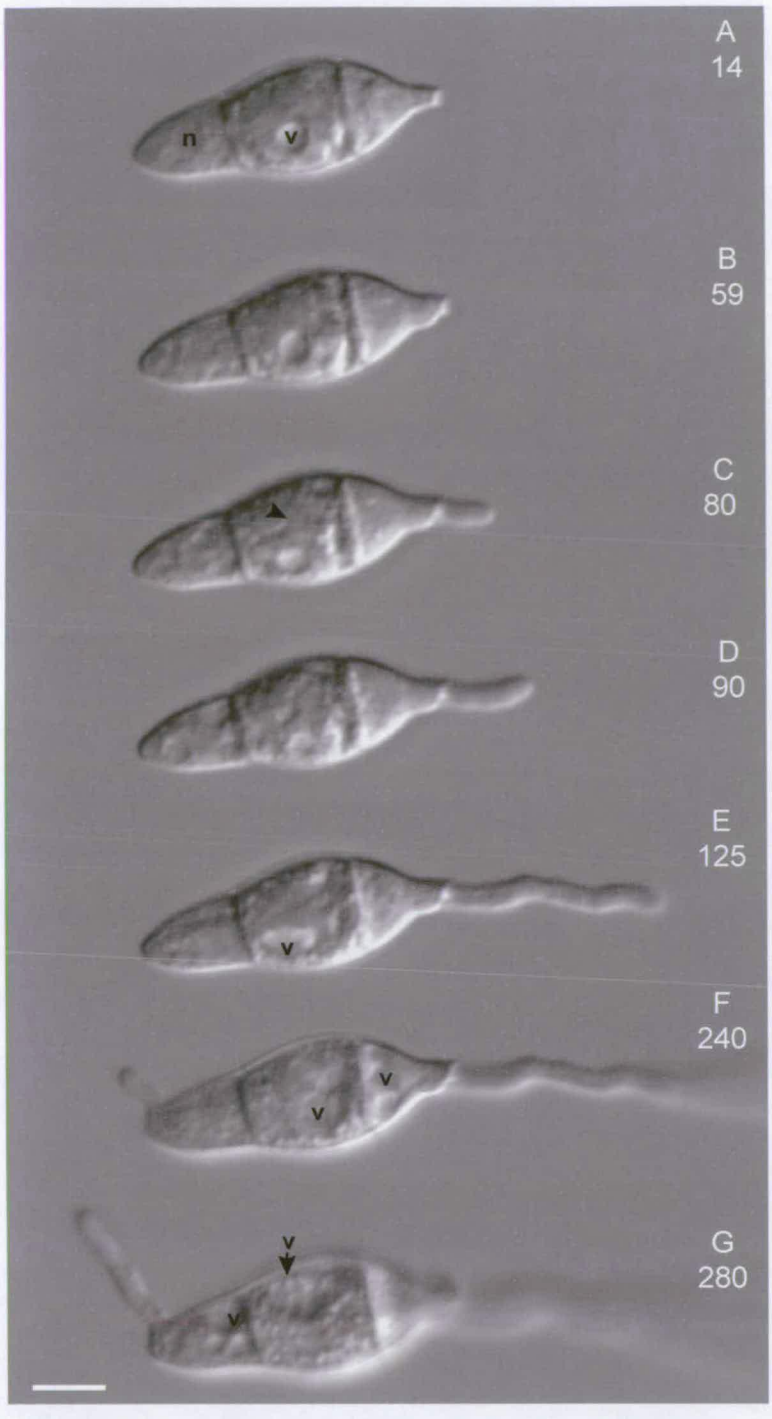

Figure 4.2: Differential interference contrast images of an individual conidium throughout germination. The numbers are min post hydration. Note that the spore initially germinates from the basal cell. Also note that the conidial cells become progressively more vacuolated. At 14 min (**A**), a round vacuole (v) is visible in the middle cell that after 125 min (**E**), appears to fuse with another to form a larger vacuole. By 280 min (**G**), a large vacuole is present in the middle cell. Also note the tubular structure (▲) in the middle cell at 80 min. Imaged using a x40 dipping objective. Bar = 5 μm.

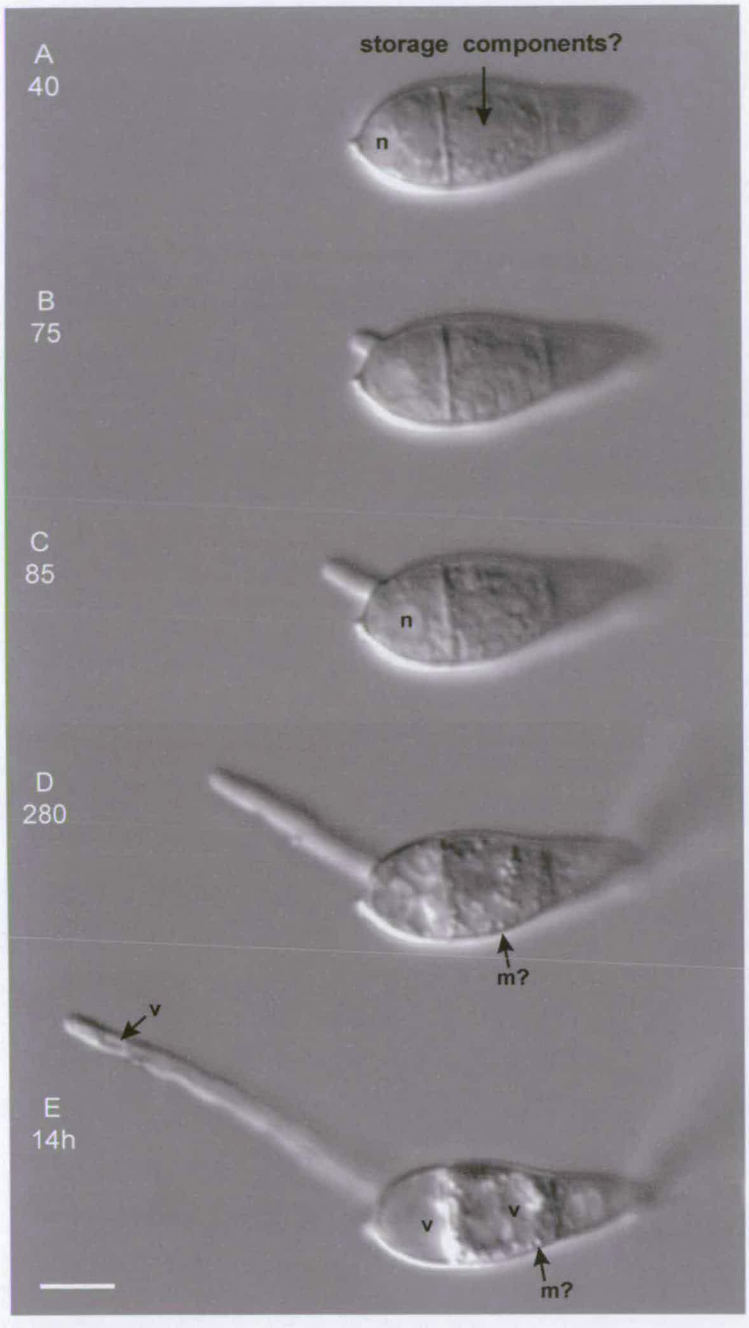

Figure 4.3: Differential interference contrast images of an individual conidium throughout germination. The numbers are min (**A**–**D**) and hours (**E**) post hydration. The spore initially germinates from the basal and then apical cell. The cellular contents become less uniform as germination proceeds; the putative storage components become less obvious and the cells become increasingly vacuolated. At 14 h (**E**), the cells are highly vacuolated and a vacuole is visible within the germ tube (v) of the basal cell. (**A**–**C**) The nucleus (n) in the basal cell moves towards the centre of the cell. Note the small round structures, particularly around the cell periphery, which could be mitochondria (m?). Imaged using a x40 dipping objective. Bar = 5 µm.

Conidia were float-harvested and after 2 min post hydration washed with sterile dH_20 (see Section 2.7.2). The x40 objective was most useful because of its greater depth of

field, which was an advantage because the conidia were not physically disturbed by fine focusing. Using this method it was possible to collect a total of nine time-courses of individual conidia throughout germination. Three representative time-courses are presented in Figs. 4.1, 4.2 and 4.3.

Figure 4.4: Differential interference contrast image of a germling, showing the mucilage associated with the germ tube (GTM). Collected at 2h 10 min post hydration. Imaged using a x40 dipping objective. Bar = 5 μm.

The conidia were attached to the substratum by STM which was clearly visible (Fig. 4.1) and mucilage associated with the germ tube was also apparent (Fig. 4.4). In ungerminated spores, there was initially little movement of subcellular contents. However, they became progressively more dynamic as germination proceeded. Images were collected with exposure times as short as 10 ms, and even with these short times, during the stages of germination that involved germ tube extension (GT_1–GT_3) the images were blurred in some regions, due to the movement of subcellular contents. Spores initially were imaged every 5 min, but this time interval was increased to 15–25 min because there were indications that the conidia were being stressed by the intense illumination required for DIC microscopy; as manifested by the non-linear rate of germ tube extension and by abnormalities in their in physical appearance.

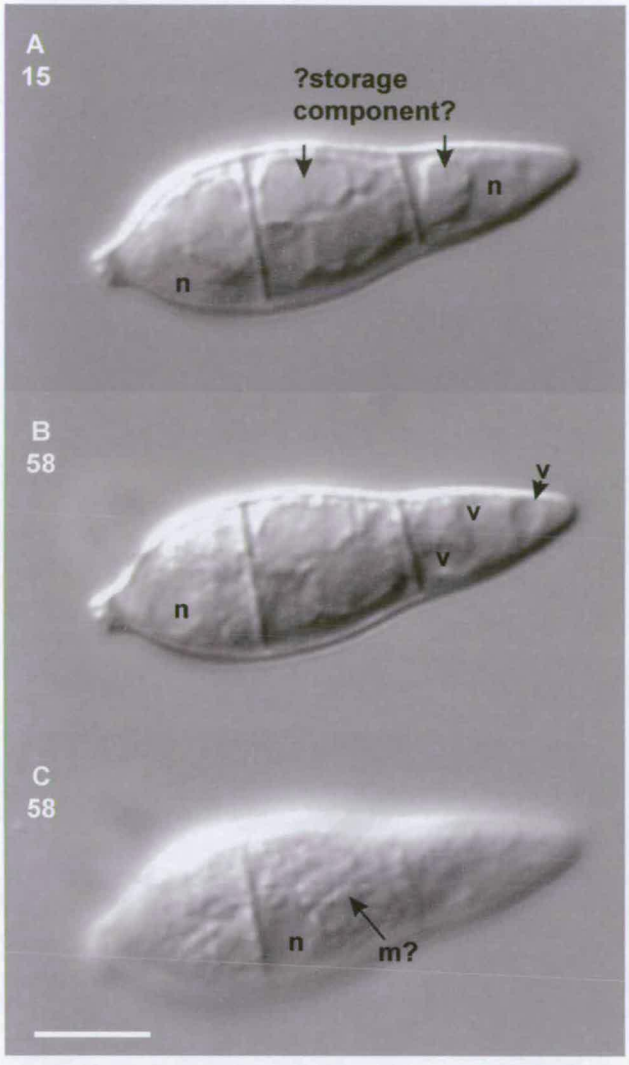

Figure 4.5: Differential interference contrast images of a conidium during germination. (**A**) At 15 min post hydration all 3 cells contain a uniform region of putative storage components and a tubular structure runs through the middle cell. (**B**) By 58 min post hydration there appear to be some small vacuoles (v) present, especially within the apical cell in which a vacuolar compartment is visible in the tip of the cell. Note that the basal cell has germinated. (**C**) This shows the upper focal plane of (**B**) in which there is evidence of elongated structures that could be mitochondria (m). The nuclei (n) are visible within the apical and basal cells (**A**) and the middle cell (**C**). Imaged using a x40 dipping objective. Bar = 5 µm.

A number of the major organelles were putatively identified and their changes in position and morphology were observed during germination. The cellular contents underwent considerable change during germination. Initially ungerminated cells characteristically contained a large uniform region that often had other small cellular components embedded within it. The composition of this uniform region was unclear, although its uniform and static nature suggested some sort of cytoplasmic storage component (e.g. Figs. 4.2A, 4.3A, 4.5A,B).

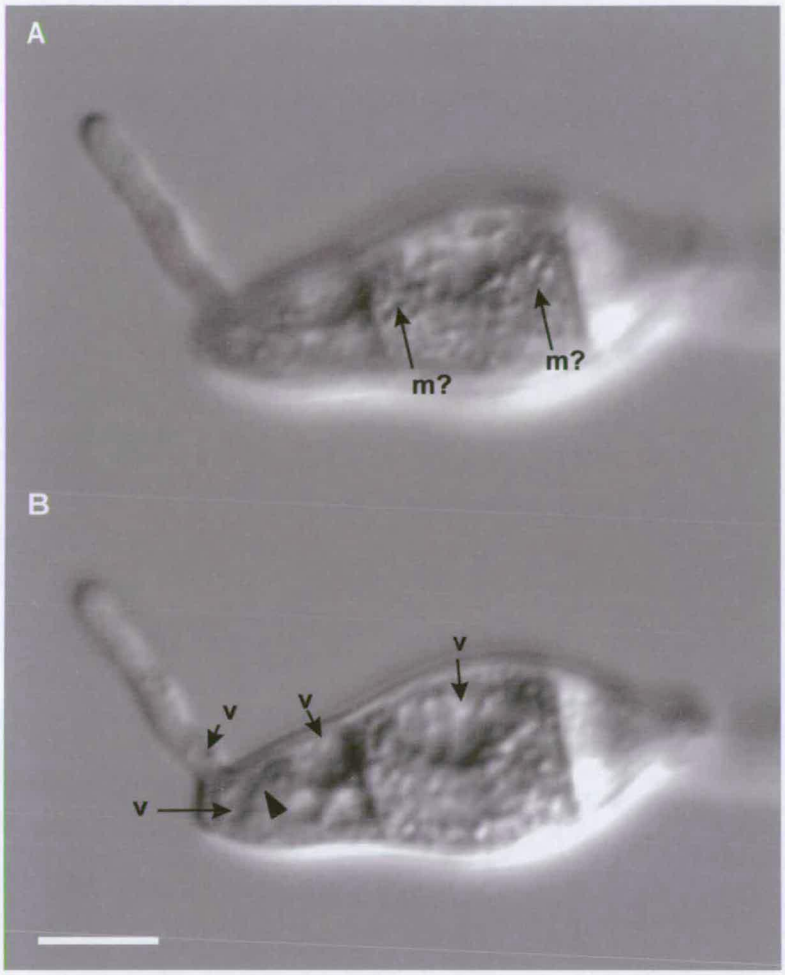

Figure 4.6: Differential interference contrast images of a germling after 4 h 40 min post hydration showing (**A**) that putative mitochondria (m?) are visible in the upper focal plane, and that (**B**) vacuoles (v) are clearly visible; in the apical cell two vacuolar compartments appear to be interconnected by a tubular structure (▲), and the large vacuole in the middle cell appears to be divided by membranes into a number of subcompartments. Please note that this is the same conidium presented in Fig. 4.2. x40 dipping objective. Bar = 5 µm.

The structures embedded within the putative storage components were tentatively identified as components of the vacuolar system. The vacuolar system appeared to become progressively larger as germination proceeded (Figs. 4.1–4.3). With this increase in size, the vacuole became more easily identifiable. There was evidence that small vacuoles fused to form larger vacuoles, although this could also be interpreted as a larger vacuole that moved into and out of the focal plane (Fig. 4.2C–E) and tubular vacuoles appeared to interconnect vacuolar compartments (e.g. Fig. 4.6B). As the germ tube extended (10–20 µm), large vacuoles in the M- and B-cells were present and often appeared to be composed of several subunits (e.g. Figs. 4.6B, 4.7B). The vacuolar system ultimately appeared to occupy most of the

cell, usually by the time that the germ tube had either differentiated or grown very long (e.g. Figs. 4.1G, 4.3E, 4.7). The conidial cytoplasm contained numerous vesicular structures that were highly dynamic and appeared to flow towards, and up, the growing germ tube. Tubular vacuoles were also observed within the germ tube (Fig. 4.3E).

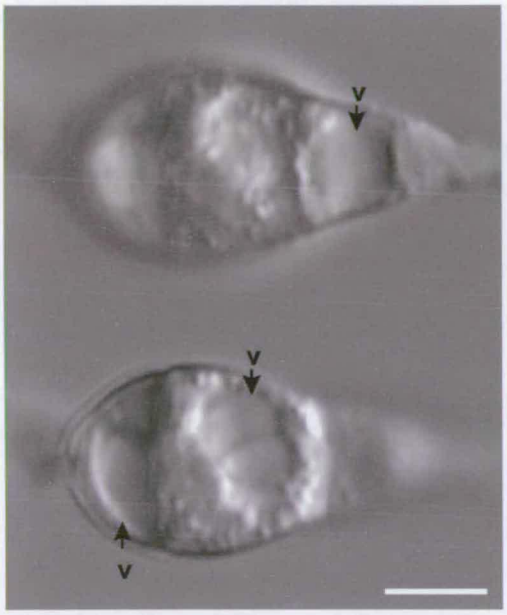

Figure 4.7: Differential interference contrast images of a germling showing two different focal planes of the conidium. The images was collected at 3 h 50 min post hydration and the spore had long (>20 µm) germ tubes from both apical and basal cells. Each cell is highly vacuolated and the middle cell vacuole appears to be composed of several subcompartments. Imaged using a x40 dipping objective. Bar = 5 µm.

The nuclei of ungerminated cells were clearly identifiable and usually appeared to be appressed to the plasma membrane in the M- and B-cells; the B-cell nucleus was usually visible near the stalk (Figs. 4.3, 4.8). The nucleus in the A-cell was usually in the centre of the cell (Figs. 4.1, 4.2A, 4.8). Due to the thickness of the M-cell, the nucleus was often absent from the focal plane (Fig. 4.5).

Nuclei were not very dynamic but were observed to slowly change their position during germination. In the M- and B-cells the nuclei often moved away from the plasma membrane during the period surrounding the emergence of a germ tube. The nucleus in the A-cell appeared to remain more or less centrally positioned but in germlings with very long germ tubes (i.e. greater than the length of the conidium) the

nuclei were sometimes absent from the germinated cell. Furthermore, in differentiated germlings and those with very long germ tubes (>24 h post hydration), the conidial cells commonly appeared to be emptied of their contents (see Figs. 3.3, 3.4 in Section 3.2.4).

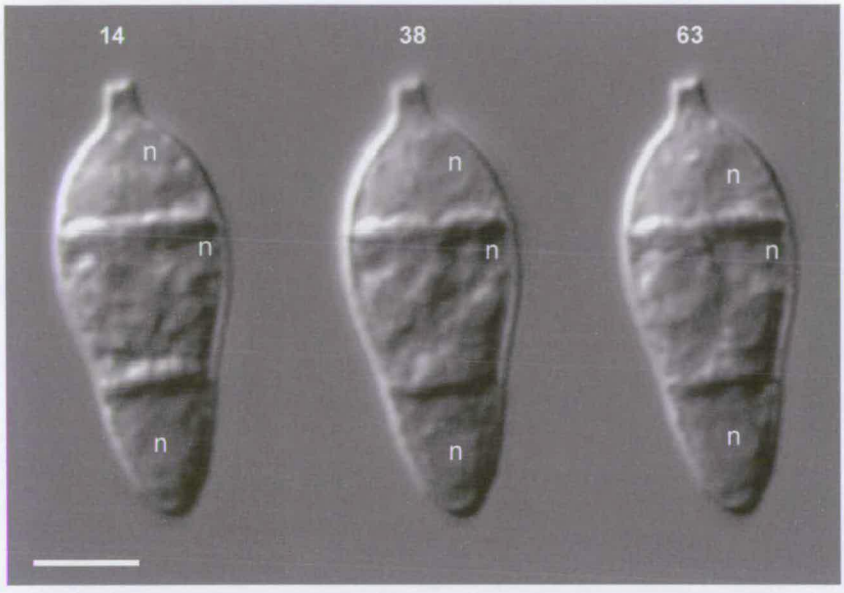

Figure 4.8: Differential interference contrast images of an ungerminated conidium, the numbers are min post hydration. Note that nuclei (n) are visible in each cell and that the basal cell nucleus moves towards the septum. Imaged using a x40 dipping objective. Bar = 5 µm.

Figure 4.9: Differential interference contrast image of a germinated conidium, collected at 60 min post hydration. Note that the image shows an upper focal plane and there are characteristically numerous small structures in this upper region of the conidial cells that might be mitochondria. Bar = 5 µm.

Structures identified as putative mitochondria were observed in the upper focal plane of the conidia, and thus near to the plasma membrane. They appeared to be small and narrow, and on occasions possibly elongated (Figs. 4.3D, 4.5C, 4.6A, 4.9).

4.2.2 Stages of conidial germination

On the basis of the appearance of conidial cells during germination as studied by DIC light microscopy, it was apparent that germlings could be categorised into 5 stages of germination. As germination is asynchronous, occurring over a period of ~3 h (see Fig. 3.1 in Section 3.2.3) and in order that direct comparisons might be made when examining organelle types, morphological stages were defined as follows.

- **UNG** (ungerminated): this is defined as the stage from hydration to the emergence of a germ tube (e.g. Fig. 4.1A).
- **EGT** (emerging germ tube): this is defined as the stage at which the germ tube is as long as it is wide, and marks the time at which polarised growth has commenced (e.g. Fig. 4.1B).
- **GT_1** (germ tube 1): this represents the first ~20 min of germ tube growth, and is defined as the period of growth during which the germ tube is longer than EGT stage but shorter than the cell from which it emerged (6–7 μm), (e.g. Fig. 4.1C).
- **GT_2** (germ tube 2): this represents the subsequent ~45 min of germ tube extension, and is defined as the period of growth during which the germ tube is longer than that in the GT_1 stage but is shorter than the length of the spore (~20 μm). This was chosen because it was found previously that differentiation occurred at mean germ tube lengths of 21–25 μm (Section 3.2.9) and because Jelitto *et al.* (1994) showed that on a range of substrata most differentiated germ tubes were of 1–20 μm in length and that on rice this represented >50% of the germling population (e.g. Fig. 4.1E).
- **GT_3** (germ tube 3): this represents the period of growth when the germ tube is longer than that in the GT_2 stage and can include differentiated germ tubes. (e.g. Figs. 4.1F, 4.3E).

4.2.3 Selection of vital organelle stains for confocal analysis of germination in live conidia

In order to image the organization and dynamics of conidial organelles during germination a range of organellar dyes were screened as suitable stains (see Fig. 2.2, Table 2.2, in Section 2.7). Dyes were initially evaluated on the following criteria:

- appropriate excitation and emission spectra in order that they could be imaged on the CLSM used in this study,
- organelle selectivity,
- rapidity of dye internalization by the conidial cells,
- influence on conidial/germling appearance in the presence of the dye at concentrations required for imaging.

With the exception of SYTO 11 (see Section 4.2.3.1), none of the dyes listed in Table 2.2 affected the physical appearance of conidia or germlings at the concentrations given. However, at higher concentrations (>10 μM) cells became granulated in appearance and germ tube growth slowed and ceased, and in some cases dyes flooded cells, indicating that they were dead.

4.2.3.1 Assessment of nuclear dyes

A range of dyes reported to be live nuclear stains (SYTO 11–16, Acridine Orange and DAPI) were assessed as suitable vital stains to image nuclear distribution and dynamics during germination. The most specific nuclear staining and best internalization into conidial cells was achieved with the SYTO dyes. The SYTO dyes stain DNA:RNA to different extents. Of those tested SYTO 11 and 15 were found to be the most selective for the nuclei, and SYTO 13, 14 and 16 stained both the nuclei and mitochondria.

The dye SYTO 12 occasionally faintly stained nuclei. However, it consistently stained bright cytoplasmic spots of ~0.6–1.0 μm in diameter. There were usually one but sometimes two or three within each conidial cell, commonly separated by ~1.5–2.0 μm. The position of the spots in the cells indicated that they were often associated with the nucleus (Fig. 4.10 cf. Fig. 4.8).

All the SYTO dyes were cytotoxic, and after ~20 min in the dye the conidial cells began to appear granular. There was a general problem staining the nucleus within the M-cell and this was especially difficult in ungerminated spores. Of those SYTO

dyes that stained the nuclei, SYTO 11 was the best internalized dye and so was chosen for subsequent analysis (e.g. Fig. 4.20 in Section 4.2.5.2).

Figure 4.10: Confocal images of two ungerminated conidia showing the bright spots characteristically stained by the nucleic acid stain SYTO 12. Imaged using a x40 dry objective. Bar = 5 μm.

4.2.3.2 Assessment of mitochondrial dyes

A range of potential mitochondrial stains was assessed for imaging mitochondria in conidia during germination. These included DASPMI, Mitotracker™ Green FM, Rhodamine hexyl ester, $DIOC_6$ and Rhodamine 123.

DASPMI and Mitotracker™ Green FM produced diffuse and non-specific staining with some evidence that the former was sequestered into the vacuolar system. Rhodamine hexyl ester and $DIOC_6$ stained the mitochondria after 45 min of incubation in the dye. In addition to staining being slow, the mitochondria were poorly stained in the B- and M-cells with both dyes (e.g. Fig. 4.11A). Rhodamine 123 was rapidly internalized into all 3 conidial cells and exhibited strong selectivity for mitochondria, and was therefore chosen for subsequent analysis (e.g. Fig. 4.24 in Section 4.2.5.3).

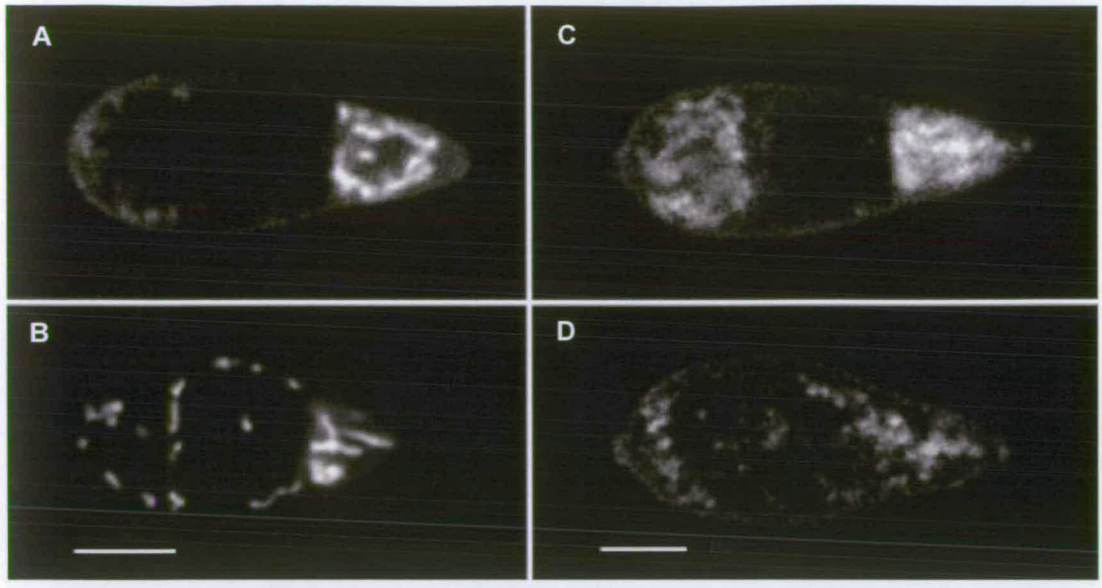

Figure 4.11: Confocal images of four ungerminated conidia stained with (**A**) $DIOC_6$, (**B**) Nile red (**C**) SYTO 13 and, (**D**) SYTO 16. Note stained the mitochondria in (**A**) and to a lesser extent (**B**) are more strongly stained in the apical cells. Imaged using a x40 dry objective. Note that bar in (**B**) applies to (**A**, **C**). Bars = 5 µm.

Five other dyes also stained mitochondria. These were the lipid stain Nile red (Fig. 4.11B), the nucleic acid stains SYTO 13, 14, and 16 (e.g. Fig. 4.11C,D), and the membrane stain FM4-64. Staining of mitochondria by FM4-64 was not as specific as some of the other dyes assessed and the mitochondria took varying times to stain, often doing so after germination. Although this delay in mitochondrial staining meant that the dye could not be used for complete time-courses of germination, it was utilized for imaging mitochondria in the latter stages of germination (e.g. Fig. 4.34 in Section 4.2.5.3).

4.2.3.3 Assessment of vacuolar dyes

A range of potential vacuolar stains were evaluated for imaging the vacuolar system within conidia during germination, including cFDA, cDCFDA, cDFFDA, FUN-1, MDY-64 and FM4-64 (Table 2.2). A common problem with the dyes assessed was that during the early stages of germination, dye uptake was usually low, resulting in diffuse staining. Attempts were made to overcome this by adding the dye at the time of hydration (i.e. the conidia were harvested in dye solution rather than being stained after hydration), but this did not sufficiently improve dye uptake. As germination commenced dye uptake commonly improved and by the GT_2 stage all the dyes evaluated were readily internalized by germlings.

The membrane stains MDY-64 and FM4-64 were also assessed. Both dyes are general membrane stains and so do not exclusively stain the vacuolar membrane. FM4-64 was less phototoxic and produced a brighter signal per μM of dye. However, it took some time until the vacuolar membrane was clearly stained, and as it did not exclusively stain the vacuole membrane it was used here only to analyse the GT_2 and GT_3 stages of germination. The dye MDY-64 was internalized by ungerminated conidia and germlings (Fig. 4.12A,B) but could not be used for live-cell time-courses of vacuolar membranes because it was phototoxic at the concentrations required to achieve a reasonable signal to noise ratio for confocal imaging.

The dyes cSNARF-1 and BCECF-AM ester are widely used fluorescent indicators for estimating intracellular pH. During some preliminary work in which attempts were made to analyse cytosolic pH in growing germlings it was discovered that cSNARF-1 and BCECF-AM ester were sequestered within the vacuolar system (Fig. 4.12C and see Fig. 4.51 in Section 4.2.5.4). The extent of sequestration varied between cells, conidia and the developmental stage of the cells. Staining was less diffuse and more localised with cSNARF-1 making it one of the better stains for UNG conidia. In addition the calcium indicator Oregon Green-AM ester was also found to be sequestered by the vacuolar system (Fig. 4.12D).

FUN-1 stains both the cytoplasm and intravacuolar structures within metabolically active cells (Haugland, 1999). It is possible to divide the fluorescence emission such that the cytoplasmic and vacuolar signal are received in different channels (i.e. different detectors) on the confocal microscope. Although the vacuolar system was poorly discriminated, brightly fluorescent bodies that might be vacuolar inclusions were present in both ungerminated and germinated conidia within the cells and germ tube (Fig. 4.13). However, with both fluorescence and confocal microscopy the dye photo-bleached rapidly.

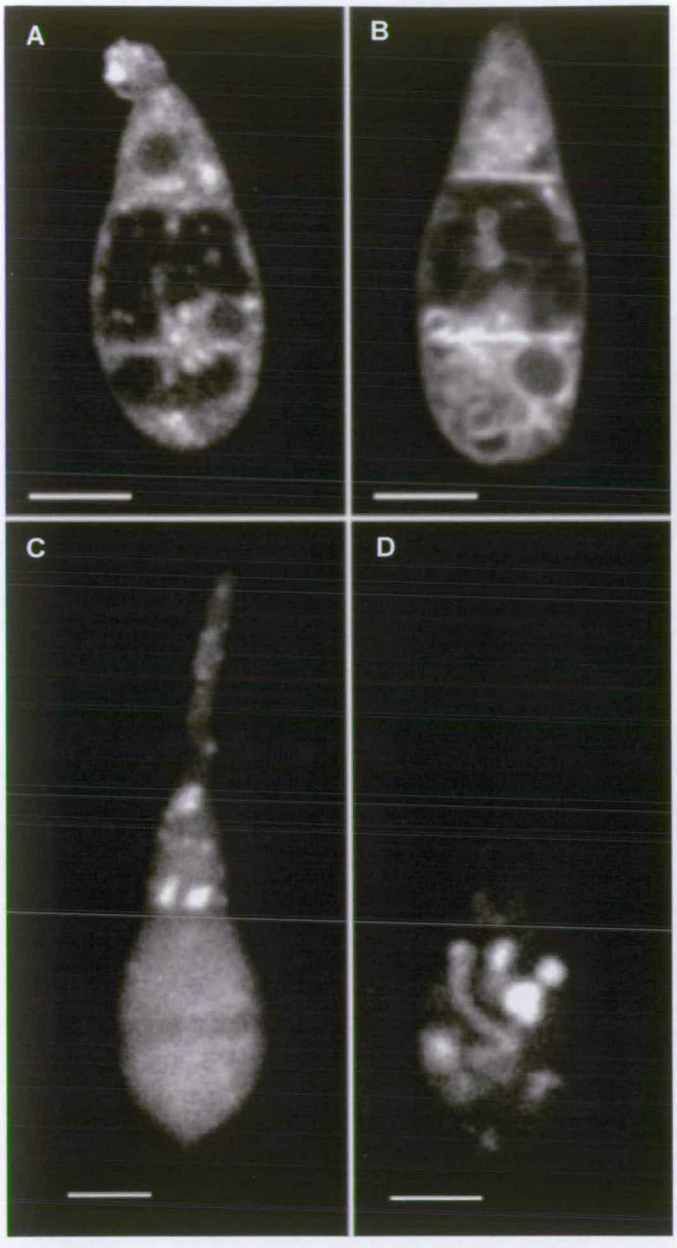

Figure 4.12: Confocal images of conidia in which components of the vacuolar system are stained. (**A**) An ungerminated conidium stained with MDY-64 (note that the STM is stained), (**B**) a GT_1 germling stained with MDY-64. Note that the dye stains the vacuole membrane but also appears to stain other membranous components of the cell. (**C**, **D**) Two germlings (GT_2 stage) stained with (**C**) BCECF-AM ester and (**D**) Oregon Green-AM ester, both of which are sequestered into the lumen of the vacuole system. Note that in (**C**) the dye is only sequestered by the vacuolar system within the apical cell and germ tube, and that in (**D**) tubular vacuoles are visible in the middle cell. Imaged using x60 (**A**,**B**) and 40 (**C**,**D**) objectives. Bars = 5 μm.

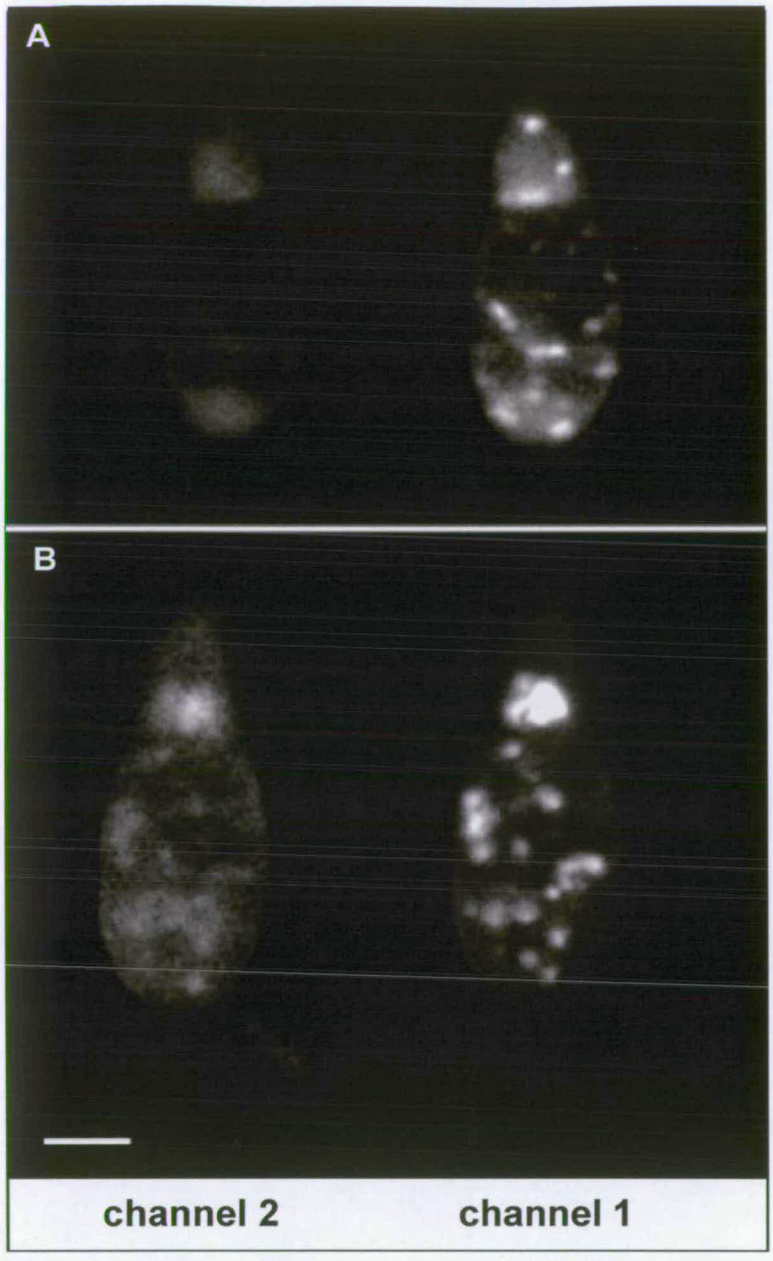

Figure 4.13: Confocal images of conidia stained with FUN-1. (**A**) An ungerminated conidium, (56 min post hydration) and (**B**) a germinated conidium, at the GT_1 stage of germination (102 min post hydration). The fluorescence signal has been divided into two channels to separate general cytoplasmic staining (**channel 2**) from fluorescence emanating from stained vacuolar inclusions (**channel 1**). Imaged using a x40 objective. Bar = 5 µm.

The vacuolar system was best discriminated by cDFFDA during germination. It was found that the optimum results were obtained if the dye was fresh, and that after 2–3 h in solution the background fluorescence often became high indicating that the dye had oxidised. Thus the dye was often washed out of solution after loading the cells (see Section 2.7.2). Although the dye became photo-bleached if over-exposed to the confocal laser, it was internalized by ungerminated spores and appeared to be the

least phototoxic of all the vacuole-selective dyes assessed (e.g. Fig. 4.38 in Section 4.2.5.4). On this basis, cDFFDA was chosen as the principal dye for live cell time-courses of vacuolar organization and dynamics. Several of the other vacuolar stains were used for correlative staining of the vacuolar network to confirm the patterns observed with cDFFDA.

4.2.4 Assessment of live-cell analysis techniques

In order to ensure that conidia and germlings were alive and unperturbed during data collection by confocal imaging, a number of experiments were performed which tested the cytotoxicity and phototoxicity of a range of dyes, including those selected for subsequent confocal microscopy (Section 4.2.3). These included an assessment of:

- percentage maximum germination and differentiation within populations of spores loaded with dye,
- germ tube growth rates in the presence of the principal dyes,
- germ tube growth rates during laser irradiation,
- germ tube growth rates in the presence the principal dyes during laser irradiation,
- pathogenicity of dye-loaded spores.

4.2.4.1 Influence of dyes on germination and differentiation

Maximum germination and differentiation (see Section 3.2.1) were assessed in the presence of the principal dyes, and some of the other more promising ones. A dye concentration of 10 μM was chosen because this was found to be the maximum required to obtain a sufficient signal for confocal microscopy (Table 2.2).

The mean percentage maximum germination was >97% for all dyes with the exception of the dyes FUN-1, MDY-64 and SYTO 11 (Table 4.1). The mean percentage maximum differentiation was >92% for all treatments except those samples stained with SYTO 11 and cSNARF-1 AM.

Dye	Target organelle	% Maximum germination	% Maximum differentiation	Total no. spores	No. of samples
Control (no dye)	-	97.9 ± 1.51	94 ± 2.77	2061	16
SYTO 11	nuclei	16.9 ± 5.29	0.0 ± 0.00	467	4
Rhodamine 123	mitochondria	98.9 ± 1.18	93.2 ± 3.13	1156	9
cDFFDA		98.9 ± 0.47	93.3 ± 2.61	964	8
FM4-64		97.4 ± 0.90	94.0 ± 0.33	702	6
MDY-64		91.6 ± 3.27	92.5 ± 2.67	655	5
cDCFDA	vacuolar	98.5 ± 1.28	95.3 ± 2.71	842	7
Oregon Green AM ester		99.1 ± 0.05	97.2 ± 1.61	329	3
BCECF		97.7 ± 1.60	94.1 ± 5.24	887	7
FUN-1		94.4 ± 4.02	92.1 ± 5.11	767	6
cSNARF-1 AM		98.7 ± 0.97	26.5 ± 21.53	858	6

Table 4.1: Mean percentage maximum germination and differentiation (measured after >21 h) in the presence of a range of fluorescent dyes (10 μM). The dyes in bold were those chosen as the principal organelle dyes for subsequent confocal imaging.

4.2.4.2 Influence of dyes on germ tube extension rate

The conidia and germlings were very sensitive to irradiation by the confocal laser. It was found that it was possible to collect entire time-courses of germination (i.e. UNG–GT_3 stages) in an individual conidium by confocal microscopy when using a x40 Plan apo objective, but not at higher magnifications (Table 2.1). At higher magnifications the intensity of laser irradiation of the cells is increased and the repeated imaging required to collect germination time-courses (i.e. UNG–GT_3 stages) usually killed the conidia.

To assess the influence of laser irradiation and dyes required to allow the collection of organellar data within living conidial cells, germlings were irradiated on the confocal microscope and germ tube extension rates were measured as described in Sections 2.8.2 and 2.11. In the first experiment, unstained conidia were scanned once every 20 min using live-cell time-course parameters (see Table 2.3) throughout germination (20–180 min post hydration). The germ tube extension rates and times of emergence were compared for the $GT^{\beta 1}$ and $GT^{\beta 2}$ categories with the data previously collected using light microscopy (Section 3.2.7.). There was no evidence that the

growth rate of germ tubes produced by laser-irradiated conidia differed from the non-laser irradiated conidia (two-tailed Students t-test: $GT^{\beta 1}$: $p = 0.45$, $GT^{\beta 2}$: $p = 0.94$, $n = 9, 5$). Similarly, there was no significant difference in germ tube emergence times (two-tailed Students t-test: $GT^{\beta 1}$: $p = 0.19$, $GT^{\beta 2}$: $p = 0.15$ $n = 9, 5$).

		Germ tube growth rate ($\mu m.min^{-1}$)		
Sample	**Time interval between scans (min)**	**before laser irradiation**	**during laser irradiation**	**Sample number**
no dye	1	0.35 ± 0.07	0.33 ± 0.08	9
	4	0.34 ± 0.03	0.35 ± 0.05	9
cDFFDA (7.5 µM)	1	0.36 ± 0.13	0.32 ± 0.08	11
	4	0.40 ± 0.11	0.40 ± 0.13	8
Rhodamine 123 (7.5 µM)	1	0.26 ± 0.08	0.13 ± 0.07	8
	4	0.28 ± 0.07	0.32 ± 0.10	10
FM4-64 (7.5 µM)	1	0.41 ± 0.06	0.41 ± 0.07	7
	4	0.34 ± 0.06	0.35 ± 0.10	8

Table 4.2: Mean germ tube growth rates before and after irradiation by the confocal laser. In each case the same germ tubes were measured before and after laser irradiation. Two successive scans were performed at intervals of either 1 or 4 min over a total of 10 or 16 min respectively. The live-cell time-course confocal parameters used are described in Table 2.3.

In the second experiment the germ tube growth rate was assessed in germlings in the presence and absence of the principal dyes used to image the vacuolar system (cDFFDA), mitochondria (Rhodamine 123) and membranes (FM4-64). Two successive laser scans were performed at intervals of either 1 or 4 min over a total of 10 or 16 min respectively (i.e. ≥10 min). Germ tube growth rates were measured before and during laser irradiation (Table 4.2).

There was no evidence that the germ tube growth rate was affected by laser irradiation in either the control (no dye), or FM4-64-loaded germlings (Table 4.2 cf Table 3.3, Section 3.2.7). There was a slight decrease in the mean germ tube growth rate at the higher scan frequency in cDFFDA-loaded germlings otherwise there was no evidence that the presence of the cDFFDA had cytotoxic or phototoxic effects.

The mean germ tube growth rate in Rhodamine 123-loaded germlings was attenuated prior to irradiation by the laser, and either (a) increased slightly when scanned every 4 min, or (b) was halved when scanned every min. Thus, although the dye does not affect the mean percentage maximum germination or differentiation (Table 4.1), evidence was obtained that Rhodamine 123 was slightly cytotoxic and that when irradiated can become phototoxic (Table 4.2).

4.2.4.3 Testing conidial pathogenicity in vivo

Having determined that differentiation occurred in the presence of the principal vital organelle dyes, an experiment was performed to assess whether dye-loaded differentiated germlings retain their pathogenicity on dye loading.

A range of dyes (see Table 4.3) was subjected to an *in vivo* pathogenicity test in which intact rice plants were inoculated with low concentrations of dye-loaded spores (Section 2.12.3). Prior to inoculation the percentage of conidia within a population that internalize each dye used in the *in vivo* pathogenicity test was assessed. In each case 100% ± 0.0 of the conidia internalized the dye (>500 conidia per sample, 4–11 samples for each dye) (see Section 2.12.3).

Treatment	Description
cDFFDA	vacuolar lumen dye
Rhodamine 123	mitochondrial dye
FM4-64	endocytic marker
MDY-64	vacuolar membrane dye
carboxySNARF-1	pH/vacuolar dye
spores only	control 1 (no dye)
water only	control 2 (no spores)

Table 4.3: Pathogenicity test inoculum treatments. Rice leaves were inoculated with *Magnaporthe grisea* conidia loaded with one of a range of dyes (10 μM). The following controls were included: (1) water only, and (2) conidial inoculum that had not been loaded with dye. Reprinted from Table 2.5, Section 2.12.3 for convenience.

All dye treatments and the 'no-dye' control resulted in the formation of lesions on the leaves, which were indicative of successful infection (Fig. 4.14). No lesions were formed on the water-only control inoculated leaves (Fig. 4.14). The external and internal characteristics of the lesions were examined. General characteristics of

lesions have been defined previously (Section 3.2.6). There were no observable differences between the leaf lesions caused by the no-dye control, and dye-loaded inocula: in all cases the lesions exhibited the same characteristics as described previously. No lesions were formed on the leaves inoculated with water only.

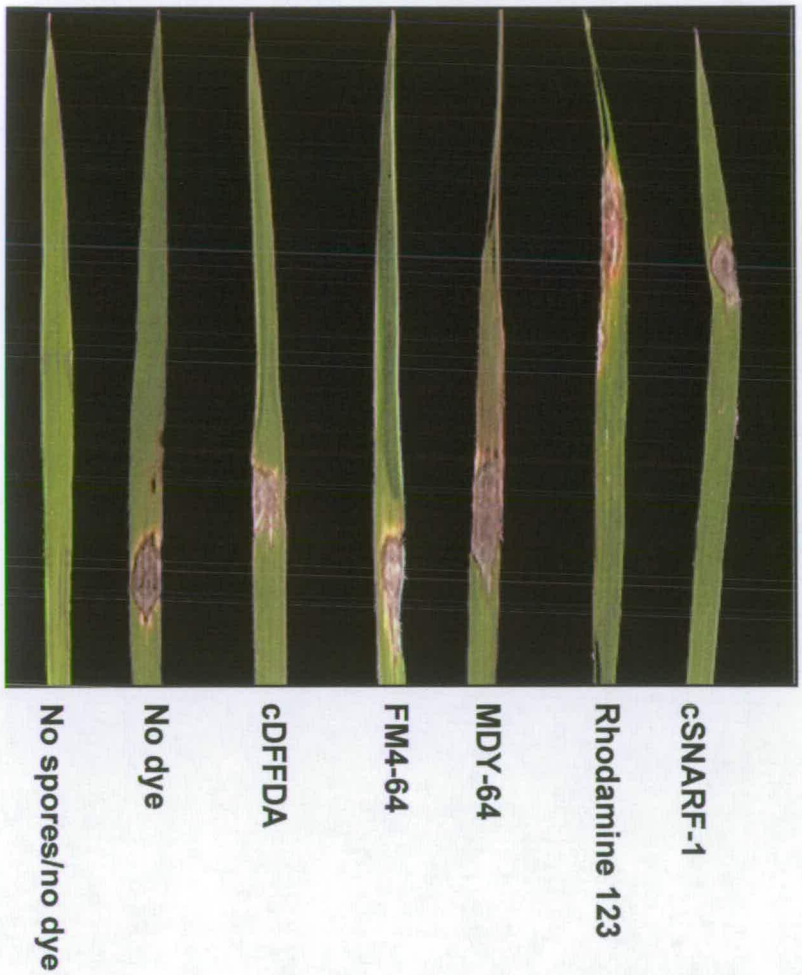

Figure 4.14: Lesions formed on rice leaves 5 days after inoculation with dye-loaded *M. grisea* conidia. Two controls were included, (1) a water only inoculum and, (2) a conidial inoculum that was not dye-loaded. Note that lesions have formed on all but the water only (no spores) inoculum.

Successful infection was scored using the following criteria:

- presence of internal hyphae within the host tissues,
- formation of conidiophores within the lesion,
- formation of conidiophores outside the lesion (lesion delimited by a brown edge).

In all treatments the above criteria were fulfilled, indicating that loading conidial inoculum with dye did not compromise the normal infection process and thus conidial pathogenicity.

4.2.5 Confocal analysis of conidial cytology during germination

Two sets of confocal imaging conditions were defined (Table 2.3): (a) "live-cell time-course" parameters which were the least damaging to conidial cells and allowed the collection of entire time-courses of germination (i.e. UNG–GT_3 stages) in an individual conidium (b) "individual image" parameters provided the highest resolution images but were ultimately deleterious to the cells (especially when a x60 oil objective was used) and thus unsuitable for entire time-courses of germination in individual conidia. As most germination occurs from the A-cell, apically germinated conidia are primarily considered in the following sections.

Between seven and ten live-cell time-courses were collected for each organelle type (except the nucleus), using the principal dye for each organelle (Section 4.2.3) to observe their distribution and dynamics during germination in individual conidia. Conidia and germlings were also sampled from the population at different stages of germination (as defined above in Section 4.2.1) in order to determine whether the observations within individual conidia were characteristic of the population and not influenced by the successive laser irradiation required to obtain individual conidial time-courses.

To refine the details of organelle morphology and organization observed with the x40 objective, spores were examined in greater detail using a x60 oil objective. At these higher magnifications, entire germination time-courses of individual spores could not be collected as the dyes were more prone to photo-bleaching and the conidia became stressed by the greater exposure to radiation resulting from the use of high-power lenses (see Section 4.2.4.2). Thus, populations of spores were examined and short time-courses were collected. Rapid time-courses (scanned every 10 sec) were also collected, but each was limited to a maximum of 10 images.

4.2.5.1 *Conidial autofluorescence during confocal analysis*

To determine whether the conidium itself might contribute to the detected signal the autofluorescence of unstained conidia during germination was assessed on the confocal microscope. The confocal parameters were those that were used to collect live-cell time-courses (Table 2.3) with blue excitation and a x60 oil objective in order to optimise the conidial exposure to the laser. The room temperature was maintained at 24 ± 1 °C. The data are shown in Figure 4.15. The minimum value on the y-axis is 10, corresponding to the value to which the black levels were set.

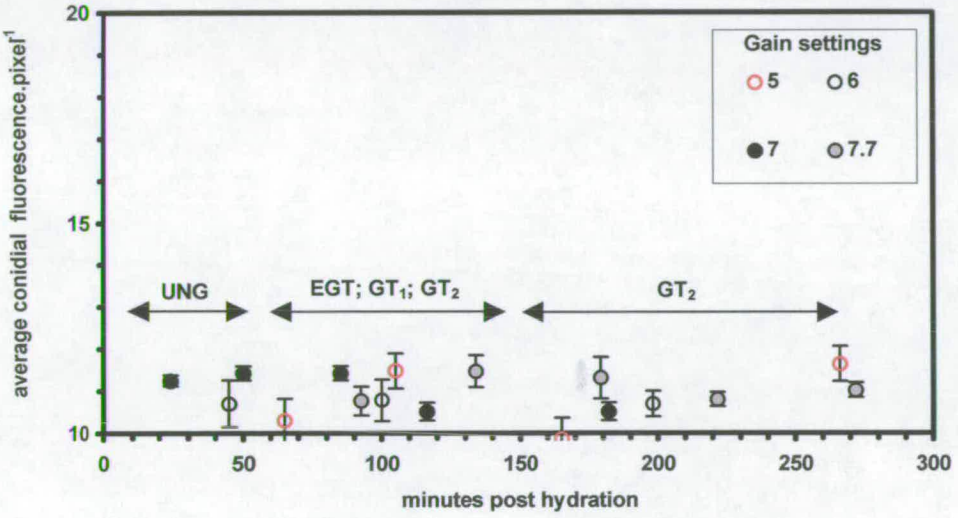

Figure 4.15: Mean conidial autofluorescence at photomultiplier gains 5, 6, 7 and 7.7 with blue excitation. Approximate stages in germination are given. Between 7–10 conidia were sampled at each data point and the vertical bars show standard deviations. Abbreviations: UNG (ungerminated); $GT_{1/2}$ (Germ tube 1 or 2; see text).

There were no observable differences between the mean conidial fluorescence collected at the four gain settings on the photomultiplier detector; gain 5 producing the highest and lowest values. The mean fluorescence values fluctuate between 10–12 in all four data sets. At the higher gains (>7.5) some faint fluorescence appeared to emanate from the vacuolar system, especially during the GT_1–GT_3 stages of germination. Thus, it was decided that gains of 5–7 (50–70%) would be used to collect organelle data.

4.2.5.2 Nuclei

In order that the position of the nuclei in each cell is clear, negative images of the SYTO 11 stained cells are shown. Each cell characteristically contained one nucleus, although on one occasion two were observed in the M-cell (Fig. 4.16).

Figure 4.16: Negative confocal image of an EGT conidium with two nuclei stained in the M-cell. Note that the A-cell nucleus is only faintly stained, that this is unusual. Stained with SYTO 11, Imaged using a x40 dry objective. Bar = 5 µm.

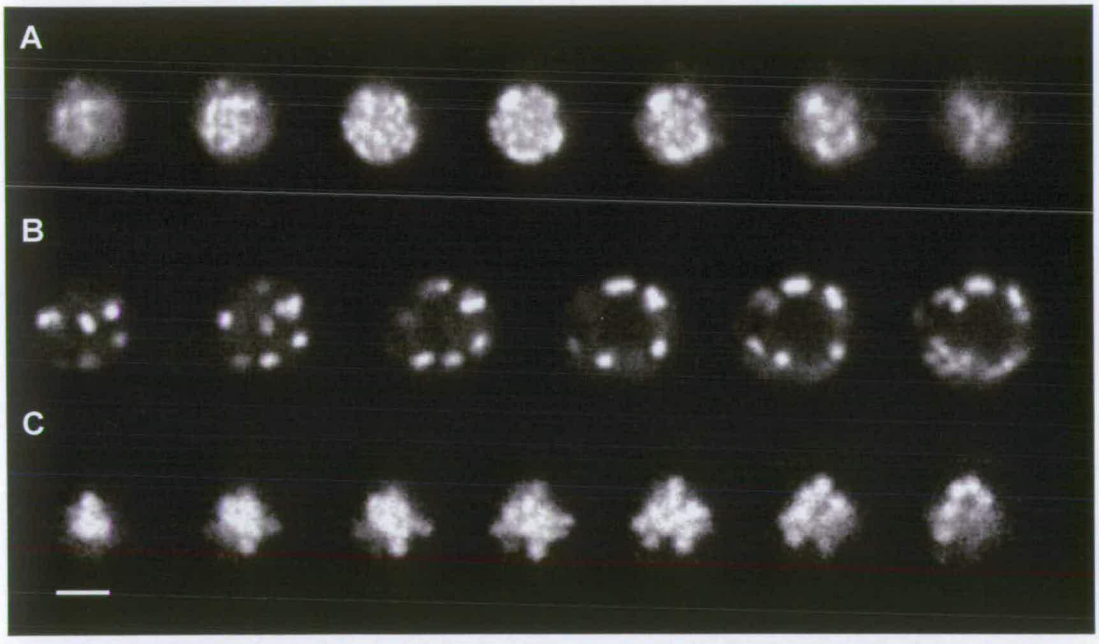

Figure 4.17: Confocal images showing three series of transverse optical sections that were collected through the apical cells of three different ungerminated conidia showing, (**A**) the nucleus (stained with SYTO 11), (**B**) the mitochondria (stained with Rhodamine 123) and (**C**) the vacuolar system (stained with cDFFDA), Imaged using a x60 objective. Bar = 2 µm.

The three different nuclei usually stained to different extents; the A- and then the B-cell nuclei being the most intensely stained. At lower dye concentrations, the M-cell nucleus was rarely visibly stained, but the structural details of the A- and B-cell

nuclei were revealed (Fig. 4.17A). In all three cells a partial ring of bright spots was often detected around the nucleus (Fig. 4.18). The diameter of the nucleus (based on A- and B-cell nuclei) was 2.3 ± 0.1 µm ($n = 13$). The M-cell nucleus commonly appeared to be smaller and to determine whether this was due to poor dye uptake, samples were refrigerated in the presence of the dye for 12 h. When fully stained, there was no evidence that there was any difference in the size of nuclei between cells.

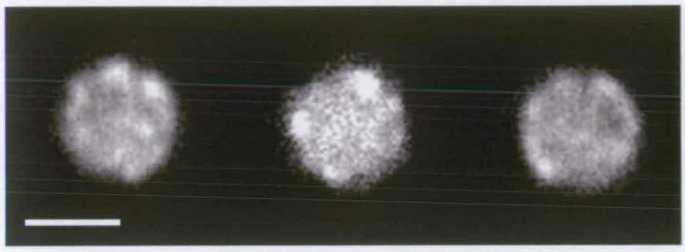

Figure 4.18 Confocal images of median sections through three different nuclei. Bright spots are characteristically present within the nucleus, and they often appear to form a rough ring around it. Stained with SYTO 11. Imaged with a x60 objective. Bar = 2 µm.

Figure 4.19: Confocal image of an ungerminated conidium at 35 min post hydration stained with the membrane dye MDY-64. Note that the nucleus is negatively stained. Dye was added 10 min post hydration. Imaged with a x60 objective. Bar = 5 µm.

Attempts were made to use the membrane dye MDY-64 to negatively stain the nuclei, but this proved unsuccessful due to the phototoxic nature of this dye over the prolonged period of laser irradiation required for live-cell time-courses (Fig. 4.19).

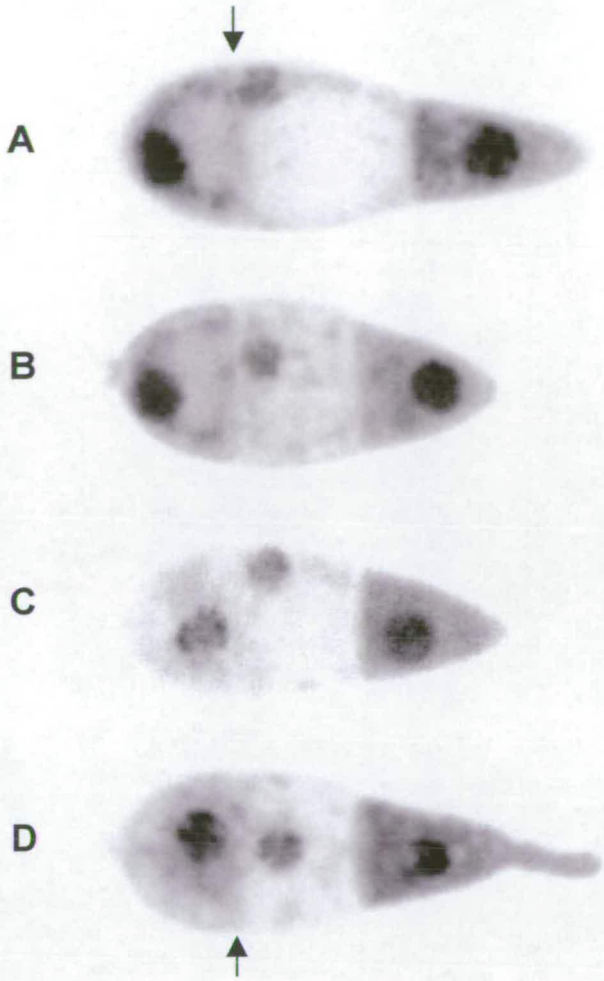

Figure 4.20: Negative confocal images of conidia and germling showing examples of the three broad categories of nuclear organization present within conidial populations during germination: (**A**) Category 1 (**B, C**) Category 2, (**D**) Category 3 (see text). Note that the conidia have been arranged so that the basal septa (→) are aligned. Stained with SYTO 11. Imaged using a x40 objective. Bar = 5 μm.

Due to the cytotoxic nature of SYTO 11, live-cell time-course data could not be collected. However, the spores appeared healthy for ~20 min in the presence of the dye and during this time no changes to the nuclear morphology or disruption to the cellular organization were observed. A population analysis was therefore performed in which the nuclear distribution in conidia was analysed at each stage of germination (UNG–GT_3 stages). Nuclear distribution was recorded within spore populations and grouped according to the stage of germination. Because SYTO11 is cytotoxic, spores were only sampled between 5–15 min post dye (See Section 4.2.3.1). The experiment

was performed four times and a total of 190 conidia were analysed. Approximately two thirds of the spore population had all three conidial nuclei stained (n = 135). The remainder were not included in the analysis.

There were three main categories (Fig. 4.20) of nuclear organization based on the B- and M-cell nuclear distribution:

- Category 1: both nuclei were closely associated with the plasma membrane. The most common positions for the nuclei were: M-cell nucleus located in the corner between the B-septum and plasma membrane, and the B-cell nucleus located in the region of plasma membrane surrounding the stalk (Fig. 4.20A)

- Category 2: either the M-cell or less frequently the B-cell nucleus moves towards the longitudinal axis of the conidium. When the M-cell nucleus changes position it was commonly alongside the B-septum and rarely in contact with the plasma membrane; occasionally it was observed in the centre of the cell (Fig. 4.20B). When the B-cell nucleus changed position it was nearer the B-septum than in Category 1, and sometimes in contact with the plasma membrane. (Fig. 4.20C)

- Category 3: both the nuclei are in alternative positions to Category 1, both being in the positions described in Category 2. At this stage they are often more-or-less parallel across the septum near the longitudinal axis of the spore. The distance between the nuclei and septum varied and on some occasions one or both the nuclei appear to be in direct contact with it (Fig. 4.20D).

In order to determine whether these three nuclear categories simply represent the variation within the population, or are determined in some way by the stage of germination, the percentage of the conidial population represented by each category was determined at each stage of germination. The UNG stage was divided into 4 sub-stages defined by time post hydration, and germinated spores into the EGT, GT_1, GT_2, or GT_3 stages of germination described previously (Section 4.2.2). Note that the

first UNG sub-stage is only 5 min in length because nuclei were not imaged until at least 15 min post hydration. The results are presented in Fig. 4.21.

The percentage of the conidial population represented by each of the three different categories changes with the defined stages of germination. Category 1 was the only nuclear pattern observed at 15–20 min post hydration, and with time becomes less common being absent from the germinated stages. The observed decrease in category 1 coincides with a gradual increase in the percentage of Category 3 within the conidial population, which continues throughout germination. Category 2 appears to be an intermediate stage. Thus, the evidence suggests that the B- and M-cell nuclei move prior to and after the emergence of the germ tube.

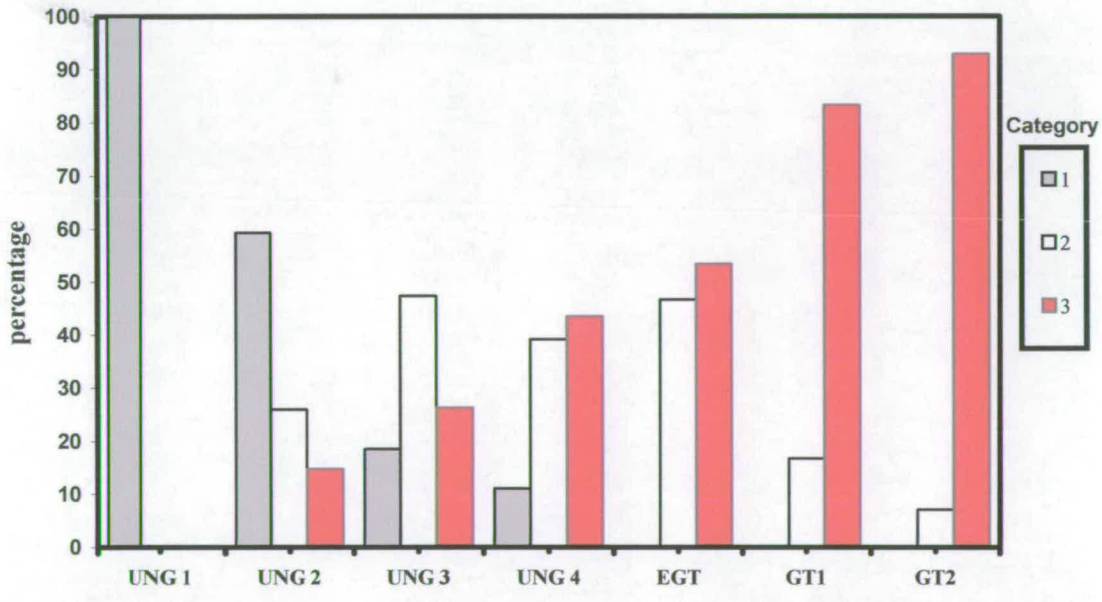

Figure 4.21: The percentage occurrence of the 3 general categories (1, 2 and 3) of nuclear distribution within conidial populations at different stages of germination. UNG 1, 2, 3 and 4 are ungerminated spores after: 15–20, 30–35, 40–50, and >60 min post hydration, respectively.

Figure 4.22: Negative confocal images of different conidia at successive stages during germination, demonstrating the likely nuclear dynamics during germination. Stained with SYTO 11. Imaged using a x40 objective. Bar = 5 μm.

Representative conidia that demonstrate the overall pattern of nuclear position during germination are shown in Fig. 4.22. The A-cell nucleus occupies the central region of

the cell, and due to the small size of the A-cell it was impossible to determine by population analysis whether the A-cell nucleus had changed its position during the UNG–GT_2 stages of germination. However, in germinated apical cells during the GT_3 stage of germination, the nucleus was often positioned towards the base of the germ tube. Occasionally it was observed to have migrated along the germ tube having become elongated in the process (Fig. 4.22F). Unstained live cell time-courses collected by DIC microscopy agree with these findings of this population analysis (e.g. Fig. 4.8).

SYTO 11 stains both DNA and RNA (Haugland, 1999). General staining of the cytoplasm was observed in all cells, and was brightest within the A- and B-cells and the germ tube (Figs. 4.20, 4.22). This could indicate that there is a higher density of cytoplasmic nucleic acid within these cells; alternatively, it could be an artefact caused by differential uptake of the dye into the different conidial cells. Nuclei within the germinated cell occasionally appeared to be larger (Fig. 4.23).

Figure 4.23: Negative confocal image of a germling at the GT_3 stage of germination. Note that the apical cell contains a large nucleus. Stained with SYTO 11. Imaged using a x40 objective. Bar = 5 μm.

4.2.5.3 Mitochondria

On the basis of the findings in presented in Table 4.2, the time intervals between images were kept as long as possible when using the principal mitochondrial dye, Rhodamine 123. In this way it was possible to collect live-cell time-courses using the CLSM parameters defined in Table 2.3 without perturbing the cells.

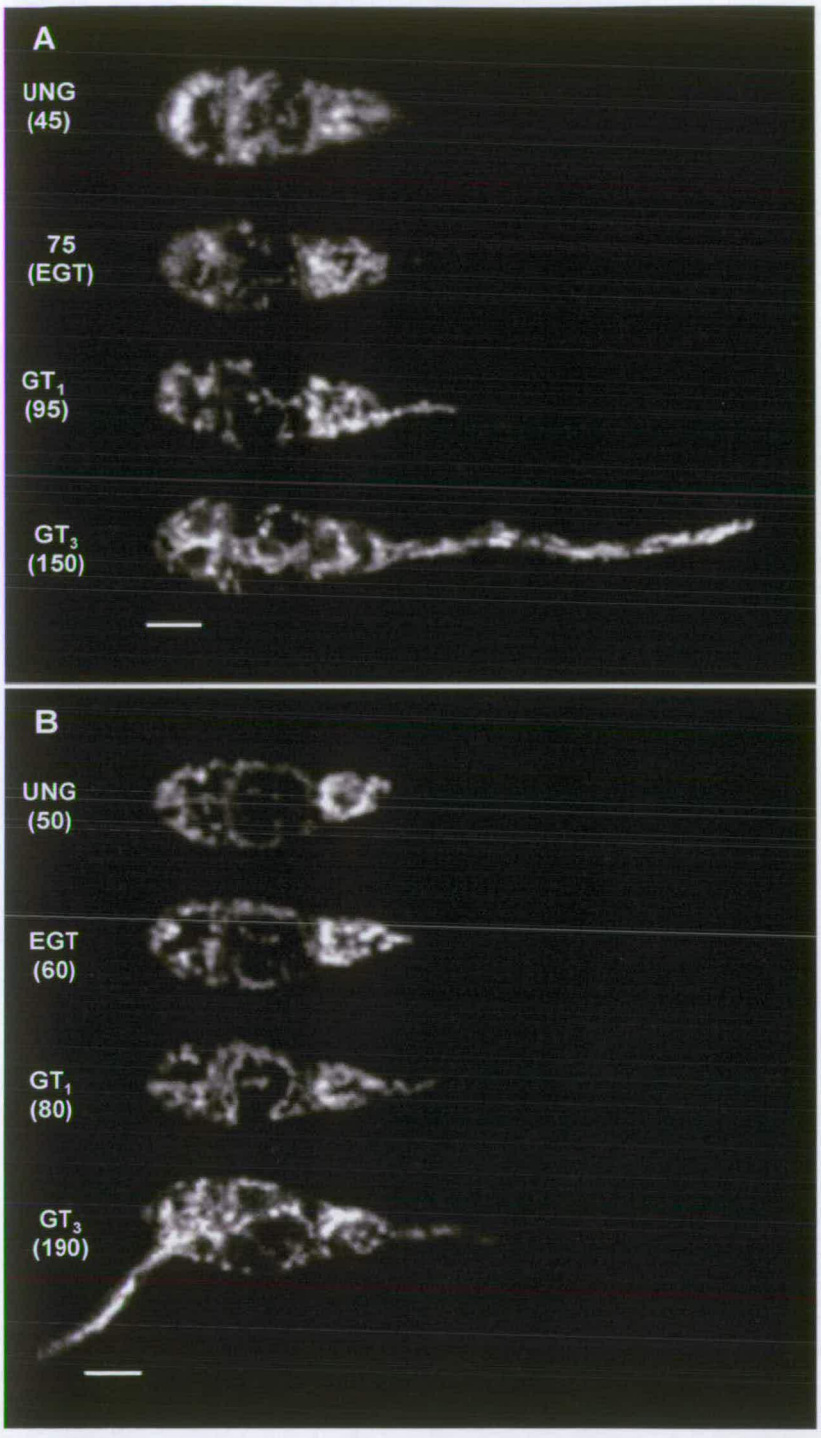

Figure 4.24: Confocal images showing two examples of live-cell time-courses of mitochondrial distribution in individual conidia throughout germination. (**A**) One germ tube is produced, from the apical cell, (**B**) two germ tubes, first from the basal cell and then from the apical cell; stages refer to the first germ tube. Images are projection of 2–3 optical sections. Stained with Rhodamine 123. Imaged using a x40 objective. Bars = 5 μm

Two examples of live-cell time-courses are shown in Figure 4.24. In general, as germination proceeded the mitochondria became progressively longer, more numerous, and polarised towards the growing germ tube. To refine the details of the mitochondrial organization and distribution, images of individual conidia were collected at different stages during germination using a x60 oil objective (Fig. 4.25).

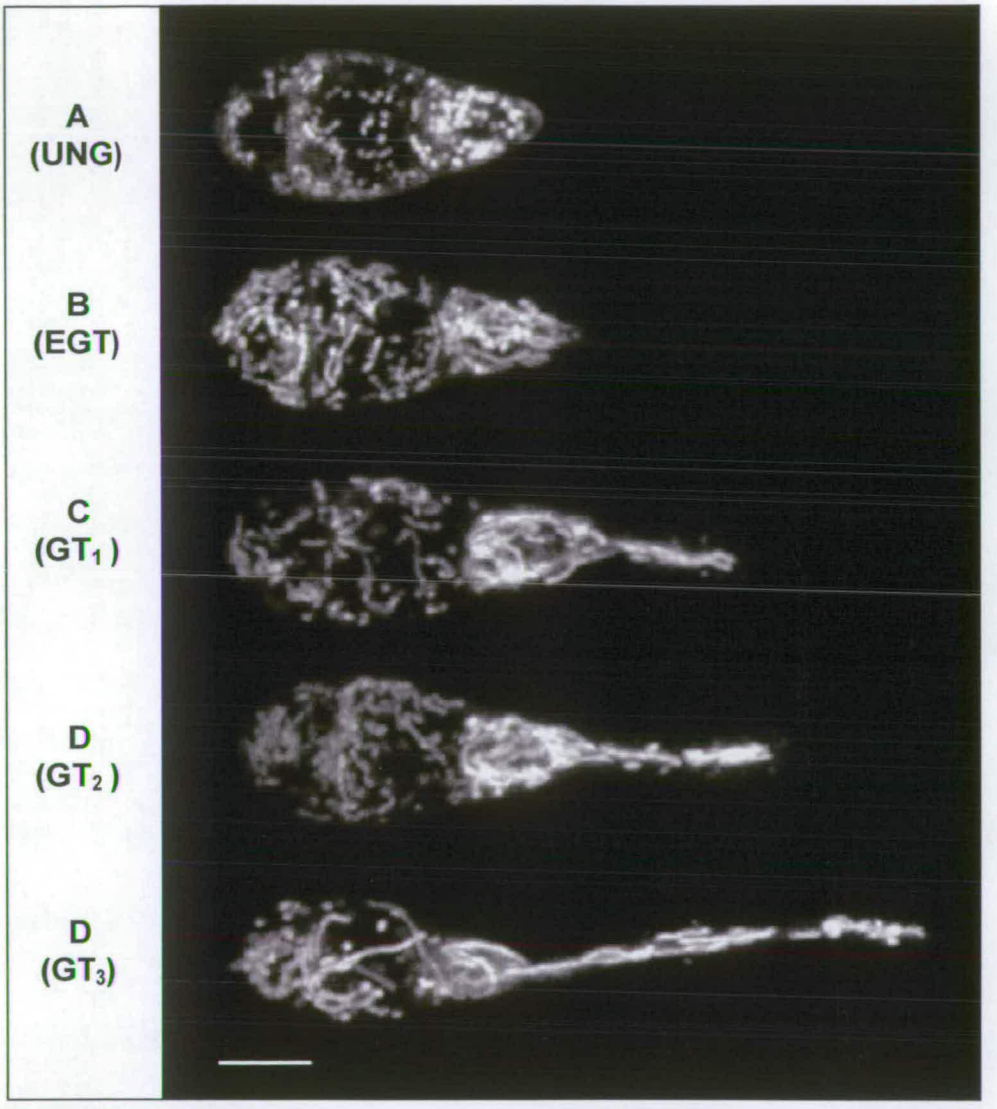

Figure 4.25: Confocal images of mitochondrial staining in representative conidia at each stage of germination (UNG–GT_3). Images are projections of optical series; (**A**) has been image processed to enhance the M- and B-cell fluorescence intensity. Stained with Rhodamine 123. Imaged using a x60 objective. Bar = 5 μm.

Mitochondria exhibited variable morphology. The principal types were either (a) small spherical to rod shaped, (e.g. Fig. 4.25A) and (b) elongated mitochondria that

were often branched (e.g. Figs 4.25C–E). Both types are ~0.4–0.5 μm in width, although the elongated mitochondria showed greater variation and could be up to 0.6 μm in width in some regions. Rhodamine 123 often stained the A-cell and/or germinated cell more brightly than the other conidial cells and this was most pronounced during the EGT–GT_1 stages of germination (e.g. Figs. 4.24A,B, 4.25).

In the M- and B-cells the mitochondria were primarily localised in the peripheral region of the conidial cells, close to the plasma membrane, throughout germination (e.g. Figs. 4.17B, 4.26). This is not always clear in a projected image (Fig. 4.27 cf. 4.25). The structures identified as putative mitochondria by DIC imaging (Figs. 4.5C, 4.6A, 4.9) correspond with the observations made here, both with respect to their dimensions and distribution within the conidia.

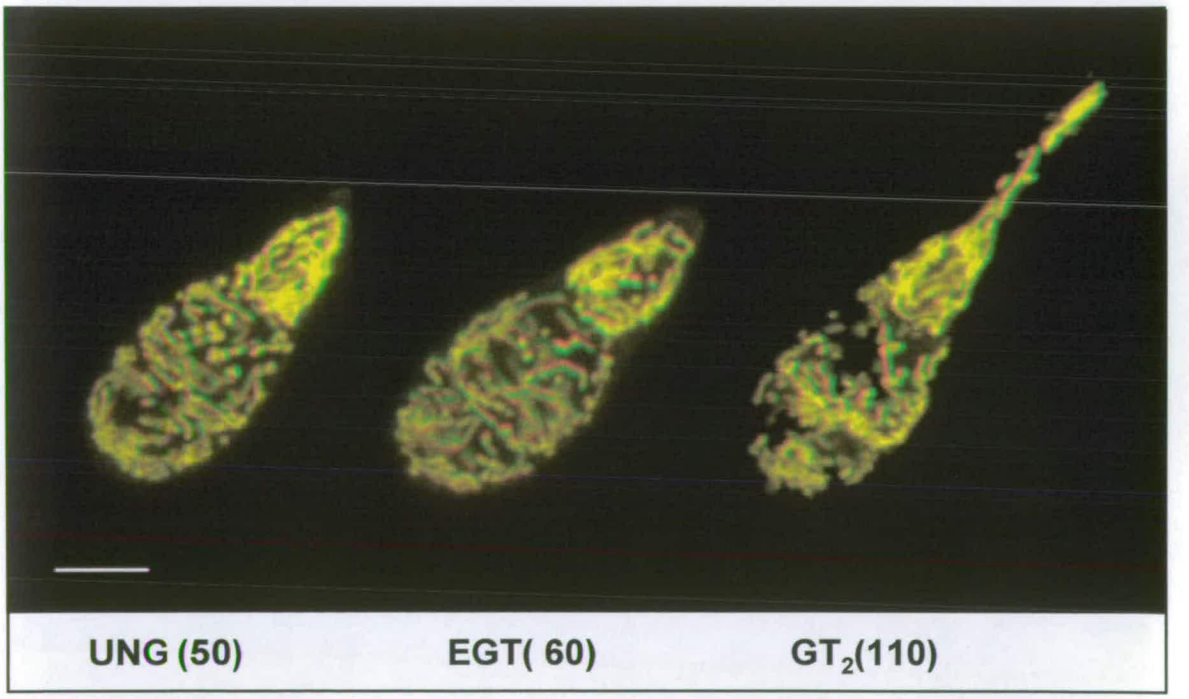

Figure 4.26: Confocal images that are projections of optical sections presented as stereo pairs of representative conidia and germlings at three different stages of germination. Note that the mitochondria are primarily peripheral in the basal and middle cells and polarised towards the germ tube in the germinated cell. The numbers are min post hydration and the dye was added at 8 (UNG, EGT images) and 95 (GT_2 image) min post hydration respectively. The GT_2 stage spore has been image processed to increase the fluorescence intensity in the B- and M-cells. Stained with Rhodamine 123. Imaged using a x60 objective. Bar = 5 μm.

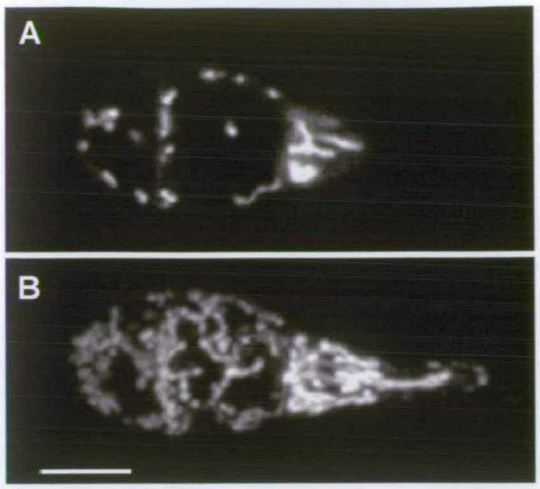

Figure 4.27: Confocal images of a germling at the GT_1 stage of germination showing (**A**) a median section though the M-cell and across the B-cell, and (**B**) the projected imaged comprised of a series of optical sections, including that shown in (**A**). Imaged using a x60 objective. Bar = 5 μm.

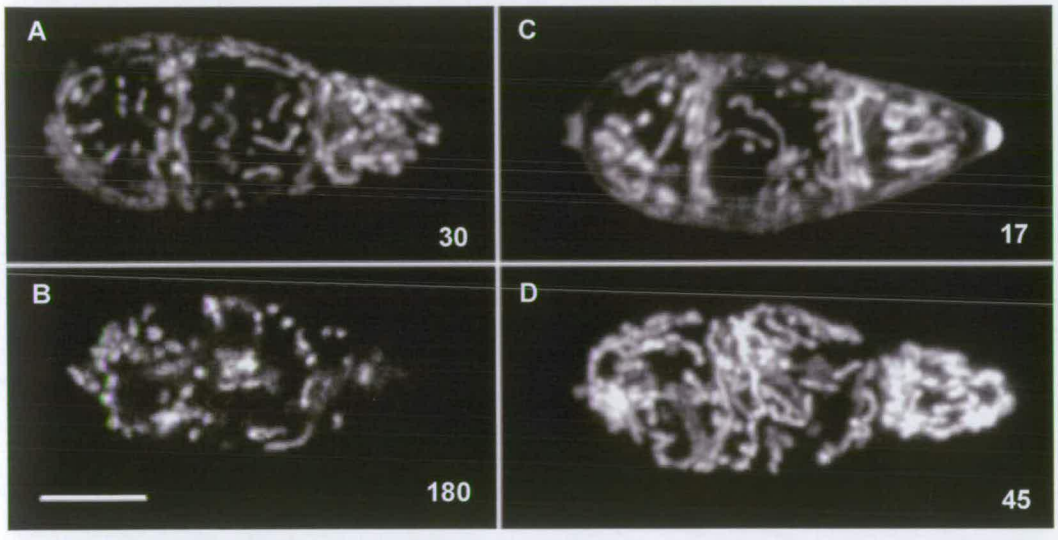

Figure 4.28 Confocal images showing examples of ungerminated spores. Small mitochondria (**A**, **B**) are commonly predominant within ungerminated conidia: however, elongated mitochondria are also present, and sometimes they predominate (**C**, **D**). Note that (**B**) is ungerminated after 180 min post hydration and still contains primarily small, spherical and rod shaped mitochondria. Stained with Rhodamine 123. Numbers are min post hydration, and the dye was added at 8 min (**A**, **C** and **D**) and 90 min (**B**) post hydration. Images are projections. Imaged using a x60 objective. Bar = 5 μm.

The density of mitochondria increased during germination, and this was most pronounced between the initial phase of the UNG stage and the EGT stages (Fig. 4.25A,B). During this early phase (<30 min post hydration) of the UNG stage, mitochondria were primarily small and spherical (~0.4–0.5 μm) and sometimes rod-shaped (similar size), with a few that were elongated, and sometimes branched

(Figs. 4.25A, 4.28A). There were no observable differences in mitochondrial morphology and organization between the different cells of ungerminated conidia during this part of the UNG stage of germination.

The small spherical and rod-shaped mitochondria were not an artefact caused by insufficient dye uptake as they were also present within ungerminated spores which had been in the dye for extended periods (Fig. 4.28B). During the rest of the UNG stage (>30 min post hydration) there was more variation in mitochondrial morphology: in particular, some spores contained a higher proportion of elongated mitochondria and these sometimes appeared to be polarised within the A-cell prior to germination (Figs. 4.28C,D, 4.26). The small spherical and rod-shaped mitochondria were present in all conidial cells throughout germination (UNG–GT_3).

By the stage at which a germ tube had emerged (EGT), the mitochondria within the germinated cell were primarily elongated and polarised towards the growing germ tube tip, and mitochondria were observed to extend into and along the length of the growing germ tube (e.g. Figs. 4.25B, 4.26). In germlings, the ungerminated cells also usually contained a higher proportion of elongated mitochondria than was observed during the UNG stage, but these appeared less numerous and shorter than in the germinated cell and generally did not exhibit polarisation towards the growing germ tube.

As the germ tube extended (GT_1–GT_2) the elongated mitochondria within the germinated cell became longer (e.g. Figs. 4.24, 4.25C,D). Although the mitochondria of the germinated cell always exhibited this elongated and polarised morphology, mitochondria in the two ungerminated conidial cells exhibited greater variation. In a conidium that had germinated from the A-cell, the B-cell often remained more or less as it had been during the EGT stage, although the M-cell usually contained a higher proportion of elongated mitochondria than at the EGT stage, but never at the same density as in the germinated cell (e.g. Figs. 4.25C,D, 4.26, 4.27). However, the

degree of elongation and polarisation of mitochondria within these two cells varied between conidia.

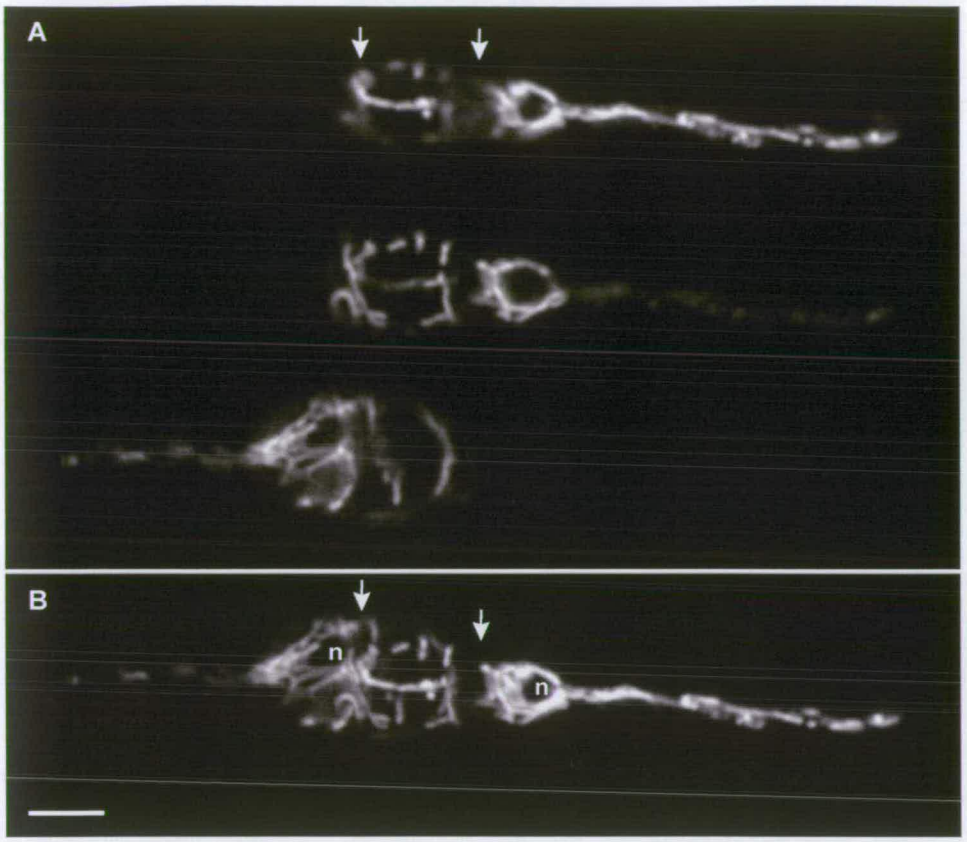

Figure 4.29: Confocal images of a germling at the GT_3 stage of germination showing three different optical sections (**A**) and a projected image (**B**). All three cells contain elongated mitochondria that are polarised towards the growing germ tubes. Note the mitochondria "stretching" between the septa (arrows) and that the nuclei (n) are surrounded by mitochondria. Stained with Rhodamine 123. Imaged using a x60 objective. Bar = 5 μm.

During the GT_3 stage, mitochondria usually maintained the organization described for the GT_2 stage and in some cases still primarily contained spherical mitochondria (Fig. 4.25E), although in others the mitochondria in the B-cell appeared more elongated (Fig. 4.24A). However, when both the A- and B-cells germinated, all three cells mainly contained elongated mitochondria, which were polarised towards the germ tube in the germinated cells (e.g. Figs. 4.24B, 4.29). In these spores the M-cell mitochondria were also usually polarised towards the germ tubes. They were observed to still be primarily peripheral (Fig. 4.30), but sometimes what appeared to be one long, or several shorter interwoven mitochondria stretched between the two

septa through the centre of the cell (Figs. 4.24B, 4.29). This was also observed in the M-cells of spores that had only germinated from one cell (4.24A).

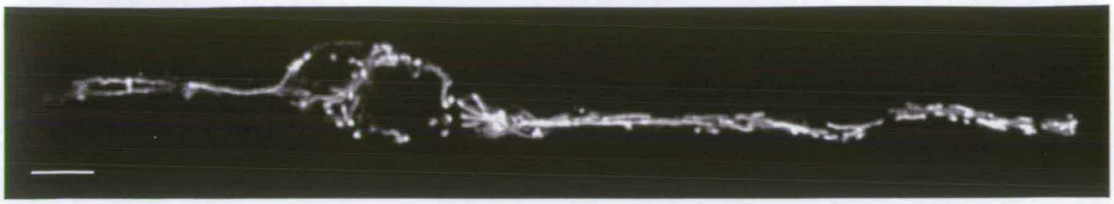

Figure 4.30: Confocal image of a germling at the GT_3 stage of germination, showing that the mitochondria are polarised towards both germ tubes and are distributed around the periphery of the middle cell. Stained with Rhodamine 123. Imaged using a x60 objective. Bar = 5 µm.

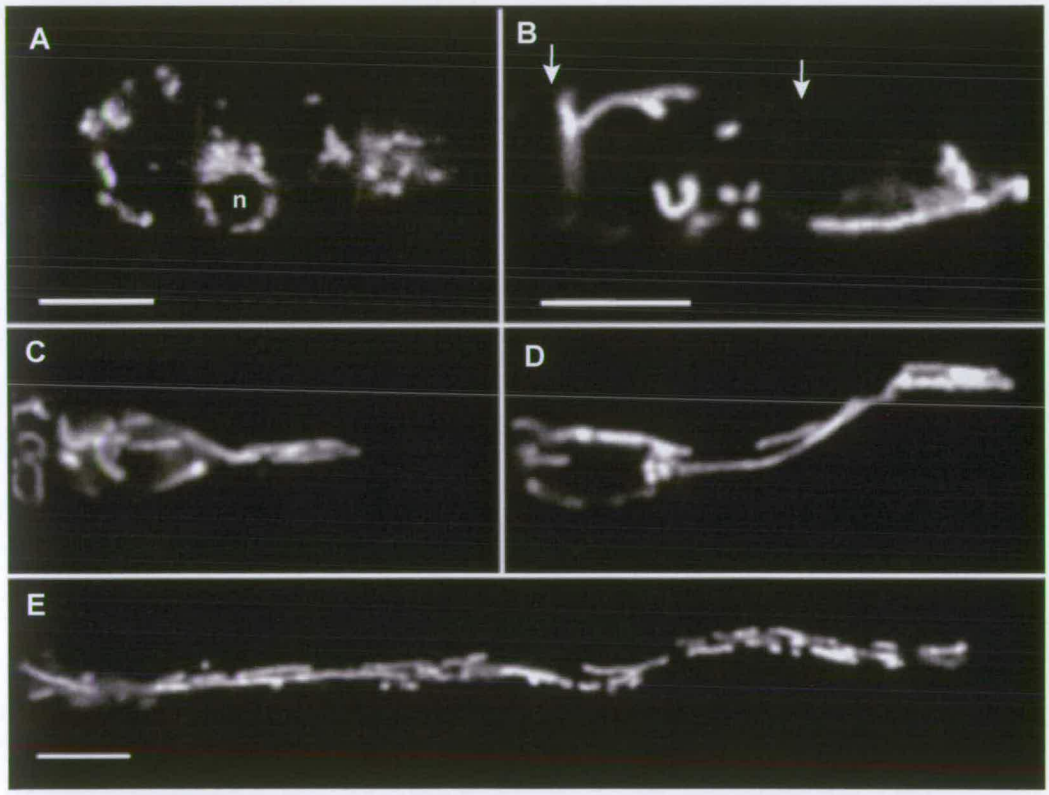

Figure 4.31: Confocal images showing some characteristics of mitochondria in conidial cells and germ tubes. (**A**) Mitochondria are commonly associated with the nucleus (n) throughout germination; this example is an ungerminated conidium. (**B**) Mitochondria are often positioned next to, and parallel to the septum (arrow); in this case the germling is at the GT_3 stage with two germ tubes. (**C–E**) Apically germinated cells at the (**C**) GT_1, (**D**) GT_2 and (**E**) GT_3 stages of germination. At all stages the mitochondria are elongated in the germinated cell and germ tube, and are closely associated with one another, sometimes appearing to be interconnected. Stained with Rhodamine 123. Imaged using a x60 objective. Bars = 5 µm.

Mitochondria were closely associated with the nuclei throughout germination (e.g. Figs. 4.29, 4.31A). They were often orientated parallel to the septa, especially within

the M-cells during the GT_2 and GT_3 stages of germination, and sometimes appeared to be continuous between the cells (e.g. Figs. 4.29, 4.31B). Elongated mitochondria were straight or curved and were frequently branched (Fig. 4.32). They were often very closely associated with one another and were observed to be interconnected (e.g. Figs. 4.31 C–E, 4.32C,D). This made it difficult to determine the precise lengths of individual mitochondria, especially within the narrow germ tube, in which many of the apparently longer mitochondria were located. Where an individual mitochondrion was clearly definable lengths of up to 15 μm have been measured.

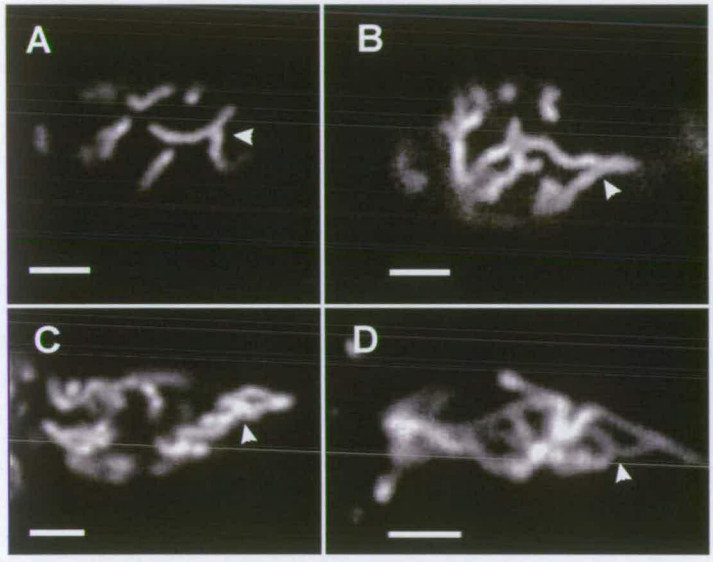

Figure 4.32: Confocal images of elongated mitochondria showing examples of, (**A**, **B**) branched mitochondria, (**C**) closely associated mitochondria and (**D**) networks formed by mitochondria in conidia at the UNG (**A**, **B**), EGT (**C**) and GT_2 (**D**) stages of germination. Stained with Rhodamine 123. Imaged using a x60 objective used. Bars = 5 μm.

Mitochondria within the conidial cells were dynamic throughout germination and there was evidence that fusion and fission occurred (Fig. 4.33). However, they were most dynamic within the growing germ tube. Elongated mitochondria were observed to repeatedly move up into the germ tube tip region, and then to retract (Fig. 4.34). Small mitochondria were also present and there was some evidence of fragmentation and fusion within the germ tube (e.g. Fig. 4.35). When a germ tube was stressed by over-exposure to the confocal laser it eventually stopped growing. This was accompanied by retraction of the mitochondria from the tip region to a subapical

position (Fig. 4.36) where they sometimes appeared to 'round-up' becoming less elongated and denser.

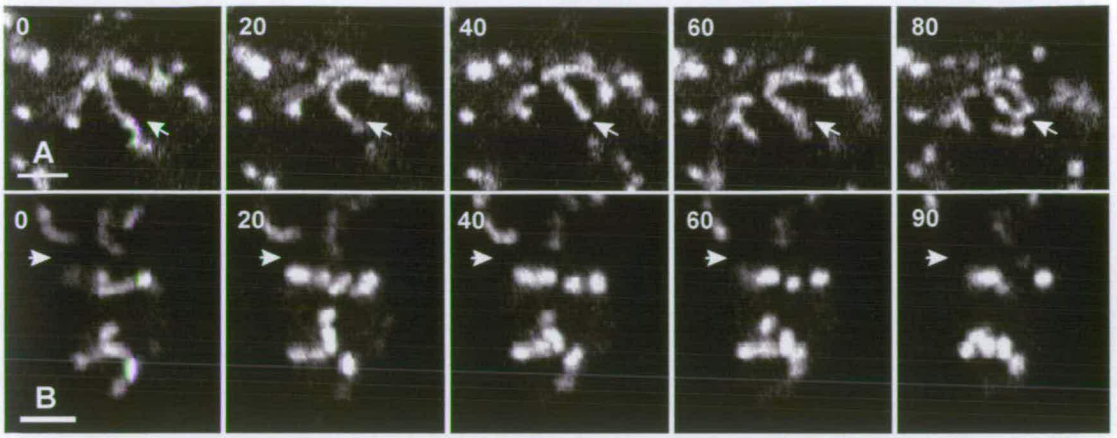

Figure 4.33: Confocal images of mitochondrial dynamics within the (**A**) middle and (**B**) apical cell of two different germlings at the GT_2 stage of germination. The numbers are seconds after the 1st image, which was collected at (**A**) 173 min and (**B**) 175 min post hydration. Note that in both examples mitochondria appear to fuse and also to exhibit movement. The arrows in (**A**) mark the same position within the cell, and in (**B**) mark the position of the A-cell septum. Stained with Rhodamine 123. Imaged using a x60 objective. Bars = 2 µm.

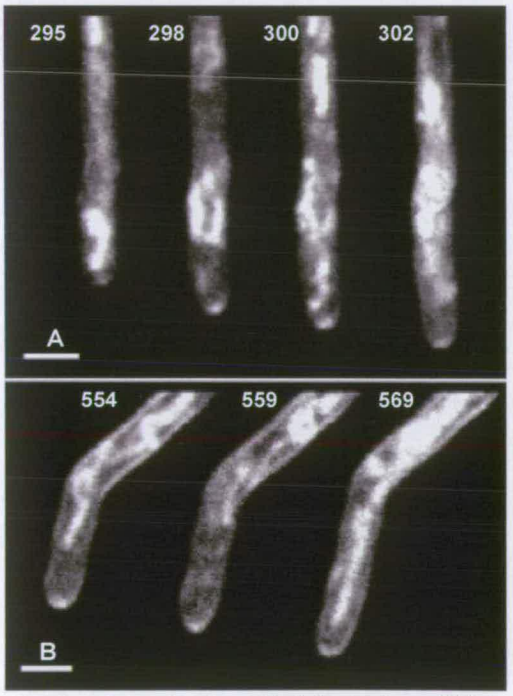

Figure 4.34: Confocal images showing mitochondrial dynamics within two different growing germ tubes (GT_3). Mitochondria typically repeatedly move into the germ tube tip region and then retract. The distance that they retract to varies and in these examples are (**A**) 1–2 µm or (**B**) 4–5 µm. The numbers are min post hydration and the dye was added at 287 and 320 min post hydration. Stained with FM4-64. Imaged using a x60 objective. Bars = 2 µm.

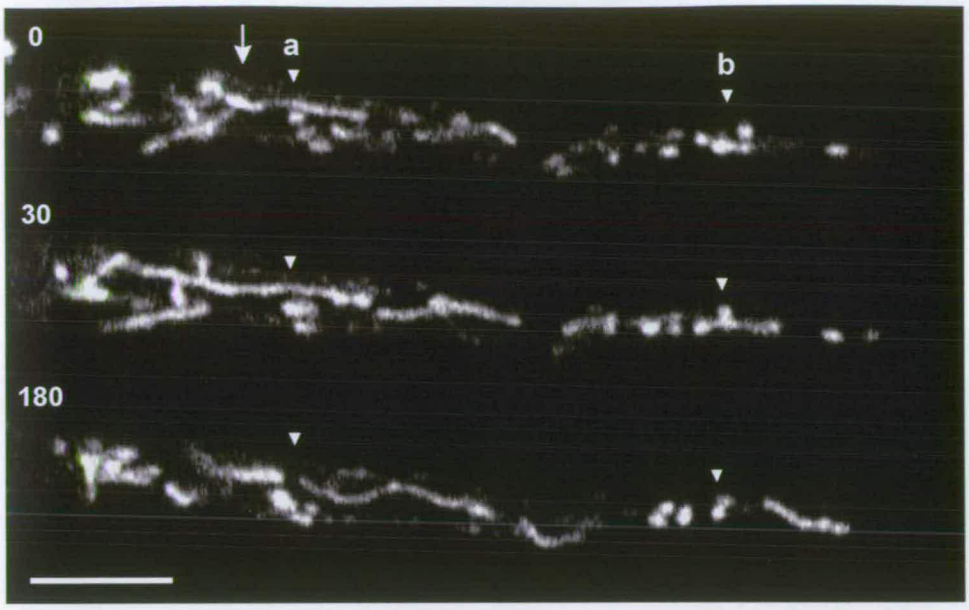

Figure 4.35: Confocal images showing mitochondrial dynamics in a germ tube produced from the apical cell of a conidium at the GT_2 stage of germination. The arrow marks the base of the germ tube. The numbers are seconds after the first image, which was collected at 3 h post hydration. The elongated mitochondrion marked by arrow (a) appears to fuse with a mitochondrion extending from the apical cell, extend into the germ tube (30 sec) and then 'break' (180 sec). At the position marked by arrow (b) smaller mitochondria exhibit dynamism, appearing to fuse (30 sec) and then separate (180 sec). Also note the elongated mitochondrion that extends towards the tip beyond these mitochondria (180 sec). Stained with Rhodamine 123. Imaged using a x60 objective. Bar = 5 µm.

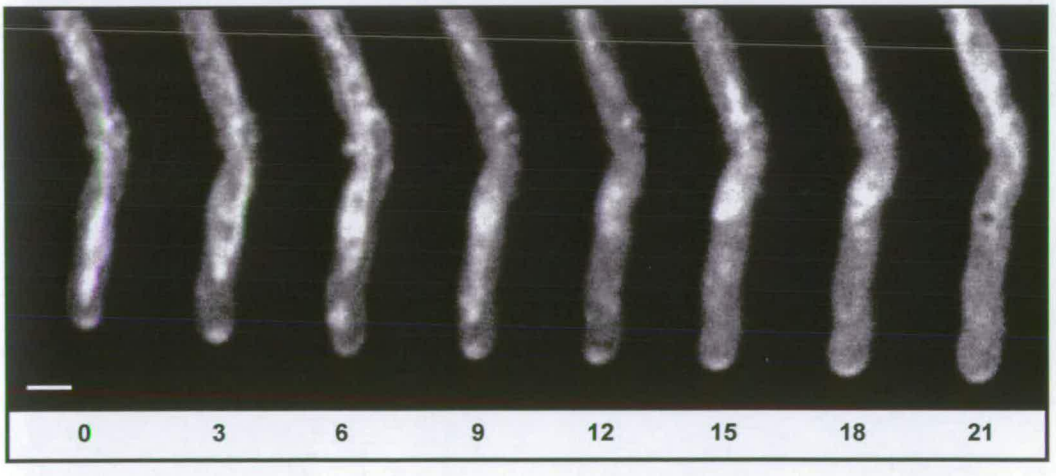

Figure 4.36: Confocal images showing mitochondrial dynamics in a germ tube produced by a conidium at the GT_3 stage of germination. Numbers are min after the first image, which was collected at 2 h 57 min post hydration. Mitochondria typically repeatedly move into the germ tube tip region and then retract. After 15–18 min they permanently retract to ~8 µm behind the tip. This coincides with the apical vesicle cluster becoming crescent-shaped at 18 min, and then disappearing at 21 min, which in turn is accompanied by the cessation of germ tube extension. Stained with FM4-64. Imaged using a x60 objective. Bar = 2 µm.

A z-series analysis (0.4–0.5 µm steps) was carried out on 13 spores. Photo-bleaching was controlled for by optically sectioning conidia in both directions: underside to upper side and *vice versa.*

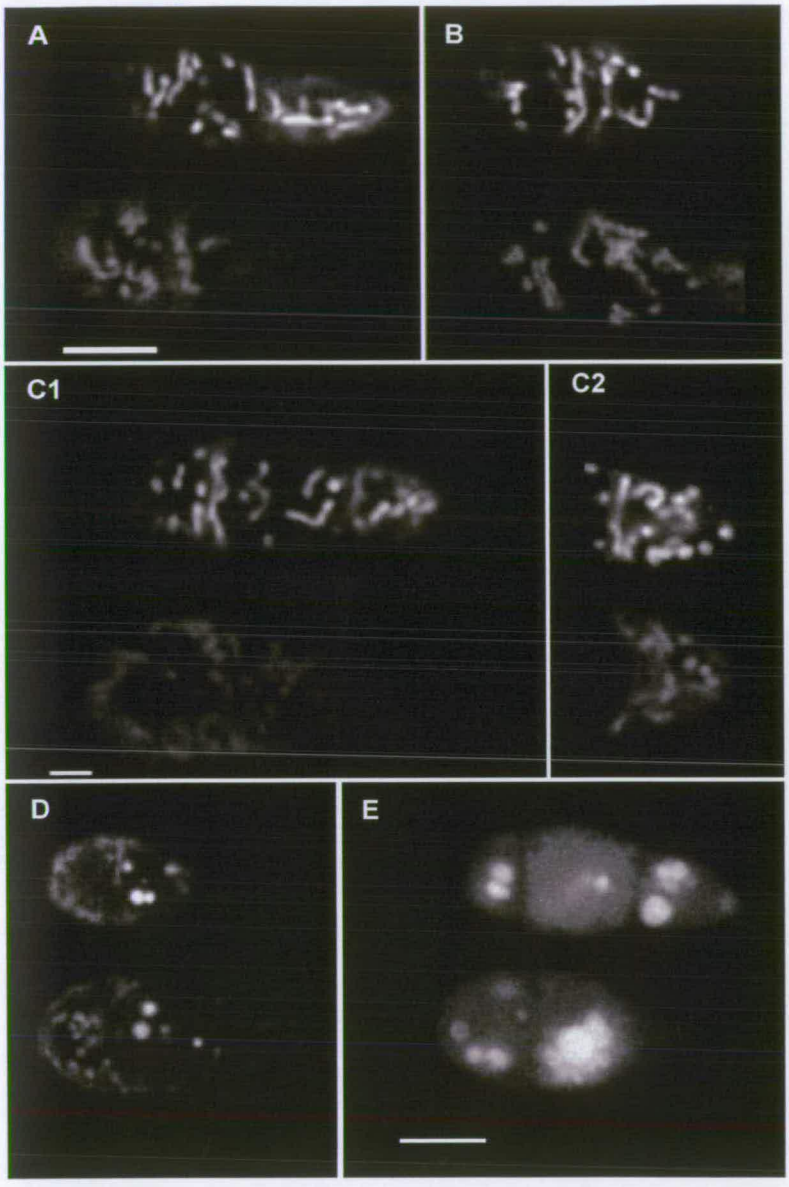

Figure 4.37 Confocal images of conidia and germlings showing the optical sections next to (*upper image* in each example), and furthest from the substratum (*lower image* in each example). Conidia (**A**) and (**B**) are ungerminated and sectioned towards the substratum, conidium (**C**) is at the EGT stage of germination and has been sectioned away from the substratum, (**C2**) is the apical cell of (**C1**). The controls are ungerminated (**D**) and germinated (**E**) and are stained with the vacuolar dye cDFFDA. Imaged using a x60 objective. Bars = 5, 2, and 5 µm respectively.

In all cases the mitochondria nearest the substratum stained more brightly than those on the opposite side of the spore, which were less fluorescent and often more

diffusely stained (Fig. 4.37A,B). This observation was confirmed in subsequent experiments. A possible explanation for this difference is that the signal is attenuated during its passage through the spore. However, although slight signal attenuation is observed with other dyes, the difference in fluorescence intensity is negligible (Fig. 4.37D,E).

4.2.5.4 Vacuolar system

Using the stain cDFFDA it was possible to image the vacuolar system in single conidia during germination using the live-cell time-course CLSM parameters (Table 2.3).

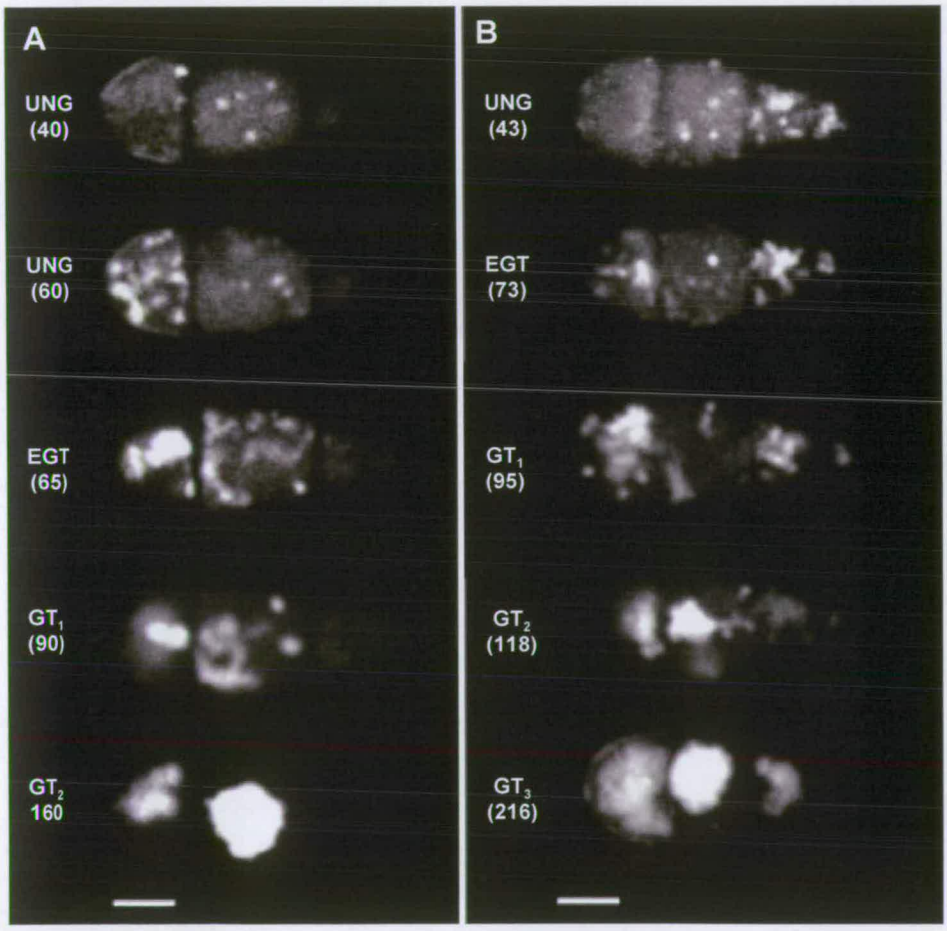

Figure 4.38: Confocal images showing two examples of live-cell time-courses of vacuolar morphology and distribution in individual conidia throughout germination. The conidium in (**A**) produces one germ tube, from the apical cell, and in (**B**) two germ tubes are produced, firstly from the basal cell (119 min) and then from the apical; stages refer to the first germ tube. Numbers are min post hydration and the dye was added at 15 min. Stained with cDFFDA. Imaged using a x40 objective. Bars = 5 µm.

In addition to using cDFFDA to sample individual conidia during germination, a number of other vacuolar dyes were also used (Table 4.1). Data were consistent between dyes, providing evidence that the presence of cDFFDA does not alter vacuolar morphology.

Two examples of live-cell time-courses are shown in Figure 4.38. The vacuolar system exhibited a variety of morphologies during germination, including small and large spherical, and globular types, and tubular vacuoles that often arose from the spherical and globular vacuoles. The morphology and dynamism varied according to the stage of germination. The main change in the morphology of the vacuolar system during germination was that it became progressively larger as germination proceeded (Fig. 4.38).

During the UNG stage of germination the vacuolar system exhibited considerable morphological variation, and the different vacuolar morphologies fell into three broad categories:

- The most common morphology observed (54% of ungerminated spores, n = 59) was a vacuolar system comprised of small (~0.5–1.0 μm in diameter), roughly spherical compartments scattered throughout the cytoplasm of all three cells and sometimes with short tubular vacuoles within the A-cell (Fig. 4.39A–C). These spores appeared to contain a rudimentary vacuolar system compared to that of other ungerminated conidial morphologies (see below). Furthermore, examples were sometimes observed in which fewer than five spherical vacuole compartments were present throughout the spores (Fig. 4.39I). It seems unlikely that this was due to insufficient dye uptake because similar observations were sometimes made after 75 min in the dye. Other categories of ungerminated vacuolar morphology were also easily stained in the same spore population, suggesting that the dye was able to enter ungerminated conidia with ease. In addition, DIC observations confirmed the presence of low numbers of small putative vacuolar spheres in ungerminated spores (Figs. 4.1A, 4.2A, 4.3A, 4.5).

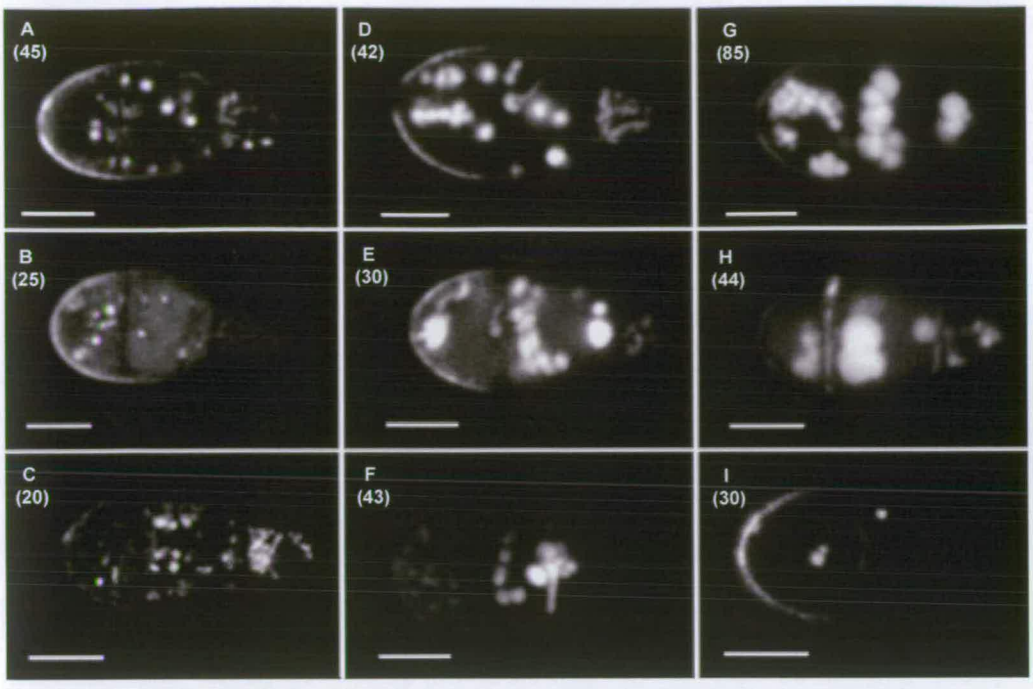

Figure 4.39: Confocal images of different ungerminated conidia showing variation in vacuolar morphology at the UNG stage of germination. Note that (**I**) was optically sectioned and there were no other stained vacuolar compartments present within the conidium. The numbers are min post hydration, dye was added at 2 min post hydration. Stained with cDFFDA. Imaged using a x40 objective. Bars = 5 μm.

- An intermediate vacuolar morphology was observed (32% of ungerminated spores, n = 59) comprised of a mixed population of small to medium (~0.5–2.0 μm in diameter), roughly spherical and globular bodies. They formed small clusters, but were generally distributed throughout each cell. Tubular vacuolar elements were commonly observed to arise from these vacuolar compartments (Fig. 4.39D–F)

- The least common vacuolar morphology observed (14% of ungerminated spores, n = 59) was that in which the M- and often B-cells contained a group of medium sized (~2–4 μm in diameter) roughly spherical and globular vacuoles (Fig. 4.39 G,H). Tubular elements were not observed to be associated with these vacuoles during the UNG stage of germination.

In general the vacuolar system of the ungerminated spore did not exhibit much dynamism, except for occasional tubular elements that "stretched" between vacuolar compartments (e.g. Figs. 4.39F, 4.40).

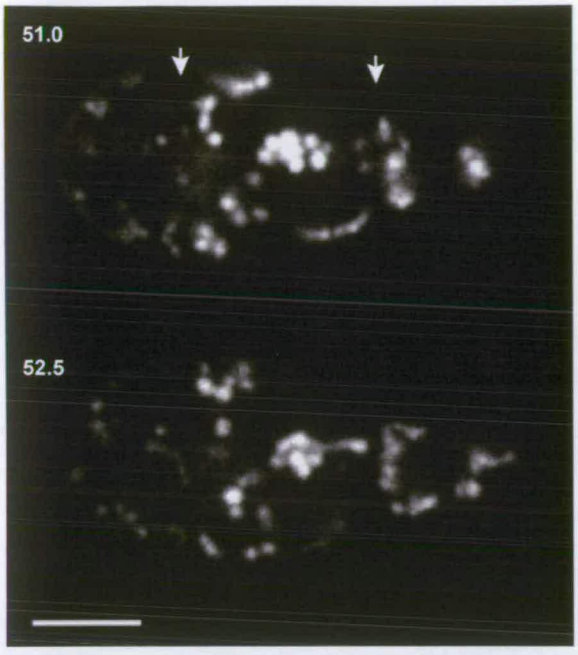

Figure 4.40: Confocal images of an ungerminated conidium showing a tubular element in the middle cell "stretching" from a group of small spherical vacuoles towards the septum (arrows). The numbers are min post hydration. Stained with cDFFDA. Imaged using a x60 objective. Bar = 5 μm.

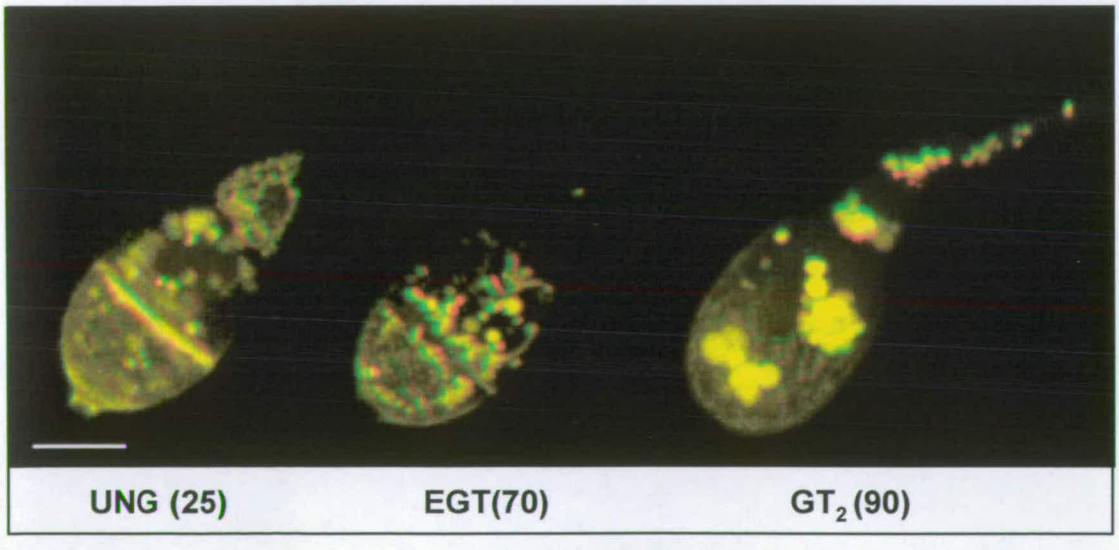

Figure 4.41: Confocal images that are projections of optical sections presented as stereo pairs of representative conidia and germlings at three different stages of germination. Numbers are min post hydration and the dye was added at 3 min. Stained with cDFFDA. Imaged using a x60 objective. Bar = 5 μm.

The variation in vacuolar morphology during the UNG stage of germination resulted in variation in the following stages of germination. By the EGT stage, the ungerminated spores that contained small roughly spherical vacuolar compartments became more like the intermediate ungerminated vacuolar category (i.e. containing a mixed population of small to medium roughly spherical and globular vacuoles), (e.g. Figs. 4.38, 4.41).

Figure 4.42: Confocal images of a germinated conidium (GT_2 stage) stained with cFDA. Note that various vacuolar morphologies are visible within the conidial cells and that (**A**) some vacuoles are localised around the apical septum, which (**B**) appears to be open, (**C**) is a different optical plane and that a line of spherical vacuoles runs from the septal pore to the base of the germ tube. The numbers are sec after the first image, which was collected at 2 h 20 min post hydration, and the dye was added at 15 min. Imaged using a x40 objective. Bar = 5 µm.

The subsequent events were as follows: as the germ tube extended during the GT_1–GT_2 stages of germination the vacuolar system became progressively larger and there was often a mixed population of vacuolar morphologies, composed of small and larger roughly spherical and globular bodies and tubular elements (e.g. Figs. 4.38, 4.42). Ultimately large groups of roughly spherical and globular vacuolar compartments formed in each cell. These were largest in the M- and then the B-cells (e.g. Figs. 4.41, 4.43). They were commonly closely associated and 3-D analysis of spores stained with the membrane dye FM4-64 provided evidence that they were

interconnected (data not shown). During germination the vacuolar system was distributed throughout the conidial cells, rather than being peripherally distributed like the mitochondria (e.g. Figs. 4.17C, 4.38, 4.41, 4.42).

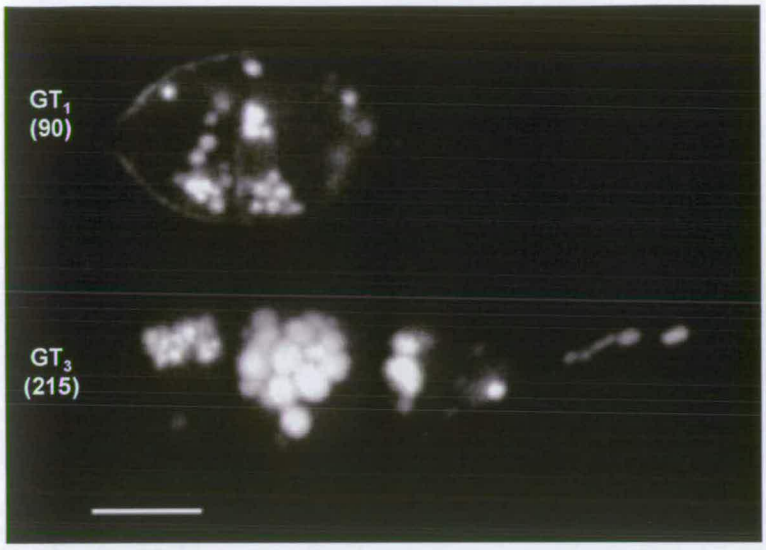

Figure 4.43: Confocal images showing an individual germling at the GT_1 and GT_3 stages of germination. Note that the vacuolar system is initially comprised of small vacuoles (GT_1) and becomes larger. Medium sized spherical vacuoles form localised groups in the middle and basal cells and a tubular vacuole is visible in the germ tube. Numbers are min post hydration and the dye was added at 15 min post hydration. Stained with cDFFDA. Imaged using a x60 objective. Bar = 5 μm.

The observed increase in vacuolar size was at least partly the result of fusion of the smaller vacuoles, and this often involved the migration of one or both of the vacuoles towards one another, and sometimes the interconnection of tubular elements (e.g. Figs. 4.38A,B, 4.44, 4.45).

Figure 4.44: Confocal images showing a time-course vacuolar morphology in the basal cell of a conidium. Note that as germination proceeds, the vacuolar system becomes larger and that vacuoles appears to fuse to form a large vacuole after 126 min. The numbers are min post hydration and the dye was added at 30 min. Stained with cDFFDA. Imaged using a x60 objective. Bar = 5 μm.

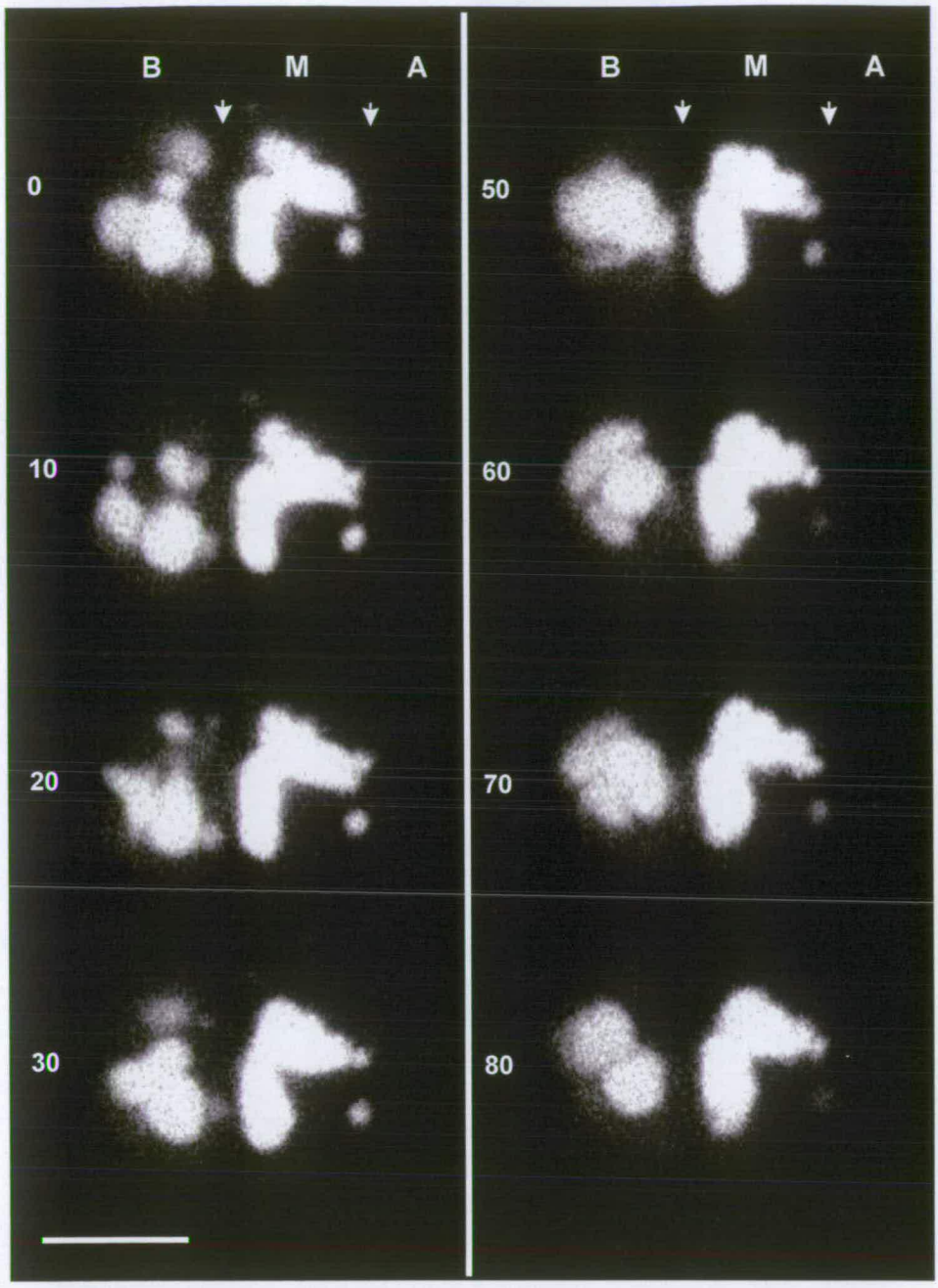

Figure 4.45: Confocal images showing vacuolar dynamics in the middle and basal cells of a germling at the GT_3 stage of germination. The vacuoles in the basal cell exhibit dynamism and appear to fuse. There is some evidence of diffusely stained vacuoles near the septum and between the main vacuolar compartments in the basal and middle cells, and that they appear to move towards the septum (10–30 sec). The apical cell vacuole is not present in the optical section. The septa between the apical (A), middle (M) and basal (B) cells are indicated by arrows and the numbers are seconds after the first image, which was collected at 4 h 4 min post hydration. Stained with cDFFDA. Imaged using a x60 objective. Bar = 5 µm.

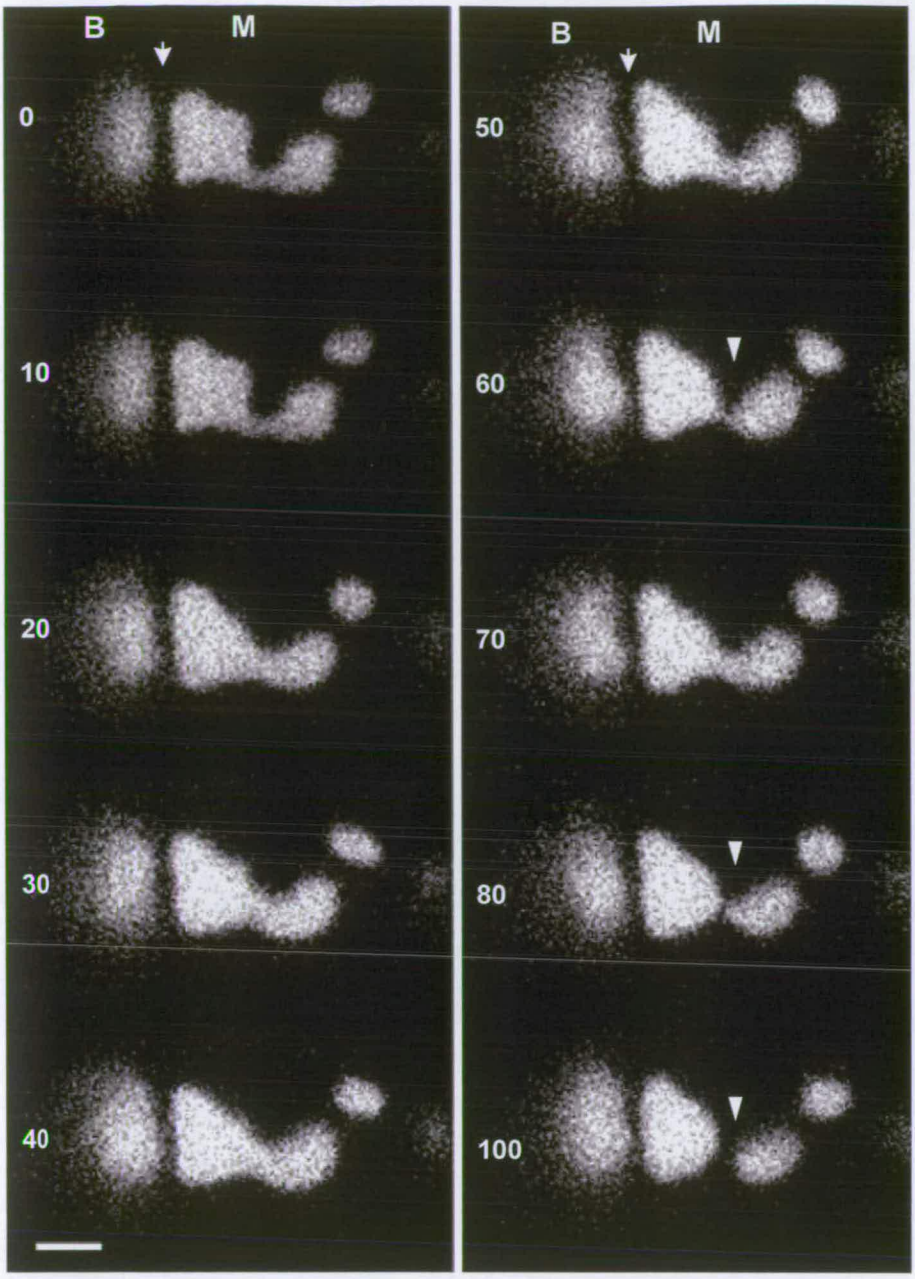

Figure 4.46: Confocal images showing vacuolar dynamics in the middle cell of a germling at the GT_3 stage of germination. The vacuoles appear to undergo fusion (0–40 sec) followed by fission (arrowhead),(60–100 sec). The septum between the middle (M) and basal (B) cells is indicated by an arrow and the numbers are seconds after the first image, which was collected at 3 h 50 min post hydration. Stained with cDFFDA, x60 Objective used. Bar = 5 µm.

Vacuoles sometimes fused and then separated (e.g. Fig. 4.46). Fusion on a more rapid and larger scale was also observed in conidial cells that were over-exposed to the confocal laser (Fig. 4.47). This type of fusion was easily distinguished from the morphological and dynamic changes of the vacuolar system within unstressed cells.

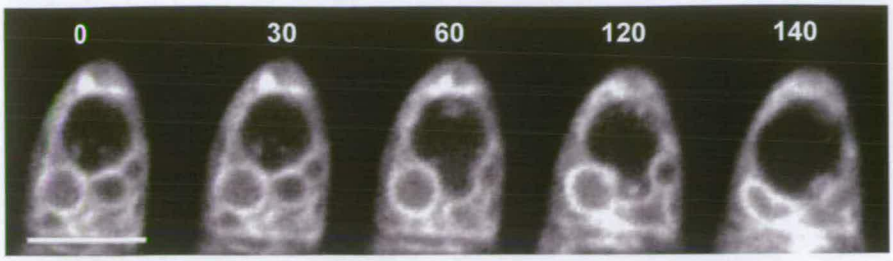

Figure 4.47: Confocal images showing rapid vacuolation in the apical cell of a germinated conidium (GT_3) that has been overexposed to the confocal laser. The numbers are sec after the first image, which was collected at 140 min post hydration. Stained with MDY-64. Imaged using a x60 objective. Bar = 5 μm.

During the GT_1–GT_2 stages, the vacuolar system was highly dynamic, exhibiting pulsatory behaviour and producing small spherical and tubular vacuoles. The tubular elements always moved in linear fashion and having emerged from one vacuole "stretched" towards one another, or towards the septum, plasma membrane, or along the germ tube (Fig. 4.48). They were transient and usually retracted back to the vacuole of origin, becoming reabsorbed (Fig. 4.49).

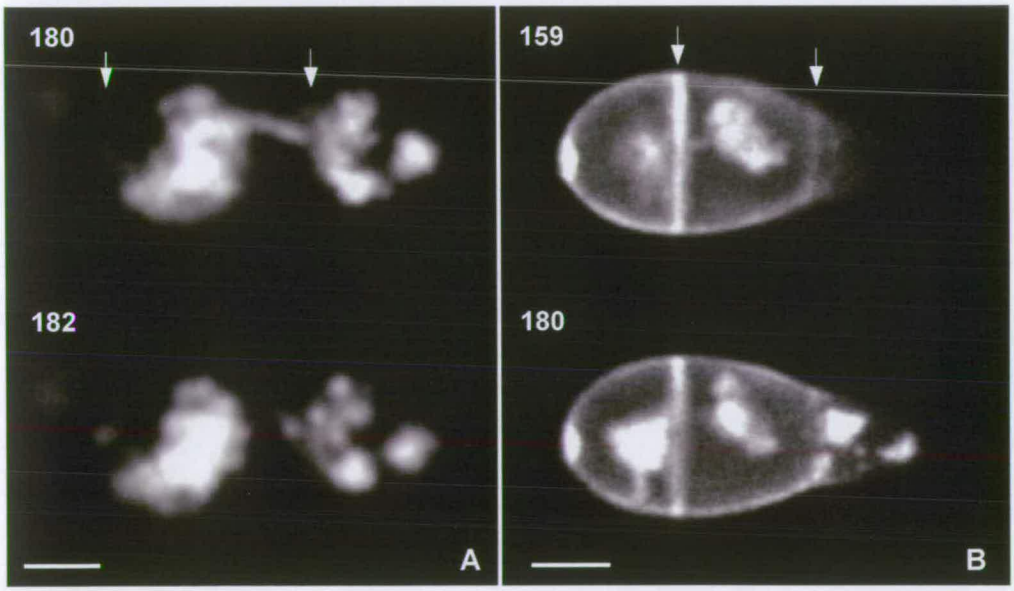

Figure 4.48: Confocal images of two germinated spores (GT_2 stage) showing vacuolar dynamics. (**A**) The middle cell vacuole transiently crosses the septum and contacts the apical cell vacuole. (**B**) Tubular vacuolar elements in the middle cell appear to contact and possibly pass through the septal pore, making contact with the basal cell vacuole which is adjacent to the septum (159 min) and 21 min later the basal cell vacuole has produced a tubular element that has moved towards to the plasma membrane. The position of the septa are marked with arrows. Numbers are min post hydration. Stained with cDFFDA. Imaged using a x40 objective. Bar = 5 μm.

Figure 4.49: Confocal image of a germinated conidium (GT_2 stage) showing the transient nature of a vacuolar tubular element. The images are 12 sec apart and collected at 3 h 36 min post hydration. The positions of the septa are marked with arrows. Stained with cDFFDA. Imaged using a x60 objective. Bar = 5 µm.

Vacuoles were never observed to produce more than one tubular vacuole simultaneously. Interestingly, these vacuolar elements appeared to be sensitive to laser irradiation, as they were less commonly observed during increased scanning by the confocal microscope laser. Small spherical vacuoles were observed to move between vacuoles, seeming to transiently fuse with one before returning to the other (Fig. 4.50).

The vacuolar system was continuous between the germinated cell and germ tube. Tubular elements extended from the germinated cell into the germ tube over distances of up to 16 µm and they were observed to retract rapidly, sometimes producing small spherical vacuoles (Fig. 4.51). There was usually a vacuole at the base of the germ tube which was most often transiently interconnected with other vacuolar compartments within the germinating cell, and from which the tubular elements and small spherical vacuoles that passed along the germ tube often originated.

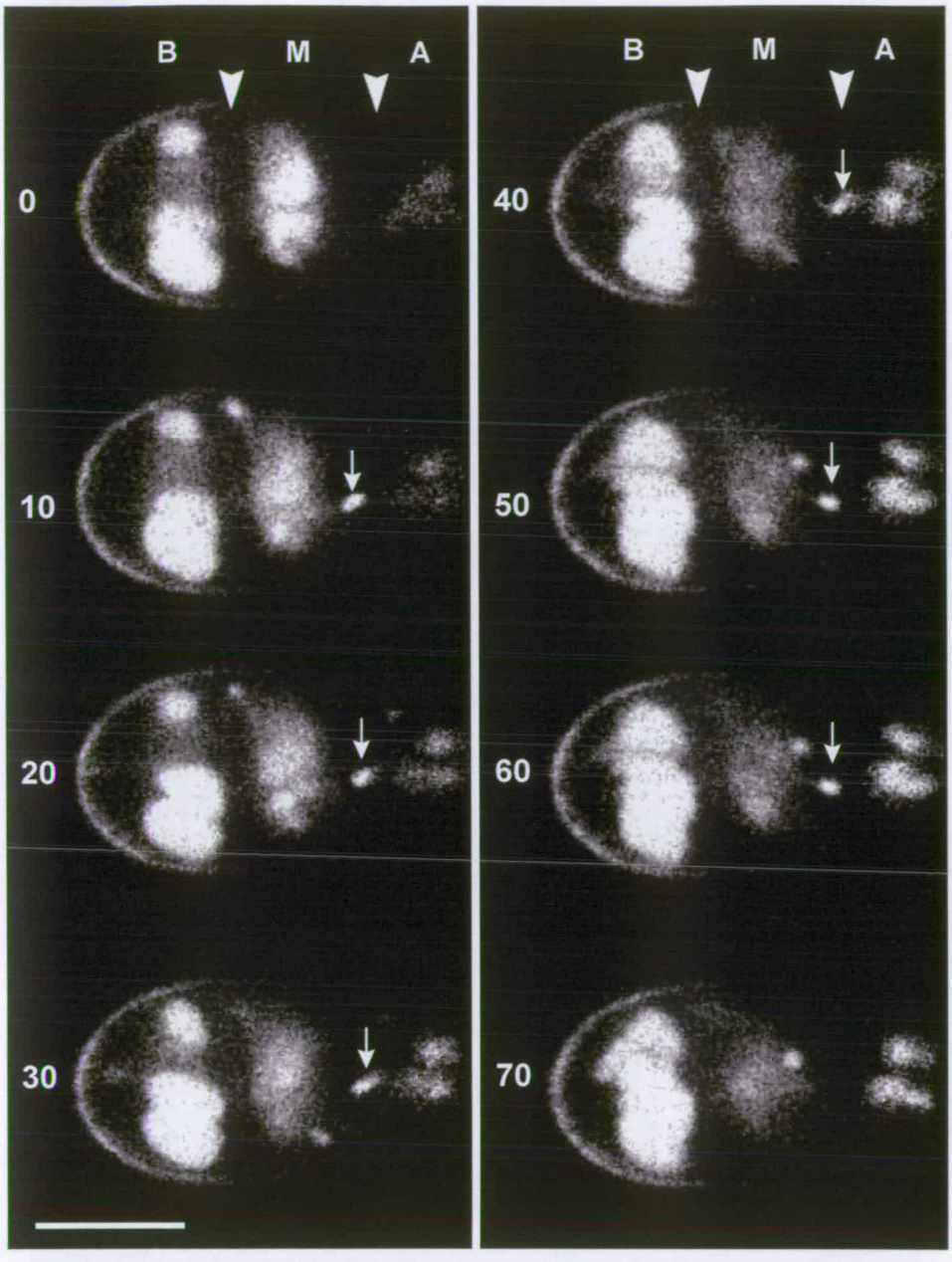

Figure 4.50: Confocal images showing vacuolar dynamics of the three conidial cells in a germling at the GT_2 stage of germination. At 10 sec a small vacuole (arrow) emerges from the large middle cell (M) vacuole and moves towards the septum (arrowhead); at 40 sec it makes transient contact with the apical cell (A) vacuole via diffusely stained "wisps", after which it returns to the middle cell vacuole. The septa between the apical (A), middle (M) and basal (B) cells are indicated by arrowheads. The numbers are seconds after the first image, which was collected at 4 h post hydration. Stained with cDFFDA, Imaged using a x60 objective. Bar = 5 μm.

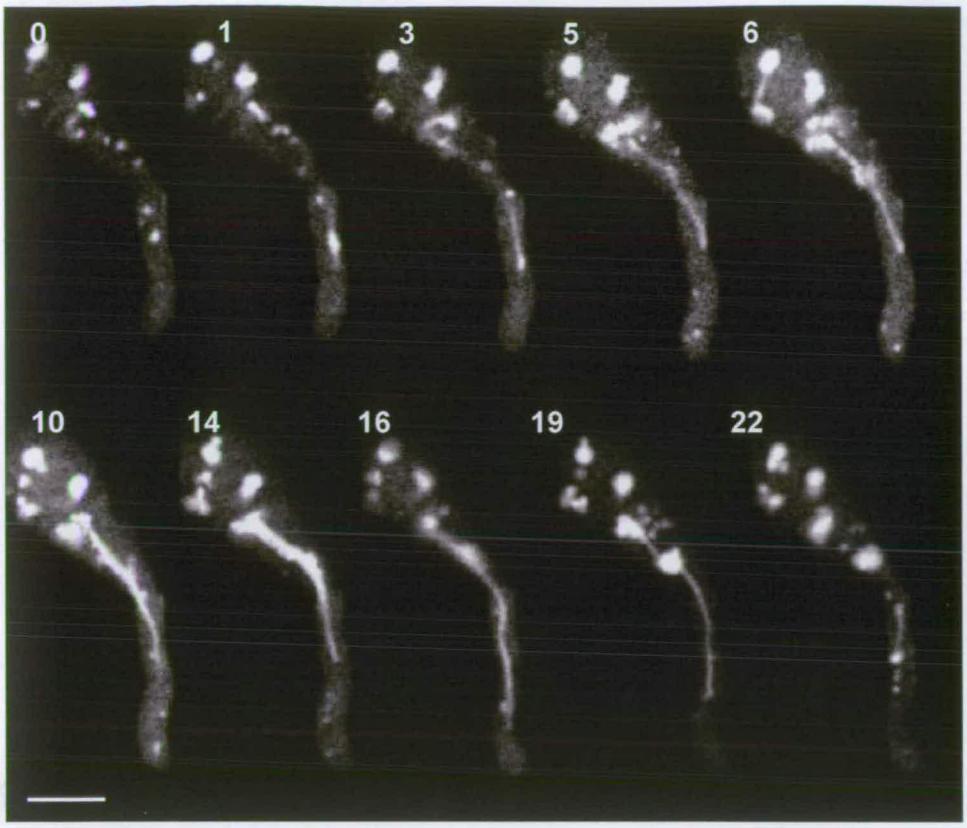

Figure 4.51: Confocal images of a growing germ tube (GT_2 stage) showing vacuolar morphology and dynamics. Tubular vacuolar elements interconnect vacuole compartments within the conidial cell and also extend into the germ tube. The numbers are min after the first image, which was collected at 2 h 40 min post hydration. Stained with cSNARF-1. Imaged using a x60 objective. Bar = 5 μm.

During further germ tube extension (GT_3 stage) the vacuolar compartments that comprised the large groups of vacuoles observed at the GT_2 stage of germination became larger and more globular (Figs. 4.38, 4.52). These vacuoles have also been characterized within unstained conidia using DIC microscopy (e.g. Figs. 4.6B, 4.7). As before, there was evidence from 3-D analysis that the vacuoles that comprised these groups were interconnected. They retained the dynamic characteristics described above, and in addition dynamic membrane-bound vacuolar inclusions were commonly observed when stained by FM4-64 or MDY-64 (Fig. 4.53). The dye FUN-1 has been reported to stain vacuolar inclusions (Haugland, 1999) and it stained small bright particles within conidia throughout germination (see Fig. 4.13, Section 4.2.3.3). A single large vacuole ultimately formed in each cell. It was comprised of one compartment, which filled the cell and was not dynamic (Fig. 5.54). These vacuoles were characteristically found in germlings that had

differentiated and sometimes in germlings with very long germ tubes. Very occasionally spores retained a more fragmented, small roughly spherical vacuolar system throughout germination. However, differentiated germlings were never observed without the vacuolar system being comprised of a large single vacuole in each cell.

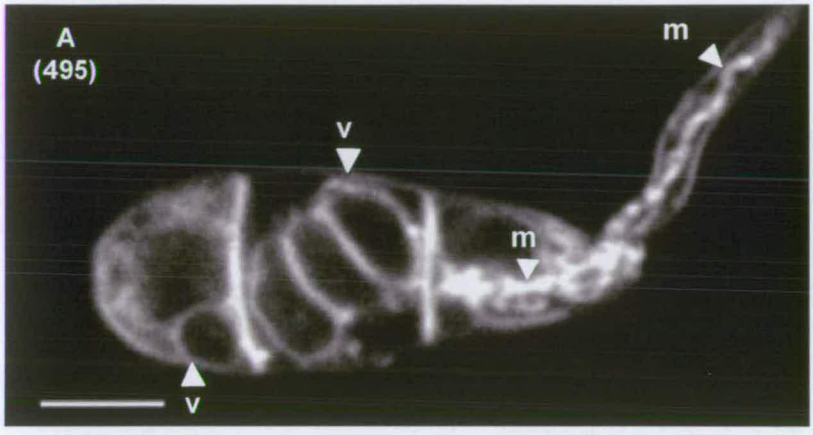

Figure 4.52: Confocal image of a germling at the GT_3 stage of germination, stained with the membrane dye FM4-64. Note the vacuoles (v) are clearly stained in the middle and basal cells and that in the middle cell the large vacuole is comprised of several subcompartments. Also note that the mitochondria (m) are stained in the germ tube and apical cell. The image was collected at 8 h 25 min post hydration and the dye was added at 45 min post hydration. Stained with FM4-64, Imaged using a x60 objective. Bar = 5 µm.

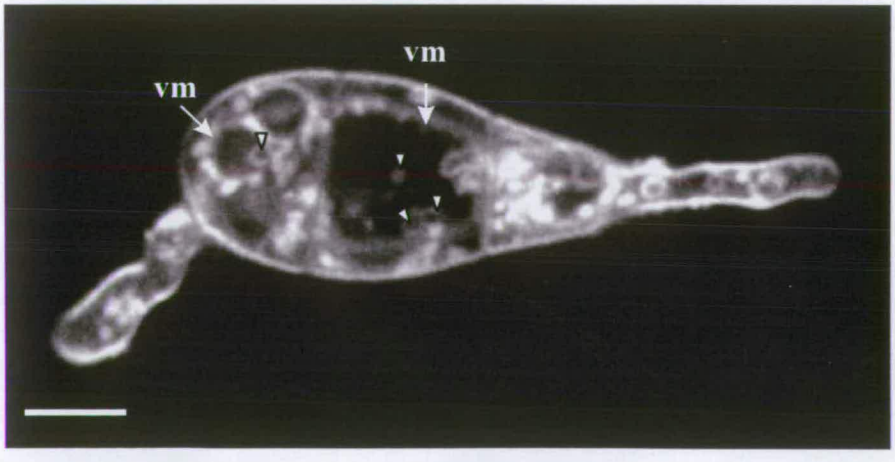

Figure 4.53: Confocal images of a germinated spore stained with the membrane stain MDY-64 showing the vacuole membrane (vm) and other membrane bound structures (arrowheads) within the vacuoles. Imaged using a x60 objective. Bar = 5 µm.

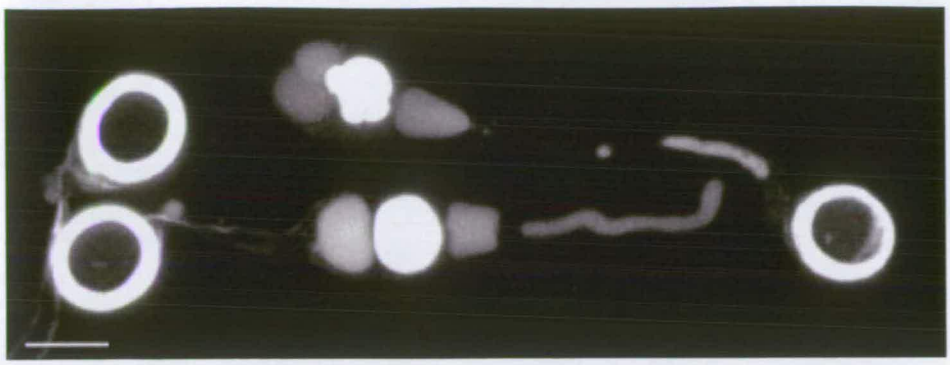

Figure 4.54: Confocal images of two differentiated germlings after 7 h post hydration, showing that each cell is filled by one large vacuolar compartment. Stained with cDFFDA. Imaged using a x60 objective. Bar = 5 μm.

Those spores that exhibited the third ungerminated vacuole category (as described above, p152) exhibited little morphological change or dynamism during germination until the GT_2 stage after which they became larger (Fig. 4.55). Note that where only one conidial cell exhibited this morphology, the vacuolar system of the other conidial cells behaved as described above (Fig. 4.55).

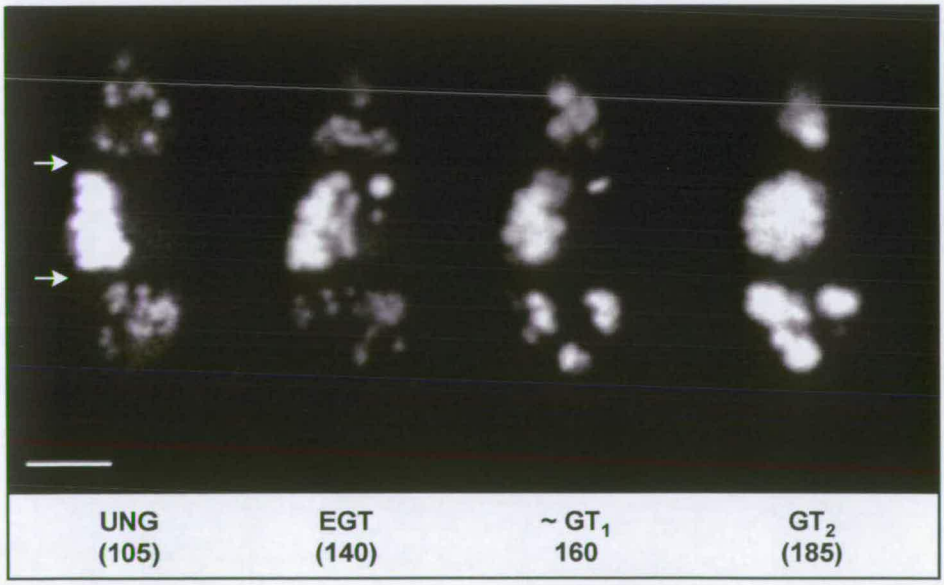

Figure 4.55: Confocal images of an individual conidium during germination. At the UNG stage of germination the middle cell contained a large globular vacuole comprised of smaller spherical vacuoles. The morphology of the large globular vacuole changes little during germination and the vacuolar compartments in the other cells behave as described in the text. Stained with cDFFDA. Imaged using a x60 objective. Bar = 5 μm.

4.2.5.5 Apical vesicle cluster

The membrane stain FM4-64 stained the apical vesicle cluster (AVC) in the growing germ tube tip (Fig. 4.56). The AVC occupied the extreme tip region extending approximately 0.5 μm behind the germ tube tip, where it was asymmetrically positioned next to the substratum.

Figure 4.56: Confocal images of germ tube tips in which the apical vesicle cluster is stained. Stained with FM4-64. Imaged using a x60 objective. Bar = 5 μm.

Studies indicated that the AVC changed position in the apical dome before a change in the orientation of germ tube growth (Fig. 4.57). There was no evidence of an unstained core region; however due to its very small size it would probably be beyond the resolving power of the confocal microscope, even if present. The AVC appeared to be very sensitive to laser scanning; a decrease in germ tube growth rate was accompanied by a change in the AVC shape to a thin crescent in the germ tube tip, which ultimately disappeared with the cessation of germ tube growth (Fig. 4.58).

Figure 4.57: Confocal images of two different germ tubes in which the apical vesicle cluster is stained. The apical vesicle cluster appears to change position as the germ tube changes its direction of growth. The numbers are min after the first image. Stained with FM4-64. Imaged with a x60 objective. Bar = 5 μm.

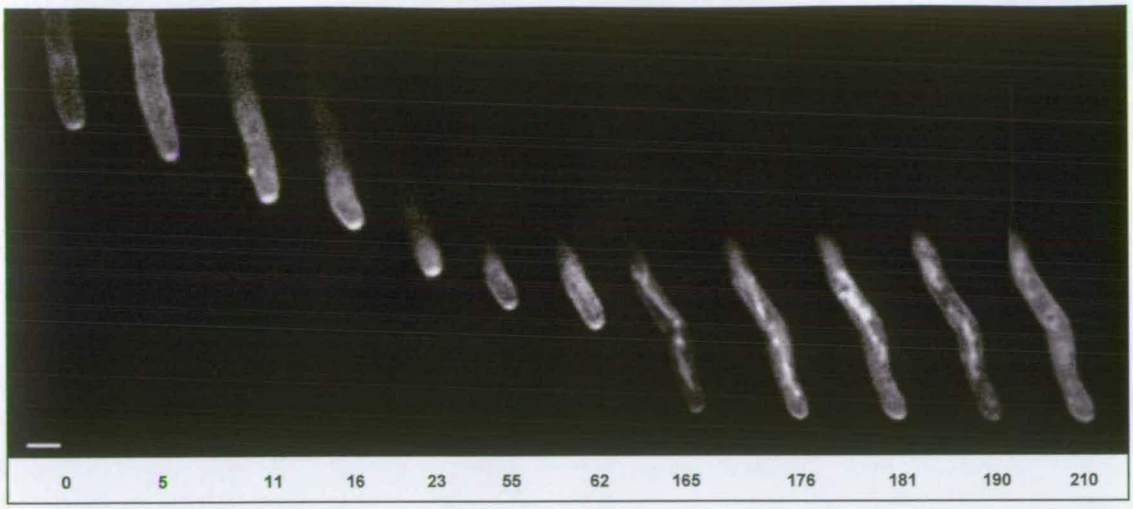

Figure 4.58: Confocal images of a growing germ tube in which the apical vesicle cluster is stained. Note that concomitant with germ tube growth slowing, the apical vesicle cluster becomes crescent shaped (165–181 min) and then disappears, and the germ tube stops growing (181 min). The times are min after the first image (0 min), which was collected at 8 min post dye and 5 h 20 min post hydration. Stained with FM4-64. Imaged using a x60 objective. Bar = 2 μm.

4.2.5.6 Peripheral spots

Brightly fluorescent spots were labelled by FM4-64. They were always located in the periphery of the germ tube and so will be referred to as peripheral spots (PS). The following observations were made.

- A number of fluorescent dyes with different staining affinities stained the PS to different degrees but the most consistent and brightest stain was FM4-64 (Table 4.3, Fig. 4.59).

- They are present throughout germination but are most dense during the EGT–GT_2 stage of germination (up to 19.4 ± 3.5 μm along the germ tube from its base; n = 14) (Fig. 4.60).

- They cover the germ tube and appear less dense at the substratum interface, where they are often absent (Fig. 4.61).

- They are produced at the germ tube tip, and are commonly observed to arise in pairs. After they are produced, PS do not change their position on the plasma membrane (Figs. 4.62, 4.63).

Figure 4.59: Confocal images of germ tubes in which the peripheral spots have been stained with a range of dyes: (**A**) FM4-64, (**B**) cFDA, (**C**) cDFFDA, (**D**) FITC-dextran (10 kDa), (**E**) MDY-64. Note that FM4-64, cFDA and cDFFDA do not stain the GTM. x60 (**A**, **C**–**E**) and x40 (**B**) objectives used. Bars = 2 µm.

- They do not change in size as the germ tube extends but size varies between individual PS (Fig. 4.62). Although variation in the size of PS was observed, they were generally ~0.4 µm in diameter when stained with FM4-64 and MDY-64. They often appear to be marginally smaller than this when stained with other dyes shown in Table 4.3, and in particular with cFDA and cDFFDA (Fig. 4.59).

- Germ tubes produce PS on hydrophobic substrata (Teflon™), hydrophilic substrata (heat treated CS) and the intermediate detCS (Fig. 4.64).

- They are extracellular. This was confirmed by the observation that the PS stained immediately on addition of FM4-64 to the external solution, and *prior to* the plasma membrane (which will always become stained before any internal structures are stained because FM4-64 is a membrane stain), (Fig. 4.65). The position of the PS relative to the cell wall was not determined (i.e. outside of the cell wall or within the periplasmic space), however, their size suggests that they must be, at least in part, outside of the cell wall. Note that although on occasions the PS appeared to be within the germ tube, that this is expected because of the small size of the germ tube relative to the depth of the optical sections: the germ tube is ~1.5 µm in diameter and has a rounded shape (e.g. Fig. 3.9C, Section 3.2.5.2), and since the z-resolution (with a x60 oil objective) is ~0.8 µm, a

median section through a germ tube would be expected to contain regions of the plasma membrane from the upper part of the optical section, and these would then appear as being located within the germ tube.

- Similar PS were also stained at the substratum interface of appressoria (Fig. 4.66).

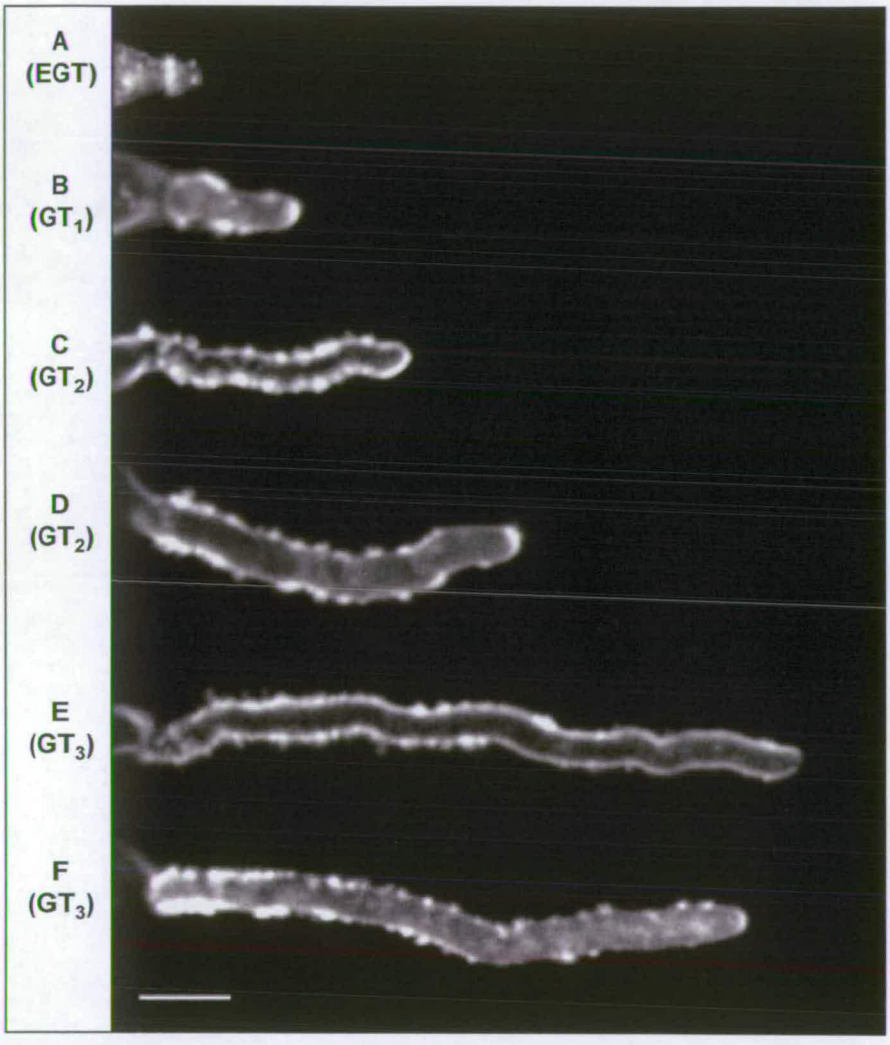

Figure 4.60: Confocal images of germ tubes produced by spores at different stages of germination showing the peripheral spots. Generally peripheral spots are not present in the later stages of germ tube extension (GT_3), but in some germ tubes they continue to be present (**F**). Note that (**A**) is stained with MDY-64 and (**B–F**) are stained with FM4-64. Imaged using a x60 objective. Bar = 5 μm.

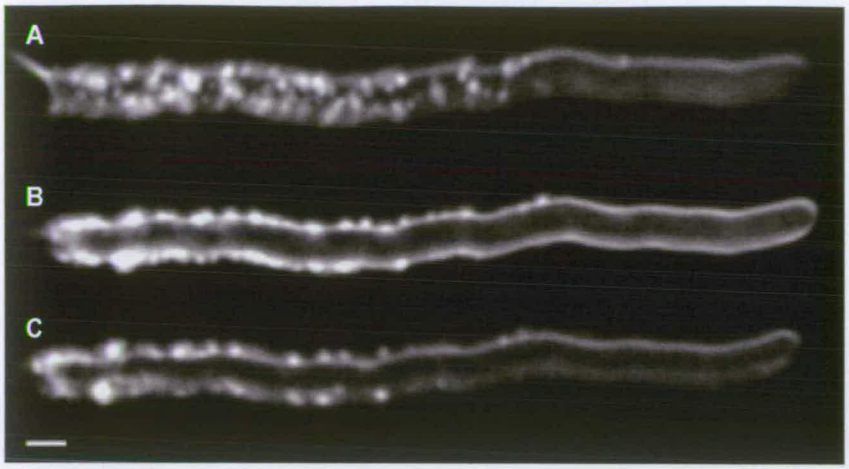

Figure 4.61: Confocal images of 3 different optical sections through a germ tube showing the distribution of the peripheral spots (PS), (**A**) is furthest from substratum and shows that the PS appear to coat the upper side of the germ tube, (**B**) is a median optical section and (**C**) is next to the substratum and shows that they appear to be absent in the region that the germ tube is in direct contact with the surface. Stained with FM4-64. Image collected at 3 h post hydration and the dye was added 5 min prior to collecting the image. Imaged using a x60 objective. Bar = 5 μm.

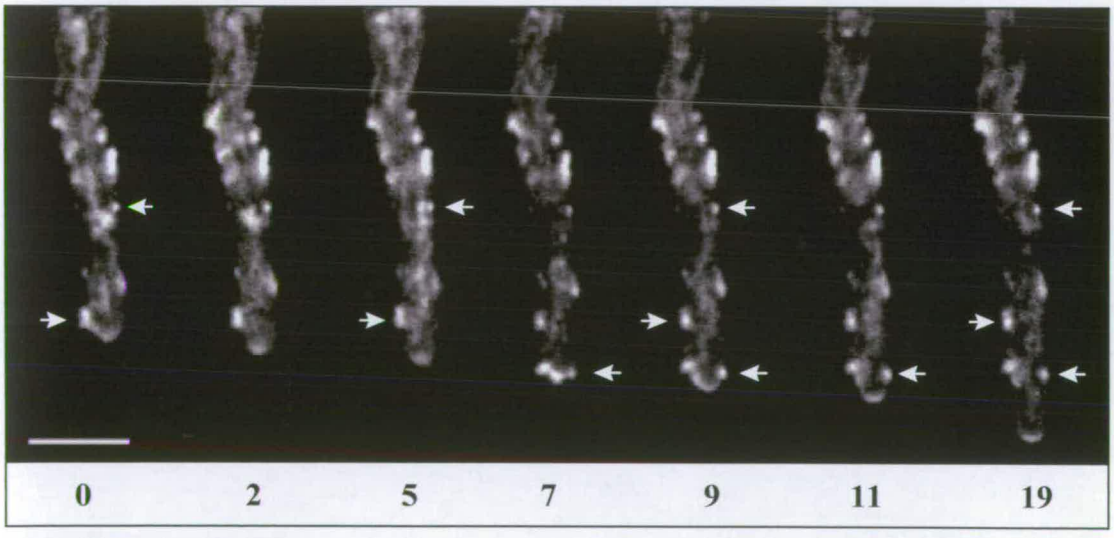

Figure 4.62:Confocal images of a growing germ tube showing that peripheral spots (arrows) are produced at the tip of the germ tube and do not move from their position at the plasma membrane. Numbers are min after the first image (0), which was collected at 1 h 2 min/10 min post hydration/dye. x60 objective used. Bar = 2 μm.

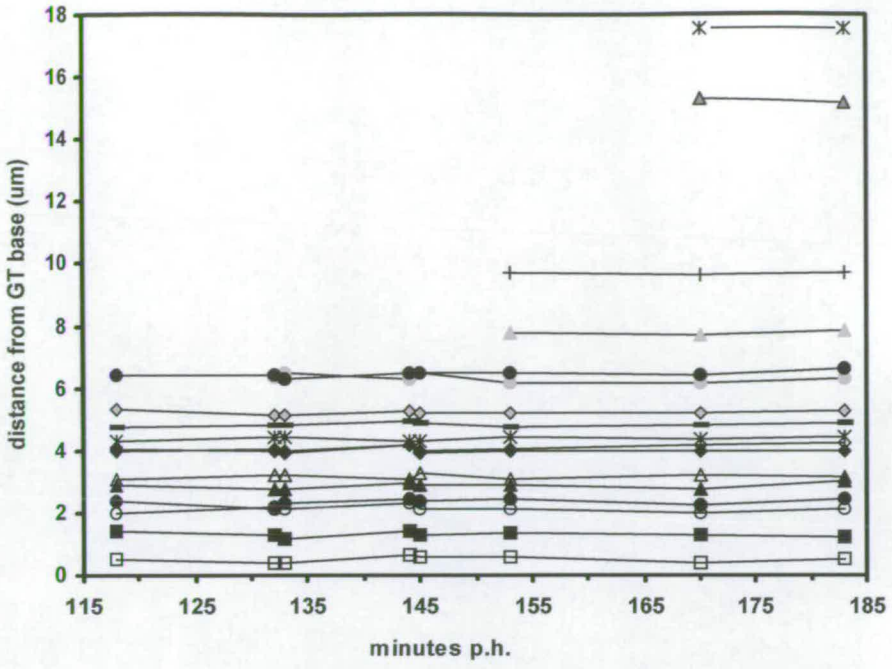

Figure 4.63: Positions of 18 peripheral spots during 60 min of germ tube growth. The distance is measured from the base of the germ tube and measurements were taken from images in which the germ tubes were stained with FM4-64 and imaged with a x60 objective.

Figure 4.64: Confocal images of three different germ tubes showing that peripheral spots are produced by germ tubes on (**A**) Teflon™, a highly hydrophobic substratum, (**B**) detCS, a moderately hydrophobic substratum, and (**C**) heat-treated CS a hydrophilic substratum. Stained with FM4-64. Imaged at (**A**) 4 h/1 min and (**B**, **C**) 4 h 20 min/3 min post hydration/post dye. Imaged using a x60 objective. Bar = 5 μm.

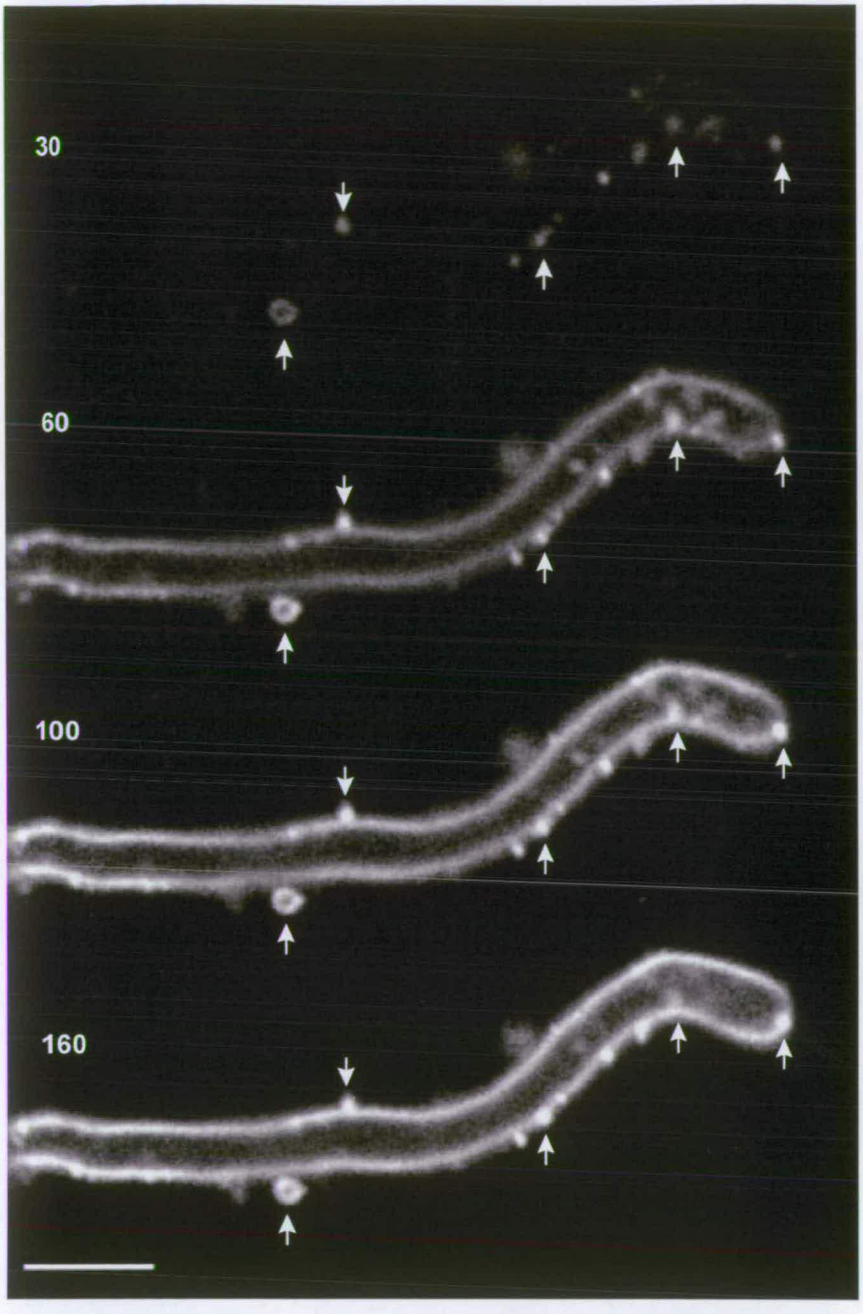

Figure 4.65: Confocal images of a germ tube stained by the dye FM4-64, and showing that the membrane-associated spots (arrows) stain before the plasma membrane. Numbers are sec post dye, which was added at 2 h 26 min post hydration. Imaged using a x60 objective. Bar = 5 µm.

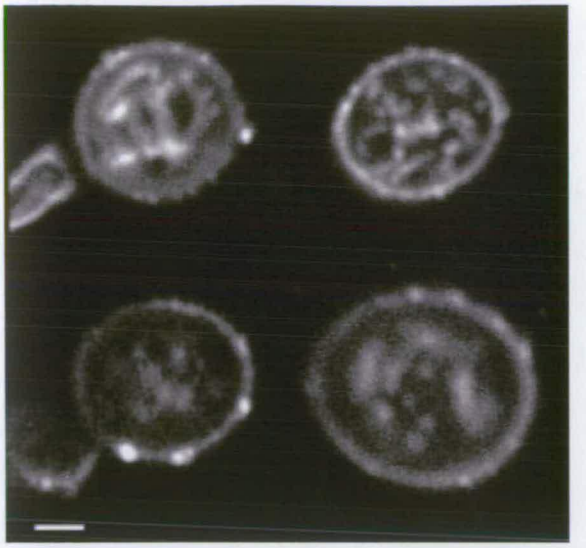

Figure 4.66: Confocal images of four appressoria stained with FM4-64 showing that there is evidence that peripheral spots are also present at the substratum interface of appressoria. Imaged using a x60 objective. Bar = 2 µm.

4.2.5.7 Mucilage associated with conidia during germination

Spore tip mucilage (STM) and germ tube mucilage (GTM) were imaged by DIC light microscopy (Figs. 4.1, 4.4). A number of dyes with different staining affinities were observed to stain STM and GTM (Fig. 4.67). The results are summarised in Table 4.3.

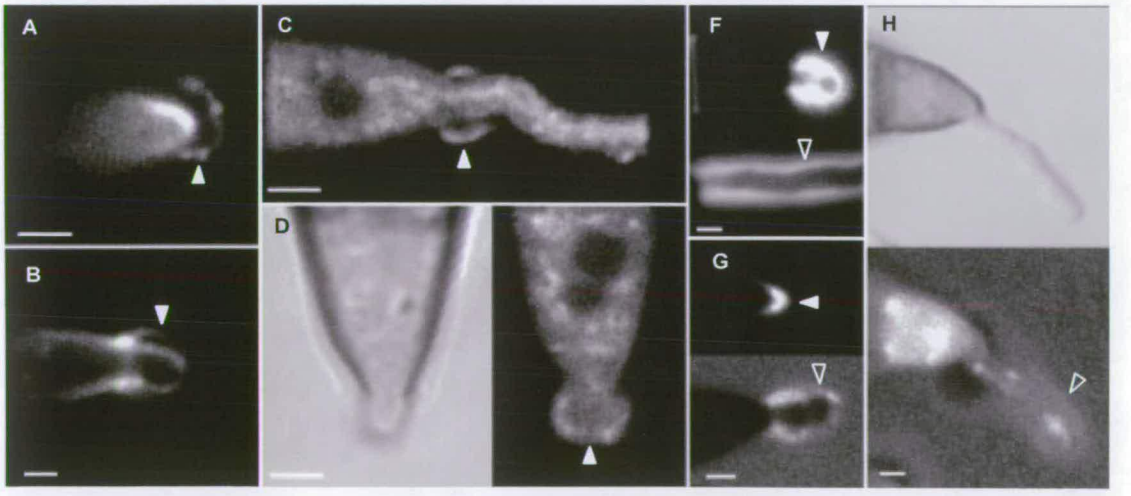

Figure 4.67: Confocal images showing examples of spore tip mucilage (STM) (white triangle) and mucilage associated with the germ tube (GTM) (black, white edged triangles), stained by (**A, B**) FM4-64 which only stains STM, (**C, D**) MDY-64, which in this case only stains STM, but is also often observed to stain GTM. (**F**) Lucifer Yellow CH and (**G**) FITC-dextran (10 kDa) stain both the STM and GTM very brightly and (**H**) FUN-1 which does not stain the STM. Note that (**D**) and (**H**) have an accompanying bright field image. Imaged using x60 (**A–D**) and x40 (**E–H**) objectives. Bars = 2 µm.

Dye	STM	GTM	PS	Staining affinity
Lucifer Yellow CH	+	+	-	aliphatic aldehydes
FITC-dextran	+	+	+	proteins (pH-sensitive fluorescence; pH 5–8)
cSNARF-1 AM	+	-	-	esterase activity (pH sensitive fluorescence)
FM4-64	+	-	+	lipophilic: including membranes and lipoproteins
MDY-64	+	~ +	+	membranes
Nile red	+	+	+	lipid
cFDA	-	-	+	esterase activity (pH sensitive fluorescence)
cDFFDA	-	-	+	esterase activity (pH sensitive fluorescence)
FUN-1	-	+	-	vacuolar inclusions in metabolically active cells

Table 4.4: A range of dyes stained the spore tip mucilage (STM), germ tube mucilage (GTM) and/or peripheral spots (PS). The degree of staining varied, but was unaffected by the stage of germination. MDY-64 sometimes stained the GTM. The information presented in the table was obtained from: Stewart, 1981; Butt *et al.*, 1989; Oparka & Read, 1994; Betz *et al.*, 1996; Haugland, 1999.

4.2.5.8 Storage compounds: glycogen

Glycogen was stained by the PAS technique using Lucifer Yellow CH as the fluorescent reporter, and then imaged by confocal microscopy (See Section 2.7.3.1). Tests were carried out to assess whether the staining observed originated exclusively from Lucifer Yellow CH-bound glycogen, or from either (a) unbound dye that had not been washed out of the cells, or (b) cellular autofluorescence caused by exposure of the cells to the acid used in the PAS reaction. There was no evidence that fluorescence originated from either of these sources.

In ungerminated conidial cells the entire cytoplasm was stained, with a central region of intense fluorescence indicating that these were rich in glycogen (Fig. 4.68). These regions were most abundant within the B- and M-cells, in which they were centrally located. The A-cell contained a smaller region of intense staining and in some cases exhibited very little staining at all. The brightly fluorescent regions within the M- and B-cells contained negatively stained spherical and sometimes tubular regions. During DIC imaging, a uniform region within the centre of the cell was identified that had a

pitted appearance, sometimes with tubular structures running though it. This region in the cell corresponds to the glycogen staining observed here. In germinated conidia the general pattern of staining was the same as in ungerminated conidia, but the fluorescence was commonly not as intense in the central region (Fig. 4.69).

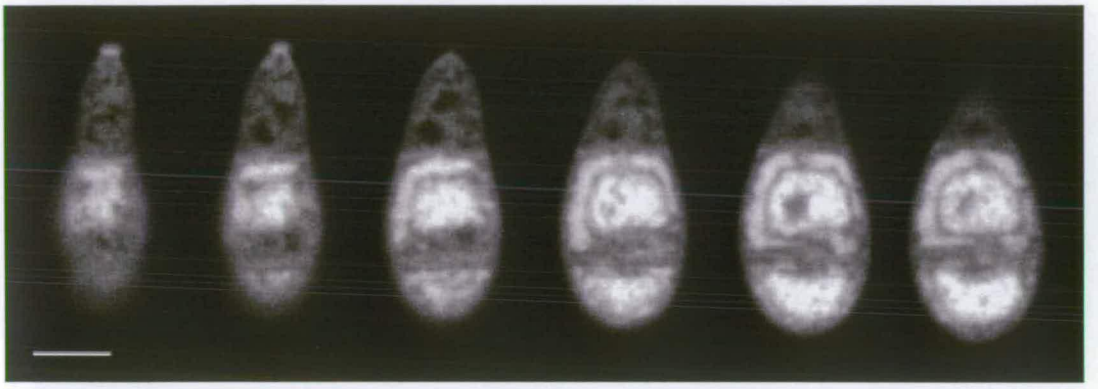

Figure 4.68: Confocal images showing optical sections through an ungerminated conidium (15 min post hydration) in which glycogen has been stained. The staining is generally much less intense within the apical cell, and in the middle and basal cells there is typically a large central region of intense staining. Note the negatively stained regions in the middle cell. Stained by the PAS technique, using Lucifer Yellow CH. Imaged using a x60 objective. Bar = 5 μm.

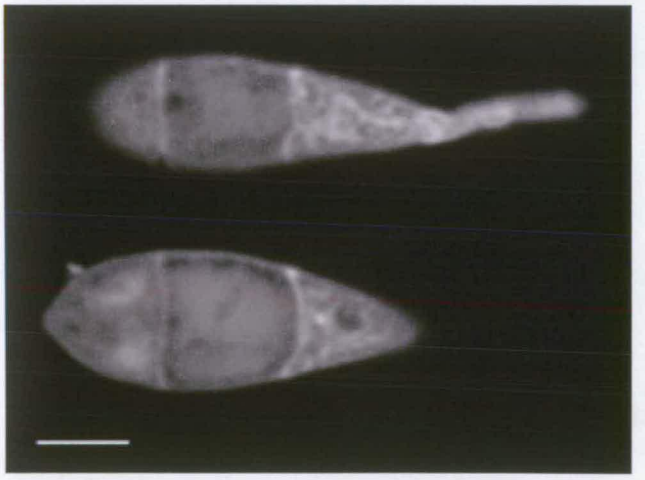

Figure 4.69: Confocal images showing two different optical sections through a germinated conidium (1 h 45 min post hydration) in which glycogen has been stained. Note that the staining is characteristically less intense in germinated spores compared to ungerminated spores (cf. Fig. 4.68). Stained by the PAS technique, using Lucifer Yellow CH. Imaged using a x60 objective. Bar = 5 μm.

4.2.5.9 Storage compounds: lipids

Attempts were made to stain lipid bodies in ungerminated conidia using the lipophilic stains Nile red, FM4-64 and MDY-64. Only diffuse fluorescence was visible after live conidia were incubated in Nile red for 30 min.

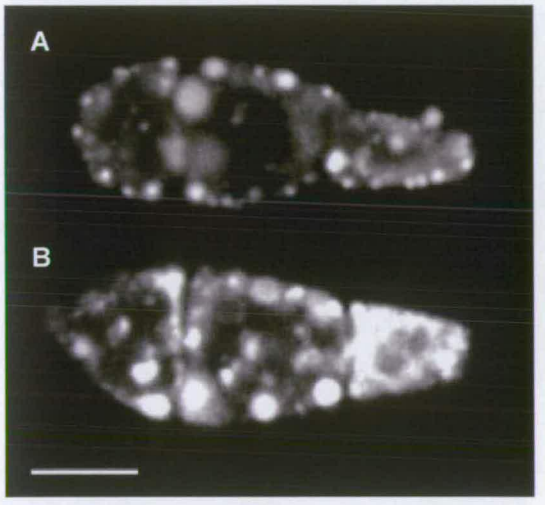

Figure 4.70: Confocal images of two ungerminated conidia that were killed by desiccation, and then stained with the lipophilic dyes (**A**) MDY-64 or (**B**) FM4-64. Brightly fluorescent large spots are characteristically stained in all three cells that could be lipid bodies. Imaged using a x60 objective. Bar = 5 µm.

Desiccated spores were stained with FM4-64 and MDY-64 (see Section 2.7.3.2). A minimum of 20 conidia were analysed for each dye. Both dyes were able to cross the plasma membrane and enter the cytoplasm, rather than being restricted to staining the endomembrane system (Haugland, 1999). The conidial cells were brightly stained with some more diffuse fluorescence that probably originated from the localisation of the dye into membranous cellular elements. Spherical structures of various sizes were also stained and the dense, even nature of the staining suggested that the structures were non-membranous and thus likely to be cellular inclusions containing lipid (Fig. 4.70). These spheres were commonly located in the corner of cells between the septa and plasma membrane within the M- and B-cells. Smaller stained spheres were located around the periphery of the cells and within the A-cell, which rarely contained large spheres.

4.3 DISCUSSION

The nuclear, mitochondrial and vacuolar system organization and dynamics were imaged in live conidia and germlings. Attention was paid to optimising the imaging conditions with respect to the dyes used, the dye concentration and the confocal microscope settings, and also with respect to the artificial substratum used for the *in vitro* system (Section 3.2.2). However, even when optimised, there was variation between spores with respect to how resilient they were, and so care had to be taken to distinguish between organelle changes in morphology and position that are part of the normal developmental stages of germination, and those changes induced by confocal imaging. In this study several changes in organelle position and morphology were symptomatic of perturbation from over-exposure to the laser: for example the mitochondria spontaneously retract from the growing germ tube tip, cells become rapidly vacuolated, and the apical vesicle cluster changes shape or even disappears. Thus, even though the conditions were optimised, the data had to interpreted with some caution and in the context of the *in vitro* system.

4.3.1 Nuclei

The problems encountered in confocal imaging of nuclei in live cells during germination meant that a population analysis had to be performed. The results were supported by observations of live conidia during germination made by DIC microscopy analysis. The conidium usually contained three nuclei, each cell being uninucleate. In other species, the spore nuclei are roughly spherical and usually centrally situated within the cell (Hawker & Abbot, 1963; Delvecchio, *et al.*, 1969; Gull & Trinci, 1971; Hoch & Staples, 1983; Mims *et al.*, 1988, 1997; Van Dyke & Mims, 1991; Roberts *et al.*, 1996; Mollicone & Longcore, 1999). In *M. grisea* the nuclei were also roughly spherical, but the B- and M-cell nuclei were rarely centrally situated in the cell. The position of the M- and B-cell nuclei changed during germination; they moved towards the longitudinal axis of the conidium, often remaining near the B-septum. The A-cell nucleus was centrally positioned within the cell throughout germination, sometimes moving towards the base of the germ tube during the latter stages. Nuclear migration only occurred during the latter stage (GT_3)

of germination, at which stage the germ tube is often developing an appressorium. During migration, the nucleus became elongated in order that it could fit the narrow germ tube; this has also been observed in other species during nuclear migration within germ tubes (Hawker & Abbot, 1963; Van Dyke & Mims, 1991). A summary of nuclear distribution and dynamics is shown in Figure 4.71A.

Germinated cells of *M. grisea* stained with DAPI have been reported to have a single brightly fluorescent spot associated with the nucleus (Bourett & Howard, 1990). In this study, cytoplasmic spots were brightly stained by the dye SYTO 12 which stains both RNA and DNA, and there was evidence that they might be associated with the nucleus. On the basis of these findings it is unclear what these structures are.

There was no evidence that nuclear division occurred during germination; in cases where the nucleus had migrated along the germ tube during the latter stage (GT_3) of germination, the germinated cell had no nucleus. Bourett & Howard (1990) analysed the nuclear cycle during germination and differentiation using DAPI in fixed cells. They reported that the nucleus in the germinated cell migrated to the proximal end of the germ tube where nuclear division occurred and one nucleus then returned to the conidium. However, Bourett & Howard (1990), analysed germlings that were differentiating, and the analysis here was restricted to the stages of germination before appressorium formation.

The conidia of *N. crassa* can contain different numbers of nuclei, and the number in a spore cell is often observed to increase during or just before germination (Schmit & Brody, 1976; Maheshwari, 1999). The number of nuclei observed in *M. grisea* conidia was constant throughout germination. On only one occasion were two nuclei observed within a single cell of an otherwise normal conidium. Multinucleate conidial cells have been previously reported in *M. grisea*, although it has been suggested that the nuclear stains used were also staining other cellular components such as lipid (Ou, 1980b). Subsequent TEM and fluorescence microscopy studies have found the cells to be uninucleate (Bourett & Howard, 1990).

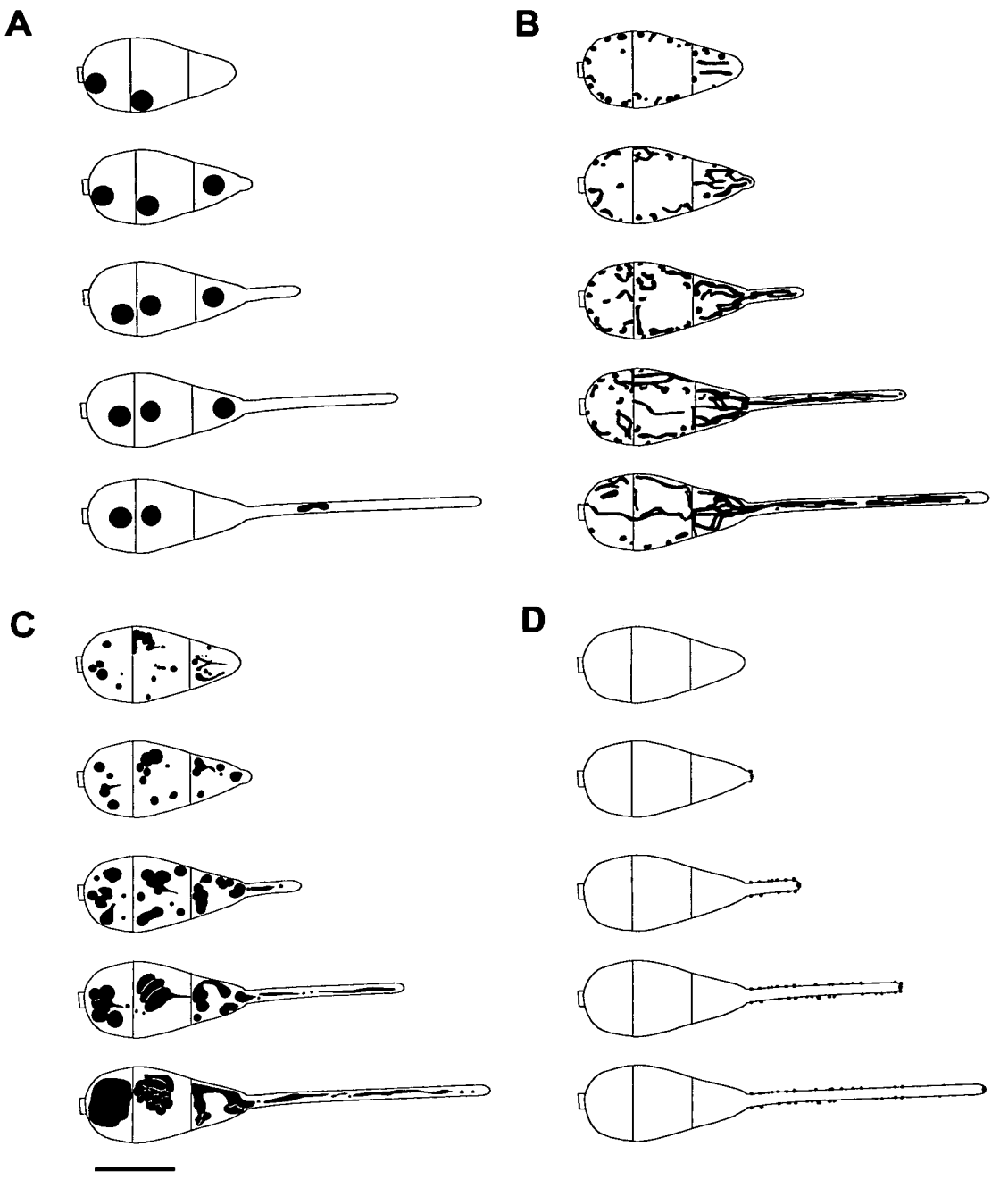

Figure 4.71: Schematic summary of the main features of the organization and distribution of (**A**) nuclei, (**B**) mitochondria, (**C**) vacuolar system, and (**D**) the peripheral spots and apical vesicle cluster in conidia during germination. Bar = 10 μm.

4.3.2 Mitochondria

It was possible to image mitochondrial morphology and dynamics within live conidia during germination. A summary of mitochondrial distribution and dynamics is shown in Figure 4.71B. The morphology of mitochondria in the germlings of *M. grisea* has

not been described previously, although they have been shown to be spherical and elongated in appressoria in which they occupy the periphery of the cell (Bourett & Howard, 1990). Mitochondria in conidia and germlings were observed in this study to be either spherical/rod shaped or elongated and often branched. As germination proceeded the conidial cell that produced the germ tube was occupied by increasingly numerous and elongated mitochondria which were polarised towards the growing germ tube, and extended into it. Mitochondria were primarily peripherally located within the M- and B-cells and seemed to be centrally located within the A-cell and germ tube, although the narrowness of the germ tubes did not allow the location of the mitochondria to be readily determined by optical sectioning. However, this interpretation has been confirmed by previous TEM studies in which mitochondria were found to be numerous in the median sections of germ tubes (Bourett & Howard, 1990). Both spherical and elongated mitochondria have been observed previously during ultrastructural studies of the ungerminated spores of other fungal species, (e.g. Mollicone & Longcore, 1999; Gull & Trinci, 1971; Mims *et al.*, 1988). The increase in elongation and number of mitochondria during spore germination has also been described in ultrastructural studies of spores of other species, and elongated mitochondria have been observed in some species to be orientated parallel to the longitudinal axis of the spore cells (e.g. Hoch & Staples, 1983; Roberts *et al.*, 1996). As in the fungal hypha, this elongated morphology is probably an adaptation to polarised growth (Markham, 1995). The fact that ungerminated cells (i.e. that do not exhibit polarised growth) contained a higher proportion of small mitochondria than elongated ones, would support this hypothesis. The growing tip of the germ tube is the most active region of the germling and will require substantial amounts of energy. An increase in the number of mitochondria, and in the amount of mitochondrial membrane, will increase the cell's ability to synthesize ATP. It should be noted that elongated mitochondria are not a prerequisite for germ tube growth. For example, the mitochondria of *Uromyces* remain smooth and near-spherical throughout germination (Hoch & Staples, 1983).

The dynamism of mitochondria in fungal hyphae is well documented, and they are recognised to be motile organelles, which are able to fuse and fragment (Steinberg, 1998). In this study, mitochondria were observed to be dynamic in all three conidial cells, but were most dynamic within the germ tube. Small spherical, rod-shaped and elongated mitochondria were present within the germ tube, and were all dynamic, exhibiting, bidirectional motility up to and from the apical region of the germ tube. Evidence was obtained that fragmentation and fusion events occurred within the mitochondrial population. There was also evidence that mitochondria extended across the septa, although the size and close association between mitochondria made it difficult to resolve the precise details of this.

Variation was observed between the different conidial cells, especially between germinated and ungerminated cells. The former contained principally elongated mitochondria that were polarised towards the growing germ tube, and the latter often contained small mitochondria typical of all three cells in an ungerminated conidium. Sometimes, however, the ungerminated cells in a germling also contained elongated mitochondria that exhibit some polarisation towards the growing germ tube. It was shown previously (Section 3.2.7) that there are two modes of germination: a conidium produces either a single germ tube or two slightly slower growing from both the A- and B-cells. One explanation for the variation observed in mitochondria morphology during germination could be that those conidia that contain elongated, polarised mitochondria in all three cells are directing the resources of the entire conidium to the production of one germ tube, and those that have, for example germinated from the A-cell and have a B-cell with mainly small spherical/rod shaped mitochondria, will subsequently produce a second germ tube from the B-cell.

Rhodamine 123 stained the mitochondria in germinated cells more intensely than ungerminated conidial cells, and in ungerminated conidia both Rhodamine 123 and $DIOC_6$ stained mitochondria in the A-cells more brightly. Both these dyes are mitochondrion-selective dyes that cross the mitochondrial membrane as a function of its membrane potential (Haugland, 1999; Butt *et al.*, 1989). These observations

provide evidence that the mitochondria are most active in the germinated cell, and that before germination the A-cell exhibits a higher degree of mitochondrial activity. As this was not observed in B-cells of ungerminated conidia it seems unlikely to be a diagnostic feature of the cell that is going to germinate, but could instead be one of the reasons why a higher proportion of the population germinate from the A-cell.

Evidence was obtained that the mitochondria near to the substratum were more intensely stained in ungerminated and germinated spores. Potential artefacts due to photobleaching were controlled for by optically sectioning in both directions (away from, and towards the surface), and problems of signal attenuation are unlikely because other dyes did not exhibit significant changes in signal intensity between the upper and lower optical sections. The apparent asymmetry in mitochondrial activity within the spore supports the hypothesis that the spore senses the surface (Read *et al.*, 1992). However, experiments in which samples were inverted, stained with other dyes (including mitochondrial stains which are not membrane potential dyes), and inoculated onto different substrata (in order to rule out any concentration of the dye at the substratum interface) are required to confirm these observations.

4.3.3 Vacuolar system

The vacuolar system of fungal spores has been reported in ultrastructural studies to be comprised of a range of morphological types, including small spherical, elongated and interconnected, elongated and branched (Hoch & Staples, 1983; Mims *et al.*, 1988, 1997; Van Dyke & Mims, 1991). Previously, in agreement with the results described here, TEM studies of *M. grisea* conidia have identified two components of the vacuolar system within conidial cells and germ tubes: one consisting of branched cisternae, and another of irregular size and shape and sometimes containing inclusion bodies (Bourett & Howard, 1994). The former was reported as having a diameter of 0.2 μm and could correspond to the tubular elements observed here. The latter could encompass the vacuoles that were neither large and globular, or tubular. A third type of vacuole was identified in the ungerminated cells of germlings and was comprised of "series of interconnected subspherical bodies" which sometimes contained inclusion bodies (Bourett & Howard, 1994). This vacuolar type was also observed in

this study, primarily after the germ tube had grown for some distance or had begun to differentiate (GT_3 stage of germination). In the TEM analysis, the vacuolar types were not observed to interconnect as they did here, and they were described as existing "in a continuous cytoplasm without any apparent connection" (Bourett & Howard, 1994).

A summary of vacuolar distribution and dynamics is shown in Figure 4.71C. The vacuolar system exhibited the most dynamism of the organelles studied here. In particular, tubular vacuoles and small vacuoles extended and retracted, and moved within the conidial cytoplasm and along the length of the growing germ tube. They were observed to interconnect different vacuolar compartments either transiently or during fusion events, and to pass through septa. The continuity of the vacuolar system between conidial cells provides evidence that the ungerminated conidial cells support the growth of the germinated cell, perhaps by delivery of breakdown products of glycogen or lipid. Tubular vacuoles were previously reported in the hyphae of a range of fungi (Rees *et al.*, 1994; Hyde & Ashford, 1997; Cole *et al.*, 1998) and it has been proposed that the tubular components of the hyphal vacuolar system are "involved in longitudinal transport of accumulated materials, in particular of nitrogen and phosphorous compounds" (Ashford, 1998). Furthermore, vacuoles are the sites of protein degradation and recycling, acting as the storage site of important metabolites, such as amino acids. They also play an important role in osmoregulation; and might also be important in cytoplasmic ion (e.g. Ca^{2+}), and pH regulation (Klionsky *et al.*, 1990). The fact that a vacuole may extend and retract into the germ tube would allow it to fulfil its functions without requiring the production of vesicles and thus membrane recycling (Ashford, 1998).

The large central vacuoles observed in yeast cells have a similar morphology to those described here in conidia at the GT_2 and GT_3 stages of germination (Weisman & Wickner, 1988). There is evidence that yeast cells undergo a cyclic pattern of vacuole fragmentation and these vacuolar morphologies in yeast cells are very similar in appearance to those observed here in the early stages of germination. It has been

suggested that the fragmented vacuoles in yeast cells might represent a physiological intermediate in vacuole biogenesis (Klionsky *et al.*, 1990) and in *M. grisea* the smaller vacuoles certainly precede and contribute to the final large globular vacuoles. A fragmented vacuolar morphology has been observed both in yeast cells in which the microtubules were disrupted and in mutants for a gene that encodes what appears to be an element of the cytoskeleton (Guthrie & Wickner, 1988; Wada & Anraku, 1992; Wada *et al.*, 1992). In hyphae of kinesin-deficient mutants of *Ustilago maydis,* the vacuolar system was comprised of small spherical vacuoles rather than the large vacuoles of the wildtype (Steinberg *et al.*, 1998). It was shown here that smaller vacuoles fuse to form large vacuoles during development of a germling and it is likely that that in *M. grisea* cytoskeletal elements such as kinesin and microtubules are important in the fusion of smaller vacuolar compartments.

The vacuolar system increases in size during germination and although fusion was observed between vacuolar compartments, this mechanism cannot solely account for observed growth of the vacuolar system because the amount of vacuole within ungerminated conidia was too small to account for the number of large globular vacuoles in the latter stages of germination (GT_2–GT_3); indeed in some extreme cases the vacuolar system was only comprised of a few small spherical bodies. The intracellular mechanisms by which this vacuolar growth occurs are poorly understood. However, in yeast cells there is evidence that growth of the vacuolar system involves *de novo* vacuolar biosynthesis and endocytosis (Klionsky *et al.*, 1990).

There is evidence that the vacuolar system increases in volume during spore germination in other filamentous fungi (e.g. Buckley *et al.*, 1966; Gull & Trinci, 1971; Hoch & Staples, 1983; Van Dyke & Mims, 1991; Steinberg *et al.*, 1998), and that the subapical regions of fungal hyphae become more vacuolated as the cytoplasm migrates forward with the growing tip (Markham, 1995; Hyde & Ashford, 1997; Cole *et al.*, 1998; Heath & Steinberg, 1999). Here, the vacuolar system became larger as the germ tube extended, and by the stage of differentiation was commonly one

large compartment that filled the cell. A function of this large vacuole could be to fill the space that the cytoplasm initially occupied in the ungerminated conidium. This would be predicted to be energetically more favourable than synthesising new cytoplasmic components and leaving the original cytoplasm behind (Heath & Steinberg, 1999), and thus a likely mechanism in a spore that has limited resources; and one that is able to complete the pre-penetration stage of infection in the absence of external nutrients.

The vacuolar system also plays a role in osmoregulation (Klionsky *et al.*, 1990). In *M. grisea* the A- and B-cells have a consistently higher turgidity than the M-cell throughout germination (Money & Howard, 1996). The vacuolar system might be responsible for controlling the differences in turgidity, which could reflect differences in the vacuolar compartments within each cell. Larger vacuoles only permanently fused within a cell, never between cells. Biochemical differences between the vacuoles in different cells could be maintained in each cell, with tubular and small spherical elements enabling controlled transfer of components. The conidial septa are open after the germ tube has emerged and there was evidence in this study that both components of the vacuolar system and mitochondria are able to pass through the septum. This is supported by TEM studies which show unoccluded open septal pores in the conidia of *M. grisea* (Money & Howard, 1996). The mechanism by which the conidium maintains differences in turgor up to 0.4 MPa with open septa is unknown (Money & Howard, 1996).

Another possible function served by the fusion of smaller vacuoles to ultimately form one large vacuole is to provide membrane for recycling to the growing tip and appressorium. One predicted outcome of change from numerous small to medium vacuoles to one large smooth compartment might be that the surface to volume ratio of the vacuolar system is reduced. The excess membrane could be transported to the growing tip to be incorporated into the growing germ tube tip, or the developing appressorium. Transport could be by either the tubular vacuolar elements or as vesicles. Furthermore, glycerol is a major subcomponent of phospholipids. The

appressorium has been demonstrated to derive its invasive force solely from turgor pressure (Howard *et al.*, 1991; Money & Howard, 1996), which is achieved by accumulating osmolytes such as glycerol in the cytoplasm during germination and germ tube growth (de Jong *et al.*, 1997). A possible source of glycerol is from the autolysis of internal membranes (de Jong *et al.*, 1997) and these might be supplied by the fusion of smaller vacuoles. This is supported by the evidence suggesting that the vacuoles in *M. grisea* conidia might degrade membranous components: internalized membranous inclusions were imaged here using MDY-64 and FM4-64 during the later stages of germination, and FUN-1 stained vacuolar inclusions throughout germination (Section 4.2.5.4). Furthermore, vacuolar inclusions were observed during a TEM study of *M. grisea* germlings (Bourett & Howard, 1994).

4.3.4 pH measurement in *M. grisea*

The role of internal pH in regulating tip growth has received considerable interest, and there is strong evidence that in *N. crassa* at least, pronounced cytoplasmic pH gradients are not essential for the regulation of tip growth (Parton *et al.*, 1997). A recent publication reported that the intracellular cytosolic pH within growing germ tubes of *M. grisea* did not change or exhibit any pronounced gradient during germination, germ tube growth or differentiation (Jelitto, 1999). It was found here that, as in several other systems (Parton *et al.*, 1997), the vacuolar system sequestered the pH dye cSNARF-1 (Fig. 4.51), and that the conidial cells and germ tubes are densely packed with dynamic organelles, such as mitochondria (Fig. 4.71). It is clear from the organelle data described in this study that Jelitto (1999) could not have consistently discriminated between cSNARF-1 signal emanating from the cytosol and that from organelles within the germ tube. Thus the conclusions drawn by the author regarding cytosolic pH need to be treated with scepticism.

4.3.5 Glycogen and lipid reserves

Spores are able to undergo the pre-penetration stage of infection in the absence of external nutrients, suggesting that they contain considerable energy reserves. Lipid and glycogen have been previously identified in TEM studies of conidia, germlings and appressoria of *M. grisea* (Money & Howard, 1996; Howard & Ferrari, 1989;

Bourett *et al.*, 1993). Evidence was obtained that the conidial cells are packed with glycogen at the UNG stage and that in germinated spores glycogen was still generally distributed throughout the conidial cells but that it stained less intensely. This finding might indicate that some glycogen had been utilized during germination, and this is supported by the findings of Thines *et al.*, (2000) who reported that glycogen is rapidly degraded during germination and then accumulates in the incipient appressorium. In a number of species there is evidence that lipid is broken down during germination (Maia *et al.*, 1994; Maxwell *et al.*, 1977; Schadeck *et al.*, 1998). Attempts to image lipids in living cells using Nile red proved unsuccessful but some success was achieved using lipophilic dyes in permeabilised cells. This technique has limited applications as it requires that the conidia are killed, but does appear to stain lipid bodies in the cell. Lipid bodies have been observed in ultrastructural studies of conidia, and as observed here, were present in the corners between the septa and plasma membrane (Money & Howard, 1996).

4.3.6 Apical vesicle cluster

The apical vesicle cluster (AVC) was imaged within growing germ tubes and was positioned near the underlying substratum. In fungal hyphae the AVC (or Spitzenkörper) is comprised of an accumulation of secretory vesicles that contribute to tip growth and displays characteristic behaviour in keeping with this function (Section 1.4.5). The AVC of *M. grisea* has been previously imaged by TEM (Bourett & Howard, 1990) but due to its small dimensions has not been characterized within living cells. It was observed here to behave in the manner expected of a vesicle cluster within a hypha, and this is consistent with it playing a role in apical extension of the germ tube.

4.3.7 Peripheral spots

The germ tubes of *M. grisea* have been previously demonstrated to have both carbohydrates and proteins associated with them (Xiao *et al.*, 1994a). In this study extra-cellular peripheral spots (PS) were found to be stained by a number of different dyes but their precise nature was not determined (Fig. 4.71E). They were not detected during SEM or DIC imaging. They do not appear to be associated with mucilage

production because dyes that stained mucilage associated with the germ tube (GTM) did not always stain the spots, even though it was clear from the MDY-64 staining that the spots are located within the GTM (Fig. 4.59E). Two other possible extracellular components of the germ tube that they could be associated with are either the production of hydrophobins, and/or enzymes. Whilst hydrophobins have been demonstrated in a range of fungi, little is known about the mechanism by which they are produced (Wessels, 1996, 1997). PS were produced at the apical tip near the AVC and it is possible that they are comprised of a membrane surrounding some extracellular compound secreted at the growing tip, because the membrane-selective dyes FM4-64 and MDY-64 produced the brightest and largest stained area for each PS of all the dyes assessed (Table 4.3). This could be explained if the PS were bounded by a membrane: the membrane-selective dyes FM4-64 and MDY-64 would stain the surrounding membrane and possibly the contents, whilst the other dyes would only to stain only the latter.

The finding that cFDA and cDFFDA stained the PS suggest that they are associated with some extracellular enzyme with esterase activity, since both are essentially nonfluorescent until it is de-esterified to fluorescein (Oparka & Read, 1994; Haugland, 1999). There is convincing evidence that some fungal pathogens produce extracellular enzymes in order to weaken the host surface and so aid the process of penetration (Howard, 1997; Hamer & Holden, 1997). Esterase activity has been localised within mucilage associated with the spores of *Erisyphe graminis* (Nicholson & Morales 1980; Nicholson *et al.*, 1988) and the uredospores of *Uromyces viciae-fabae* have been demonstrated to produce serine esterases (including one with cutinase activity) that promote spore adhesion (Deising *et al.*, 1992). Although there is evidence that *M. grisea* is able to penetrate the host solely by physical force (Howard *et al.*, 1991) this could be facilitated by extracellular digestive enzymes (e.g. cutinases) produced by the fungus. *M. grisea* has been demonstrated to possess a gene that encodes a cutinase, and although it is not essential for pathogenesis the production of cutinase might aid infection in a number of other ways (Sweigard *et al.*, 1992a;b). In addition to being involved in the

degradation of host surface polymers, extracellular enzyme production could also aid adhesion, and play a role in host-pathogen signalling (Köller, 1991; Howard, 1997; Hamer & Holden, 1997).

5. EVIDENCE FOR ENDOCYTOSIS DURING CONIDIAL GERMINATION

5.1 INTRODUCTION

There is increasing evidence for the occurrence of endocytosis within filamentous fungi and it is thought that it could play a central role in hyphal tip growth (Ashford, 1998; Hoffman & Mendgen, 1998; Fischer-Parton *et al.*, 2000; Read & Hickey, 2000). Although there is evidence that germ tubes of some filamentous fungi endocytose (Hoffman & Mendgen, 1998; Fischer-Parton *et al.*, 2000), there have been no such studies on spores of filamentous fungi. It has been proposed that endocytosis in fungal cells could play important roles in the detection of signals from the host, internalization of nutrients, and in polarised tip growth (Fischer-Parton *et al.*, 2000; Read & Hickey, 2000). Such processes could be important during the pre-penetration phase of infection and the latter is crucial for successful infection of the host. The **principal objective** of the research described in this chapter was to establish whether the conidia of *M. grisea* undergo endocytosis during germination.

Useful methods for investigating the occurrence of endocytosis in live cells involve the application of endocytic markers such as Lucifer Yellow CH, FITC-dextran or FM4-64, which can be imaged by fluorescence or confocal microscopy. The uptake of these dyes has been characterized within animal, plant and yeast cells, and to some extent in fungal hyphae, but never in germinating fungal spores (Hawes *et al.*, 1995; Ashford, 1998; Fischer-Parton *et al.*, 2000). The **first aim** of this study was to determine whether any of these dyes were internalized by conidia during germination and to characterize that uptake. Endocytosis is an energy-dependent process and as such is expected to be arrested by inhibitors of energy production, such as sodium azide and exposure to low temperatures (Vida & Emr, 1995). The **second aim** of this study was to examine the influence of these inhibitory treatments on the internalization of endocytic markers by conidia of *M. grisea* during germination.

The order in which cellular components are stained by a fluorescent marker of endocytosis will in theory allow one to map the vesicle trafficking network. In practice the size of the cellular components (in particular the vesicles) coupled with the resolution of the confocal microscope, can be limiting factors (Fischer-Parton *et al.*, 2000). The **third aim** of this study was to characterize the sequential staining of different organelles by an endocytic marker and identify components of the vesicle trafficking network involved during conidial germination.

5.2 RESULTS

5.2.1 Internalization of endocytic markers

The principal dyes utilized in this study were Lucifer Yellow CH and FITC-dextran (10 kDa), both of which are reported to be markers of fluid phase endocytosis (Hawes *et al.*, 1995; Ashford, 1998), and the membrane selective stain FM4-64 (see Table 2.2, Fig. 2.2 in Section 2.7). All three dyes were internalized by germlings (Fig. 5.1). Lucifer Yellow CH and FITC-dextran both appeared to be localised within the vacuolar system (Fig. 5.1A,B), and FM4-64 stained the membranes of a number of cellular components, including components of the vacuolar system (Fig. 5.1C).

5.2.2 An assessment of inhibitors of endocytosis

To investigate whether these three dyes were internalized by endocytosis or by some other mode of entry into the conidial cells, two treatments were assessed as inhibitors of dye internalization. The treatments were cooling of conidia to 4 °C, and exposure to the metabolic inhibitor sodium azide (see Section 2.13). The dye FM4-64 was used for this experiment because it produced the most intense signal of the three endocytic dyes used in this study (e.g. Fig. 5.1C).

Conidia were incubated at 24 °C, 7 °C and 4 °C in the presence of FM4-64. The degree of dye internalization was qualitatively assessed. At 24 °C, conidia internalized significant amounts of dye within 35 min post dye (Fig. 5.2A). Loading the dye at 7 °C significantly inhibited this uptake (Fig. 5.2B), and loading at 4 °C resulted in almost complete inhibition (Fig. 5.2C).

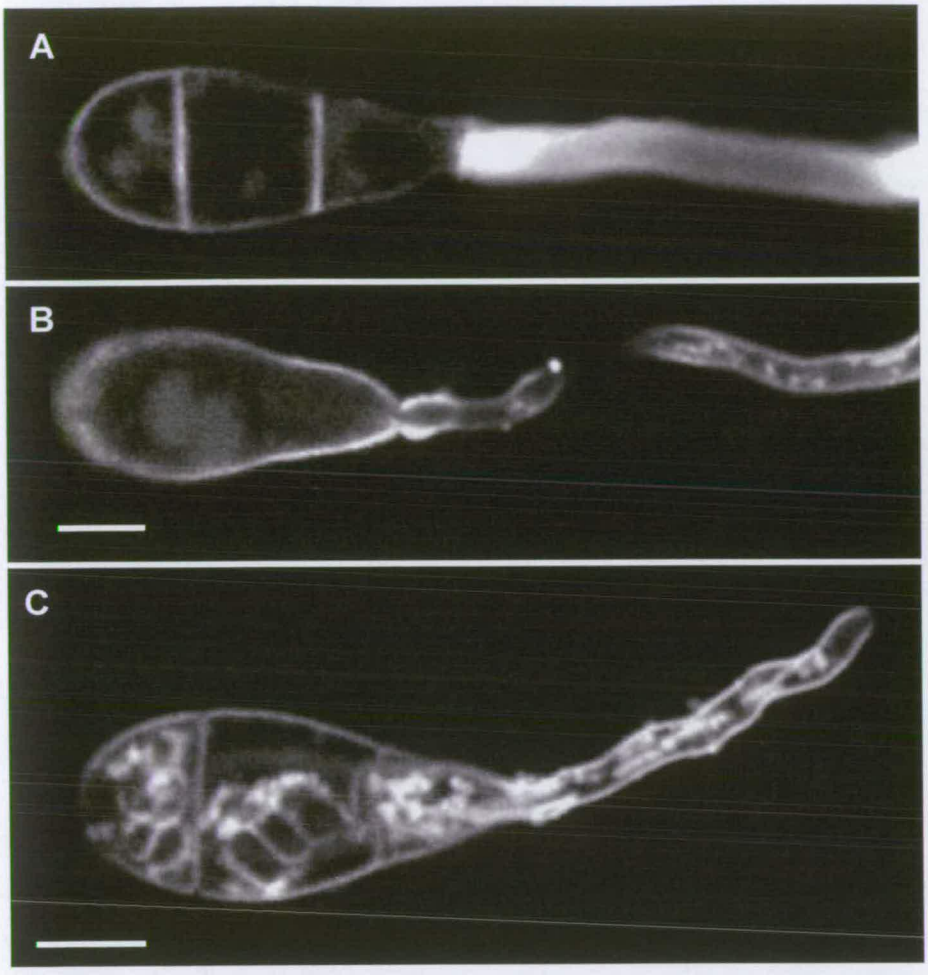

Figure 5.1: Confocal images of germlings stained with the endocytic markers (**A**) Lucifer Yellow CH, (**B**) FITC-dextran (10 kDa), and (**C**) FM4-64, and showing that conidial cells and germ tubes internalize the dyes. (**A**, **B**) Both Lucifer Yellow CH and FITC-dextran appear to be localised in components of the vacuolar system, (**C**) FM4-64 stains the vacuolar membranes in the middle and basal cells, and there is evidence of mitochondrial staining within the germinated apical cell and germ tube. Note that in (**A**) the germ tube contents are obscured by staining of extracellular mucilage. Dyes were added at 15 min post hydration, and the images were collected at (**A**), 3 h 45 min, (B) 4 h 45 min and (C) 3 h 53 min post hydration. Imaged using a x60 objective. Bars = 5 µm.

Conidia were incubated in 10–100 mM sodium azide in the presence of FM4-64. The degree of dye internalization was then qualitatively assessed after 14–22 min post dye (Fig. 5.3). The greatest and most repeatable inhibition of dye internalization was produced by sodium azide at a concentration of 100 mM (Fig. 5.3D).

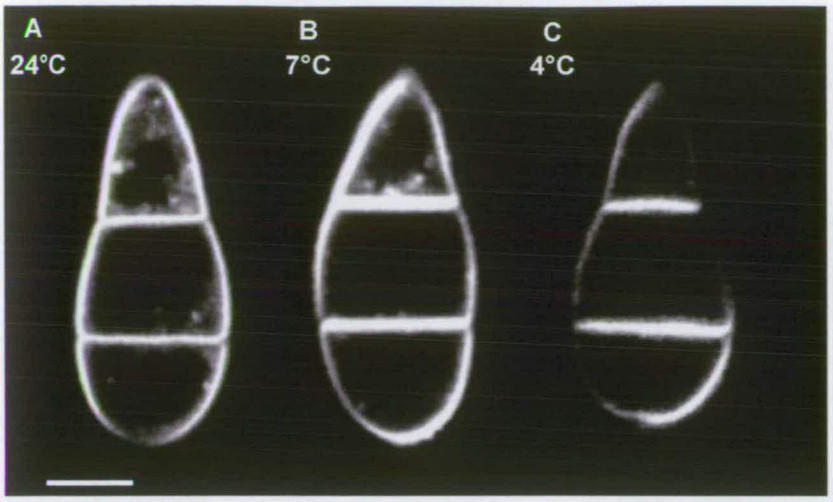

Figure 5.2: Confocal images showing inhibition of FM4-64 uptake into conidia by cooling. Conidia were imaged at 65 min post hydration after incubation in FM4-64 at (**A**) 24 °C, (**B**) 7 °C, and (**C**) 4 °C. The dye was added at (**A**, **B**) 30 min and (**C**) 15 min post hydration. Note that (**C**) has had 15 min longer in the dye and yet no dye was internalized. Imaged using a x60 objective. Bars = 5 µm.

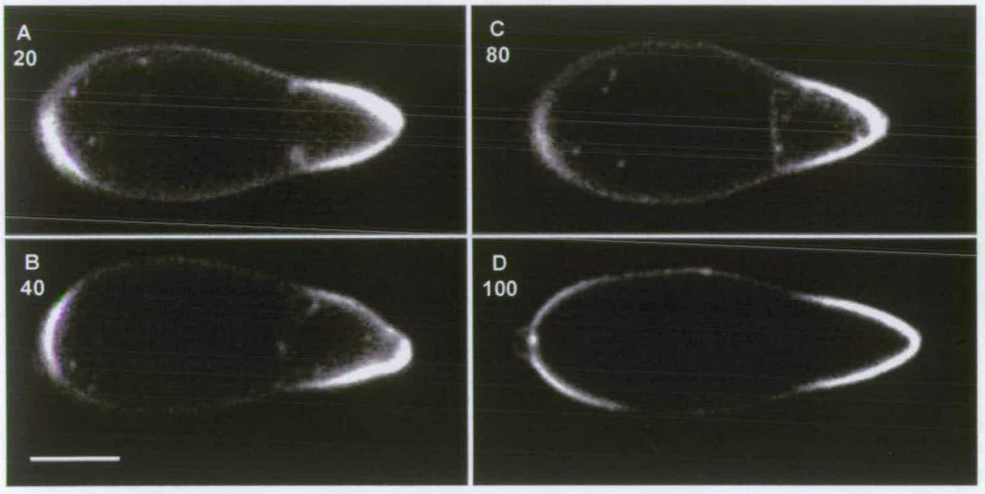

Figure 5.3: Confocal images showing inhibition of FM4-64 uptake into conidia by exposure to the metabolic inhibitor sodium azide. The numbers refer to the concentration of sodium azide (mM) and the images were collected at (**A**) 22 min and (**B–D**) 14 min after the dye was added. Sodium azide was added 2 min before the dye. Imaged using a x60 objective. Bar = 5 µm.

To determine whether 100 mM sodium azide was cytotoxic, and whether the observed inhibitory effect was reversible, percentage germination was measured immediately after washing sodium azide out of the inoculum, and then again after at least 22 h (to measure maximum germination, see Sections 2.10 and 3.2.1), (Table 5.1). Conidial germination was inhibited by exposure to 100 mM sodium azide, and washing it out of the inoculum reversed this inhibition. Maximum germination (>22 h after treatment) was unaffected by all sodium azide treatments except for

those in which conidia had been incubated in the inhibitor for 24 h. On the basis of these findings, a concentration of 100 mM was chosen for subsequent inhibition experiments, as it provided the best inhibition of dye internalization (Fig. 5.3) and did not kill the conidia; the observed inhibition of germination was reversible in samples that were incubated in sodium azide for up to 3 h.

		Percentage germination	
Treatment	Period of exposure to treatment (h)	immediately after treatment	>22 h after treatment
24 °C	3	97.1 ± 1.4	99.2 ± 0.7
4 °C	3	0.0 ± 0.0	99.0 ± 0.8
sodium azide	1	0.2 ± 0.5	98.3 ± 1.1
sodium azide	2	0.5 ± 0.6	97.1 ± 1.4
sodium azide	3	1.2 ± 1.4	97.8 ± 1.5
sodium azide	24	0.1 ± 0.2	72.7 ± 9.8

Table 5.1: Inhibition of conidial germination by cooling to 4 °C or by exposure to 100 mM sodium azide. Following each treatment, samples were washed in 24 °C dH_2O and then incubated at 24 °C. Mean conidial germination was assessed immediately after each treatment, and then again at least 22 h later (to determine maximum germination). Samples sizes were 100–150 conidia each, and the values presented are the mean of 4–8 samples ± the standard deviation.

The influence on germination of cooling to 4 °C was also examined. Germination was inhibited at 4 °C but this inhibition was reversed on warming to 24 °C, with no effect on maximum germination (Table 5.1).

5.2.3 Characterization of dye internalization and the influence of sodium azide and cooling

A more detailed quantitative approach was adopted to characterize dye internalization and the influence of cooling and sodium azide. The methods used are described in Sections 2.8.3 and 2.13. There was no evidence that the presence of sodium azide or cooling influenced either autofluorescence (Section 4.2.5.1) or dye fluorescence.

Two different types of time-course experiments were carried out:

- *population time-courses* in which conidia were randomly sampled from the population at each time point allowing mean dye fluorescence values to be calculated,

- *individual time-courses* in which individual conidia were repeatedly sampled over time, allowing data for each time point to be presented either for a single conidium, or as mean values for all replicates.

All experiments were performed at least twice. However, because of the large variation in dye fluorescence values, in spite of the constant dye concentrations and confocal parameters, data could not often be pooled.

5.2.3.1 Lucifer Yellow CH and FITC-dextran

Both Lucifer Yellow CH and FITC-dextran internalization was characterized and the influence of exposure to 100 mM sodium azide and cooling to 4 °C was assessed.

Experiments were performed two or three times and representative fluorescence data for each dye are presented in Figure 5.4. In both cases an increase in dye fluorescence within conidia was detected but only after germination had commenced (> 3 h post dye), and this dye uptake was inhibited by both sodium azide and cooling to 4 °C (Figs. 5.4, 5.5).

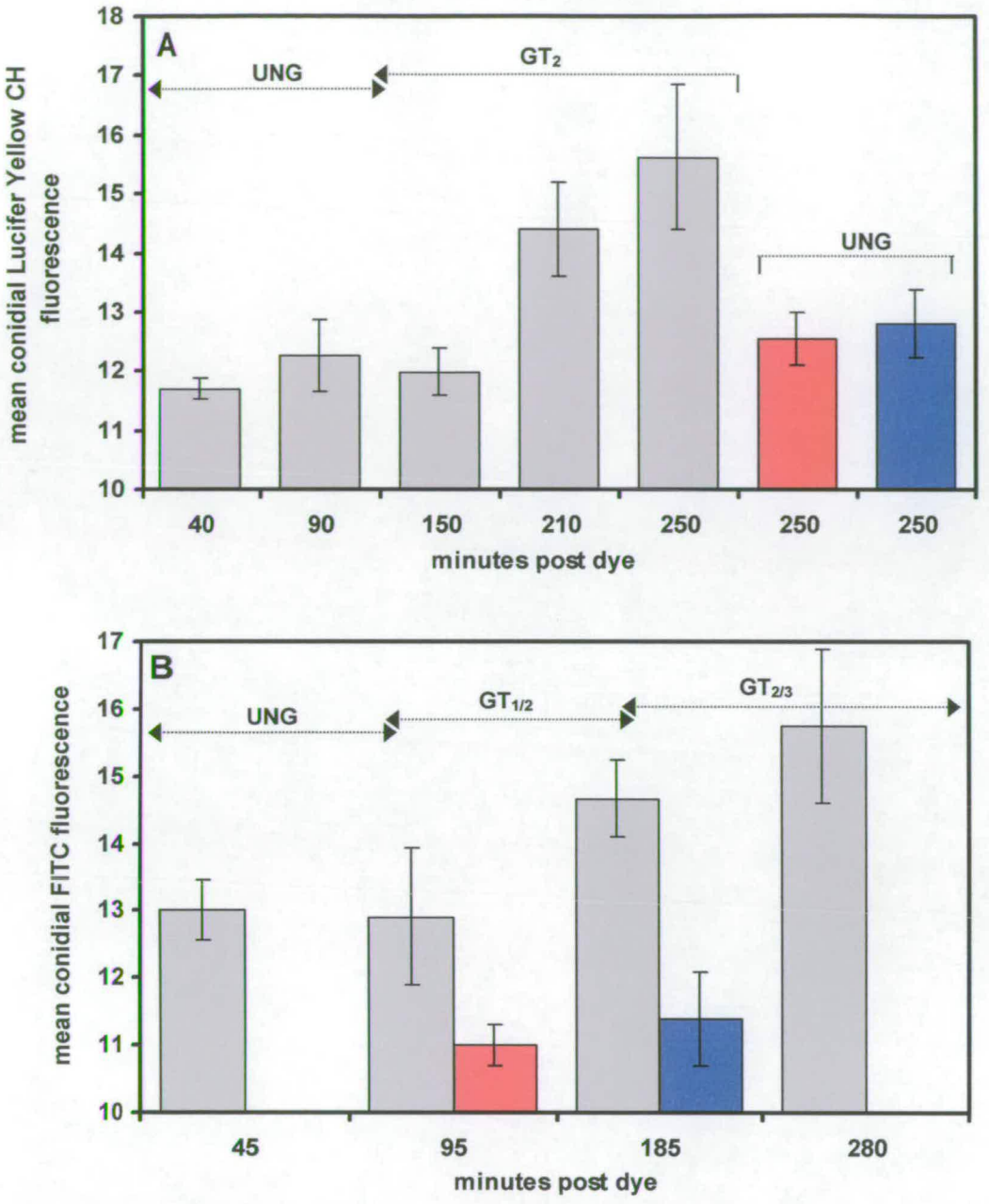

Figure 5.4: (**A**) Lucifer Yellow CH and (**B**) and FITC-dextran (10 kDa) internalization within conidia incubated at 24 °C (■), in the presence of 100 mM sodium azide (■) and at 4 °C (■). Note that in both, the mean conidial dye fluorescence increases with time at 24 °C, but that samples that were treated with sodium azide or cooled to 4 °C have a significantly lower mean dye fluorescence. The stages of germination are indicated. Sodium azide was added at 2 min post hydration, and the dye was added at 15 min post hydration. Data were extracted from population time-courses with total spore counts of (**A**) 52 and (**B**) 42, with 5–18 conidia sampled at each time point. The values are mean conidial Lucifer Yellow CH/FITC fluorescence per pixel and the vertical bars are standard deviations.

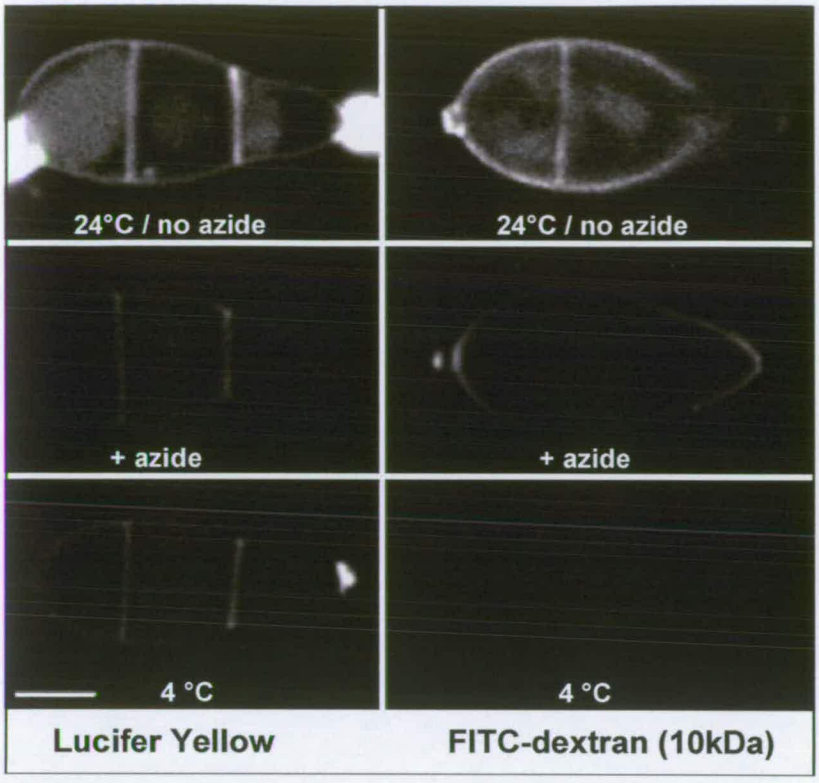

Figure 5.5:Confocal images showing inhibition of Lucifer Yellow CH and FITC-dextran (10 kDa) uptake into conidia by 100 mM sodium azide and cooling. Samples were incubated either at 24 °C in the presence or absence of sodium azide, or at 4 °C. Dyes were added at 15 min post hydration and the images were collected at 4 h 5 min (Lucifer Yellow CH) and 3 h 30 min (FITC-dextran) after the addition of the dye. Note that the 24 °C samples have germinated but that those treated with sodium azide or that were cooled, have not. Imaged using a x60 objective. Bars = 5 μm.

5.2.3.2 FM4-64

A more detailed analysis was performed using FM4-64, because of the three endocytic markers used, it appeared to be the better marker for the components of the endocytic pathway in conidial cells (Fig. 5.1). Dye internalization was characterized within individual conidia throughout germination (45 min to 6 h post hydration). The experiment was repeated and the data from both experiments are presented as mean conidial FM4-64 fluorescence (Fig. 5.6A). Mean conidial FM4-64 fluorescence increased throughout germination until 250 min post dye (~5 h post hydration).

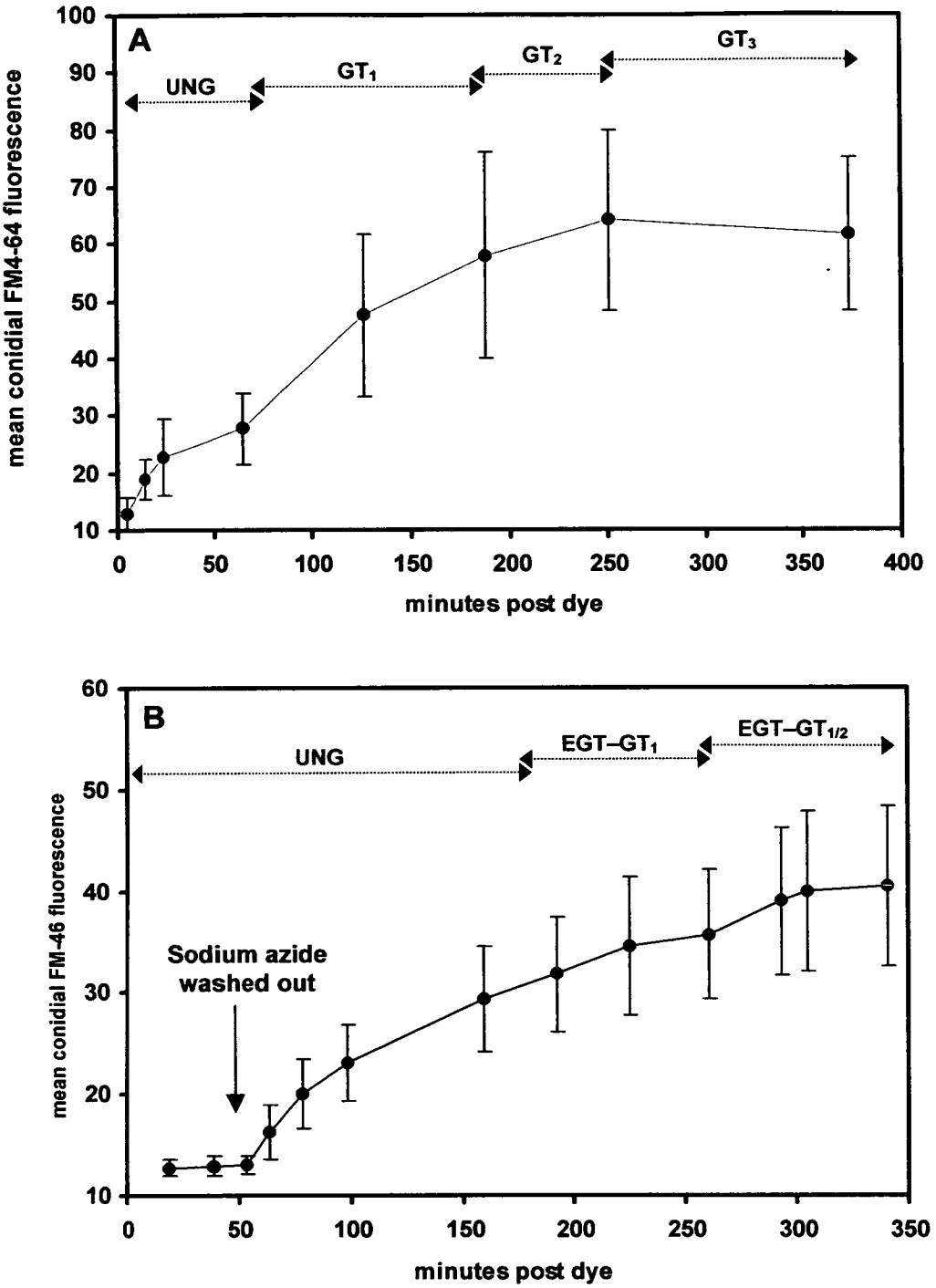

Figure 5.6: Internalization of FM4-64 by conidia during germination. (**A**) Conidia were incubated at 24 °C, and the dye was added at 45 min post hydration. (**B**) Conidia were incubated at 24 °C, in the presence of 100mM sodium azide, and after it was washed out of the inoculum at 50 min post dye. Sodium azide was added at 30 min post hydration and the dye was added 3 min later. Approximate stages of germination are indicated. Data from (**A**) 18 and (**B**) 12 individual time-courses are presented here as mean conidial FM4-64 fluorescence per pixel. The vertical bars are standard deviations.

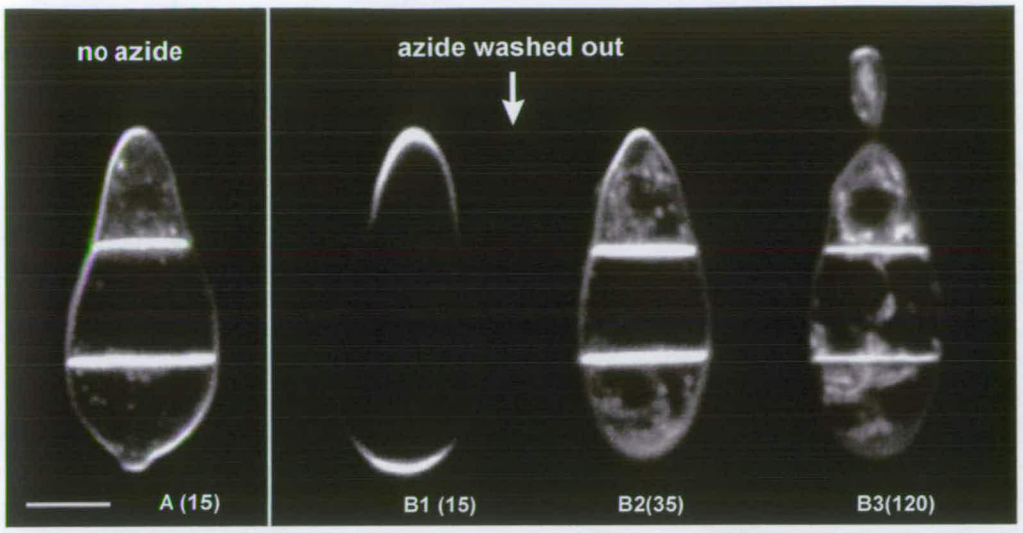

Figure 5.7: Confocal images showing that FM4-64 uptake into conidia is inhibited by exposure to 100 mM sodium azide, and that this inhibition is reversible. (**A**) An ungerminated conidium after 15min of incubation in the dye. (**B1-B3**) Time-course of a single conidium: (**B1**) ungerminated conidium after 15 min of incubation in the dye in the presence of sodium azide; note that this spore has been incubated in FM4-64 for the same period as (**A**) and exhibits no dye uptake, (**B2**) sodium azide was washed out at 22 min post dye (and new dye added) and the conidium was imaged at 35 min after the dye was first added; note that this was 13 min after the azide was washed out and that the staining of the conidium resembles (**A**), (**B3**) the conidium has germinated, and all three cells have internalized the dye. Numbers are min post dye and the azide was added 3 min before the dye. Imaged using a x60 objective. Bar = 5 μm.

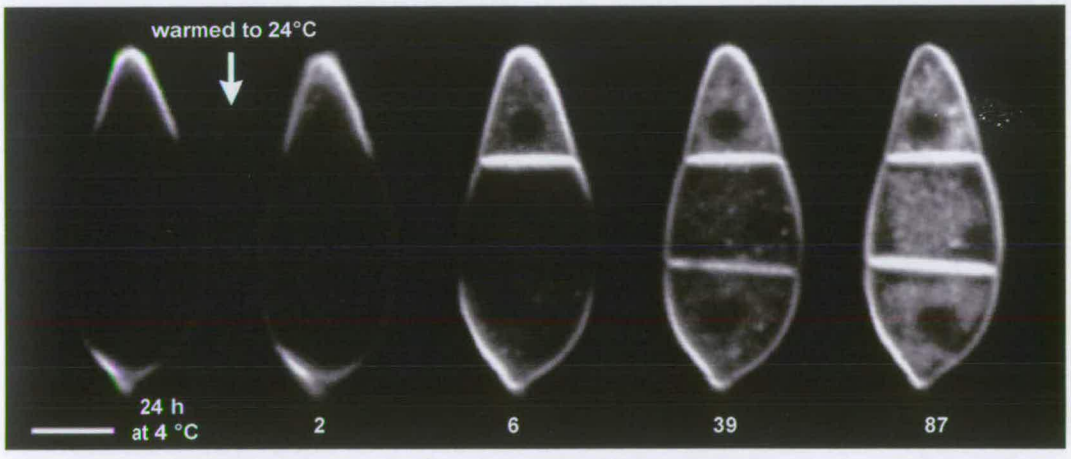

Figure 5.8: Confocal images of an individual conidium showing that internalization of FM4-64 is inhibited by cooling to 4 °C, and that this inhibition is reversible. The conidium was incubated at 4 °C for 24 h in the presence of FM4-64, and imaged (on a cold microscope stage); after which it was incubated at 24 °C. The numbers (2–87) are min at 24 °C. Note that as the conidium warms, dye is internalized by the cells, and that by 39 min at 24 °C, all three cells have internalized the dye. After 87 min at 24 °C, internal membranes are clearly stained. The conidium subsequently germinated. Imaged using a x60 objective. Bar = 5 μm.

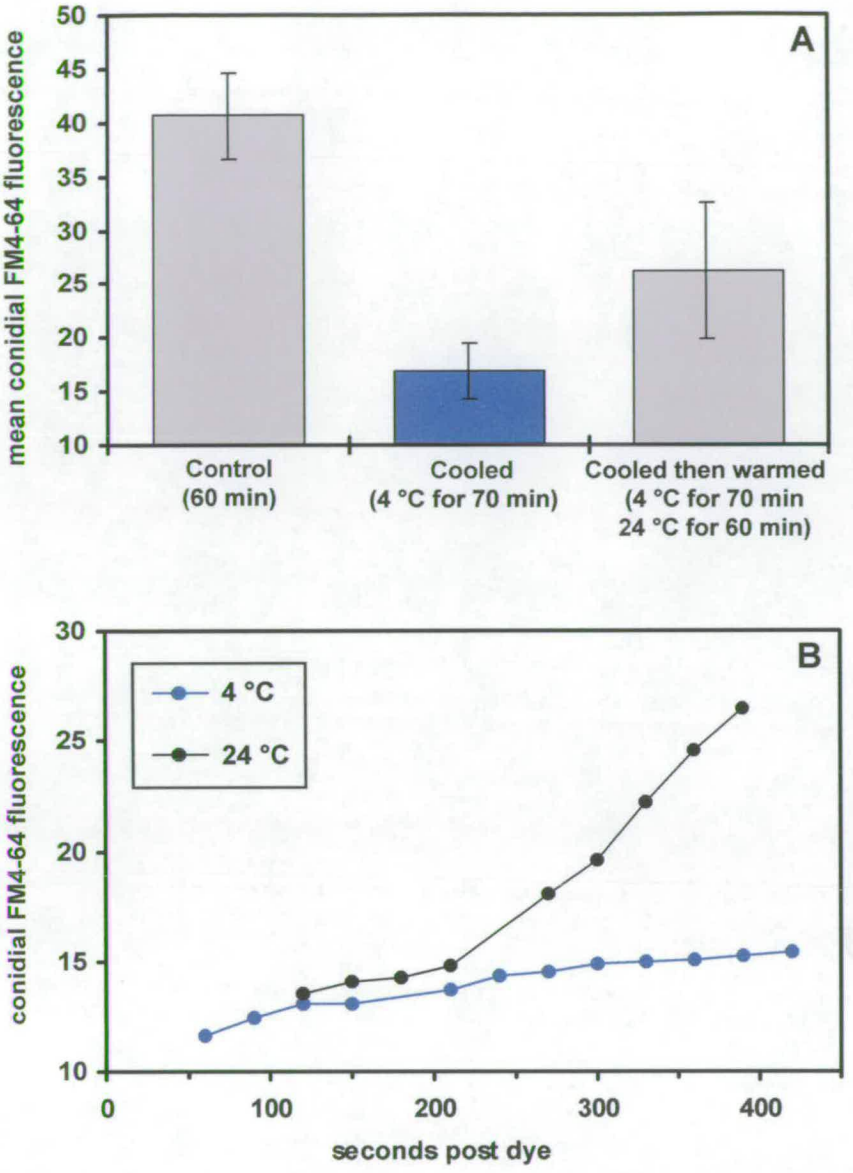

Figure 5.9: The influence of cooling to 4 °C on internalization of FM4-64 into conidia. (**A**) A population experiment in which samples were incubated in dye at either 24 °C for 60 min, or at 4 °C for 70 min, followed by 60 min at 24 °C (= 130 min post hydration). The dye was added at 15 min post hydration. All conidia were ungerminated. A total of 27 conidia were counted (8–10 per treatment). (**B**) FM4-64 internalization into two conidia, one at 24 °C and the other at approximately 4 °C. Measurements were collected between 60 and 420 sec after adding the dye. The dye was added at 20 min post hydration and both conidia were ungerminated. Values are (**A**) mean conidial FM4-64 fluorescence per pixel and vertical bars are standard deviations and (**B**) conidial FM4-64 fluorescence per pixel.

The influence of exposure to 100 mM sodium azide on dye internalization was examined. An individual time-course was performed (n = 12) over a period of several hours during which the sodium azide was washed out of the inoculum. Conidial FM4-64 fluorescence data are expressed as mean values over time and are presented in Figure 5.6B. Exposure to sodium azide inhibited dye internalization, and after it was washed out of the inoculum, mean conidial FM4-64 fluorescence increased and the spores germinated (Figs. 5.6B, 5.7). Germination was delayed as it commenced at ~2 h after the inhibitor was washed out of the inoculum (previously shown to start ~50 min post hydration; see Fig. 3.1, Section 3.2.3).

The influence of cooling on FM4-64 uptake into conidia was also examined. Maintaining the temperature at 4 °C significantly inhibited FM4-64 internalization. Subsequent warming of the conidia to 24 °C resulted in the uptake of the dye into the conidial cells (Figs. 5.8, 5.9A). It was possible to image an individual conidium at ~4 °C by cooling the apparatus, including the microscope stage (see Section 2.13.2). However, the sample still warmed gradually with time. Thus, the period over which an individual cooled conidium could be imaged was limited. The conidial fluorescence values for one conidium that was incubated at 24 °C and another that was incubated at 4 °C are shown in Figure 5.9B. Although the cooled spore fluorescence gradually increases, the fluorescence of the spore maintained at 24 °C increases at a much greater rate during the 400 sec post dye (= 6.7 min period of observation). Both cooling experiments were repeated and yielded quantitatively similar results.

5.2.3.3 Nile red

It was possible that the treatments used to inhibit endocytosis (i.e. sodium azide and cooling to 4 °C) also had more general effects on the conidia that could influence mechanisms of dye internalization other than endocytosis. To test whether these treatments were acting as specific metabolic inhibitors, the experiments described above (Sections 5.2.3.1 and 5.2.3.2) were repeated using the dye Nile red which is reported to freely diffuse into cells (Butt *et al.*, 1989; Haugland, 1999).

Conidia freely internalized the Nile red, but dye internalization over time differed from the three endocytic markers by reaching a maximum after 30 minutes after the dye was added (Fig. 5.10A). There was no evidence that incubation in the presence of 100 mM sodium azide influenced the uptake of Nile red (Fig. 5.10A). However, although there was considerable variation within the population, there was evidence that cooling to 4 °C suppressed dye internalization but only to a limited extent (Fig. 5.10B).

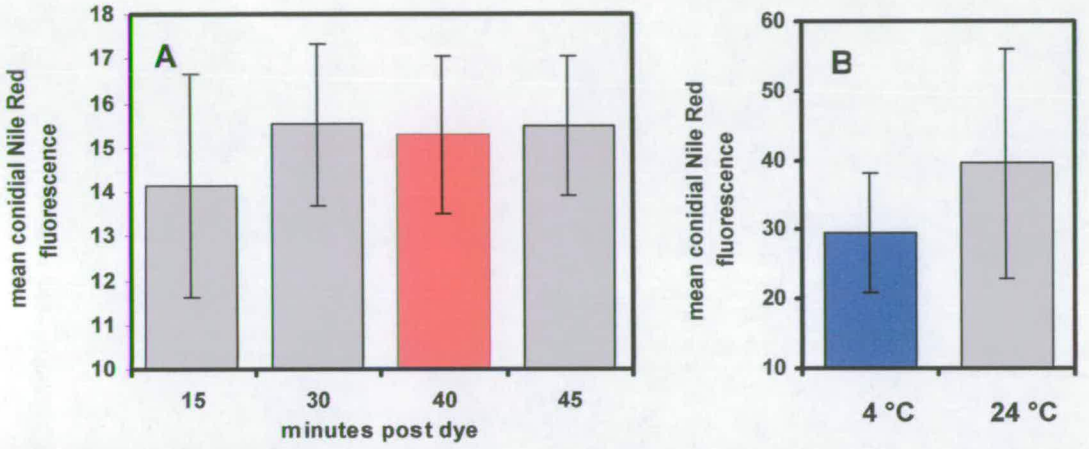

Figure 5.10: **(A)** Time-course of Nile red uptake by conidia at 24 °C (■), note that the 40 min time point sample was incubated in 100 mM sodium azide (■) for 42 min and that there is no significant difference in mean fluorescence. A total of 35 spores were counted (7–10 per time point). **(B)** Nile red uptake by conidia incubated at 4 °C (■) for 60 min and then incubated at 24 °C (■) for a further 60 min. Nine and five conidia were sampled respectively. Dye was added at 5 min post hydration in both experiments. In both **(A)** and **(B)** values were extracted from a population time-course and are presented as mean conidial Nile red fluorescence per pixel. The vertical bars are standard deviations.

5.2.4 Further evidence that conidia and germlings are able to internalize by endocytosis

Propidium iodide (PI) stains DNA and is reported to be membrane impermeant (Haugland, 1999). Here it was observed that conidia internalized PI (at concentrations used in Section 2.15) after over 3 h of incubation in the dye. The germlings were healthy (mean germ tube growth rate = 0.33 ± 0.6 $\mu m.min^{-1}$) and the dye did not stain the nucleus, but instead appeared to be localised in regions of the cell that could be vacuolar compartments (Fig. 5.11). It was also observed that the free acid of cSNARF-1, which has also been reported to be membrane-impermeant,

was internalized by live conidial germlings after periods of >1.5 h of incubation in the dye (data not shown).

Figure 5.11: Confocal image showing internalization of the dead-cell stain propidium iodide in a living germling. The dye was added at 5 min post hydration, and the image was collected at 3 h later. Imaged using a x60 objective. Bar = 5 μm.

5.2.5 Characterization of endocytosis during germination using the dye FM4-64

A more detailed study was made of FM4-64 internalization in order to characterize endocytosis within living conidia during germination.

5.2.5.1 Sequential staining of organelles with FM4-64

The order in which membranous conidial cellular components were stained was highly repeatable (n = 25). Example time-courses are presented in Figures 5.12 and 5.13.

- **Plasma membrane**: the membrane selective dye FM4-64 stained the plasma membrane (e.g. Figs. 5.12A, 5.13A, 5.14A) but not the cell wall (Fig. 5.15). The plasma membrane became stained within seconds of adding the dye to the spores (Fig. 5.14A, also see Fig. 4.65, Section 4.2.5.6). There was variation in the intensity of plasma membrane fluorescence within any one conidium, this might have been at least in part due to optical sectioning of the plasma membrane. After approximately 10 min the plasma membrane was usually brightly stained and often appeared to be very thick in regions (e.g. Figs. 5.2A, 5.12B, 5.13B). This effect was probably partially caused by flare from intense fluorescence. However, this did not account for other cases in which fluorescence intensity of the plasma

membrane was lower (e.g. Fig. 5.12D). Another possible explanation for the variation in the thickness of the stained plasma membrane is that some endocytic vesicles were stained and that they were concentrated near the sites of their production.

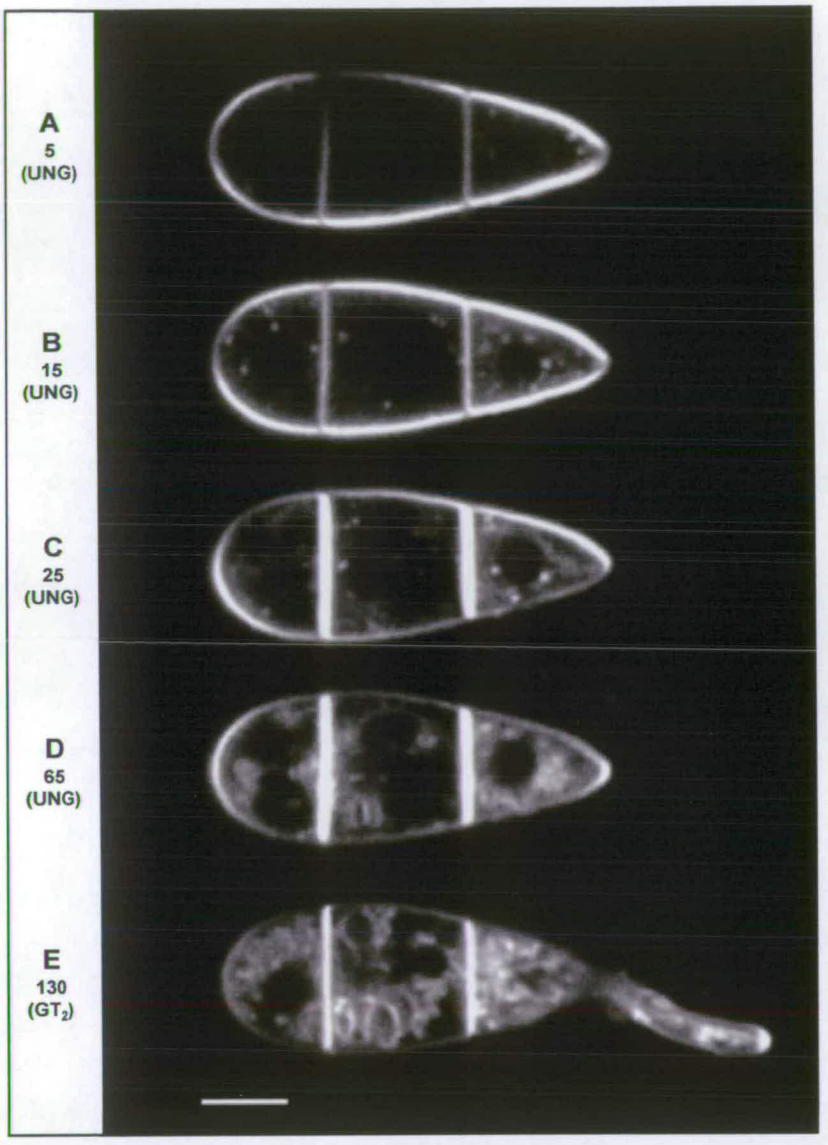

Figure 5.12: Confocal images of an individual conidium showing the time-dependent staining of organelles with FM4-64. Note that the conidium germinates from the apical cell. The numbers are min post dye, and the dye was added at 45 min post hydration. Imaged using a x60 objective. Bar = 5 µm.

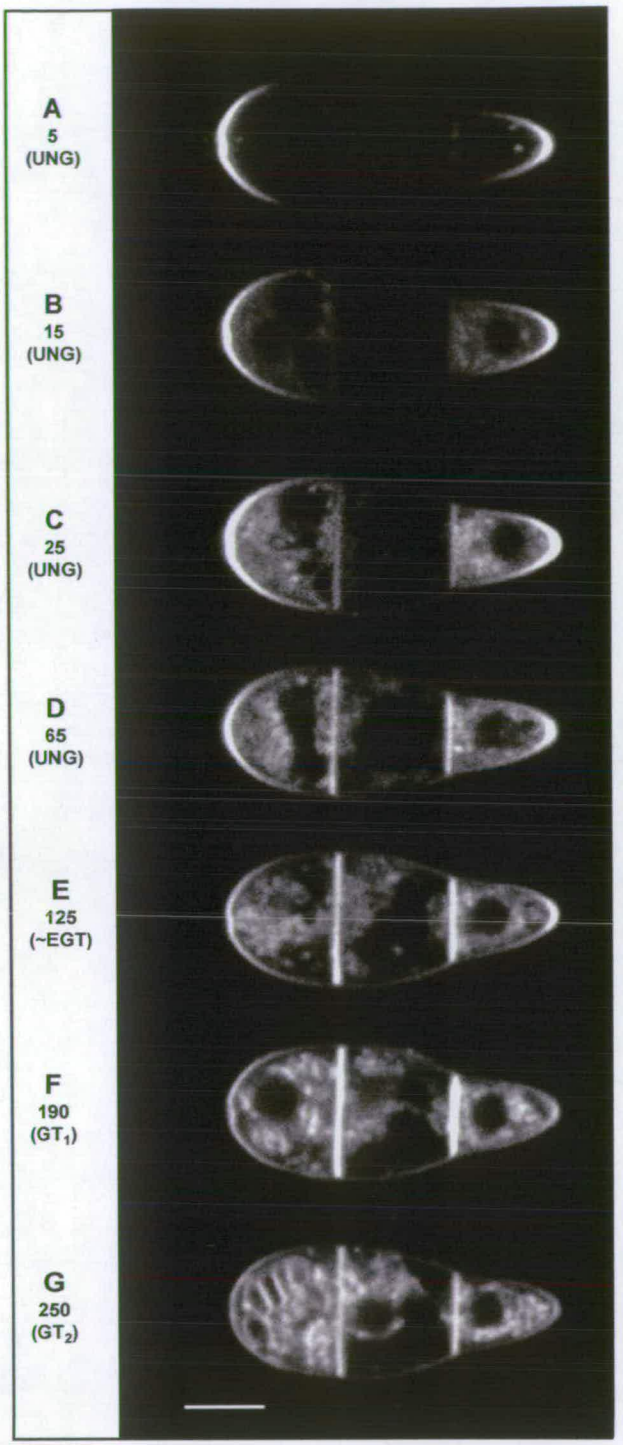

Figure 5.13: Confocal images of an individual conidium showing the time-dependent staining of organelles with FM4-64. Initially, (**A**) diffuse fluorescence is visible and ultimately, (**G**) vacuolar membrane is clearly stained. Note that the conidium germinates from the basal cell but that the germ tube is not visible because it is not within the optical section. The numbers are min post dye, and the dye was added at 45 min post hydration. Imaged using a x60 objective. Bar = 5 μm.

Figure 5.14: Confocal images of an individual conidium showing the sequence of staining with FM4-64 within the apical cell. (**A**) at 100 sec after the addition of the dye the plasma membrane is stained, (**B**) by 150 sec in the dye there is clearly diffuse fluorescence within the cell, but primarily near to the plasma membrane. (**C**) After 210 sec in the dye, a bright spot (putative endosome) is clearly stained in the tip of the cell. The numbers are sec post hydration. Imaged using a x60 objective. Bar = 5 µm.

To determine whether the conidia changed size as a result of putative plasma membrane internalization by endocytosis, a comparison of the size of conidia was made by overlaying the plasma membrane profile of median sections at the UNG stage with the GT_2 within the same spore (data not shown). This analysis was performed on 5 conidia and no change in conidial size was found.

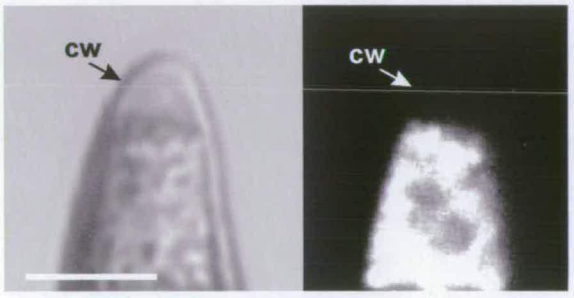

Figure 5.15: The apical cell of a conidium killed by desiccation and then flooded with FM4-64. Note that the cell wall (cw) does not stain. Imaged using a x60 objective. Bar = 5 µm.

- **Diffuse fluorescence within the cytoplasm**: initially (~1–2 min post dye) diffuse fluorescence was observed associated with the inner side of the plasma membrane. This was especially visible in the A-cell tip, which could be partly due to the close proximity of the plasma membrane in that region (e.g. Figs. 5.12A, 5.13A, 5.15B). The source of this diffuse fluorescence was beyond the resolution of the confocal microscope. However, diffuse fluorescence within the cytoplasm has previously been interpreted as emanating from endocytic vesicles (Fischer-Parton *et al.*, 2000).

- **Motile fluorescent spots**: small brightly stained fluorescent spots (~0.4 μm in diameter) were visible in the cytoplasm after the diffuse fluorescence (Figs. 5.3A–C, 5.12A,B, 5.13A, 5.14C). The earliest observation of these fluorescent spots was 2 min post dye and they were always found to be present within 4 min post dye (n = 11). They were highly dynamic, and appeared to move back and forth between the plasma membrane, septum and centre of the cells. Similar spots have previously been observed in fungal hyphae and interpreted as putative endosomes (Fischer-Parton *et al.*, 2000).

- **Septa**: the plasma membrane associated with the septa characteristically stained within the first 30 min post dye and this appeared to occur by the movement of the dye through the plasma membrane, into the membrane present on either side of the septum (Figs. 5.7B, 5.8, 5.12, 5.13, also see Fig. 5.21 in Section 5.2.5.2). The timing of septal staining varied between spores and between septa within the same spore.

- **Other unidentified organelles**: a general increase in cellular FM4-64 fluorescence followed staining of the putative endosomes (e.g. Fig 5.12B–D, 5.13B–F). This was partly due to fluorescence from unidentified small to medium sized membrane-bounded organelles. These were characteristically stained in all cells, distributed throughout the cytoplasm and often appeared to have a convoluted profile (e.g. Figs. 5.13D–F, 5.16). They became stained after the putative endosomes, and prior to identifiable vacuolar membrane staining (e.g. Fig. 5.13D–G). They were observed throughout germination and appeared to exhibit some dynamism. The morphology and position of these organelles within the cells makes it very unlikely that they were mitochondria, particularly because they were not positioned in the cell periphery and were never observed to be elongated in germinated cells (see Section 4.2.5.3). Although some of the staining could have originated from the vacuolar membrane, the morphology and density did not resemble that of the vacuolar system or elements of the vacuolar system,

and did not become larger as germination commenced (see Section 4.2.5.4), (Fig. 5.16).

Figure 5.16: Confocal images of the basal cell of an individual conidium showing examples of the unidentified membrane-bound organelles that are stained prior to the vacuolar membrane. They do not change size or shape as the germ tube grows. Numbers are min post hydration, the dye was added at 17 min post hydration. Imaged using a x60 objective. Bar = 5 µm.

- **Vacuolar membrane**: the typically small vacuoles are present within conidia at the UNG stage of germination (see Section 4.2.5.4) were difficult to positively identify, partly because of their size, and partly due to the general FM4-64 fluorescence in the cells by this stage. The earliest convincing observations of stained vacuole membrane were after 45 min post dye (Fig. 5.17), although structures resembling components of the vacuolar system were observed as early as 16–19 min post dye.

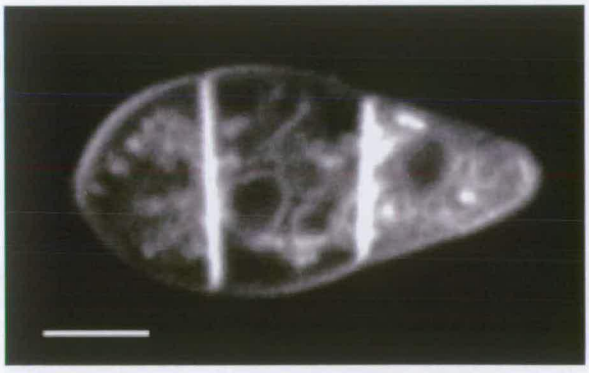

Figure 5.17: Confocal image of an ungerminated conidium stained with FM4-64 for 45 min and showing that the vacuolar membrane in the middle cell is stained. The dye was added at 73 min post hydration. Imaged using a x60 objective. Bars = 5 µm.

Identification of vacuolar membrane was easiest once the conidium had germinated (GT_1–GT_3), (e.g. Figs. 5.1C, 5.12E, 5.13G) because the vacuolar compartments are larger at this stage of germination (see Section 4.3, Fig. 4.71).

- **Mitochondria**: mitochondria in the germ tubes were frequently observed to become stained. The timing of mitochondrial staining varied depending on the stage of germination. During the GT_1 to GT_2 stages of germination, mitochondria within the germ tube were observed to stain after 1 h 35 min in the dye but sometimes took as long as 3 h (n = 11), but in longer germ tubes (GT_3 stage) they were observed to stain as early as 8 min and always by 65 min after the dye was added (n = 8) (Fig. 5.18).

  Identifiably stained mitochondria were not observed within conidial cells during the early stages of germination (UNG–GT_1). This might be expected in the M- and B-cells because the images in this experiment were collected as median sections and mitochondria are primarily located in the peripheral regions of these cells (see Section 4.2.5.3). However, elongated, polarised mitochondria were not observed within the germinated A-cell during the UNG–GT_1 stages of germination. It is possible that the high levels of cellular FM4-64 fluorescence masked any mitochondrial staining. In the later stages of germination (GT_2–GT_3) mitochondria were observed within the germinated conidial cells and the germ tube (Fig 5.1, also see Fig. 4.52 in Section 4.2.5.4).

- **Nuclear envelope**: fluorescence was occasionally observed at the periphery of the nuclei in conidia after germination (EGT–GT_2), (Fig 5.19). The source of this apparent staining of the nuclear envelope might have been other membranous cellular components that are closely associated with the nucleus, such as ER, or possibly the vacuolar membrane pressed against the nucleus.

Figure 5.18: Confocal images of a growing germ tube (GT_3 stage) pulse labelled with FM4-64 and showing that the mitochondria and apical vesicle cluster are stained. In this example the mitochondria stain after 57 min and before 63 min post dye. Note that at this stage of germination, mitochondria in the germ tubes have been observed to stain within 8 min after addition of the dye. The numbers are min post dye, which was added at 5 h 12 min post hydration. Imaged using a x60 objective. Bar = 2 µm.

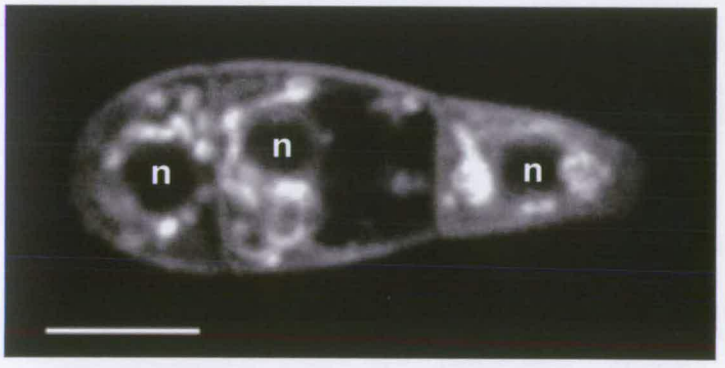

Figure 5.19: Confocal image of a germling (EGT stage) stained with FM4-64 showing the fluorescence occasionally observed to be associated with the periphery of the nucleus (n). Imaged using a x60 objective. Bar = 5 µm.

- **Apical vesicle cluster**: to determine how rapidly the apical vesicle cluster (AVC) became stained (see Section 4.2.5.5), germlings were incubated for 1 min in FM4-64 and the dye was then washed out of the inoculum. This effectively pulse labelled the plasma membrane and subsequent membranes that were stained. It

also prevented the plasma membrane staining from being too high and so masking AVC staining at the germ tube tip (Fig. 5.18). The AVC stained faintly within 2 min after the dye was added, and after approximately 5 min it was brightly stained and highly visible.

5.2.5.2 Initiation of endocytosis in ungerminated spores

Having established that endocytosis occurs during germination and within ungerminated spores after 45 min post hydration (Figs. 5.6A, 5.12, 5.13), experiments were performed to determine the stage after hydration at which endocytosis is initiated. Spores were float-harvested in dye solution and imaged from the time the spore settled on the surface of the CS (~1 min post hydration) to 35 min post dye/hydration. Spores were harvested in dye solution (rather than adding dye to the solution after harvesting) to ensure that the rate that of dye diffusion in the solution was not a variable. A total of 12 conidia were analysed in this manner.

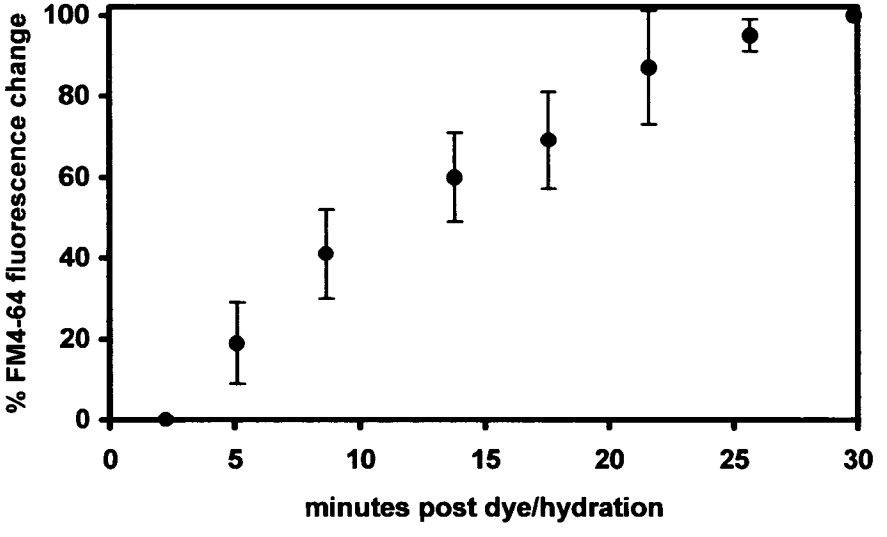

Figure 5.20: Time-course of the change in mean conidial FM4-64 fluorescence over the first 30 min post hydration and dye (added at the time of hydration), showing that the dye is internalized by conidia during this period. The data was extracted from 12 individual conidial time-courses and is expressed as percentage change in FM4-64 fluorescence (grey scale) per pixel over the first 30 min post hydration. The vertical bars are standard deviations.

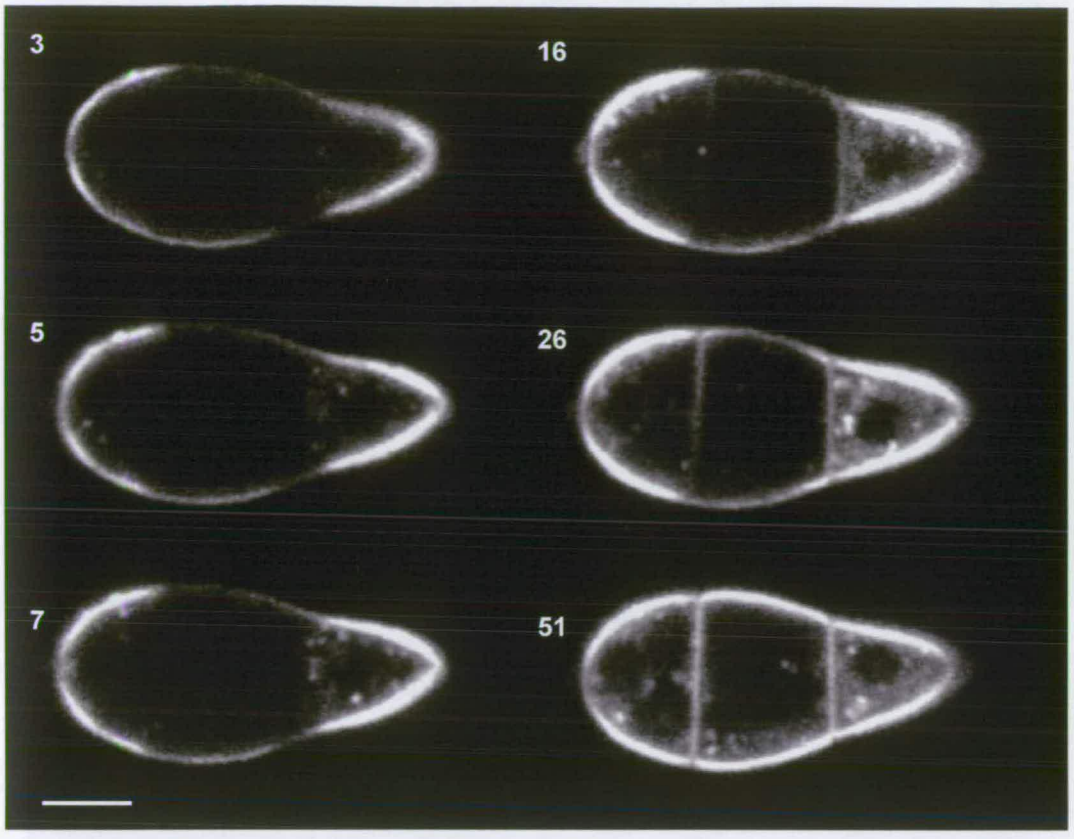

Figure 5.21: Confocal images of an individual conidium showing the time-dependent pattern of staining with FM4-64 during the first 51 min post hydration. Note that the apical cell visibly internalizes dye after three min. The spore is ungerminated during this period of observation but subsequently germinated. Note that the numbers are min post hydration and dye (harvested in dye solution). Imaged using a x60 objective. Bar = 5 µm.

All conidia internalized the dye during the first 30 min post hydration, but the degree of dye internalization and thus fluorescence intensity varied considerably between conidia. In order that the data might be compared, mean FM4-64 fluorescence was expressed as percentage change over the period of 1–30 min post dye/hydration and the means of these values are plotted in Fig. 5.20. The mean value for conidial FM4-64 fluorescence per pixel at 1–3 min post hydration/dye was 13.9 ± 1.8. Between 2–5 min post hydration there was a 20% increase in mean conidial FM4-64 fluorescence, demonstrating that conidia do internalize the dye during the first few min post hydration. This was confirmed by image data in which dye was visibly internalized by conidia as early as 2–3 min post hydration (Fig. 5.21).

A comparison of the rates of endocytosis (measured as rate of increase in the percentage change in mean FM4-64 fluorescence over the period of measurement)

during the periods of 0–30 min post hydration (Fig. 5.20), and 45–75 min post hydration (data from Fig. 5.6A) found no detectable differences (rate = 3.4 and 3.6 percent change in fluorescence per min, respectively n = 12, n = 15).

5.2.6 Evidence that different conidial cells exhibit different rates of FM4-64 internalization

Differences in the rate and extent of dye internalization were observed between cells within the same conidium during germination (e.g. Fig. 5.21). The A-cell was always the first to visibly internalize the dye, and this was most prominent in the tip region of the cell. After a brief lag (typically ~3 min) the B-cell also began to internalize the dye. The M-cell was the last to exhibit visible intracellular FM4-64 fluorescence, and the time lag between it and the A-cell varied.

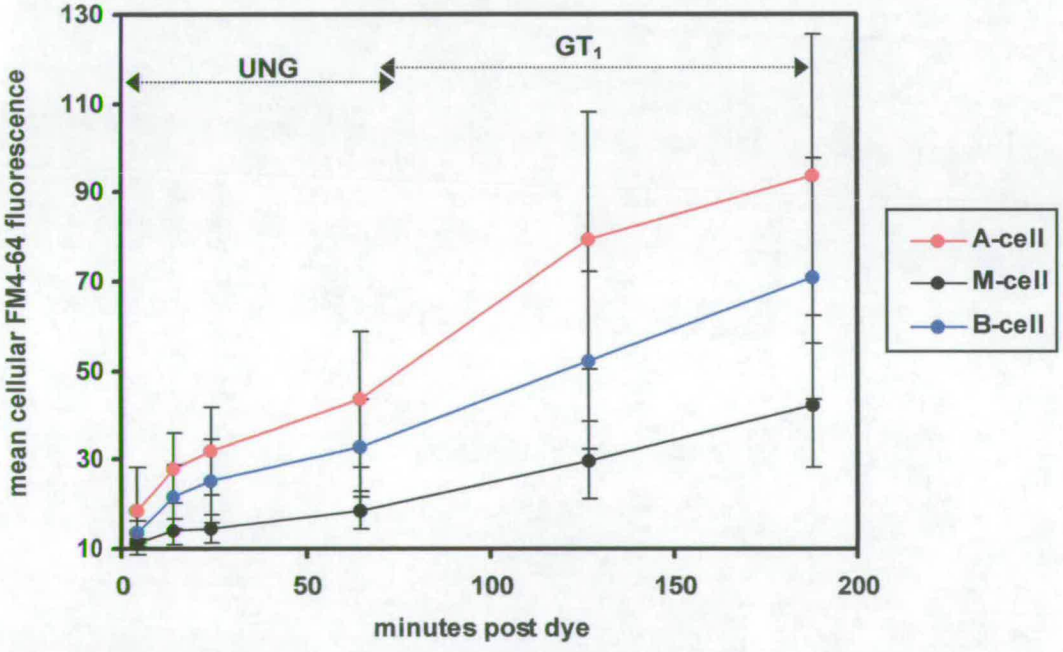

Figure 5.22: A time-course of FM4-64 internalization into the three conidial cells during germination, showing the different rates of dye uptake. The apical (A-cell) and basal (B-cell) cells initially internalize the dye at a faster rate than the middle cell (M-cell). Note that the A-cell values are significantly different from the M-cell values. Dye was added at 45 min post hydration. The data were extracted from 18 individual conidial time-courses and the values are mean cellular FM4-64 fluorescence per pixel. The vertical bars are standard deviations.

When the data shown in Figure 5.6A are plotted as mean cellular FM4-64 fluorescence (rather than conidial), it is apparent that the M-cell exhibits a lower rate of dye internalization than the other two cells (Fig. 5.22). Furthermore, the A- and B-cells are more fluorescent than the M-cell throughout the period examined. Note that the standard deviations are large due to variation within the conidial population, but that the mean A-cell fluorescence is significantly higher than that of the M-cell throughout the period of observation.

5.2.7 Evidence that endocytosis in differentiated germlings occurs within the appressorium but not within the conidium

An analysis to determine whether endocytosis occurs in the conidia and/or appressoria of differentiated germlings was carried out. Data were collected after 10 and 35 min post dye from six differentiated germlings. The dye was added at 6 h post hydration. The results are shown in Figure 5.23 and a representative differentiated germling is shown in Figure 5.24.

There was negligible dye internalization by the conidial cells during the period of 0–35 min post dye, and this is clear from the images shown in Figure 5.24, in which the plasma membrane is the only stained component of the conidium. Although there was much variation between appressoria with respect to the degree of dye internalization (evident from the large standard deviation values), all six appressoria internalized the dye between 0 and 35 min post dye. It should be noted that one germling produced values that were three times greater than the others. However, it has been included in the analysis so that the data represents the true variation within the spore population. The germ tube was not measured due to its small size although the images revealed that they also internalized some dye (Fig 5.24).

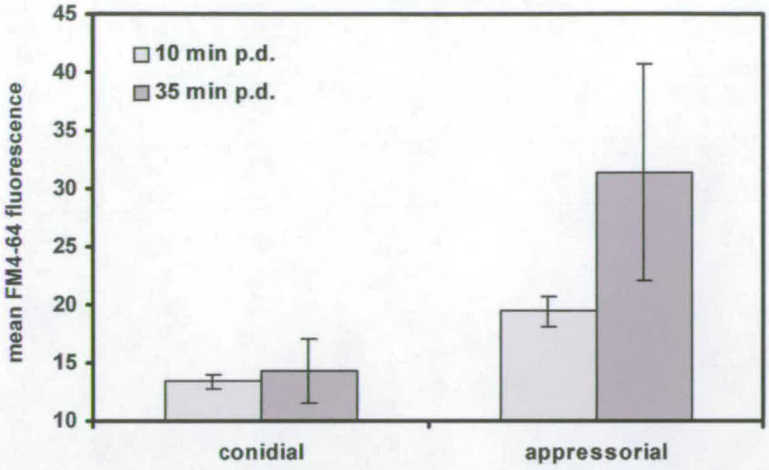

Figure 5.23: FM4-64 internalization within the conidia and appressoria at 10 and 35 min post dye showing that compared to the appressoria the conidia internalized negligible amounts of the dye over this period. The dye was added at 6 h post hydration. Data was extracted from 6 individual time-courses and is expressed as mean conidial and appressorial FM4-64 fluorescence per pixel. The vertical bars are standard deviations. Abbreviations post dye (p.d.).

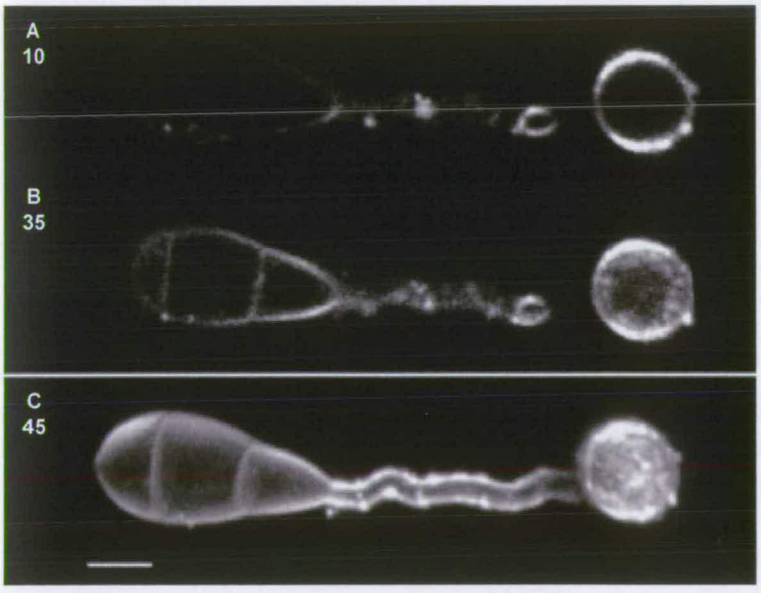

Figure 5.24: Confocal images showing internalization of FM4-64 by a differentiated germling. The numbers are min post dye, which was added at 6 h post hydration. (**A, B**) Only the plasma membrane is stained in the conidium whilst the appressorium clearly internalizes the dye between 10 and 35 min post dye. (**C**) A projected image of the germling which was optically sectioned after 45 min post dye; note that throughout the conidium only the plasma membrane is clearly stained and that the appressorium has internalized the dye and is brightly stained. Imaged using a x60 objective. Bar = 5 μm.

5.3 DISCUSSION

The findings here that three endocytic markers (Lucifer Yellow CH, FITC-dextran and FM4-64) were internalized by conidia and appressoria provides evidence that endocytosis occurs during the pre-penetration phase of the infection cycle of *M. grisea*. The finding that the uptake of these dyes by conidia was reversibly inhibited by sodium azide and cooling, provides evidence that the process by which these dyes are internalized is an active one and not simply by passive diffusion. Furthermore, the staining of organelles by the membrane selective dye FM6-64 was shown to be time-dependent and consistent with internalization by endocytosis, and distribution of the dye to different organelles via the vesicle trafficking network (Fischer-Parton *et al.*, 2000; Read & Hickey, 2000).

5.3.1 Internalization of endocytic markers by conidia

Lucifer Yellow CH was chosen because it has been used extensively as a fluid-phase endocytic marker in animals, plants and yeast cells. However, in recent years it has fallen from favour because it was found that in plant and animal cells the dye was carried across membranes by an organic anion transporter (Hawes *et al.*, 1995). There is evidence that similar anion transporters are also present in the vacuolar membrane of the fungus *Pisolithus tinctorius*, indicating that Lucifer Yellow CH might be internalized by mechanisms other than endocytosis (Cole *et al.*, 1997). In *Ustilago maydis*, mutants thought to be defective for a microtubule-dependant motor enzyme involved in the vesicle trafficking network were unable to accumulate Lucifer Yellow CH within the vacuolar system, but FM4-64 was still readily internalized (Steinberg *et al.*, 1998). The second marker for fluid-phase endocytosis used in this study was FITC-dextran (10 kDa). This is potentially a much better marker since it is too large to diffuse or to be carried across the plasma membrane, but is predicted to be able to cross the cell wall (Cole *et al.*, 1997). It was also observed to be internalized by conidia of *M. grisea* and thus provides the first direct evidence that filamentous fungi undergo fluid-phase endocytosis.

The styryl dye FM4-64 inserts into the outer leaflet of the plasma membrane bilayer and is believed to be unable to enter cells by unfacilitated diffusion (Betz *et al.*, 1996; Fischer-Parton *et al.*, 2000). It has been utilised as a marker of components of the vesicle trafficking network in animal and yeast cells and also more recently in fungal hyphae and there is strong evidence arising from these studies that the dye is internalized by endocytosis (Betz *et al.*, 1996; Hoffman & Mendgen, 1998; Fischer-Parton *et al.*, 2000; Read & Hickey, 2000). In this study, intracellular FM4-64 fluorescence was quantified, to provide a measure of the amount of plasma membrane internalized by the fungal cells, and it was shown that FM4-64 is internalized by the ungerminated conidia, germlings and by the appressoria of *M. grisea*.

Conidia incubated in either of the 2 fluid-phase markers showed no significant increase in fluorescence unless incubated in the dye for extended periods and thus after germination had occurred. On the basis of these findings alone it might be concluded that endocytosis does not occur until after the production of a germ tube, and even that the germ tube is solely responsible for the endocytic internalization of the dyes. However, by using the dye FM4-64 it was possible to demonstrate that endocytosis occurred within 2 minutes after hydration of the conidium. The likely explanation for this disparity between the two sets of results is that the fluid phase endocytosis markers were diluted within the lumen of the variously stained membranous components, whilst FM4-64 remains concentrated within the membrane and thus provided a strong enough signal to image dye internalization by conidia prior to germination.

5.3.2 Inhibition of dye internalization and the mode of internalization

Endocytosis is an active process. The use of treatments that inhibit the production of energy have been previously cited as evidence that dyes are internalized by endocytosis (Vida & Emr, 1995; Hoffman & Mendgen, 1998). In this study internalization of all three endocytic markers assessed was inhibited by the presence of 100 mM sodium azide and by cooling to 4 °C. Furthermore, both these inhibitory

treatments were demonstrated to be reversible. Although both exposure to sodium azide and cooling will inhibit the production of ATP and so endocytosis (Vida & Emr, 1995; Hoffman & Mendgen, 1998) they could have other effects on the conidial cells. In particular, cooling would be predicted to alter membrane fluidity (Ellar, 1978). Thus, these inhibitory treatments might also suppress other mechanisms of dye uptake, such as passive diffusion (Alberts *et al.*, 1989). Controls were performed using the hydrophobic probe Nile red that is readily membrane permeant (Butt *et al.*, 1989; Oparka & Read, 1994; Haugland, 1999). Conidial Nile red fluorescence reached a maximum after approximately 30 min rather than increasing over an extended period of time (~3 h) as in the case of FM4-64 fluorescence. This provided confirmation that Nile red was internalized by diffusion, because it increased in concentration within the cells until it reached equilibrium. There was no evidence that Nile red internalization by conidial cells was inhibited by the presence of sodium azide, but the data did suggest that cooling has some effect on membrane permeability. However, the extent of inhibition of Nile red internalization at 4 °C was too small to account for that observed in the case of the 3 endocytic marker dyes. Thus, the evidence supports the hypothesis that the three markers (Lucifer Yellow CH, FITC-dextran and FM4-64) do not enter cells by passive diffusion.

Whether the dyes enter cells by some other mechanism, such as via carrier proteins in the plasma membrane, has not been controlled for here; sodium azide is predicted to affect ATP-driven carrier proteins, and also the electrochemical gradient across the plasma membrane. However, the localisation of staining by FM4-64 and the order and timing in which this staining occurs is more consistent with uptake via the endocytic pathway rather than directly from the cytoplasm (See Fig. 1.3, Section 1.5). Indeed when FM4-64 was introduced directly into the cytoplasm of desiccated permeabilised conidial cells, the pattern of staining was very different to that observed here (Fig. 4.70, Section 4.2.5.9). One of the main differences is that fluorescence was associated with lipid bodies and although this was performed with dead cells, some degree of lipid staining might be expected if the dye were released directly into the cytoplasm. It was concluded from these results and in the light of

previous findings (Vida & Emr, 1995; Hoffman & Mendgen, 1998; Fischer-Parton *et al.*, 2000; Read & Hickey, 2000) that the most likely route of uptake of the dye FM4-64 into conidial cells is by endocytosis.

5.3.3 Time-dependent staining of organelles with FM4-64

The order and timing in which components of the endomembrane system are stained by FM4-64 was characterized and in general, agreed with previous findings in *N. crassa* (Fischer-Parton *et al.*, 2000; Read & Hickey, 2000). The order of staining is expected to reflect the routes by which membrane passes through the vesicle trafficking network to different organelles. Thus, some of the unidentified, stained, membrane-bounded cellular components can be tentatively identified by their morphology, behaviour and the order in which they became stained (see Fig. 1.3, Section 1.5).

- The diffuse fluorescence observed during the first minutes after the addition of FM4-64 probably emanated primarily from stained endocytic vesicles.
- The most likely candidates for the small brightly stained spots are endosomes (see Fischer-Parton *et al.*, 2000; Read & Hickey, 2000) and they will thus be referred to as putative endosomes. It should be noted that these could also be Golgi equivalents.
- In animal cells and budding yeast the vesicle trafficking network includes a retrograde pathway that links the endosomal system with the Golgi and ER (Satiat-Jeunemaitre *et al.*, 1995). It has been predicted that such pathways also exist in filamentous fungi (Fischer-Parton *et al.*, 2000; Read & Hickey, 2000). The convoluted unidentified structures, which were observed here to stain before the vacuole and to remain present throughout germination, could be Golgi equivalents. Although Golgi equivalents have been identified within the hyphae of *M. grisea* it should be noted that in a study utilising the pharmacological agent brefeldin A, which is known to affect specific endomembrane organelles, there was no evidence for a retrograde pathway between the Golgi and ER (Bourett & Howard, 1994; Satiat-Jeunemaitre *et al.*, 1995; Bourett & Howard, 1996).

Mitochondria did become stained, but they primarily observed within germ tubes. Mitochondrial staining by FM4-64 has been observed previously within fungal hyphae after extended period of incubation within the dye (Fischer-Parton et al., 2000). Continuity between the outer membrane of the mitochondria and the ER system has been described in various cells including hyphae and could account for this staining (Bracker & Grove, 1971; Franke & Kartenback, 1971). However, these studies utilized chemical fixation techniques and so the data must be interpreted with caution (see Section 1.4). An alternative interpretation is that vesicle trafficking occurs between the mitochondria and other endomembrane components; for example lipid transfer from the ER to the mitochondria might occur via vesicle trafficking rather than by phospholipid-exchange proteins. Mitochondria were consistently observed to stain more rapidly in longer germ tubes and the significance of this is unclear. It might be indicative of greater uptake of FM4-64 at this stage, although faint staining of mitochondria was not evident in germ tubes sampled earlier. There could also be some biological significance to this finding relating to the amount of vesicle trafficking or perhaps the degree of contact between the mitochondria and ER during germination.

There was evidence that the nuclear envelope became stained by FM4-64. Previous studies on fungal hyphae using FM4-64 found no evidence of nuclear envelope staining (Fischer-Parton *et al.*, 2000; Read & Hickey, 2000). It is possible that some other component of the endomembrane system was stained and one possible candidate is the ER. In *A. nidulans,* use of green fluorescent protein targeted to the ER has revealed that the ER surrounds the nucleus in the fungal hyphae (Fernández-Ábalos *et al.*, 1998), and in fungal spores the ER is often observed to be in association with the nucleus (e.g. Gull & Trinci, 1971; Mollicone & Longcore, 1999). It has been demonstrated in animal and plant cells and in several fungal species that the rough ER and outer nuclear membrane are continuous (Beckett *et al.*, 1974; Stryer, 1988; Evans & Graham, 1989; Morre, 1990) and this might explain how the nuclear envelope could be stained by FM4-64.

5.3.4 Differential rates of dye internalization

The rate and extent to which FM4-64 was internalized into the different conidial cells was also examined. The quantitative data supports the hypothesis that A- and B-cells internalize the dye at a greater rate and to a greater extent than the M-cell. Some care must be taken when interpreting this data because the values were extracted from median sections in different cells, and the surface:volume ratio differs between the 3 cells: in other words if all three cells were endocytosing at the same rate per unit plasma membrane, the A-cell would be the brightest and the M-cell might very well be the dimmest. However, the possibility that the three conidial cells exhibit different rates and initiation times of endocytosis is supported by the order of staining of putative endosomes. These were always observed to stain earliest within the A-cell and sometimes the B-cell and last within the M-cell after a considerable time lag.

5.3.5 Evidence for endocytosis in the germ tube and appressorium

It was not possible to prove that the dye within the germ tubes originated from dye internalized by endocytosis at the germ tube plasma membrane, because it might have been transferred from the endocytosing conidium. Diffuse fluorescence, putative endosomes and staining of internal membranes were observed within the germ tubes (e.g. Figs. 5.1, 5.18, 5.24). However, internalization of FM4-64 into the germ tube was not quantified in this study. This was mainly because of the narrow germ tube width (~1.5 μm). This has two implications (1) the optical sections could include additional signal from plasma membrane or external cellular features (e.g. peripheral spots, see Section 4.2.5.6) because the z-resolution (with a x60 oil objective) is ~0.8 μm (see Section 2.8.4) which accounts for nearly half the height of a germ tube, (2) the intense fluorescence from the germ tube plasma membrane reduces the available area within the cell from which a sufficient signal could be extracted without flare from the plasma membrane signal skewing the data. Reduction in dye concentration generally reduced the internal signal too greatly to allow the extraction of meaningful data.

Preliminary data was collected that provides evidence that endocytosis takes place within the appressorium and that this might occur during the period of expansion. A

septum occluded by electron dense material has been observed to form at the base of the germ tube during the early stages of differentiation (Bourett & Howard, 1990). This implies that cellular contents can no longer pass into the appressorium from the germ tube after this stage and so rules out transfer of FM4-64 internalized by the germ tube. The data was collected at 6 h post hydration during which time appressorium expansion could still be occurring depending on the time of germination (see Table 1.3, Section 1.3.4). In mature appressoria, a layer of melanin is positioned just outside the plasma membrane, which serves as a barrier to solute flux but not to water (Howard & Ferrari, 1989; Howard & Valent, 1996). The finding that FM4-64 was internalized by the appressoria means that the dye was able to access the plasma membrane and so implies that melanisation (which occurs after expansion, see Table 1.3, p20) was not complete and that the appressoria were still expanding.

5.3.6 Possible functions of endocytosis in conidia and germlings

The results suggest that conidia are undergoing endocytosis within minutes of hydration and thus usually prior to making contact with the rice leaf. Endocytosis continues throughout germination until an appressorium is formed and no detectable difference was found when the rate of FM4-64 internalization was compared between 2–30 and 45–75 min post hydration. The possible functions within the ungerminated spore are unclear, in part because the conidia of *M. grisea* are able to germinate in pure dH_2O and thus in the absence of host signals, or external nutrients. A potentially significant finding was that the two cells that usually germinate appeared to be most active in endocytosis. Evidence was obtained during this study that germ tubes do not emerge from the conidium randomly. They appear to emerge nearer the substratum, and in positions opposite to germ tubes that have already arisen from the same conidium (see Sections 3.2.4, 3.3.5). Recently evidence was obtained that conidia of *B. graminis* internalized low-molecular weight materials with physical properties similar to cutin monomers and it was proposed that the uptake of external signals could play a role in the site and direction of germ tube emergence (Neilson *et al.*, 2000). Endocytosis might serve to internalize external signals from the host surface, or possibly from conidial cells within the same conidium and other conidia.

Furthermore, there is evidence that *M. grisea* both produces and responds to pheromones (Beckerman *et al.*, 1997; Shen *et al.*, 1999). Another possible function of endocytosis in ungerminated conidia is recycling membrane delivered during secretion. There is evidence in other species that spores secrete enzymes prior to germination (Nicholson & Morales 1980; Nicholson *et al.*, 1988; Deising *et al.*, 1992; Pascholati *et al.*, 1992) and if this were occurring then the membrane equilibrium might be maintained by endocytosis: excess membrane delivered to the plasma membrane in the form of secretory vesicles might be recycled by endocytosis.

The possible functions of endocytosis within a germling are clearer than within ungerminated conidia. Most of those possible functions proposed within fungal hyphae apply since the germ tube also exhibits tip growth. These include recycling of membrane, and membrane protein and lipids, transport of membrane proteins and lipids to the vacuole for degradation and the uptake of molecules (Section 1.5.2). Evidence was obtained in this study that the germ tube exhibits directional growth on the rice leaf (Section 3.3.5). Contact sensing might occur via a number of mechanisms (Read *et al.*, 1992b), one of which is the perception of host signals, which might occur via endocytosis. Endocytosis could serve a function during differentiation of the germ tube to form an appressorium. This requires that there is a change from polarised tip growth to localised swelling and might require changes in the phospholipid composition of the plasma membrane at the germ tube tip (Markham *et al.*, 1993). One of the proposed functions of endocytosis is in the recycling of membrane proteins and lipids (Section 1.5.2).

A number of possible functions for endocytosis within fungal hyphae could also apply to the expanding appressorium. If the appressorium secretes compounds at the substratum interface such as enzymes to aid penetration of the underlying host, endocytosis might be required to retrieve the membrane and thus maintain the appressorial turgidity required for penetration of the host (Howard *et al.*, 1991a; Money & Howard, 1996). Filasomes are the best candidates for endocytic vesicles within *M. grisea* and they have been found to be abundant in the region of the

appressorium/substratum interface in *M. grisea* and in other fungi (Howard, 1981; Bourett & Howard, 1991; Howard 1994). In addition, during appressorium expansion the cytoplasm is abundant in cytoplasmic vesicles and smooth cisternae, again a finding common to other fungal species (Bourett & Howard, 1991; Howard 1994). However, since the controls were not performed on differentiated germlings and the experiment was performed only once, the findings are speculative, but deserve further attention.

6. FUTURE WORK

- Study the directional growth of germ tubes in relation to other germ tubes produced by the same conidium.
- Examine the influence of external conditions on the mode of germination within the conidial population.
- Use the method developed to kill individual conidial cells, to determine the role of each conidial cell in influencing germ tube growth rate and direction.
- Use multi-photon confocal microscopy to analyse organelle dynamics and organization in living cells taking advantage of the fact that this technique is potentially less phototoxic.
- Further analyse mitochondrial activity during germination, in particular the apparent asymmetry at the substratum.
- Compare and contrast data collected from imaging living conidia during germination with freeze-substitution TEM studies on conidia and germlings.
- Use green fluorescent protein (GFP) targeted to different organelles, in particular to the Golgi and ER, and make comparisons with results obtained using vital fluorescent dyes in living cells.
- Study endocytosis in germ tubes and within appressoria during germination in more detail.
- Screen for mutants compromised in endocytosis and vesicle trafficking, using the membrane-selective dye FM4-64.
- Combine the techniques used here for live cell analysis, with a genetic approach to analyse spore germination.

REFERENCES

1. Adachi, K. & Hamer, J. E. (1998) Divergent cAMP signalling pathways regulate growth and pathogenesis in the rice blast fungus *Magnaporthe grisea*. *Plant Cell* **10**, 1361–1373.

2. Agrios, G. N. (1988) *Plant Pathology*. Academic Press, London.

3. Alberts, B., Bray, D., Lewis, J., Raff, M., Roberts, K. & Watson, J. D. (1989) *Molecular Biology of the Cell*. Garland Publishing, New York.

4. Allaway, W. G., Ashford, A. E., Heath, I. B. & Hardham, A. R. (1997) Vacuolar reticulum in oomycete hyphal tips: an additional component of the Ca^{2+} regulatory system. *Fungal. Genet. Biol.* **22**, 209–220.

5. Altre, J. A., Vandenberg, J. D. & Cantone, F. A. (1999) Pathogenicity of *Paecilomyces fumosoroseus* isolates to diamondback moth, *Plutella xylostella*: correlation with spore size, germination speed, and attachment. *J. Invertebr. Pathol.* **73**, 332–338.

6. Apoga, D. & Jansson, H. (2000) Visualisation and characterization of the extracellular matrix of *Bipolaris sorokiniana*. *Mycol. Res.* **104**, 564–575.

7. Araki, F. & Miyagi, Y. (1977) Effects of fungicides on penetration by *Pyricularia oryzae* as evaluated by an improved cellophane method. *J. Pest. Sci.* **2**, 457–461.

8. Ashford, A. E. (1998) Dynamic pleiomorphic vacuole systems: are they endosomes and transport compartments in fungal hyphae? *Adv. Bot. Res.* **28**, 119–159.

9. Au, D. W. T., Jones, E. B. G., Moss, S. T. & Hodgkiss, I. J. (1996) The role of mucilage in the attachment of conidia, germ tubes, and appressoria in the saprobic aquatic Hyphomycetes *Lemonniera aquatica* and *Mycocentrospora filiformis*. *Can. J. Bot.* **74**, 1789–1800.

10. Bagga, S. & Straney, D. (1999) Modulation of cAMP and phosphodiesterase activity by flavonoids which induce spore germination of *Nectria haematococca* MP VI (*Fusarium solani*). *Physiol. Mol. Plant Pathol.* **56**, 51–61.

11. Bainbridge, A. & Stedman, O. J. (1979) Dispersal of *Erisyphe* and *Mycopodium clavatum* spores near to the source in a barley crop. *Ann. Appl. Biol.* **91**, 187–198.

12. Bainbridge, B. W., Valentine, B. P. & Markham, P. (1979) The use of temperature-sensitive mutants to study wall growth. In *Fungal Walls and Hyphal Growth*, (Burnett, J. H. & Trinci, A. P. J., eds), pp. 71–92, Cambridge University Press, Cambridge.

13. Baker, B., Zambryski, P., Staskawicz, B. & Dinesh-Kumar, S. P. (1997) Signalling in plant-microbe interactions. *Science* **276**, 726–733.

14. Barr, D. J. S. & Hadland–Hartmann, V. E. (1978) Zoospore ultrastructure in the genus *Rhizophydium* (Chytridiales). *Can. J. Bot.* **56**, 2380–2404.

15. Bartnicki-Garcia, S., Bartnicki, D. D., Gierz, G., Lopez-Franco, R. & Bracker, C. (1995) Evidence that Spitzenkörper behaviour determines the shape of a fungal hypha – a test of the hyphoid model. *Exp. Mycol.* **19**, 153–159.

16. Bartnicki-Garcia, S., Ruiz-Herrera, J. & Bracker, C. (1979) Chitosomes and chitin synthesis. In *Fungal Walls and Hyphal Growth*, (Burnett, J. H. & Trinci, A. P. J., eds), pp. 149–168, Cambridge University Press, Cambridge.

17. Beakes, G. (1981) Ultrastructure of the Phycomycete nucleus. In *The Fungal Nucleus*, (Gull, K. & Oliver, S. G., eds), pp. 1–37, Cambridge University Press, Cambridge.

18. Bechinger, C., Giebel, K. F, Schnell, M., Leiderer, P., Deising, H. B. & Bastmeyer, M. (1999) Optical measurements of invasive forces exerted by appressoria of a plant pathogenic fungus. *Science* **285**, 1896–1899.

19. Beckerman, J. L., Naider, F. & Ebbole, D. J. (1997) Inhibition of pathogenicity of the rice blast fungus by *Saccharomyces cerevisiae* α-factor. *Science* **276**, 1116–1119.

20. Beckett, A. (1981) Ultrastructure and behaviour of nuclei and associated structures within the meiotic cells of Euascomycetes. In *The Fungal Nucleus*, (Gull, K. & Oliver, S. G., eds), pp. 37–61, Cambridge University Press, Cambridge.

21. Beckett, A., Heath, I. B. & McLaughlin, D. J. (1974) *An Atlas of Fungal Ultrastructure*. Longman, London

22. Bergeron, V., Bonn, D., Martin, J. Y. & Vovelle, L. (2000) Controlling droplet deposition with polymer additives. *Nature* **405**, 772–775.

23. Betz, W. J., Mao, F. & Orlovich, D. A. (1996) Imaging exocytosis and endocytosis. *Fungal. Genet. Biol.* **6**, 365–371.

24. Blakeman, J. P. (1980) Behaviour of conidia on aerial plant surfaces. In *The Biology of* Botrytis, (Coley-Smith, J. R., Verhoeff, K. & Jarvis, W. R., eds), pp. 115–151, Academic Press, London.

25. Blatt, M. E., Leyman, B. & Geelen, D. (1999) Tansley Review No. 108: Molecular events of vesicle trafficking and control by SNARE proteins in plants. *New Phytol.* **144**, 418.

26. Bölker, M. and Kahmann, R. (1993) Sexual pheromones and mating responses in fungi. *Plant Cell* **5**, 1461–1469

27. Bonman, J. M. (1992) Foliar diseases: blast. In *Compendium of Rice Diseases* (Webster, R. K. & Gunnel, P. S., eds), pp. 14–17, *Am. Phytopathol. Soc.*, St. Paul, Minnesota:

28. Bourett, T. M. & Howard, R. J. (1990) *In vitro* development of penetration structures in the rice blast fungus *Magnaporthe grisea*. *Can. J. Bot.* **68**, 329–342.

29. Bourett, T. M. & Howard, R. J. (1991) Ultrastructural immunolocalization of actin in a fungus. *Protoplasma* **163**, 199–202.

30. Bourett, T. M. & Howard, R. J. (1992) Actin in penetration pegs of the fungal rice blast pathogen, *Magnaporthe grisea*. *Protoplasma* **168**, 20–26.

31. Bourett, T. M. & Howard, R. J. (1994) Enhanced labelling of concanavalin A binding sites in fungal endomembranes using a double-sided, indirect method. *Mycol. Res.* **98**, 769–775.

32. Bourett, T. M. & Howard, R. J. (1996) Brefeldin A-induced structural changes in the endomembrane system of a filamentous fungus, *Magnaporthe grisea*. *Protoplasma* **190**, 151–163.

33. Bourett, T. M., Picollelli, M. A. & Howard, R. J. (1993) Postembedment labelling of intracellular concanavalin A-binding sites in freeze-substituted fungal cells. *Exp. Mycol.* **17**, 223–235.

34. Bourret, J. A., Flora, L. L. & Carnell, L. (1991) Cyclic AMP regulation of fructose metabolism in germinating *Pilobolus longipes* spores. *Exp. Mycol.* **15**, 44–54.

35. Bracker, C. E. & Grove, S. N. (1971) Continuity between cytoplasmic endomembranes and outer mitochondrial membranes in fungi. *Protoplasma* **73**, 15–34.

36. Bracker, C. E., Morré, D. J. & Grove, S. N. (1996) Structure, differentiation, and multiplication of Golgi apparatus in fungal hyphae. *Protoplasma* **194**, 250–274.

37. Brambl, R. (1981) Respiration and mitochondrial biogenesis during fungal spore germination. In *The Fungal Spore: Morphogenetic Controls*, (Turian, G. & Hohl, H. R., eds), pp. 585–604, Academic Press, London.

38. Brambl, R., Dunkle, L. D. & Van Etten, J. L. (1978) Nucleic acid and protein synthesis during fungal spore germination. In *The Filamentous Fungi, Developmental Biology* Vol 3, (Smith, J. E. & Berry, D. R., eds), pp. 94–118, Arnold, London.

39. Brambl, R. & Handschin, B. (1976) Mitochondrial biogenesis during fungal spore germination: products of mitochondrial protein synthesis *in vivo*. *Arch. Biochem. Biophys.* **175**, 606–617.

40. Brambl, R., Plesofky-Vig, N., Hammet, J. R. & Russel, P. J. (1987) Preserved polyadenylated ribonucleic acid in dormant conidia of *Neurospora crassa* and new RNA synthesis during spore germination. *Exp. Mycol.* **11**, 317–330.

41. Braun, E. J. & Howard, R. J. (1994) Adhesion of fungal spores and germlings to host surfaces. *Protoplasma* **181**, 202–212.

42. Brown, W. (1922) On the germination and growth of fungi at various temperatures and in various concentrations of oxygen and carbon dioxide. *Ann. Bot.* **36**, 257–283.

43. Buckley, P. M., Sjaholm, V. E. & Sommer, N. F. (1966) Electron microscopy of *Botrytis cinerea* conidia. *J. Bacteriol.* **91**, 2037–2044.

44. Butt, T. M., Staples, R. C. & Leger, R. J. S. (1989) Use of fluorochromes in the study of fungal cytology and differentiation. *Exp. Mycol.* **13**, 303–320.

45. Caesar–Ton That, T. C., Hoangvan, K., Turian, G. & Hoch, H. C. (1987) Isolation and characterization of coated vesicles from filamentous fungi. *Eur. J. Cell Biol.* **43**, 189–194.

46. Calvo-Mendez, C, Martinez-Pacheco, M, Ruiz-Herrera, J. (1987) Regulation of orthinine decarboxylase activity in *Mucor bacilliformis* and *Mucor rouxii*. *Exp. Mycol.* 270–277.

47. Carver, T. L. W., Kunoh, H., Thomas, B. J. and Nicholson, R. L. (1999) Release and visualization of the extracellular matrix of conidia of *Blumeria graminis*. *Mycol. Res.* **103**, 547–560.

48. Choi, W. & Dean, R. A. (1997) The adenylate cyclase gene MAC1 of *Magnaporthe grisea* controls appressorium formation and other aspects of growth and development. *Plant Cell* **9**, 1973–1983.

49. Choi, W., Kang, S., Lee, Y. & Lee, Y. (1998) Cyclic AMP restores appressorium formation inhibited by polyamines in *Magnaporthe grisea*. *Phytopathology* **88**, 58–62.

50. Christensen, C. M. (1965) *The Molds and Man.* University of Minnesota Press, Minneapolis.

51. Chuang, J. S. & Schekman, R. W. (1996) Differential tracking and timed localization of two chitin synthase proteins, Chs2p and Chs3p. *J. Cell Biol.* **135**, 597–610.

52. Chumley, F. G. & Valent, B. (1990) Genetic analysis of melanin-deficient, non-pathogenic mutants of *Magnaporthe grisea*. *Mol. Plant-Microbe Interact.* **30**, 359–372.

53. Clement, J. A., Martin, S. G., Porter, R., Butt, T. M. & Beckett, A. (1993) Germination and the role of extracellular matrix in adhesion of urediniospores of *Uromyces viciae-fabae* to synthetic surfaces. *Mycol. Res.* **97**, 585–593.

54. Clement, J. A., Porter, R., Butt, T. M. & Beckett, A. (1994) The role of hydrophobicity in attachment of urediniospores and sporelings of *Uromyces viciae-fabae*. *Mycol. Res.* **98**, 1217–1228.

55. Clutterbuck, A. J. (1995) Molecular Biology. In *The Growing Fungus* (Gow, N. A. R. & Gadd, G. M., eds), pp. 255–274, Chapman & Hall, London.

56. Cole, G. T. (1981) Techniques for examining developmental and ultrastructural aspects of conidial fungi. In *Biology of Conidial Fungi* (vol 2), (Cole, G. T. & Kendrick, B., eds), pp. 577–634, Academic Press, London.

57. Cole, G. T. (1986) Models of cell differentiation in conidial fungi. *Microbiol. Rev.* **50**, 95–132.

58. Cole, G. T. (1990) The conidial fungi. In *Atlas of Fungal Ultrastructure*, (A.E. Vassilyev, ed.), Komarov Botanical Institute, Leningrad.

59. Cole, G. T. & Samson, R. A. (1979) *Patterns of development in conidial fungi.* Pitman, London.

60. Cole, L., Hyde, G. J. & Ashford, A. E. (1997) Uptake and compartmentalisation of fluorescent probes by *Pisolithus tinctorius* hyphae: evidence for an anion transport mechanism at the tonoplast but not for fluid–phase endocytosis. *Protoplasma* **199**, 18–29.

61. Cole, L., Orlovich, D. A. & Ashford, A. E. (1998) Structure, function and motility of vacuoles in filamentous fungi. *Fungal. Genet. Biol.* **24**, 86–100.

62. Coleman, J., Evans, D. & Hawes, C. (1988) Plant coated vesicles. *Plant Cell Env.* **11**, 669–684.

63. Collinge, A. J. & Trinci, A. P. J. (1974) Hyphal tips of wild type and spreading colonial mutants of *Neurospora crassa*. *Arch. Microbiol.* **99**, 353–368.

64. Collins, T. J. (1996) *Appressorium Induction in the Cereal Rusts*. Ph.D. thesis, University of Edinburgh.

65. Collins, T. J. & Read, N. D. (1997) Appressorium induction by topographical signals in six cereal rusts. *Physiol. Mol. Plant Pathol.* **51**, 169–179.

66. Daly, J. M., Knoche, H. W. & Wiese, M. V. (1967) Carbohydrate and lipid metabolism during germination of uredospores of *Puccinia graminis tritici*. *Plant Physiol.* **42**, 1633–1642.

67. Dayton, J. S., Sumi, M., Nanthakumar, N. N. & Means, A. R. (1997) Expression of a constitutively active Ca^{2+}/calmodulin-dependant kinase in *Apsergillus nidulans* spores prevents germination and entry into the cell cycle. *J. Biol. Chem.* **272**, 3223–3230.

68. Deacon, J. W. (1997) *Modern Mycology*. Blackwell Science, Cambridge.

69. Dean, R. A., Blackmon, B. P., Brooks, J. C., Gilbert, R. D., Liu, S., Mitchell, T. K., Shieh, M. T. & Zhu, H. (1996) Cell surface communication in appressorium development by *Magnaporthe grisea*. In *Molecular Aspects of Pathogenicity and Resistance: Requirement or Signal Transduction*, (Mills, D., Kunoh, H., Keen, N. T. & Mayama, S, eds), pp. 59–71, APS Press, Minnesota.

70. Deising, H., Nicholson, R. L., Haug, M., Howard, R. J. & Moss, S. T. (1992) Adhesion pad formation and the involvement of cutinase and esterases in the attachment of uredospores to the host cuticle. *Plant Cell* **4**, 1101–1111.

71. Deising, H., Rauscher, M., Haug, M. & Heiler, S. (1995) Differentiation and cell wall degrading enzymes in the obligately biotrophic rust fungus *Uromyces viciae-fabae*. *Can. J. Bot.* **73**, S624–S631.

72. de Jong, J. C., McCormack, B. J., Smirnoff, N. & Talbot, N. (1997) Glycerol generates turgor in rice blast. *Nature* **389**, 244–245.

73. Delvecchio, V. G., Corbaz, R. & Turian, G. (1969) An ultrastructural study of hyphae, endoconidia and chlamydospores of *Thielaviopsis basicola*. *J. Gen. Microbiol.* **58**, 23–27.

74. d'Enfert, C. (1997) Fungal spore germination: insights from the molecular genetics of *Aspergillus nidulans* and *Neurospora crassa*. *Fungal. Genet. Biol.* **21**, 163–172.

75. Derksen, J., Rutten, T., Lichtscheidl, I. K., Dewin, A. H. N., Pierson, E. S. & Rongen, G. (1995) Quantitative analysis of the distribution of organelles in tobacco pollen tubes – implications for exocytosis and endocytosis. *Protoplasma* **188**, 267–276.

76. DeZwaan, T. M., Carroll, A. M., Valent, B. & Sweigard, J. A. (1999) *Magnaporthe grisea* Pth11p is a novel plasma membrane protein that mediates

appressorium differentiation in response to inductive substrate cues. *Plant Cell* **11**, 2013–2030.

77. Diamond, J. (1997) *Guns, Germs and Steel*. Hutchinson, New York.

78. Dixon, K. P., Xu, J. -R., Smirnoff, N. & Talbot, N. J. (1999) Independent signalling pathways regulate cellular turgor during hyperosmotic stress and appressorium-mediated plant infection by *Magnaporthe grisea*. *Plant Cell* **11**, 2045–2058.

79. Dobinson, K. F. & Hamer, J. E. (1992) *Magnaporthe grisea*. In *Molecular Biology of Filamentous Fungi, Berlin, August 24–29, 1991*, (Stahl, U. & Tudzynski, P., eds), pp. 67–86, Proceedings of the EMBO–Workshop. Weinheim, Germany: VCH.

80. Dulic, V., Egerton, M., Elguindi, I., Raths, S., Singer, B. & Riezman, H. (1991) Yeast endocytic assays. *Meth. Enzymol.* **194**, 697–710.

81. Dutta, S. K., Lafayette, L. & Austin, W. L. (1981) Gene level control. In *The Fungal Spore: Morphogenetic Controls*, (Turian, G. & Hohl, H. R., eds). Academic press, London.

82. Elbein, A. D. (1974) The metabolism of ∝, ∝-trehalase. *Adv. Carbohydr. Chem. Biochem.* **30**, 256–277.

83. Ellar, D. J. (1978) Membrane fluidity in microorganisms. In *Companion to Microbiology: Selected Topics for Further Study*, (Bull, A. T. & Meadow, P. M., eds.), pp. 265–298, Longman Group, London.

84. Epstein, L., Laccetti, L., Staples, R. C., Hoch, H. C. & Hoose, W. A. (1985) Extracellular proteins associated with induction of differentiation in bean rust uredospore germlings. *Phytopathology* **75**, 1073–1076.

85. Evans, W. H. & Graham, J. M. (1989) *Membrane Structure and Function.* IRL Press at Oxford University Press, Oxford.

86. Fernández-Ábalos, J. M., Fox, H., Pitt, C. & Doonan, J. H. (1998) Plant-adapted green fluorescent protein is a versatile vital reporter for gene expression, protein localization and mitosis in the filamentous fungus, *Aspergillus nidulans. Mol. Microbiol.* **27**, 121–130.

87. Fischer, R. (1999) Nuclear movement in filamentous fungi. *FEMS Microbiol. Rev.* **23**, 39–68.

88. Fischer-Parton, S., Parton, R. M., Hickey, P. C., Dijksterhuis, J., Atkinson, H. A. & Read, N. D. (2000) Confocal microscopy of FM4-64 as a tool for analysing endocytosis and vesicle trafficking in living fungal hyphae. *J. Microsc.* **198**, 246–259.

89. Franke, W. W. & Kartenbeck, J. (1971) Outer mitochondrial membrane continuous with endoplasmic reticulum. *Protoplasma* **73**, 35–41.

90. Garraway, M. O. & Evans, C. E. (1984) *Fungal Nutrition and Physiology.* John Wiley & Sons, New York.

91. Gilbert, R. D., Johnson, A. M. & Dean, R. A. (1996) Chemical signals responsible for appressorium formation in the rice blast fungus *Magnaporthe grisea. Physiol. Mol. Plant Pathol.* **48**, 335–346.

92. Girardin, H., Paris, S., Rault, J., Bellon-Fontaine, M-N. & Latgé, J-P. (1999) The role of the rodlet structure on physicochemical properties of *Aspergillus* conidia. *Lett. Appl. Microbiol.* **29**, 364–369.

93. Gold, R. E. & Mendgen, K. (1991) Rust basidiospore germlings and disease initiation. In *The Fungal Spore and Disease Initiation in Plants and Animals*, (Cole, G. T. & Hoch, H. C., eds), pp. 67–100, Plenum Press. New York.

94. Gooday, G. W. (1995) Cell walls. In *The Growing Fungus*, (Gow, N. A. R. & Gadd, G. M., eds), pp. 41–62, Chapman & Hall, London.

95. Gottlieb, D. (1950) The physiology of spore germination in fungi. *Bot. Rev.* **16,** 229–257.

96. Gottleib, D. (1976) Carbohydrate metabolism and spore germination. In *The Fungal Spore*, (Weber, D. J. and Hess, W. M., eds), pp. 141–163. John Wiley and Sons, New York.

97. Gow, N. A. R. (1995) Tip growth and polarity In *The Growing Fungus*, (Gow, N. A. R. & Gadd, G. M., eds), pp. 277–299, Chapman & Hall, London.

98. Grove, S. N. (1978) The cytology of hyphal tip growth. In *The Filamentous Fungi*, (Smith, J. E. & Berry, D. R., eds), pp. 28–48, Edward Arnold, London.

99. Grove, S. N. & Bracker, C. (1970) Protoplasmic organization of hyphal tips among fungi: vesicles and Spitzenkörper. *J. Bacteriol.* **104**, 989–1009.

100. Gruenberg, J. & Maxfield, F. R. (1995) Membrane transport in the endocytic pathway. *Curr. Opin. Cell Biol.* **7**, 552–563.

101. Gull, K. (1978) Form and function of septa in filamentous fungi. In *The Filamentous Fungi,* (Smith, J. E. & Berry, D. R., eds), pp. 78–93, Edward Arnold, London.

102. Gull, K. & Trinci, A. P. J. (1971) Fine structure of spore germination in *Botrytis cinerea. J. Gen. Microbiol.* **68**, 207–220.

103. Guthrie, B. A. & Wickner, W. (1988) Yeast vacuoles fragment when microtubules are disrupted. *J. Cell Biol.* **107**, 115–120.

104. Hall, A. A., Bindslev, L., Rouster, J., Rasmussen, A. W., Oliver, R. P. & Gurr, S. J. (1999) Involvement of cAMP and protein kinase A in conidial differentiation by *Erisyphe graminis* f. sp. *hordei*. *Mol. Plant-Microbe Interact.* **12**, 960–968.

105. Hamer, J. E. & Holden, D. W. (1997) Linking approaches in the study of fungal pathogenesis: a commentary. *Fungal. Genet. Biol.* **21**, 11–16.

106. Hamer, J. E., Howard, R. J., Chumley, F. G. & Valent, B. (1988) A mechanism for surface attachment in spores of a plant pathogenic fungus. *Science* **239**, 288–290.

107. Hamer, J. E. & Talbot, N. (1998) Infection-related development in the rice blast fungus *Magnaporthe grisea*. *Curr. Opin. Microbiol.* **1**, 693–697.

108. Hashioka, Y. (1965) Effects of environmental factors on development of causal fungus, infection, disease development, and epidemiology in rice blast disease. In *The Rice Blast Disease: Proceedings of a Symposium at the International Rice Research Institute*, pp. 153–161, John Hopkins Press, Baltimore.

109. Hashioka, Y. (1972) Fine structure of the rice blast: IX scanning electron microscopical observations on appressoria of the rice blast fungus and other species of *Pyricularia*. *Res. Bull. Fac. Agr.* **33**, 65–73.

110. Haugland, R. P. (1999) *Handbook of Fluorescent Probes and Research Chemicals*, (7th Edn), Molecular Probes Inc., Eugene.

111. Hawes, C., Crooks, K., Coleman, J. & Satiat-Jeunemaitre, B. (1995) Endocytosis in plants: fact or artefact? *Plant Cell Environ.* **18**, 1245–1252.

112. Hawker, L. E. & Abbot, P. M. (1963) An electron microscope study of maturation and germination of sporangiospores of two species of *Rhizopus*. *J. Gen. Microbiol.* **32**, 295–298.

113. Heath, I. B. (1981) Mechanisms of nuclear division in fungi. In *The Fungal Nucleus*, (Gull, K. & Oliver, S. G., eds), pp. 85–112, Cambridge University Press, Cambridge.

114. Heath, I. B. (1995) The cytoskeleton. In *The Growing Fungus,* (Gow, N. A. R. & Gadd, G. M., eds), pp. 99–134, Chapman & Hall, London.

115. Heath, I. B. & Steinberg, G. (1999) Mechanisms of hyphal tip growth: tube dwelling amoebae revisited. *Fungal. Genet. Biol.* **29**, 79–93.

116. Heath, M. C., Howard, R. J., Valent, B. & Chumley, F. G. (1992) Ultrastructural interactions of one strain of *Magnaporthe grisea* with goosegrass and weeping lovegrass. *Can. J. Bot.* **70**, 779–87.

117. Heath, M. C., Valent, B., Howard, R. J. & Chumley, F. G. (1990) Interactions of two strains of *Magnaporthe grisea* with rice, goosegrass and weeping lovegrass. *Can. J. Bot.* **68**, 1627–1637.

118. Hegde, Y. & Kolattukudy, P. E. (1997) Cuticular waxes relieve self-inhibition of germination and appressorium formation by the conidia of *Magnaporthe grisea*. *Physiol. Mol. Plant Pathol.* **51**, 75–84.

119. Hein, L., Ishii, K., Coughlin, S. R. & Kobilka, B. K. (1994) Intracellular targeting and trafficking of thrombin receptors: a novel mechanism for representation of a G protein-coupled receptor. *J. Biol. Chem.* **269**, 27719–27726.

120. Henricksen, G. H., Taylor, A. R., Brownlee, C. & Assman, S. M. (1995) Laser microsurgery of higher plant cell walls permits patch clamp access. *Plant Physiol.* **110**, 1068.

121. Heritage, L. & Evans, E. G. V. (1996) *Introduction to Microbiology.* Cambridge University Press.

122. Ho, W-H., Ranghoo, V. M., Hyde, K. D. & Hodgkiss, I. J. (1999) Ascal ultrastructural study in *Annulatascus hongkongensis* sp. nov., a freshwater ascomycete. *Mycologia* **91**, 885–892.

123. Hoch, H. C. (1986) Freeze-substitution of fungi. In *Ultrastructure Techniques for Microorganisms*, (Aldrich, H. C. & Todd, W. J., eds), pp. 183–212, Springer-Verlag, Berlin.

124. Hoch, H. C. & Staples, R. C. (1983) Ultrastructural organization of the non-differentiated uredospore germling of *Uromyces phaseolis* variety *typica*. *Mycologia* **75**, 795–824.

125. Hoch, H. C. & Staples, R. C. (1991) Signalling for infection structure formation. In *The Fungal Spore and Disease Initiation in Plants and Animals*, (Cole, G. T., ed.), pp. 3–24, Plenum Press, New York.

126. Hoch, H. C., Staples, R. C., Whitehead, B., Comeau, J. & Wolf, E. D. (1987) Signalling for growth orientation and cell differentiation by surface topography in *Uromyces*. *Science* **235**, 1659–1662.

127. Hoffman, H-P. & Avers, C. J. (1973) Mitochondrion of yeast: ultrastructural evidence for one giant, branched organelle per cell. *Science* **181**, 749–751.

128. Hoffman, J. & Mendgen, K. (1998) Endocytosis and membrane turnover in the germ tube of *Uromyces fabae*. *Fungal. Genet. Biol.* **24**, 77–85.

129. Holthius, J. C. M., Nichols, B. J. & Pelham, H. R. B. (1998) The syntaxin Tlg1p mediates trafficking of chitin synthase III to polarized growth sites in yeast. *Mol. Biol. Cell* **9**, 3383–3397.

130. Hooke, R. (1665) *Micrographia: or Some Physiological Description of Minute Bodies Made by Magnifying Glasses with Observations and Inquiries Thereupon.* London: Martyn Allestry – Printers to the Royal Society.

131. Howard, R. J. (1981) Ultrastructural analysis of hyphal tip cell growth in fungi: Spitzenkörper, cytoskeleton and endomembranes after freeze-substitution. *J. Cell Sci.* **48**, 89–103.

132. Howard, R. J. (1994) Cell Biology of Pathogenesis. In *Rice Blast Disease* (Zeigler, R. S., Leong, S. A. & Teng, P. S., eds), pp. 3–22, CAB International with International Rice Research Institute, Oxon.

133. Howard, R. J. (1997) Breaching the outer barriers – cuticle and cell wall penetration. In *Plant Relationships*, (Carrol & Tudzynski, eds), pp. 43–60, Springer-Verlag, Berlin.

134. Howard, R. J. & Aist, J. R. (1979) Hyphal tip ultrastructure of the fungus *Fusarium*: improved preservation by freeze-substitution. *J. Ultrastruct. Res.* **66**, 224–234.

135. Howard, R. J., Bourett, T. M. & Ferrari, M. A. (1991a) Infection by *Magnaporthe*: an *in vitro* analysis. In *Electron Microscopy of Plant Pathogens* (Mendgen, K. & Lesemann, D. E., eds), pp. 251–264, Springer-Verlag, Berlin.

136. Howard, R. J. & Ferrari, M. A. (1989) Role of melanin in appressorium function. *Exp. Mycol.* **13**, 403–418.

137. Howard, R. J., Ferrari, M. A., Roach, D. H. & Money, N. P. (1991b) Penetration of hard substrates by a fungus employing enormous turgor pressures. *Proc. Natl. Acad. Sci. U. S. A.* **88**, 11281–11284.

138. Howard, R. J. & O'Donnell, K. L. (1987) Freeze substitution of fungi for cytological analysis. *Exp. Mycol.* **11**, 250–269.

139. Howard, R. J. & Valent, B. (1996) Breaking and entering: host penetration by the fungal rice blast pathogen *Magnaporthe grisea*. *Annu. Rev. Microbiol.* **50**, 491–512.

140. Hudler, W. G. (1998) *Magical Mushrooms, Mischievous Molds*. Princeton University Press, Chichester.

141. Hunsley, D. & Gooday, G. W. (1974) The structure and development of septa in *Neurospora crassa*. *Protoplasma* **82**, 125–146.

142. Hyde, G. J. & Ashford, A. E. (1997) Vacuole motility and tubule-forming activity in *Pisolithus tinctorius* hyphae are modified by environmental conditions. *Protoplasma* **198**, 85–92.

143. Hyde, G. J., Davies, D., Perasso, L., Cole, L. & Ashford, A. E. (1999) Microtubules, but not actin microfilaments, regulate vacuole motility and morphology in hyphae of *Pisolithus tinctorius*. *Cell Motil. Cytoskeleton* **42**, 114–124.

144. Hyde, K. D., Moss, S. T., & Jones, E. B. J. (1997) Ultrastructure of germination and mucilage production in *Halosphaeria appendiculata* (Halosphaeriaceae). *Mycoscience* **38**, 45–53

145. Ingold, C. T. (1964) Possible spore discharge mechanism in *Pyricularia*. *Trans. Br. Mycol. Soc.* **47**, 573–559.

146. Ingold, C. T. (1971) *Fungal Spores: Their Liberation and Dispersal.* Oxford University Press, London.

147. International Rice Research Institute (1997) *IRRI Rice facts.* Manilla: International Rice Research Institute.

148. Jeffree, C. E. (1996) Structure and ontogeny of plant cuticles. In *Plant Cuticles*, (Kerstiens, G., ed.), pp. 33–82, BIOS Scientific Publishers, Oxford.

149. Jelitto, T. C. (1999) Confocal ratio imaging of cytoplasmic pH during germ tube growth and appressorium induction by *Magnaporthe grisea. New Phytol.* **144**, 499–506.

150. Jelitto, T. C., Page, H. A. & Read, N. D. (1994) Role of external signals in regulating the pre-penetration phase of infection by the rice blast fungus, *Magnaporthe grisea. Planta* **194**, 471–477.

151. Jones, G. L., Bailey, J. A. & O'Connell, R. J. (1995) Sensitive staining of fungal extracellular matrices using colloidal gold. *Mycol. Res.* **99**, 576–573.

152. Jones, L. & O'Shea, P. (1994) The electrostatic nature of the cell surface of *Candida albicans*: a role in adhesion. *Exp. Mycol.* **18**, 111–120.

153. Kaminskyj, S. G. & Day, A. W. (1984) Chemical induction of infection structures in rust fungi. *Exp. Mycol.* **8**, 63–72.

154. Kershaw, M. J. & Talbot, N. J. (1998) Hydrophobins and repellents: proteins with fundamental roles in fungal morphogenesis. *Fungal. Genet. Biol.* **23**, 18–33.

155. Khurana, N., Saxenam R. K. Gupta, R. & Rajam, M. V. (1996) Polyamines as modulators of microcycle conidiation in *Aspergillus flavus*. *Microbiology* **142**, 517–523.

156. Kim, C. K. (1994) Blast management in high input, high yield potential, temperate rice ecosystems. In *Rice Blast Disease*, (Zeigler, R. S., Leong, S. A. & Teng, P. S., eds), pp. 451–464, CAB International with International Rice Research Institute, Oxon.

157. Kim, W. K. (1971) Folate and polyamine content of undifferentiated and differentiated wheat stem rust uredosporelings. *Can. J. Bot.* **49**, 1112–1122.

158. Klein, J. (2000) Smart polymer solutions. *Nature* **405**, 745–747.

159. Klionsky, D. J. (1997) Protein transport from the cytoplasm into the vacuole. *J. Membr. Biol.* **157**, 105–115.

160. Klionsky, D. J., Herman, P. K. & Emr, S. D. (1990) The fungal vacuole: composition, function, and biogenesis. *Microbiol. Rev.* **54**, 266–292.

161. Koga, H. (1994) Hypersensitive death, autofluorescence, and ultrastructural changes in cells of leaf sheaths of susceptible and resistant near-isogenic lines of rice (Pi–zt) in relation to penetration and growth of *Pyricularia oryzae*. *Can. J. Bot.* **72**, 1463–1477.

162. Kolattukudy, P. E. (1980) Cutin, suberin and waxes. In *The Biochemistry of Plants, (Vol. 4): Lipids: Structure and Function*, (Stumpf, P. K., ed.), pp. 571–645, Academic Press, New York.

163. Kolattukudy, P. E. & Köller, W. (1983) Fungal Penetration of the first line defensive barriers of plants. In *Biochemical Plant Pathology*, (Callow, J. A., ed.), pp. 79–114, John Wiley & Sons, New York.

164. Kolattukudy, P. E., Rogers, L. M., Li, D., Hwang, C-S. & Flaishman, M. A. (1995) Surface signalling in pathogenesis. *Proc. Natl. Acad. Sci. U. S. A.* **92**, 4080–4087.

165. Kunoh, H., Yamaoka, N., Yoshioka, H. & Nicholson, R. L. (1988) I. Contact-mediated changes in morphology of the conidium surface. *Exp. Mycol.* **12**, 325–335.

166. Kuo, K. & Hoch, H. C. (1995) Visualization of the extracellular matrix surrounding pycnidiospores, germlings, and appressoria of *Phyllosticta ampelicida*. *Mycologia* **87**, 759–771.

167. Kuo, K. & Hoch, H. C. (1996) Germination of *Phyllosticta ampelicida* pycnidiospores: prerequisite of adhesion to the substratum and the relationship of substratum wettability. *Fungal Genet. Biol.* **20**, 18–29.

168. Kwon, Y. H., Hoch, H. C., Staples, R. C. (1991) Cytoskeletal organisation in *Uromyces* urediospore germling apices during appressorium formation. *Protoplasma* **163**, 37–50.

169. Lacey, J. (1981) The aerobiology of conidial fungi. In *Biology of Conidial Fungi* (Vol. 1), (Cole, G. T. & Kendrick, B., eds), pp. 373–416, Academic Press, London.

170. Lange, L. & Olson, L. (1998) The fungal zoospore: its structure and biological significance. In *Zoosporic Plant Pathogens – A Modern Perspective*, (Buczacki, S. T., ed.), pp. 1–42, Academic Press, London.

171. Lee, Y-H. & Dean, R. A. (1993) cAMP regulates infection structure formation in the plant pathogenic fungus *Magnaporthe grisea*. *Plant Cell* **5**, 693–700.

172. Leung, H. & Shi, Z. (1994) Genetic regulation of sporulation in the rice blast fungus. In *Rice Blast Disease*, (Zeigler, R. S., Leong, S. A. & Teng, P. S., eds), pp. 35–50, CAB International with International Rice Research Institute, Oxon.

173. Leung, H. & Taga, M. (1988) *Magnaporthe grisea* (*Pyricularia* species) the blast fungus. *Adv. Plant Pathol.* **6**, 175–188.

174. Lingappa, B. T. & Sussman, A. S. (1959) Endogenous substrates of dormant, activated and germinating ascospores of *Neurospora tetrafirma*. *Plant Physiol.* **34**, 466–473.

175. Liu, S. & Dean, R. A. (1997) G protein ∝ subunit genes control growth, development, and pathogenicity of *Magnaporthe grisea*. *Mol. Plant-Microbe Interact.* **10**, 1075–1086.

176. Liu, Z. M. & Kolattukudy, P. E. (1999) Early expression of the calmodulin gene, which precedes appressorium formation in *Magnaporthe grisea*, is inhibited by self-inhibitors and requires surface attachment. *J. Bacteriol.* **181**, 3571–3577.

177. López-Franco, R. & Bracker, C. (1996) Diversity and dynamics of the Spitzenkörper in growing hyphal tips of higher fungi. *Protoplasma* **195**, 90–111.

178. Lovett, J. S. (1976) The regulation of protein metabolism during spore germination. In *The Fungal Spore: Form and Function*, (Weber, D. J. & Hess, W. M., eds), pp. 189–242, John Wiley, New York.

179. Macko, V. (1981) Inhibitors and stimulants of spore germination and infection structure formation in fungi. In *The Fungal Spore: Morphogenetic Controls*, (Turian, G. & Holh, H. R., eds), pp. 565–584, Academic Press, New York.

180. Maheshwari, R. (1999) Microconidia of *Neurospora crassa*. *Fungal Genet. Biol.* **26**, 1–18.

181. Maia, L. C., Kimbrough, J. W. & Benny, G. L. (1994) Ultrastructure of spore germination in *Gigaspora albida* (Glomales). *Mycologia* **86**, 343–349.

182. Markham, P. (1995) Organelles of filamentous fungi. In *The Growing Fungus* (Gow, N. A. R. & Gadd, G. M., eds), pp. 75–98, Chapman & Hall, London.

183. Markham, P., Robson, G. D., Bainbridge, B. W. & Trinci, A. P. J. (1993) Choline: its role in the growth of filamentous fungi and the regulation of mycelial morphology. *FEMS Microbiol. Rev.* **104**, 300.

184. Martin, M. & Gay, J. L. (1983) Ultrastructure of conidium development in *Erisyphe pisi*. *Can. J. Bot.* **61**, 2472–2495.

185. Maxwell, D. P., Armentrout, V. N. & Graves, J L B. (1977) Microbodies in plant pathogenic fungi. *Ann. Rev. Phytopathol.* **15**, 119–134.

186. McKeen, W. E., Mitchell, N. & Smith, R. (1967) The *Erisyphe cichoracearum* conidium. *Can. J. Bot.* **45**, 1489–1496.

187. McKerracher, L. J. & Heath, I. B. (1986a) Fungal nuclear behaviour analysed by ultraviolet microbeam irradiation. *Cell Motil. Cytoskeleton* **6**, 5–47.

188. McKerracher, L. J. & Heath, I. B. (1986b) Polarized cytoplasmic movement and inhibition of saltations induced by calcium mediated effects of microbeams in fungal hyphae. *Cell Motil. Cytoskeleton* **6**, 136–145.

189. McKerracher, L. J. & Heath, I. B. (1987) Cytoplasmic migration and intracellular organelle movements during tip growth of fungal hyphae. *Exp. Mycol.* **11**, 79–100.

190. Mellman, I. (1996) Endocytosis and molecular sorting. *Annu. Rev. Cell. Dev. Biol.* **12**, 575–625.

191. Mendgen, K., Bachmem, U., Stark–Urnau, M. & Xu, H. (1995) Secretion and endocytosis at the interface of plants and fungi. *Can. J. Bot.* **73**, S640–S648.

192. Mendgen, K. & Deising, H. (1993) Tansley Review No. 48: infection structures of fungal plant pathogens – a cytological and physiological evaluation. *New Phytol.* **124**, 193–213.

193. Mennucci, L., Rojas, S. & Camargo, E. P. (1975) Polyamines and orthinine decarboxylase activity during growth and differentiation in *Blastocladiella emersonii*. *Biochem. Biophys. Acta* **404**, 249–256.

194. Mercure, E. W., Leite, B. & Nicholson, R. L. (1994) Adhesion of ungerminated conidia of *Colletotrichum graminicola* to artificial hydrophobic surfaces. *Physiol. Mol. Plant Pathol.* **45**, 421–440.

195. Mims, C. W., Liljebjelke, K. A. & Richardson, E. A. (1995) Surface morphology, wall structure, and initial adhesion of conidia of the powdery mildew fungus *Uncinuliella australiana*. *Phytopathology* **85**, 352–358.

196. Mims, C. W., Roberson, R. W. & Richardson, E. A. (1988) Ultrastructure of freeze-substituted and chemically fixed basidiospores of *Gymnosporangium juniper-virginianae*. *Mycologia* **80**, 356–364.

197. Mims, C. W., Rogers, M. A. & Van Dyke, C. G. (1997) Ultrastructure of conidia and conidium germination in the plant pathogenic fungus *Alternaria cassiae*. *Can. J. Bot.* **75**, 252–260.

198. Mims, C. W. & Snetselaar, K. M. (1991) Teliospore maturation in the smut fungus *Sporisorium sorghi*; an ultrastructural study using freeze substitution fixation. *Bot. Gaz.* **152**, 1–7.

199. Mitchell, T. K. & Dean, R. A. (1995) The cAMP-dependent protein kinase catalytic subunit is required for appressorium formation and pathogenesis by the rice blast fungus *Magnaporthe grisea*. *Plant Cell* **7**, 1869–1878.

200. Mollicone, M. R. N. & Longcore, J. E. (1999) Zoospore ultrastructure of *Gonapodya polymorpha*. *Mycologia* **91**, 727–734.

201. Money, N. P. (1999) Fungus punches its way in. *Nature* **401**, 332–333.

202. Money, N. P. & Howard, R. J. (1996) Confirmation of a link between fungal pigmentation, turgor pressure, and pathogenicity using a new method of turgor measurement. *Fungal Genet. Biol.* **20**, 217–227.

203. Morré, D. J. (1990) Endomembrane system of plants and fungi. In *Tip Growth in Plant and Fungal Cells*, (Heath, I. B., ed.), pp. 183–210, Academic Press, London.

204. Moss, M. A. & Trevathan, L. E. (1987) Environmental conditions conducive to infection of rye grass by *Pyricularia grisea*. *Phytopathology* **77**, 863–866.

205. Mukherjee, S., Soe, T. T. & Maxfield, F. R. (1999) Endocytic sorting of lipid analogues differing solely in the chemistry of their hydrophobic tails. *J. Cell Sci.* **144**, 1271–1284.

206. Nicholson, R. L. & Epstein, L. (1991) Adhesion of fungi to the plant surface: prerequisite for pathogenesis. In *The Fungal Spore and Disease Initiation in Plants and Animals*, (Cole, G. T. & Hoch, H. C., eds), pp. 3–24, Plenum Press, New York.

207. Nicholson, R. L. & Moraes, W. B. C. (1980) Survival of *Colletotrichum graminicola*: importance of the spore matrix. *Phytopathology* **70**, 225–261.

208. Nicholson, R. L., Yoshioka, H., Yamaoka, N. & Kunoh, H. (1988) II. Release of esterase enzyme from conidia in response to a contact stimulus. *Exp. Mycol.* **12**, 336–349.

209. Nielsen, K. A., Nicholson, R. L., Carver, T. L. W., Kunoh, H. & Oliver, R. P. (2000) First touch: an immediate response to surface recognition in conidia of *Blumeria graminis*. *Physiol. Mol. Plant Pathol.* **56**, 63–70.

210. Oakley, B. R. & Rinehart, J. E. (1985) Mitochondria and nuclei move by different mechanisms in *Aspergillus nidulans*. *J. Cell Biol.* **101**, 2392–2397.

211. Oparka, K. J. & Read, N. D. (1994) The use of fluorescent probes for studies of living plant cells. In *Plant Cell Biology: A Practical Approach*. pp. 27–50, Oxford University Press, Oxford.

212. Orlovich, D. A. & Ashford, A. E. (1998) Structure, function, and motility of vacuoles in filamentous fungi. *Fungal. Genet. Biol.* **24**, 86–100.

213. Ou, S. H. (1980a) A look at worldwide rice blast disease control. *Plant Dis.* **64**, 439–445.

214. Ou, S. H. (1980b) Pathogen variability and host resistance in rice blast disease. *Ann. Rev. Phytopathol.* **18**, 167–187.

215. Ou, S. H. (1985) *Rice Diseases*. Commonwealth Mycological Institute, Kew.

216. Padmavati, M., Sakthivel, K. V., Thara, K. V. & Reddy, A. R. (1997) Differential sensitivity of rice pathogens to growth inhibition by flavanoids. *Phytochemistry* **46**, 499–502.

217. Parton, R. M., Fischer, S., Malhó, R., Papasouliotis, O., Jelitto, T. C., Leonard, T. & Read, N. D. (1997) Pronounced cytoplasmic gradients are not required for tip growth in plant and fungal cells. *J. Cell Sci.* **110**, 1187–1198.

218. Pascholati, S. F., Yoshioka, H., Kunoh, H. & Nicholson, R. L. (1992) Preparation of the infection court by *Erysiphe graminis* f. sp. *hordei*: cutinase is a component of the conidial exudate. *Physiol. Mol. Plant Pathol.* **41**, 53–59.

219. Peng, Y. L. & Shishiyama, J. (1988) Temporal sequence of cytological events in rice leaves infected with *Pyricularia oryzae*. *Can. J. Bot.* **66**, 730–735.

220. Perfect, S. E., Hughes, H. B., O'Connel, R. J., & Green, J. R. (1999) *Colletotrichum:* a model genus for studies on pathology and fungal-plant interactions. *Fungal Genet. Biol.* **27**, 186–198.

221. Philips, R. (1981) *Mushrooms and Other Fungi of Great Britain & Europe.* Pan Books, London.

222. Picton, J. M. & Steer, M. W. (1983) Membrane recycling and the control of secretory activity in pollen tubes. *J. Cell Sci.* **63**, 303–310.

223. Pitt, D., Barnes, J. C. & Weber, D. J. (1998) Teaching techniques for mycology. 4. Demonstration of Koch's postulates with *Phytophthora erythroseptica*. *Mycologist* **12**, 56–58.

224. Podila, G. K., Rogers, L. M. & Kolattukudy, P. E. (1993) Chemical signals from avocado surface wax trigger germination and appressorium formation in *Colletotrichum gloeosporioides*. *Plant Physiol.* **103**, 267–272.

225. Rajam, M. V. (1993) Polyamine biosynthesis inhibitors: new protectants against fungal plant disease. *Curr. Sci.* **65**, 683–692.

226. Ramsbottom, J. (1929) *Fungi: An Introduction to Mycology*. Ernest Benn Limited, London.

227. Rawlinson, C. J. (1979) Light leaf spot of oilseed rape: an appraisal with comments on strategies for control. In *Proceedings of the 1979 British Crop Protection Conference – Pests and Diseases*, pp. 137–143.

228. Read, N. D. (1994) Cellular nature and multicellular morphogenesis of higher fungi. In *Shape and Form in Plants and Fungi*, (Ingram, D. S. & Hudson, A., eds), pp. 251–270, Academic Press, London.

229. Read, N. D., Allan, W. T. G., Knight, H., Knight, M. R., Malhó, R., Russel, A., Shacklock, P. S. & Trewavas, A. J. (1992a) Imaging and measurement of cytosolic free calcium in plant and fungal cells. *J. Microsc.* **166**, 57–86.

230. Read, N. D. & Beckett, A. (1996) Ascus and ascospore morphogenesis. *Mycol. Res.* **100**, 1281–1314.

231. Read, N. D. & Hickey, P. C. (2000) The vesicle trafficking network and tip growth in fungal hyphae. In *Cell Biology of Plant and Fungal Tip Growth*, (Geitmarn, A., Cresti, M. & Heath, I. B., eds). IOS Press, Amsterdam.

232. Read, N. D., Kellock, L. J., Collins, T. J. & Gundlach, A. M. (1997) Role of topography sensing for infection–structure differentiation in cereal rust. *Planta* **202**, 163–170.

233. Read, N. D., Kellock, L. J., Knight, H. & Trewavas, A. J. (1992b) Contact sensing during infection by fungal pathogens. In *Perspectives in Plant Recognition*, (Callow, J. A. & Green, J. R., eds), pp. 137–172, Cambridge University Press, Cambridge.

234. Rees, B., Sheperd, V. A. & Ashford, A. E. (1994) Presence of a motile tubular vacuole system in different phyla of fungi. *Mycol. Res.* **98**, 985–992.

235. Rees, G. & Jones, E. B. G. (1984) Observations on the attachment of spores of marine fungi. *Bot. Mar.* **27**, 145–160.

236. Rieder, S. E., Banta, L. M., Kohrer, K. McCafferty, J. M. & Emr, S. D. (1996) Multilamellar endosome-like compartment accumulates in the yeast vps28 vacuolar protein sorting mutant. *Mol. Biol. Cell* **7**, 985–999.

237. Riggs, W. & Mims, C. W. (2000) Ultrastructure of chlamydospore development in the plant pathogenic fungus *Thielaviopsis basicola*. *Mycologia* **92**, 123–129.

238. Roberson, R. W. (1992) The actin cytoskeleton in hyphal cells of *Sclerotium rolfsii*. *Mycologia* **84**, 41–51.

239. Roberson, R. W. & Fuller, M. S. (1988) Ultrastructural aspects of the hyphal tip of *Sclerotium rolfsii* preserved by freeze substitution. *Protoplasma* **146**, 143–149.

240. Roberts, D. R. J., Mims, C. W. & Fuller, M. S. (1996) Ultrastructure of the ungerminated conidium of *Blumeria graminis* f. sp. *hordei*. *Can. J. Bot.* **74**, 231–237.

241. Roberts, S. K., Dixon, G. K., Dunbar, S. J. & Sanders, D. (1997) Laser ablation of the cell wall and localized patch clamping of the plasma membrane in the filamentous fungi *Aspergillus*: characterisation of an anion efflux channel. *New Phytol.* **137**, 579–585.

242. Ruiz–Herrera, J. & Calvo-Mendez, C. (1987) Effect of orthinine decarboxylase inhibitors on the germination of sporangiospores of *Mucorales*. *Exp. Mycol.* **11**, 287–296.

243. Sachs, M. S. & Yanofsky, C. (1991) Developmental expression of genes involved in conidiation and amino acid biosynthesis in *Neurospora crassa*. *Dev. Biol.* **148**, 117–128.

244. Sadasivan, T. S., Suryanarayanan, S. & Ramakrishnan, L. (1965) Influence of temperature in rice blast disease. In *The Rice Blast Disease: Proceedings of a Symposium at the International Rice Research Institute, July, 1963*. pp. 163–171. John Hopkins Press, Baltimore.

245. Satiat-Jeunemaitre, B., Cole, L., Mao, F. & Hawes, C. (1996) Brefeldin A effects in plant and fungal cells: something new about vesicle trafficking? *J. Microsc.* **181**, 162–177.

246. Schadeck, R. J. G., Buchi, D. F. & Leite, B. (1998) Ultrastructural aspects of *Colletotrichum graminicola* conidium germination, appressorium formation and penetration on cellophane membranes: focus on lipid reserves. *J. Submicrosc. Cytol. Path.* **30**, 555–561.

247. Schmit, J. C. & Brody, S. (1976) Biochemical genetics of *Neurospora crassa* conidial germination. *Bacteriol. Rev.* **40**, 1–41.

248. Seiler, S., Plamman, M. & Schliwa, M. (1999) Kinesin and dynein provide novel insights into the roles of vesicle traffic during cell morphogenesis in *Neurospora*. *Curr. Biol.* **9**, 779–785.

249. Shahjahan, A. K. M. (1994) Practical approaches to rice blast management in tropical Monsoon ecosystems, with special reference to Bangladesh. In *Rice*

Blast Disease, (Zeigler, R. S., Leong, S. A. & Teng, P. S., eds), pp. 465–488, CAB International with International Rice Research Institute, Oxon.

250. Shaw, B. D. & Hoch, H. C. (1999) The pycnidiospore of *Phyllosticta ampelicida*: surface properties involved in substratum attachment and germination. *Mycol. Res.* **103**, 915–924.

251. Shaw, B. D., Kuo, K. & Hoch, H. C. (1998) Germination and appressorium development of *Phyllosticta ampelicida* pycnidiospores. *Mycologia* **90**, 258–268.

252. Shen, W. C., Bobrowicz, P. & Ebbole, D. J. (1999) Isolation of pheromone precursor genes of *Magnaporthe* genes. *Fungal Genet. Biol.* **27**, 253–263.

253. Shepherd, V. A., Orlovich, D. A. & Ashford, A. E. (1989) A dynamic continuum of dynamic pleiomorphic tubules and vacuoles in growing hyphae of a fungus. *J. Cell Sci.* **104**, 495–507.

254. Shepherd, V. A., Orlovich, D. A. & Ashford, A. E. (1993) Cell-to-cell transport via motile tubules in growing hyphae of a fungus. *J. Cell Sci.* **105**, 1173–1178.

255. Sheppard, C. R. J. and Shotton, D. M. (1997) *Confocal Laser Scanning Microscopy*. BIOS Scientific Publishers, Oxford.

256. Shull, V. & Hamer, J. E. (1994) Genomic structure and variability in *Pyricularia grisea*. In *Rice Blast Disease*, (Zeigler, R. S., Leong, S. A. & Teng, P. S., eds), pp. 65–86, CAB International with International Rice Research Institute, Oxon.

257. Smart, M. G. (1991) Plant cell wall as a barrier to fungal invasion. In *The Fungal Spore and Disease Initiation in Plants and Animals*, (Cole, G. T., ed.), pp. 47–66, Plenum Press, New York.

258. Smith, C. W. (1995) *Crop Production, Evolution, and Technology*. John Wiley & Sons, New York.

259. Smith, H. (1999) More than just a surface thing: rice infection by *Magnaporthe grisea*. *Plant Cell* **11**, 1815–1817.

260. Smith, J. E. & Berry, D. R. (1974) The fungal spore. In *Introduction to Biochemistry of Fungal Development*, pp. 80–105. Academic Press, London.

261. Sokal, R. R. & Rohlf, F. J. (1987) *Introduction to Biostatistics*. W. H. Freeman and Company, New York.

262. Som, T. & Kolaparthi, S. R. (1994) Developmental decisions in *Aspergillus nidulans* are modulated by ras activity. *Mol. Cell Biol.* **14**, 5333–5348.

263. Steer, M. W. (1988) Plasma membrane turnover in plants. *J. Exp. Bot.* **39**, 987–996.

264. Steinberg, G. (1998) Organelle transport and molecular motors in fungi. *Fungal Genet. Biol.* **24**, 161–177.

265. Steinberg, G. (2000) The cellular roles of molecular motors in fungi. *Trends Microbiol.* **8**, 162–168.

266. Steinberg, G., Schliwa, M., Lehmler, C., Bölker, M., Kahmann, R. & McIntosh, J. R. (1998) Kinesin from the plant pathogenic fungus *Ustilago maydis* in vacuole formation and cytoplasmic migration. *J. Plant Sci.* **111**, 2235–2246.

267. Stevens, L., McKinnon, I. M. & Winther, M. D. (1976) Polyamine and orthinine metabolism during the germination of conidia of *Aspergillus nidulans*. *J. Biochem.* **158**, 235–241.

268. Stryer, L. (1988) *Biochemistry*. W. H. Freeman & Company, New York

269. Subramanian, C. V. (1968) *Pyricularia oryzae*. In: *C. M. I. Descriptions of Pathogenic Fungi and Bacteria*. No. 169, The Eastern Press, London.

270. Suelmann R., Sievers N. & Fischer R. (1997) Nuclear traffic in fungal hyphae: *in vivo* study of nuclear migration and positioning in *Aspergillus nidulans*. *Mol. Microbiol.* **25**, 757–769.

271. Sundberg, W. J. (1978) Hymenial cytodifferentiation in basidiomycetes. In *The Filamentous Fungi, Dev. Biol.*, (Vol 3), (Smith, J E. & Berry, D R., eds), pp. 298–314, Arnold, London.

272. Sussman, A. S. (1981) Environmental controls: ecological aspects. Discussant's introduction. In *The Fungal Spore*. (Turian, G. & Hoch, H C., eds), pp. 377–384, Academic Press, London.

273. Sweigard, J. A., Chumley, F. G. & Valent, B. (1992a) Cloning and analysis of CUT1, a cutinase gene from *Magnaporthe grisea*. *Mol. Gen. Genet.* **232**, 174–182.

274. Sweigard, J. A., Chumley, F. G. & Valent, B. (1992b) Disruption of a *Magnaporthe grisea* cutinase gene. *Mol. Gen. Genet.* **232**, 183–190.

275. Tabor, C. W. & Tabor, H. (1985) Polyamines in microorganisms. *Microbiol. Rev.* **49**, 81–99.

276. Talbot, N. J. (1995) Having a blast: exploring the pathogenicity of *Magnaporthe grisea*. *Trends Microbiol.* **10**, 9–16.

277. Talbot, N. J., Ebbole, D. J. & Hamer, J. E. (1993) Identification and characterization of MPG1, a gene involved in pathogenicity from the rice blast fungus *Magnaporthe grisea*. *Plant Cell* **5**, 1575–1590.

278. Talbot, N. J., Kershaw, M. J., Wakely, G. E., de Vries, O. H. M., Wessels, J. G. H. & Hamer, J. E. (1996) MPG1 encodes a fungal hydrophobin involved in surface interactions during infection–related development by *Magnaporthe grisea*. *Plant Cell* **8**, 985–999.

279. Taylor, A. R. & Brownlee, C. (1992) Localized patch clamping of plasma membrane of a polarized plant cell. *Plant Physiol.* **99**, 1686–1688.

280. Taylor, A. R., Manison, N., Fernandez, C., Wood, J. & Brownlee, C. (1996) Spatial organisation of calcium signalling involving in cell wall volume control in the *Fucus* rhizoid. *Plant Cell* **8**, 2015–2031.

281. Teng. P. S. (1994) Epidemiological basis for blast management. In *The Rice Blast Disease*, (Zeigler, R. S., Leong, S. A. & Teng, P. S., eds), pp. 409–434, CAB International in association with The International Rice Research Institute, Oxon.

282. Terhune, B. T. & Hoch, H. C. (1993) Substrate hydrophobicity and adhesion of *Uromyces* urediospores and germlings. *Exp. Mycol.* **17**, 241–252.

283. Thevelein, J. M. (1988) Regulation of trehalose activity by phosphorylation–dephosphorylation during developmental transitions in fungi. *Exp. Mycol.* **12**, 1–12.

284. Thines, E. Weber, R. W. S. & Talbot, N. J. (2000) MAP kinase and protein kinase A-dependent mobilization of triacylglycerol and glycogen during appressorium turgor generation by *Magnaporthe grisea*. *Plant Cell* **12**, 1703–1718.

285. Torralba, S., Raudaskoski, M., Pedregosa, A. M. & Laborda, F. (1998) Effects of cytochalasin A on apical growth, actin cytoskeleton organization and enzyme secretion in *Aspergillus nidulans*. *Microbiology* **144**, 45–53.

286. Tsao, P. W. & Tsao, P. H. (1970) Electron microscopic observations on the spore wall and 'operculum' formation in chlamydospores of *Thielaviopsis basicola*. *Phytopathology* **60**, 613–616.

287. Uchiyama, T., Ogasawara, N., Nanba, Y. & Itô, H. (1979) Conidial germination and appressorial formation of the plant pathogenic fungi on the cover-glass or cellophane coated with various lipid components of plant leaf waxes. *Agric. Biol. Chem.* **43**, 383–384.

288. Uchiyama, T. & Okuyama, K. (1990) Participation of *Oryzae* leaf wax in appressorium formation by *Pyricularia oryzae*. *Phytochemistry* **29**, 91–92.

289. Valent, B. (1990) Rice blast as a model system for plant pathology. *Phytopathology* **80**, 33–36.

290. Valent, B. & Chumley, F. G. (1991) Molecular genetic analysis of the rice blast fungus, *Magnaporthe grisea*. *Ann. Rev. Phytopathol.* **29**, 443–467.

291. Valent, B., Farral, L. & Chumley, F. G. (1991) *Magnaporthe grisea* genes for pathogenicity and virulence identified through a series of backcrosses. *Genetics* **127**, 87–101.

292. Van Dyke, G. C. & Mims, C. W. (1991) Ultrastructure of conidia germination, and appressorium development in the plant pathogenic fungus *Colletotrichum truncatum*. *Can. J. Bot.* **69**, 2455–2467.

293. Van Laere, A. J. (1995) Intermediary metabolism. In *The Growing Fungus*, (Gow, N A. R. & Gadd, G M., eds), pp. 211–238, Chapman & Hall, London.

294. Van Laere, A. J., Van Assche, J. A. & Fursch, B. (1987) The sporangiospore: dormancy and germination. In *The Phycomyces*, (Cerdá-Olmedo, E. & Lipson, E. D., eds), pp. 247–279, Cold Spring Harbour Laboratory: CSH.

295. Vida, T. A. & Emr, S. D. (1995) A new vital stain for visualizing vacuolar membrane dynamics and endocytosis in yeast. *J. Cell. Biol.* **128**, 779–792.

296. Wada, Y. & Anraku, Y. (1992) Genes for directing vacuolar morphogenesis in *Saccharomyces cerevisiae*: II. VAM7, a gene for regulating morphogenic assembly of the vacuoles. *J. Biol. Chem.* **267**, 18671–18675.

297. Wada, Y., Ohsumi, Y. & Anruka, Y. (1992) Genes for directing vacuolar morphogenesis in *Saccharomyces cerevisiae*: I. isolation and characterization of two classes of vam mutants. *J. Biol. Chem.* **267**, 18665–18670.

298. Warwar, V. & Dickman, M. B. (1996) Effects of calcium and calmodulin on spore germination and appressorium development in *Colletotrichum trifolii*. *Appl. Environ. Microbiol.* **62**, 74–79.

299. Watanabe, K., Parberry, D. G., Kobayashi, T. & Doi, Y. (2000) Conidial adhesion and germination of *Pestalotiopsis*. *Mycol. Res.* **104**, 962–968.

300. Watts, C. & Marsh, M. (1992) Endocytosis: what goes in and how? *J. Cell Biol.* **103**, 1–8.

301. Weber, R. W. S., Wakely, G. E. & Pitt, D. (1998) Histochemical and ultrastructural characterization of fungal mitochondria. *Mycologist* **12**, 174–179.

302. Webster, J. & Davey, R. A. (1984) Sigmoidal conidial shape in aquatic fungi. *Trans. Br. Mycol. Soc.* **83**, 43–52.

303. Wedlich-Sölder, R., Kahmann, R. & Steinberg, G. (2000) A putative endosomal t-SNARE links exo- and endocytosis in the phytopathogenic fungus *Ustilago maydis*. *EMBO J.* **19**, 1974–1986.

304. Weete, J. D. (1981) Lipids in fungal growth and reproduction. In *The Fungal Spore: Morphogenetic Controls*, (Turian, G. & Hohl, H. R., eds), pp. 463–485, Academic press, London.

305. Weintraub, R. L., Miller, W. E. & Schantz, E. J. (1958) Chemical stimulation of germination of spores of *Pyricularia oryzae*. *Phytopathology* **48**, 7–10.

306. Weisman, L. S., Bacallo, R. & Wickner, W. (1987) Multiple methods of visualising the yeast vacuole permit evaluation of its morphology and inheritance during the cell cycle. *J. Cell Biol.* **105**, 1539–1547.

307. Weisman, L. S. & Wickner, W. (1988) Intervacuole exchange in the yeast zygote: a new pathway in organelle communication. *Science* **241**, 589–591.

308. Wessels, J. G. H. (1986) Cell wall synthesis in apical hyphal growth. *Int. Rev. Cytol.* **104**, 387–413.

309. Wessels, J. G. H. (1996) Fungal hydrophobins: proteins that function at an interface. *Trends Plant Sci.* **1**, 9–15.

310. Wessels, J. G. H. (1997) Hydrophobins: proteins that change the nature of the fungal surface. In *Advances in Microbial Physiology* (vol. 38), (Poole, R. K., ed.), pp. 1–45. Academic Press, London.

311. Wheeler, M. H. & Bell, A. A. (1988) Melanins and their importance in pathogenic fungi. *Curr. Top. Med. Microbiol.* **2**, 338–387.

312. Wheeler, M. H. & Greenblatt, G. A. (1988) The inhibition of melanin biosynthetic reactions in *Pyricularia oryzae* by compounds that prevent rice blast disease. *Exp. Mycol.* **12**, 151–160.

313. Wilson, T. P., Canny, M. J. & Lefcovitch, L. P. (1990) Breakdown of cytoplasmic vacuoles: a model of endomembrane rearrangement. *Protoplasma* **155**, 144–152.

314. Woloshuk, C. P., Sisler, H. D., Tokousbalides, M. C. & Dukty, S. R. (1980) Melanin biosynthesis in *Pyricularia oryzae*: site of tricyclazole inhibition and pathogenicity of melanin-deficient mutants. *Pestic. Biochem. Physiol.* **14**, 256–264.

315. Woloshuk, C. P., Wolkow, P. M. & Sisler, H. D. (1981) The effect of three fungicides, specific for the control of rice blast disease, on the growth and melanin biosynthesis of *Pyricularia oryzae* Cav. *Pestic. Sci.* **12**, 86–90.

316. Wu, Q., Sandrock, T. M., Turgeon, B. G., Yoder, O. C., Wirsel, S. G. & Aist, J. R. (1998) A fungal kinesin required for organelle motility, hyphal growth, and morphogenesis. *Mol. Biol. Cell* **9**, 89–101.

317. Wynn, W. K. & Staples, R. C. (1981) Tropisms of fungi in host recognition. In *Plant Disease Control: Resistance and Susceptibilty*, (Staples, R. C. & Toenniessen, G. H., eds), pp. 45–69, Wiley Interscience, New York.

318. Xiao, J., Ohshima, A., Kamakura, T., Ishiyama, T. & Yamaguchi, I. (1994a) Extracellular glycoprotein(s) associated with cellular differentiation in *Magnaporthe grisea*. *Mol. Plant-Microbe Interact.* **7**, 639–644.

319. Xiao, J., Watanabe, T., Kamakura, T., Ohshima, A. & Yamaguchi, I. (1994b) Studies on cellular differentiation of *Magnaporthe grisea*. Physicochemical

aspects of substratum surfaces in relation to appressorium formation. *Physiol. Mol. Plant Pathol.* **44**, 227–236.

320. Xu, J. R. & Hamer, J. E. (1996) MAP-kinase and cAMP signalling regulate infection structure formation and pathogenic growth in the rice blast fungus, *Magnaporthe grisea*. *Genes Dev.* **10**, 2696–2706.

321. Xu, J. R., Urban, M., Sweigard, J. A. & Hamer, J. E. (1997) The CPKA gene of *Magnaporthe grisea* is essential for appressorium penetration. *Mol. Plant-Microbe Interact.* **10**, 187–194.

322. Yang, Z. & Dickman, M. B. (1999) *Colletotrichum trifolii* mutants disrupted in the catalytic subunit of cAMP-dependent protein kinase are nonpathogenic. *Mol. Plant-Microbe Interact.* **12**, 430–439.

323. Zhu, Y., Chen, H., Fan, J., Wang, Y., Li, Y., Chen, J., Fan, J., Yang, S., Hu, L., Leung, H., Mew, T. W., Teng, P. S., Wang, Z. & Mundt, C. C. (2000) Genetic diversity and disease control in rice. *Nature* **406**, 718–722.

324. Ziman, M., Chuang, J. S. & Schekman, R. W. (1996) Two proteins involved in chitin synthesis populate a compartment of the *Saccharomyces cerevisiae* endocytic pathway. *Mol. Biol. Cell* **7**, 1909–1919.

325. Ziman, M., Chuang, J. S., Tsung, M., Hamamoto, S. & Schekman, R. W. (1998) Chs6p–dependent anterograde transport from the chitosome to the plasma membrane in *Saccharomyces cerevisiae*. *Mol. Biol. Cell* **9**, 1565–1576.

Journal of Microscopy, Vol. 198, Pt 3, June 2000, pp. 246–259.
Received 7 January 2000; accepted 3 March 2000

Confocal microscopy of FM4-64 as a tool for analysing endocytosis and vesicle trafficking in living fungal hyphae

S. FISCHER-PARTON, R. M. PARTON, P. C. HICKEY, J. DIJKSTERHUIS, H. A. ATKINSON & N. D. READ

Institute of Cell and Molecular Biology, University of Edinburgh, Rutherford Building, Edinburgh EH9 3JH, U.K.

Key words. Confocal microscopy, endocytosis, FM1-43, FM4-64, fungal hyphae, Spitzenkörper, tip growth, TMA-DPH, vesicle trafficking.

Summary

Confocal microscopy of amphiphilic styryl dyes has been used to investigate endocytosis and vesicle trafficking in living fungal hyphae. Hyphae were treated with FM4-64, FM1-43 or TMA-DPH, three of the most commonly used membrane-selective dyes reported as markers of endocytosis. All three dyes were rapidly internalized within hyphae. FM4-64 was found best for imaging the dynamic changes in size, morphology and position of the apical vesicle cluster within growing hyphal tips because of its staining pattern, greater photostability and low cytotoxicity. FM4-64 was taken up into both the apical and subapical compartments of living hyphae in a time-dependent manner. The pattern of stain distribution was broadly similar in a range of fungal species tested (*Aspergillus nidulans, Botrytis cinerea, Magnaporthe grisea, Neurospora crassa, Phycomyces blakesleeanus, Puccinia graminis, Rhizoctonia solani, Sclerotinia sclerotiorum* and *Trichoderma viride*). With time, FM4-64 was internalized from the plasma membrane appearing in structures corresponding to putative endosomes, the apical vesicle cluster, the vacuolar membrane and mitochondria. These observations are consistent with dye internalization by endocytosis. A speculative model of the vesicle trafficking network within growing hyphae is presented.

Introduction

Vesicle trafficking is fundamental to numerous activities in eukaryotic organisms, and underlies many of the basic processes involved in cell growth and differentiation. The vesicle trafficking network includes exocytosis and endocytosis (Gruenberg & Clague, 1992; Rothman, 1994). In filamentous fungi a reasonable amount is understood about exocytosis, whereas very little is known about endocytosis.

Correspondence to: Nick Read. Tel: +44 (0)131 650 5335; fax: +44 (0)131 650 5392; e-mail: nick.read@ed.ac.uk

Most of our current understanding of vesicle trafficking in filamentous fungi is concerned with tip growth and is based upon ultrastructural studies (e.g. Grove & Bracker, 1970; Howard, 1981), pharmacological treatments (e.g. Howard & Aist, 1980), analyses of mutants (Wu *et al.*, 1998; Seiler *et al.*, 1999) and mathematical modelling of vesicle trafficking in relation to tip growth (e.g. Bartnicki-Garcia *et al.*, 1989). During tip growth, extension of the hypha is confined to a region occupying only a few micrometres at the hyphal apex and involves highly polarized exocytosis. Secretory vesicles deliver membrane, cell wall precursors and wall-building enzymes to the hyphal tip, and many extracellular enzymes released into the surrounding medium are also believed to be secreted from this region (reviewed by Wessels, 1993).

In higher fungi (i.e. members of the Ascomycota, Basidiomycota and Deuteromycota) vesicle trafficking to the apex during tip growth is highly organized and involves the activity of a specific, multicomponent organelle complex which, in most cases, is called the Spitzenkörper (= 'apical body'). This structure is predominated by secretory vesicles which make up what is commonly described as an 'apical vesicle cluster' (Grove & Bracker, 1970; López-Franco & Bracker, 1996). The dynamic behaviour of the Spitzenkörper has indicated that it is intimately associated with the precise growth pattern of the hyphal apex (Girbardt, 1957; Bartnicki-Garcia *et al.*, 1995; López-Franco & Bracker, 1996).

From studies of tip-growing plant cells (Steer & Steer, 1989; Miller *et al.*, 1997) it has been suggested that membrane recycling via endocytosis is a critical part of the process of apical extension. However, reports of the existence of endocytosis in filamentous fungi have been conflicting. Work by Caesar-Ton That *et al.* (1987) identified a fraction from hyphae of *Neurospora crassa* that was rich in coated vesicles and possessed a major polypeptide with a molecular weight similar to that of the heavy chain of

clathrin, the major coat protein of endocytic vesicles in animal and plant cells (Hawes *et al.*, 1995; Mellman, 1996). However, convincing ultrastructural evidence for clathrin-coated vesicles or pits in fungal hyphae is lacking. Evidence against the occurrence of endocytosis in filamentous fungi was obtained by Cole *et al.* (1997), who were unable to observe uptake of membrane-impermeant fluorescent probes by fluid-phase endocytosis into hyphae of the basidiomycete *Pisolithus tinctorius*. Recently, uptake of the membrane-selective endocytosis marker FM4-64 by germ tubes of *Uromyces fabae* (Hoffmann & Mendgen, 1998) and hyphae of *N. crassa* and *Trichoderma viride* (Read *et al.*, 1998) has been taken as positive evidence for membrane internalization by endocytosis.

Amphiphilic styryl dyes, such as FM4-64, insert into the outer leaflet of the plasma membrane and are believed not to directly enter intact cells by unfacilitated diffusion (Illinger & Kuhry, 1994; Betz *et al.*, 1996). They have, therefore, been widely used as fluorescent reporters of endocytosis and other components of the vesicle trafficking network in animal cells (e.g. Betz *et al.*, 1996) and the budding yeast (Vida & Emr, 1995; Rieder *et al.*, 1996).

In this paper we have used confocal imaging of amphiphilic styryl dyes to study endocytosis and vesicle trafficking in living fungal hyphae. Although we tested three of these dyes (FM4-64, FM1-43 and TMA-DPH), most of our work has concentrated on FM4-64 because of its superior properties. Time courses of FM4-64 staining have been performed and considerable emphasis placed on imaging the stained apical vesicle cluster within growing hyphal tips. Possible pathways of dye internalization and distribution have been assessed. However, our analysis supports the view that endocytosis and vesicle trafficking are probably the predominant pathways by which FM4-64 is internalized and distributed between organelles within hyphae. Based on the interpretation of our results in the context of current knowledge in other cell types, we present a speculative model of the vesicle trafficking network within growing hyphae.

Materials and methods

Dyes and other chemicals

The dyes FM4-64, FM1-43 and TMA-DPH were obtained from Molecular Probes Inc. (Eugene, OR, U.S.A.). All other chemicals were supplied by Sigma (Poole, U.K.).

Fungal material

The following fungi were used: *Aspergillus nidulans* (R153 from Fungal Genetics Stock Center [FGSC], Arcata, CA, U.S.A.); *Botrytis cinerea* (from the Plant Disease Control Group, DuPont Co., Wilmington, DE, U.S.A.); *Magnaporthe grisea* (strain 0-42 from B. Valent, DuPont Co.); *Neurospora crassa* 74 A (strain 262 from FGSC); *Phycomyces blakesleeanus* (isolated from soil by P. Hickey, Edinburgh, U.K.); *Puccinia graminis* f. sp. *tritici* (isolate 84 from the National Institute for Agricultural Botany, Cambridge, U.K.); *Rhizoctonia solani* (No. 283 from E. E. Butler, University of California, Davis, U.S.A.); *Sclerotinia sclerotiorum* (from T. S. Abney, Purdue University, IN, U.S.A.); and *Trichoderma viride* (No. 2011 from J.F. Tuite, Purdue University).

Growth conditions and dye loading

Aspergillus nidulans, *B. cinerea* and *P. blakesleeanus* were grown on 2% w/v malt extract solidified with 2% w/v agar. Twenty-four-hour-old cultures of *P. blakesleeanus* and 48-h-old cultures of *A. nidulans* and *B. cinerea* were used for experiments. Agar bearing the leading edge of the colony was cut out and carefully placed, hypha side down, in liquid malt extract medium containing 25 μM FM4-64 on a glass coverslip.

Magnaporthe grisea was grown on oatmeal agar at 24 °C in continuous light (as described in Jelitto *et al.*, 1994). Conidia were harvested from 10-day-old cultures, inoculated onto glass coverslips in distilled water and incubated in darkened humid chambers. The resultant germlings were stained with 7.5 μM FM4-64.

Neurospora crassa, *R. solani*, *S. sclerotiorum* and *T. viride* were grown on Vogel's medium N (Vogel, 1956) plus 2% w/v sucrose (VMS medium) and prepared for microscopic observation on coverslips, as described by Parton *et al.* (1997). After 10 min of loading with 6.4 μM FM4-64, the medium containing dye was replaced with fresh medium lacking dye. *Neurospora* hyphae were similarly stained with 6.4 μM FM1-43 or 10 μM TMA-DPH. Additionally, *N. crassa* was grown on a thin layer of VMS medium solidified with 2% w/v agarose evenly spread on a glass coverslip (Parton *et al.*, 1997). Shortly before imaging, the mycelium was covered with 100 μL liquid VMS medium containing 6.4 μM FM4-64. For double staining of *N. crassa* hyphae with Rhodamine 123 and FM4-64, the stains were added sequentially. Firstly, 10 μM Rhodamine 123 was applied in 100 μL liquid VMS medium for at least 30 min then a further 100 μL medium containing 6.4 μm FM 4-64 was added.

Puccinia graminis urediospores (obtained from uredia on wheat as described by Read *et al.*, 1997) were inoculated onto glass coverslips and subsequently incubated in a humid chamber for 3–5 h to allow germ tubes to form. Germlings were loaded with dye by placing 20 mM HEPES-buffer (pH 7.2) containing 3.2 μM FM4-64 over them, followed by a coverslip supported by strips of lithographer's tape (No. 616, Scotch Brand).

For time course experiments, osmotic shock during dye

application was avoided by acclimatizing hyphae to standard liquid medium before experimentation.

Confocal microscopy

For routine confocal microscopy we employed a Bio-Rad MRC 600 confocal laser scanning microscope fitted with a 25 mW argon laser and connected to a Nikon Diaphot TMD inverted microscope with epifluorescence equipment (all supplied by Bio-Rad Microscience, Hemel Hempstead, U.K.). The laser power used was 1 or 3% of full intensity. Excitation was at 514 nm, and fluorescence was detected at >550 nm. Simultaneous confocal fluorescence images and corresponding brightfield images were collected. A $\times 40$ dry plan apo (NA 0.95) and a $\times 60$ oil immersion plan apo (NA 1.4) objective were used.

UV confocal microscopy of TMA-DPH was performed using a Leica TCS NT confocal microscope (Leica Microsystems Heidelberg GmbH, Germany) fitted with a 2 W UV argon laser. The Leica system was also equipped with a 100 mW argon ion laser, which allowed simultaneous imaging of Rhodamine 123 and FM4-64 without 'bleed through' of signal between the two channels used (488 nm excitation; Rhodamine 123 fluorescence detected at 530/30 nm, FM4-64 fluorescence detected at >640 nm). A $\times 63$ water immersion plan apo (NA 1.2) objective was used.

Results

Application and imaging styryl dyes in hyphae

Amongst the most commonly used fluorescent dyes for imaging endocytosis in living cells are the styryl-based dyes FM4-64, FM1-43 and TMA-DPH (Figs 1A, 2A and 3A, Illinger & Kuhry, 1994; Betz *et al.*, 1996; Haugland, 1996). These compounds were tested in *N. crassa*. All three dyes were found to be taken up by both apical and subapical hyphal compartments in a time-dependent manner: immediate staining of the plasma membrane was followed by dye internalization and staining of organelles. All dyes stained the apical vesicle cluster within the Spitzenkörper (Figs 1B, 2B and 3B), although considerable differences were observed in the patterns of organelle staining and in the photosensitivity and phototoxicity of each dye.

The staining pattern with each dye was examined over the apical 50 μm of hyphae, 40 min after dye application (Figs 1B, 2B and 3B). At that time FM4-64 had clearly stained the plasma membrane and Spitzenkörper region, with a more diffuse background staining of the cytoplasm. Staining of organelles was also evident but not marked. There was little staining of mitochondria (Fig. 1B). In addition, FM4-64 caused little disturbance to apical extension, even with repeated laser scanning at 15 s intervals over periods of 10 min when imaged with a $\times 40$ dry plan apo (NA 0.95) objective. The extension rate of dye-loaded hyphae imaged in this way was 16.7 ± 1.1 μm min^{-1} (SE) ($n = 11$), whilst the extension rate of control hyphae lacking dye was 17.2 ± 0.3 μm min^{-1} (SE) ($n = 10$). FM1-43 staining of the Spitzenkörper was similar except that it photobleached much more rapidly, making it more difficult to follow with time. In addition, the elongated mitochondria were more intensely stained with FM1-43 (cf. Figs 2B and 1B) unless the period of FM4-64 staining was significantly extended (Fig. 4). As with FM4-64, little significant effect on growth was observed (data not shown). TMA-DPH stained the plasma membrane and Spitzenkörper but the latter was less clearly stained than with FM4-64 (cf. Figs 3B and 1B). The cytoplasm was diffusely stained with TMA-DPH but pronounced staining of organelles was lacking (Fig. 3B). Repeated scanning with the UV laser led to drastic photobleaching of TMA-DPH and cessation of apical extension within three or four scans. These limitations render TMA-DPH useless for the type of prolonged examination required to image the dynamic behaviour of the Spitzenkörper or other aspects of vesicle trafficking.

Characteristics of FM4-64 internalization

Examination of early dye uptake within hyphal tips revealed that after immediate plasma membrane staining, signs of internalized dye could first be discerned as early as 30 s following dye application, and more clearly after 60 s (Fig. 5). Initial dye internalization was observed by contrast adjusting images and could be seen as a slight staining of the apical cytoplasm, most obviously in a 10–15 μm long region commonly 8–10 μm from the apical pole. Discrete, roughly spherical fluorescent organelles, ~ 0.75 μm in diameter, which corresponded in size and in their time of appearance to the putative endosomes visualized by FM4-64 staining in budding yeast cells (Vida & Emr, 1995), were first discernible 110 s after dye application. These organelles tended to be more numerous or obvious in a particular region behind the extreme tip although the precise distance of this zone from the apical pole varied between hyphae (data not shown). Spitzenkörper staining was first evident after 180 s (Fig. 5). Subsequently, the Spitzenkörper region and the small, roughly spherical organelles became brighter whilst numerous other small organelles also became stained. In hyphae stained for longer than $\sim$ 15 min, numerous roughly circular regions of dye exclusion, $\sim$2–3 μm in diameter, could be seen up to within $\sim$20 μm of the tip (Figs 1B and 4). These regions of dye exclusion correspond to the size and location of nuclei (Zalokar, 1959). Staining of nuclear membranes was never observed.

The subapical compartments we investigated after staining with FM4-64 were within the peripheral growth zone of the mycelium (i.e. the mycelial region needed to maintain the maximum extension rate of the colony's leading hyphae) and possessed unplugged septa. These hyphal

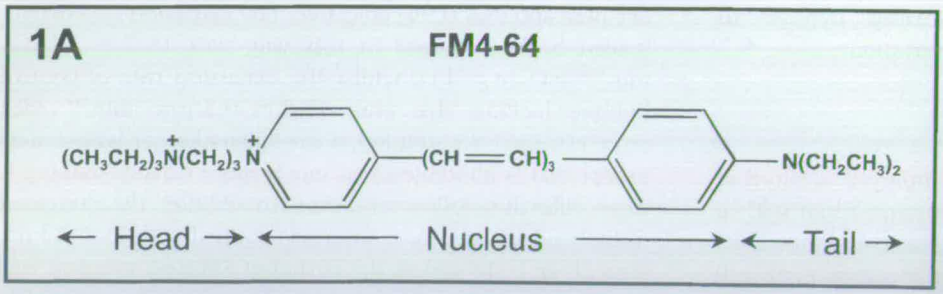

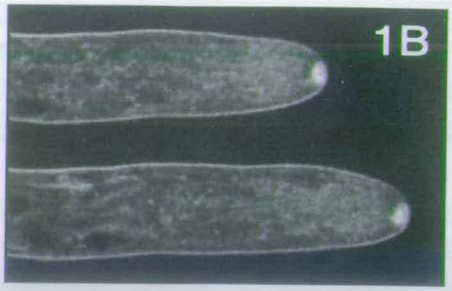

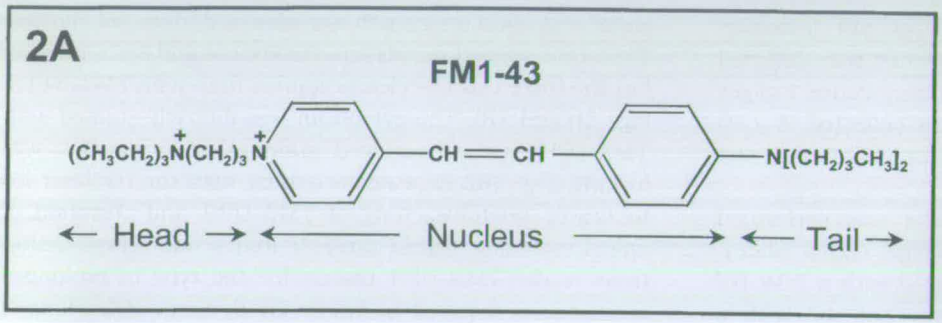

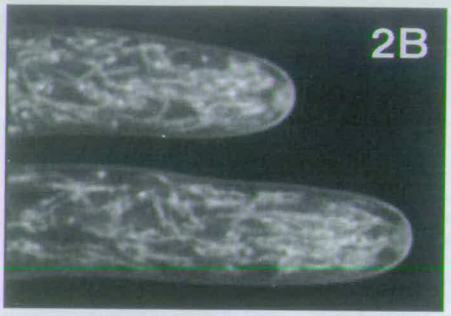

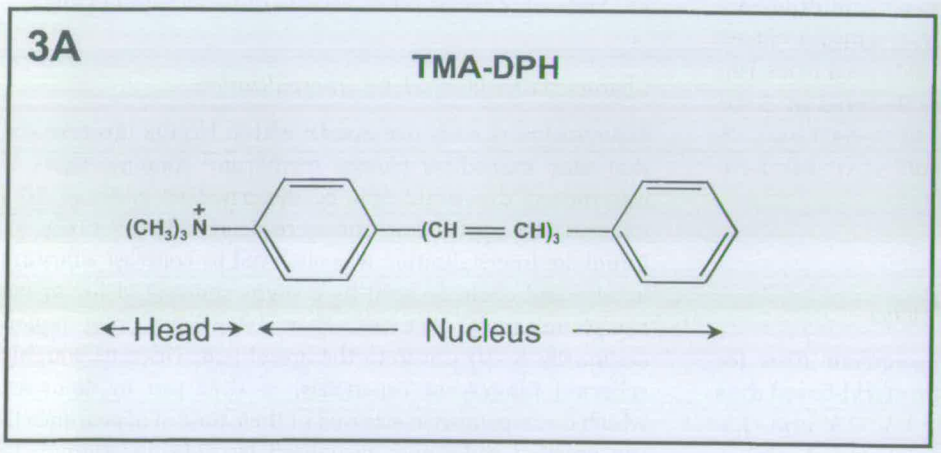

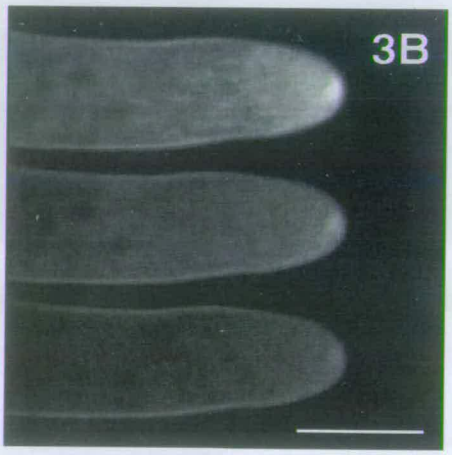

Fig. 1. (A) Molecular structure of endocytosis marker dye FM4-64. (B) Confocal image of growing hyphal tip of *Neurospora crassa* stained for 40 min with FM4-64; images 30 s apart; hyphal extension rate = 12.0 μm min^{-1}.

Fig. 2. (A) Molecular structure of endocytosis marker dye FM1-43. (B) Confocal image of growing hyphal tip of *Neurospora crassa* stained for 40 min with FM1-43; images 30 s apart; hyphal extension rate = 15.3 μm min^{-1}.

Fig. 3. (A) Molecular structure of endocytosis marker dye TMA-DPH. (B) Confocal image of growing hyphal tip of *Neurospora crassa* stained for 40 min with TMA-DPH; images 1 s apart; growth rate not determined.

Note the staining of elongated mitochondria in Fig. 2(B) but not in Figs 1(B) and 3(B). Bar = 10 μm.

compartments are metabolically very active and contribute to tip growth by the vectorial transport of cytoplasm and organelles towards growing hyphal apices (Trinci, 1971). In these compartments (Fig. 6) the immediate staining of the plasma membrane after dye application was followed within 1–2 min by the appearance of faintly stained roughly spherical organelles, ~0.75 μm in diameter, which were similar in appearance to the previously described organelles in the apical hyphal compartments. These organelles were distinct from the similarly sized, more-or-less spherical mitochondria found in subapical regions. This was shown by double staining with FM4-64 and the mitochondrion-selective stain, Rhodamine 123, which did not colocalize (Fig. 7). With time, FM4-64 staining increased in the small spherical organelles which were not mitochondria, and also in the surrounding cytoplasm and other organelles, until the small spherical organelles could no longer be clearly distinguished (3–9 min in Fig. 6). The large spherical vacuole, normally found lying adjacent to the septum of subapical hyphal compartments, was originally visible as a zone of dye exclusion. Initial staining of the vacuole membrane was observed after 9 min and the degree of staining increased thereafter (Fig. 6). Strong staining of the septum, lined on each

Fig. 4. Confocal image of a growing hyphal tip of *Neurospora crassa* stained for 105 min; hyphal extension rate = 11.5 μm min^{-1}. Note pronounced staining of elongated mitochondria (cf. Fig. 2B) and cytoplasmic region of dye exclusion (asterisk) which probably represents an unstained nucleus. Bar = 10 μm.

side by the plasma membrane, was also often observed. The intense dye fluorescence associated with the plasma membrane remained relatively constant during experiments in which dye was continuously present in the extracellular medium.

Application of FM4-64 in the presence of the metabolic inhibitor sodium azide inhibited dye internalization but still allowed staining of the plasma membrane of apical and subapical hyphal compartments (Fig. 8).

FM4-64 uptake into the apical hyphal region of different fungal species (Fig. 9) was broadly similar to that recorded for *N. crassa* (Fig. 5). However, there were clear differences between species in the rate and extent to which FM4-64 was taken up into organelles, most obviously the elongated mitochondria within hyphal tips. *Aspergillus nidulans*, in particular, accumulated FM4-64 more rapidly (i.e. within 30 min) within these mitochondria (Fig. 9D).

Staining of Spitzenkörper in different species

In higher fungi (Ascomycota, Deuteromycota and Basidiomycota) the Spitzenkörper is a highly dynamic and pleomorphic multicomponent structure believed to contain the secretory vesicles responsible for tip growth (Grove & Bracker, 1970; López-Franco & Bracker, 1996). López-Franco & Bracker (1996) investigated Spitzenkörper morphology in the unstained hyphal tips of 32 species using computer-enhanced phase-contrast microscopy. In the present study, we have compared FM4-64 staining of the apical vesicle cluster within the Spitzenkörper of seven higher fungal species: *N. crassa* (Fig. 9A), *S. sclerotiorum*

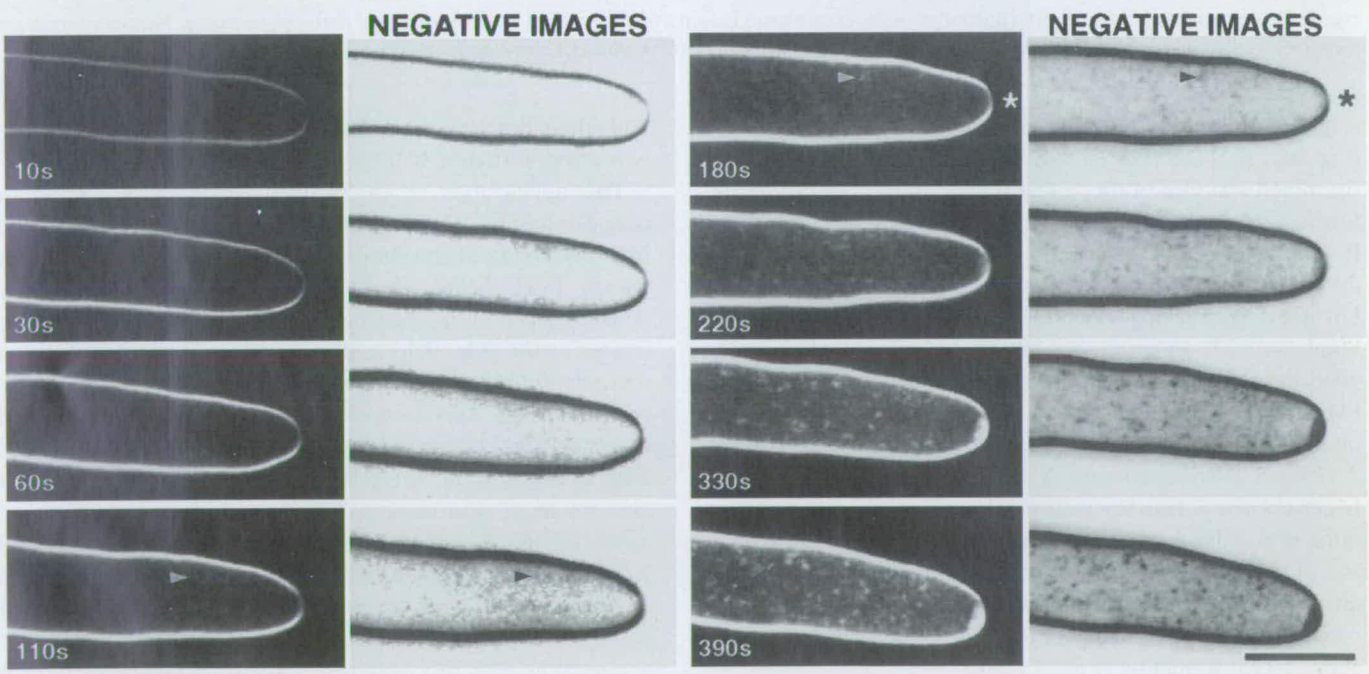

Fig. 5. Time course of FM4-64 internalization within the hyphal tip of *Neurospora crassa*. Numbers indicate time(s) after dye application (continuous loading). Confocal fluorescence images (median optical sections) are displayed alongside the same images contrast adjusted and shown in 'negative', in which dye-stained structures appear dark. Early uptake of dye is more easily seen in the contrast-adjusted negative images. The earliest signs of dye internalization can be seen after 30 s, most prominently within a (10–15 μm) region 8–10 μm from the apical pole. Small, roughly spherical organelles (arrowheads) are first evident between 110 s and 180 s. Staining of the Spitzenkörper region (asterisk) is first seen 180 s after dye application. Hyphal extension continued at an average rate of 21 μm min^{-1} throughout the time course. Bar = 10 μm.

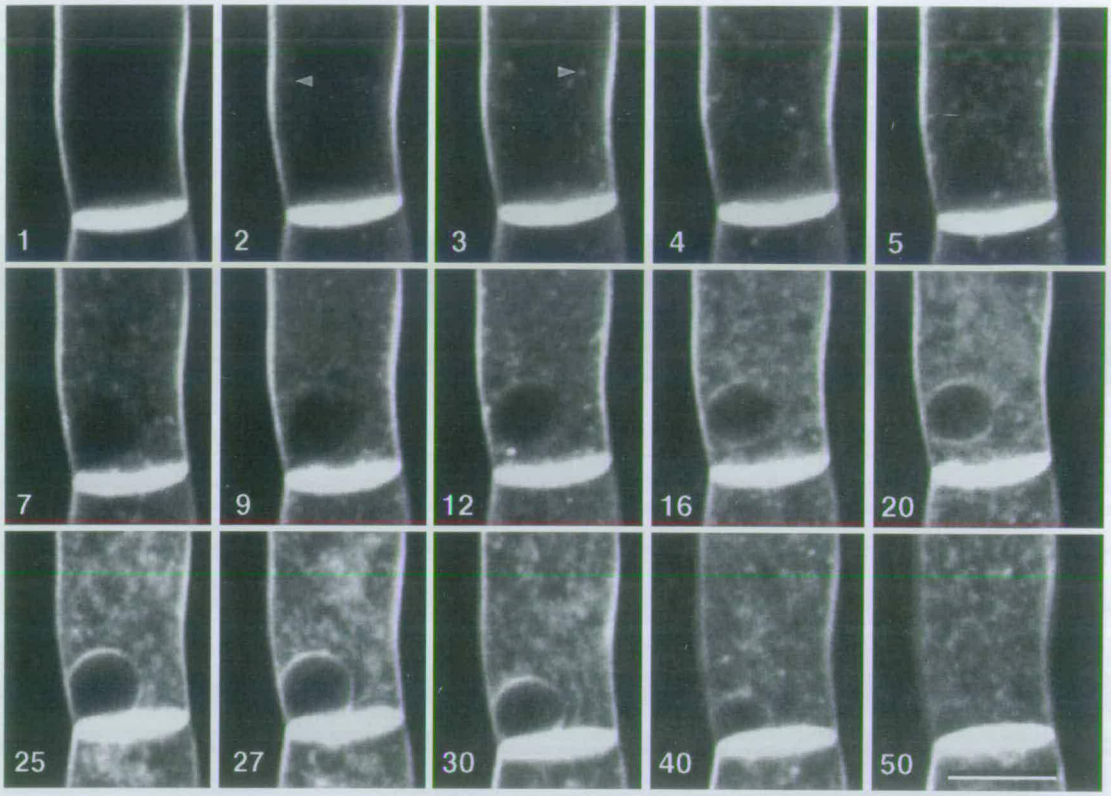

Fig. 6. Time course of FM4-64 internalization with continuous loading of a subapical hyphal region of *Neurospora crassa*. Numbers indicate time (min) after dye application. Small, roughly spherical structures (arrowheads) are clearly visible after 2 min. Bar = 10 μm.

(Fig. 9B), *M. grisea* (Fig. 9C), *A. nidulans* (Fig. 9D), *T. viride* (Fig. 9E), *R. solani* (Fig. 9F) and *B. cinerea* (Fig. 10). We also examined staining of the apical vesicle cluster within germ tubes of the basidiomycete rust fungus, *P. graminis* (Fig. 9G). It should be noted that the rust germ tube has been described previously as possessing an apical vesicle cluster but not a Spitzenkörper (Littlefield & Heath, 1979; Hoch & Staples, 1983; Kwon *et al.*, 1991). In general, there was good agreement between the morphologies of the brightly FM4-64 stained apical vesicle clusters with the unstained phase-dark Spitzenkörper of vegetative hyphae of *N. crassa, T. viride, S. sclerotiorum* and *R. solani* previously described by López-Franco & Bracker (1996). Our unpublished observations of the dynamic changes in position, morphology and size of the stained apical vesicle cluster of each species were also in agreement with previous descriptions of Spitzenkörper behaviour (Bartnicki-Garcia *et al.*, 1995; López-Franco *et al.*, 1995; Riquelme *et al.*, 1998).

After staining with FM4-64, the Spitzenkörper of *N. crassa, S. sclerotiorum, A. nidulans, T. viride, R. solani and B. cinerea* (Figs 9A, B, D–F and 10) were all visible as brightly fluorescent structures, which commonly had a distinct area of reduced fluorescence within them. In those species previously examined by López-Franco & Bracker (1996), the area of reduced fluorescence observed here correlates with their descriptions of the Spitzenkörper core. This core was often particularly large in *S. sclerotiorum* (Fig. 9B).

The appearance of the Spitzenkörper of *N. crassa* in optical sections (Fig. 9A) was roughly round but showed high variability in the shape and size of the core region, and varied from being circular to horseshoe-shaped. The Spitzenkörper of *A. nidulans* lacked an obvious negatively stained core (Fig. 9D) and was often surrounded by a diffusely fluorescent vesicle cloud (not shown). The Spitzenkörper of *S. sclerotiorum* (Fig. 9B), *T. viride* (Fig. 9E) and *B. cinerea* (Fig. 10) were roughly similar: more-or-less round with a central roughly circular core region which was most obvious in *S. sclerotiorum*. The Spitzenkörper of *R. solani* appeared as an irregularly shaped, bright horseshoe-like structure surrounding a darker core region. The germ tubes of *M. grisea* were very narrow, making it difficult to discern details of Spitzenkörper morphology. The Spitzenkörper appeared as a slightly flattened, sometimes crescent-shaped, band within the apical dome of the germ tube (Fig. 9C). The germ tubes of *P. graminis* possessed an FM4-64 stained vesicle cloud, which was most often rounded in shape yet highly pleiomorphic (Fig. 9G).

López-Franco *et al.* (1994, 1995) reported that the Spitzenkörper in many higher fungi was accompanied by one or more smaller migratory Spitzenkörper (called satellite

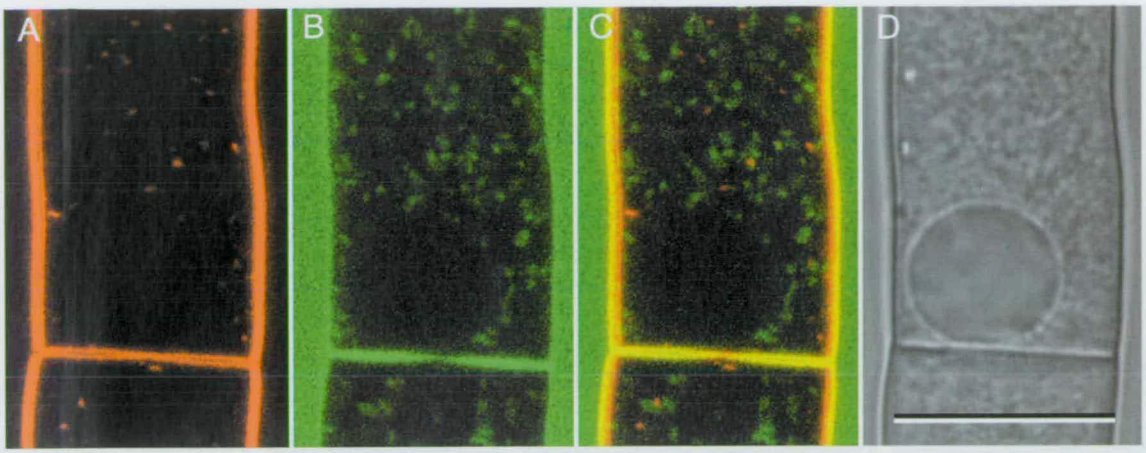

Fig. 7. Pseudocoloured confocal images of the subapical region of a *Neurospora crassa* hypha double stained with (A) FM4-64 loaded for ~4 min (red) and (B) Rhodamine 123 loaded continuously (green). (C) Overlay of (A) and (B) showing that putative endosomes labelled with FM4-64 are distinct from mitochondria labelled with Rhodamine 123 (colocalization = yellow). (D) Corresponding bright field image. Bar = 15 μm.

Spitzenkörper). FM4-64 was found to clearly stain satellite Spitzenkörper in *S. sclerotiorum*, *T. viride* (Fig. 9E) and *B. cinerea* (Fig. 10). Such satellites were most frequently observed in *B. cinerea*. Satellite Spitzenkörper generally emerged adjacent to the plasma membrane a few micrometres behind the main Spitzenkörper, migrated to the apex and finally merged with the main Spitzenkörper within 15 s (Fig. 10).

Finally, we also imaged the FM4-64 stained apical vesicle cluster of the lower fungus *P. blakesleeanus* (Fig. 9H). This fungus belongs to the Zygomycota, which have been reported to possess a crescent-shaped band of apical vesicles instead of a Spitzenkörper (Grove & Bracker, 1970). FM4-64 staining revealed a crescent-shaped zone of bright fluorescence in a zone corresponding to the expected location of these vesicles.

Discussion

In the present paper we have demonstrated FM4-64 staining of hyphae in a range of fungal species, spanning the Ascomycota, Deuteromycota, Basidiomycota and Zygomycota. We have shown that FM4-64 is clearly an excellent stain for tracking the apical vesicle cluster or main Spitzenkörper and satellite Spitzenkörper. FM4-64 also has significant potential for the study of endocytosis and other aspects of vesicle trafficking in living fungal hyphae. Below, we discuss how, with the aid of this dye, we can gain a better understanding of endocytosis and the vesicle trafficking network of hyphae.

Does endocytosis occur in filamentous fungi?

Little is known about endocytosis in filamentous fungi and neither physiological nor ultrastructural analyses have provided concrete evidence that it even occurs (Ashford, 1998). The best evidence for its occurrence so far available are reports of the uptake of FM4-64 by fungal hyphae (Hoffmann & Mendgen, 1998; Read *et al.*, 1998). Our current results further substantiate this with observations of FM4-64 uptake by nine different fungal species. In contrast to this, it is interesting to note that Cole *et al.* (1998) did not observe uptake of FM4-64 by healthy hyphae of *Pisolithus tinctorius* (Basidiomycota). The reason for this difference in results is unclear. Cole *et al.* (1997) also found that membrane-impermeant fluorescent probes, such as Lucifer Yellow carbohydrazide (LYCH), which is used as an indicator of fluid-phase endocytosis in budding yeast (Dulic *et al.*, 1991), were not taken up into hyphae of

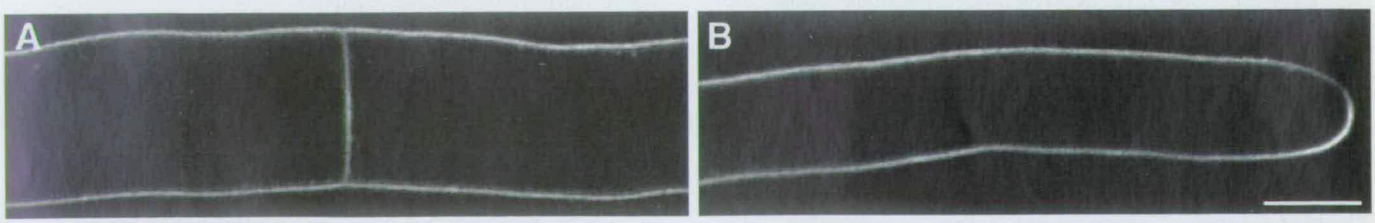

Fig. 8. Confocal images of (A) subapical and (B) apical hyphal compartments of *Neurospora crassa* loaded with FM4-64 for 45 min in the presence of 10 mM sodium azide (note that the sodium azide was added to hyphae 2 min before applying the dye). Bar = 10 μm.

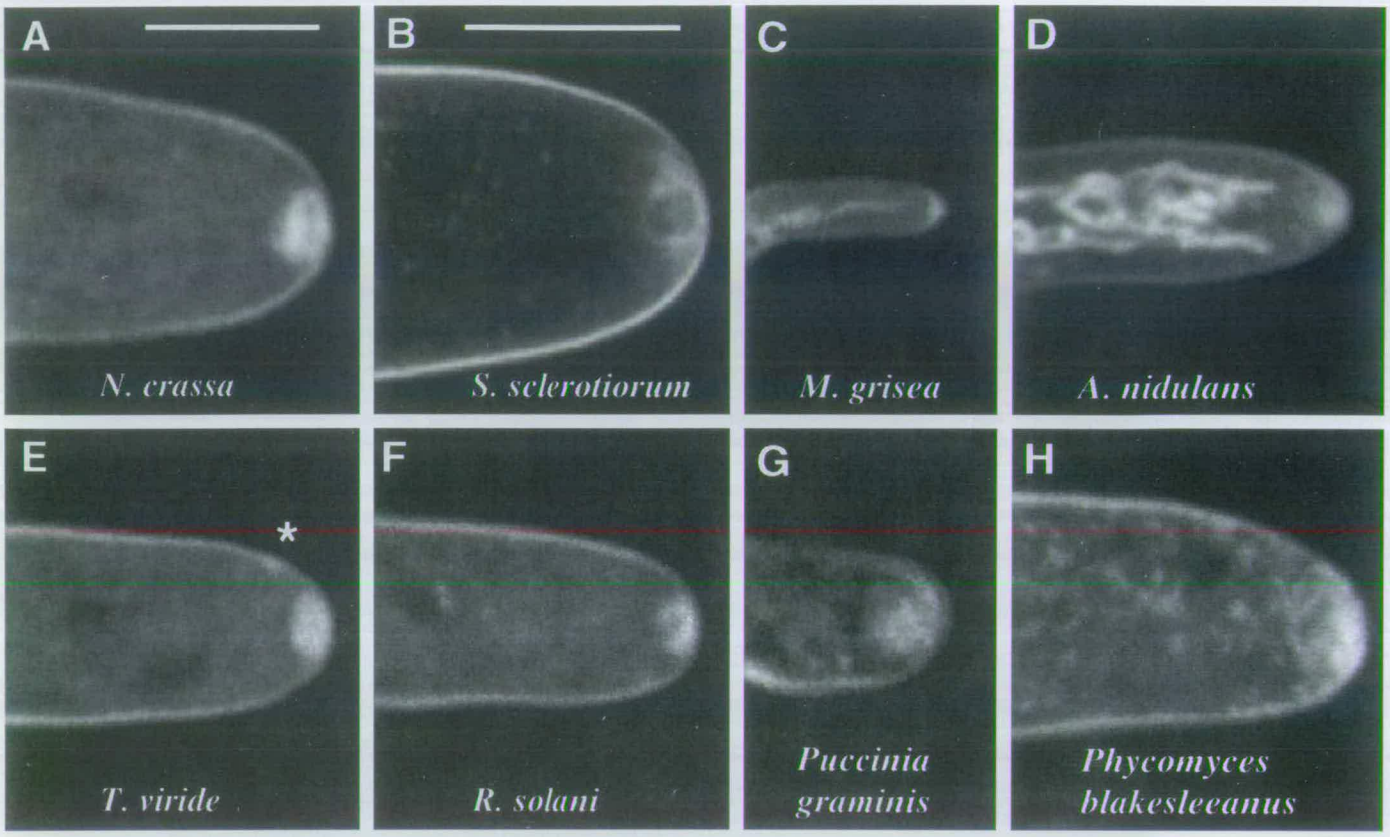

Fig. 9. Confocal images of growing hyphal tips of different species stained with FM4-64: (A) *Neurospora crassa*, (B) *Sclerotinia sclerotiorum*, (C) *Magnaporthe grisea*, (D) *Aspergillus nidulans*, (E) *Trichoderma viride* (asterisk indicates a satellite Spitzenkörper), (F) *Rhizoctonia solani*, (G) *Puccinia graminis*, (H) *Phycomyces blakesleeanus*. Bar in (A) for (A), (C)–(H), = 5 μm. Bar in (B) = 10 μm.

P. tinctorius (fluid-phase endocytosis involves the uptake of molecules in the lumen of endocytic vesicles). We found that although FM4-64 was rapidly internalized by *N. crassa*, LYCH and Oregon Green 488 10 kDa dextran did not appear to be taken up into hyphae of this fungus even after long periods of immersion in the dye (unpublished results).

In the light of such seemingly contradictory evidence, questions still need to be raised as to the occurrence of endocytosis in filamentous fungi and whether the styryl dyes do in fact reliably report endocytosis in filamentous fungi. In the absence of good evidence from other experimental techniques, the burden of proof presently lies heavily upon the FM4-64 data and is critically dependent upon the assumption that FM4-64 is internalized by endocytosis (Fig. 11A). This is certainly believed to be the case where it has been used with animal and yeast cells (Cochilla *et al.*, 1999).

Evidence supporting endocytic uptake of FM4-64

The FM4-64 molecule is composed of three elements (Fig. 1A): a hydrophobic tail (which promotes partitioning into membranes), a dicationic head (which prevents passage across membranes), and a body or nucleus (which determines the spectral properties of the dye). The structure of this dye therefore places a significant energetic barrier to direct passage across the plasma membrane (Betz *et al.*, 1996). Evidence against FM4-64 entering budding yeast cells by unfacilitated diffusion was obtained by inhibiting dye internalization in the presence of the metabolic inhibitor sodium azide, or by applying dye at low temperature (Vida & Emr, 1995). This was confirmed for fungal hyphae by our experimental observations with azide reported here. Similar inhibition was also obtained by Fischer-Parton (1999) when *Neurospora* hyphae were loaded with dye at 4 °C; when the temperature was subsequently increased to 25 °C normal dye uptake occurred.

Whilst unfacilitated diffusion of styryl dyes across membranes is unlikely, it is known that membrane phospholipids, which would similarly be expected to be resistant to passage from one side of membranes to the other, are able to cross over with the aid of flippases (Menon, 1995). Flippases are enzymes that facilitate the movement of specific phospholipids from one leaflet of the lipid bilayer of membranes to the other. Their activity is an essential requirement for membrane biosynthesis. In mammalian

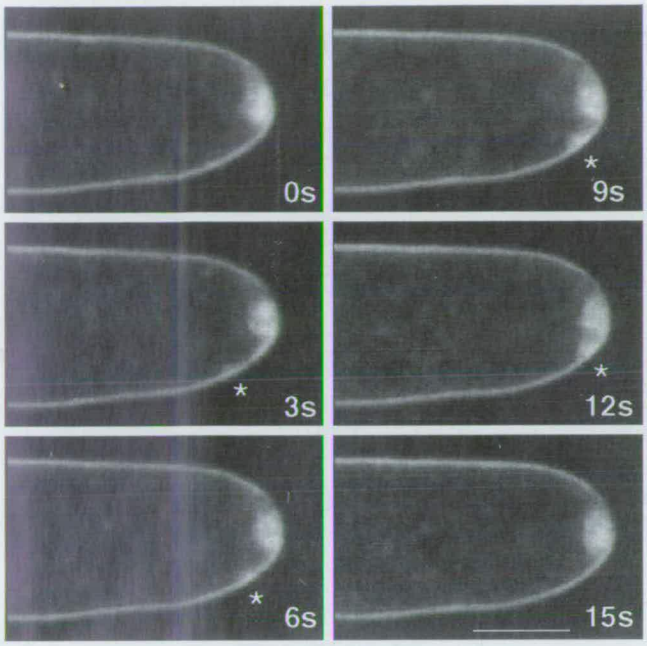

Fig. 10. Confocal images of an FM4-64-stained satellite Spitzenkörper (asterisk) of *Botrytis cinerea* showing a time course (in s) of different stages in its formation, migration and fusion with the main Spitzenkörper. Bar = 5 μm.

cells they have been identified in both the plasma membrane and endoplasmic reticulum (ER) (Menon, 1995) but they have not, to our knowledge, been described in fungi. It is conceivable that the action of flippases could provide an alternative mechanism for the internalization of FM4-64, FM1-43 and TMA-DPH (Fig. 11B). Once dye has been translocated to the inner leaflet of the plasma membrane by flippase activity, lipid transfer proteins may then transport dye molecules to the cytosolic face of the membranes of other organelles (Fig. 11B). Lipid transfer proteins have been identified in numerous eukaryotic cells, including filamentous fungi (Record *et al.*, 1998). Alternatively, owing to the water solubility of these dyes and reversible incorporation into many membranes, they could enter the cytosol from the cytoplasmic face of the plasma membrane and then label the external leaflet of organelle membranes (Illinger & Kuhry, 1994; Betz *et al.*, 1996). However, Illinger & Kuhry (1994), who used TMA-DPH to follow endocytosis in mammalian cells, recognized the possible significance of flippase activity for dye uptake but provided strong experimental evidence to discount it. Further evidence to support endocytic uptake comes from neuronal preparations, where it was shown that FM1-43 is confined to synaptic vesicles (Henkel *et al.*, 1996). Even stronger evidence that FM4-64 uptake follows an endocytic pathway comes from mutants in budding yeast defective in the vesicle trafficking network, in which styryl dye transport to the vacuole was inhibited (Vida & Emr, 1995). Indeed, in budding yeast FM4-64 has been successfully used in a fluorescence assisted cell sorter to screen for proteins involved in endocytosis (Gaynor *et al.*, 1998).

Our observations of the time-dependent sequence of FM4-64 internalization, with staining appearing in a defined sequence of organelles, is consistent with uptake by endocytosis as described for styryl dyes applied to animal and yeast cells (reviewed in Cochilla *et al.*, 1999). In these latter systems, the first obvious stained organelles have been identified as, or proposed to be, early endosomes (Vida & Emr, 1995; Cochilla *et al.*, 1999). The roughly spherical ~0.75 μm organelles observed here correspond well to this and thus we now refer to them as putative endosomes. However, it must be emphasized that endosomes have not yet been identified at the ultrastructural level in filamentous fungi.

The case for endocytosis in fungal hyphae

Although inconclusive, it is clear that uptake of FM4-64, FM1-43 and TMA-DPH provide the best evidence to date for endocytosis in filamentous fungi. The case for endocytosis in fungal hyphae is further supported by the wealth of knowledge available from research with the budding yeast fungus. Endocytosis and components of the endocytic pathway have been well characterized in this organism at the genetic, biochemical and ultrastructural levels (Pelham, 1997; Geli & Riezman, 1998; Prescianotto-Baschong & Riezman, 1998).

There is an array of physiological functions carried out in animal, plant and yeast cells which are mediated by endocytosis (Dulic *et al.*, 1991; Hawes *et al.*, 1995; Mellman, 1996; Geli & Riezman, 1998). Evidence that such activities are also carried out in filamentous fungi strengthens the case for endocytosis. Our data are consistent with the interpretation that endocytosis occurs in both apical and subapical hyphal compartments. At present we do not know exactly what roles endocytosis might serve in these different compartments. Nevertheless, based on what is known about the biology of hyphae and about endocytosis in other organisms we can speculate generally as to possible roles that endocytosis may serve in filamentous fungi.

Removal of excess plasma membrane. It has been suggested that, in pollen tubes, insertion of membrane by the fusion of vesicles delivering cell wall components to the apex exceeds the membrane necessary for tip extension (Picton & Steer, 1983). The most likely retrieval mechanism for superfluous membrane is endocytosis (Steer, 1988). This is supported by Derksen *et al.* (1995), who identified a zone 6–15 μm behind the tip with a concentration of clathrin-coated pits implicating it as a major site of endocytosis. In rust germ tubes, Hoffman & Mendgen (1998) observed initial FM4-64 uptake within a region 5–20 μm away from the apical pole, indicating active endocytosis in that zone. This broadly matches our observations of early uptake in *N. crassa*. Calculations of the amount

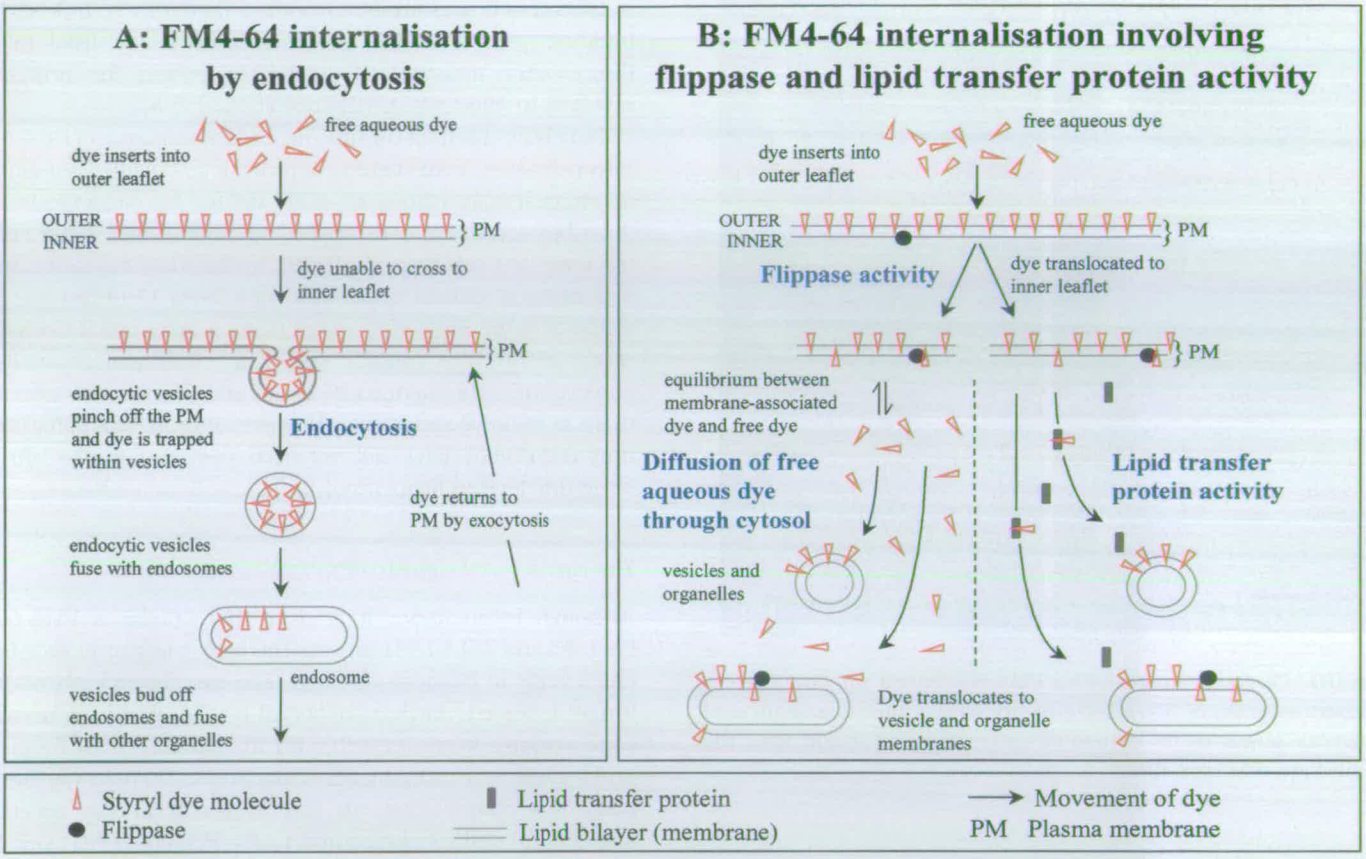

Fig. 11. Diagrams outlining possible alternative pathways of FM4-64 uptake by fungal hyphae. (A) Endocytic pathway of internalization. (B) Internalization involving the activity of flippases and lipid transfer proteins.

of apical vesicle membrane relative to the volume of these vesicles in fungal hyphae have indicated that a significant excess of membrane relative to wall material is probably added during hyphal tip growth (C. E. Bracker, personal communication, 1998). In subapical compartments endocytosis may be important for retrieving excess membrane delivered by secretory vesicles during septum formation.

Recycling of membrane proteins. Endocytosis in apical hyphal compartments may function in tip growth by providing a means for retrieving displaced membrane proteins (e.g. ion channels and cell wall-building enzymes) and returning them to the tip for re-use. In budding yeast, there is strong evidence that two of the three chitin synthases in the plasma membrane are recycled back to the plasma membrane via endocytosis (Chuang & Schekman, 1996; Ziman *et al.*, 1996, 1998; Holthuis *et al.*, 1998). It makes economic sense for a hypha to recycle and reuse some of the proteins involved in tip growth rather than to synthesize all of these proteins *de novo*. As discussed in the following section, rapid recycling of membrane proteins in hyphae may occur via endosomes and/or satellite Spitzenkörper.

Transport of membrane proteins and lipids to the vacuole for degradation. Our findings showed that spherical vacuoles in *N. crassa* became stained with FM4-64 in a manner similar to that reported for the vacuole of budding yeast, which functions as the site of degradation of plasma membrane proteins (Vida & Emr, 1995; Wendland *et al.*, 1998).

Uptake of molecules in the fluid phase of endocytic vesicles. This may be important for the uptake of certain nutrients (Dulic *et al.*, 1991).

Receptor-mediated uptake of ligands. It has been shown that, in budding yeast, the mating pheromone α-factor and its plasma membrane receptor are internalized by receptor-mediated endocytosis (Wendland *et al.*, 1998). Although filamentous fungi produce pheromones (Bölker & Kahmann, 1993), their mechanism of internalization has not been studied.

Tracking the vesicle trafficking network in fungal hyphae

FM4-64 was found to be of low toxicity and relatively resistant to photobleaching during repeated imaging. This makes it an excellent dye for following dynamic processes in living cells over time without perturbing those processes. Confocal imaging has allowed us to visualize putative endosomes and other organelles (e.g. mitochondria and vacuoles). However, it should be emphasized that visualization of individual vesicles is beyond

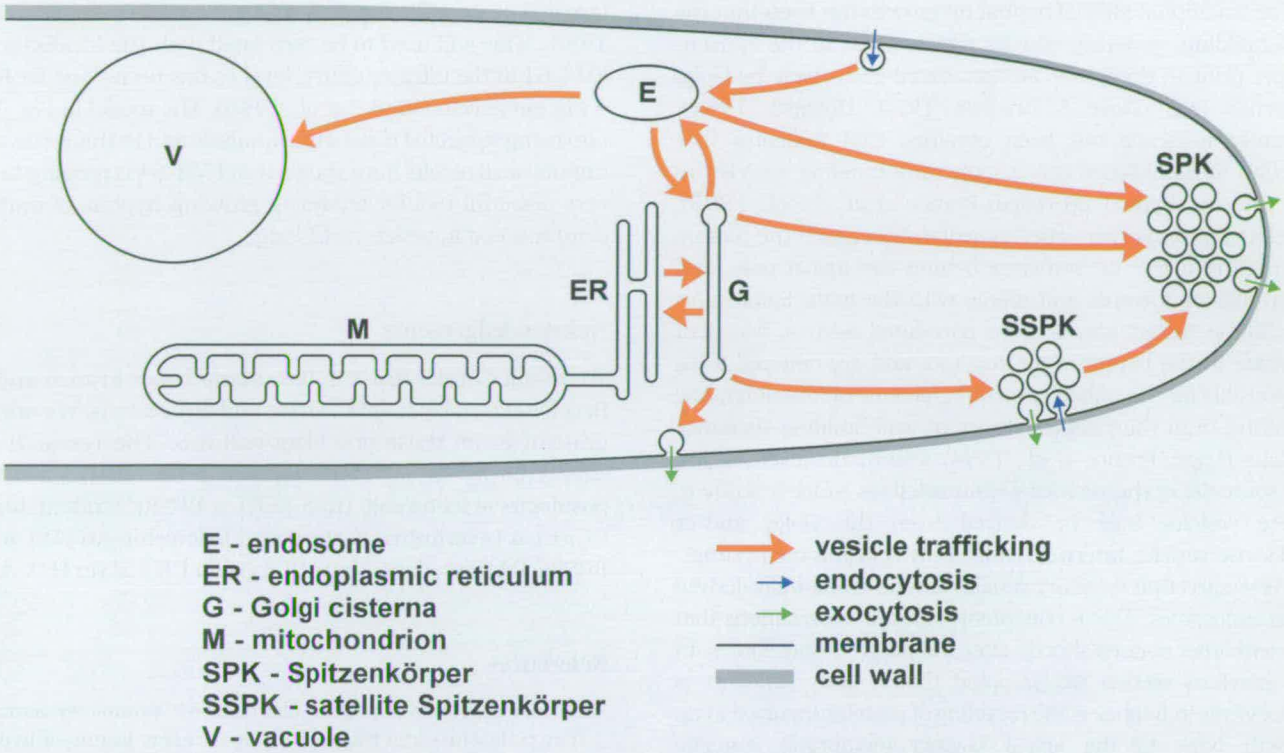

Fig. 12. A hypothetical model of the organization of the vesicle trafficking network in a growing hypha based upon the pattern of FM4-64 staining.

the limits of the imaging techniques employed here. This is because the vesicles are very small (typically < 100 nm in diameter) and are present at a high density within the hyphal cytoplasm. The diffraction limitation of fluorescence imaging means that such small, closely spaced fluorescing vesicles cannot be individually identified because they appear blurred together (Betz & Angleson, 1997).

On the basis of our observations with FM4-64 uptake we have proposed a speculative model (Fig. 12) which interprets our observations in the context of current knowledge of the vesicle trafficking pathways in yeast and animal cells (e.g. Mellman, 1996; Pelham, 1997; Geli & Riezman, 1998).

Our observation of diffuse fluorescence within the cytoplasm within 30 s of adding FM4-64 to hyphae may be interpreted as primarily representing a cloud of stained endocytic vesicles. Although endocytic vesicles have not been identified at the ultrastructural level, possible candidates are filasomes (Howard, 1981). These are vesicles possessing a fibrillar coating that contains actin (Bourett & Howard, 1991; Roberson, 1992). These coated vesicles were found to be concentrated principally in the first 12 μm of growing hyphal tips of the basidiomycete *Sclerotium rolfsii* (Roberson, 1992). This is consistent with our observations of initial dye internalization in a localized region behind the apical dome. The first FM4-64-stained organelles that we could visualize clearly in hyphae were small and roughly spherical and, as previously discussed, are interpreted as putative endosomes. In other cell types endosomes function as sorting compartments for proteins and lipids, and are classified into two functional types: 'early' and 'late' endosomes (Ashford, 1998; Prescianotto-Baschong & Riezman, 1998; Mukherjee *et al.*, 1999).

In subapical compartments, the next obviously stained organelle was the large spherical vacuole. This pattern of staining was similar to that in budding yeast, in which staining of yeast vacuolar membranes followed that of putative endosomes (Vida & Emr, 1995). In addition to the large spherical vacuoles, the vacuolar system in hyphae also consists of an extensive tubular network in both subapical and apical compartments (Ashford, 1998). We have also found that the membranes of these tubular vacuoles in apical hyphal compartments become clearly stained after prolonged immersion in FM4-64 (unpublished results).

In addition to vacuolar membranes we would also expect that both the Golgi and ER of fungal hyphae would become stained with FM4-64 via retrograde pathways which connect the endosomal system, Golgi and ER, as occurs in budding yeast (Pelham, 1997; Fig. 12). Staining by FM4-64 of these membranes in fungal hyphae would provide an explanation for the observed increase in staining of other organelles in the cytoplasm with time. However, it should also be stressed that the staining of the small, roughly spherical organelles proposed earlier to be endosomes could conceivably be Golgi instead.

The traditional view of hyphal tip growth has been that the wall-building, secretory vesicles which reside in the Spitzenkörper prior to exocytosis are generated exclusively by Golgi cisternae (e.g. Grove & Bracker, 1970; Howard, 1981). Recently, evidence has been obtained that indicates that satellite Spitzenkörper also supply wall-building vesicles to the growing hyphal tip (López-Franco *et al.*, 1994, 1995). Satellite Spitzenkörper arise immediately beneath the plasma membrane a few micrometres behind the apical pole, and then migrate towards and merge with the main Spitzenkörper. These fusion events were correlated with a transient increase in the hyphal extension rate and are believed to be responsible for the pulsed growth behaviour of fungal hyphae resulting from the pulsed delivery of wall-building secretory vesicles (López-Franco *et al.*, 1994, 1995). However, as yet, the source(s) of the vesicles within satellites is/are unknown. These vesicles may be derived from the Golgi and/or endocytic vesicles internalized from the plasma membrane.

We suggest that secretory vesicles may be additionally derived from endosomes. This is consistent with our observations that Spitzenkörper stained shortly after the putative endosomes. In the previous section we proposed that a likely function of endocytosis in hyphae is the recycling of proteins involved in tip growth back to the apical plasma membrane. Satellite Spitzenkörper may also have a role in this process. However, the longer route for recycling these proteins from endosomes to the Spitzenkörper via the Golgi cannot be discounted (Fig. 12).

Mitochondria were always stained by FM4-64 with longer incubation times than necessary to stain Spitzenkörper or putative endosomes, and these times varied between species. A possible explanation of this phenomenon, still consistent with FM4-64 internalization by endocytosis, is that FM4-64 stains mitochondria through direct contact with the ER (Fig. 12). Continuity between the ER and the outer mitochondrial membrane has been shown at the ultrastructural level in various cells including hyphae (Bracker & Grove, 1971; Franke & Kartenbeck, 1971). We found that FM4-64 and FM1-43 stained mitochondria at different rates in any one species and the rates of staining varied between species. An explanation for this may be found in the recent finding that fluorescent lipid analogues undergo endocytic sorting to different organelles in animal cells solely on the basis of differences in the chemistry of their hydrophobic tails (Mukherjee *et al.*, 1999). Variations between species (e.g. *N. crassa* and *A. nidulans*) in the composition of their organelle membranes may also explain the differential rates at which their mitochondria become stained by FM4-64.

The hypothetical model of vesicle trafficking presented in Fig. 12 now needs to be rigorously tested and, in particular, endocytic intermediates and components of the secretory pathways need to be identified and characterized. Towards this aim, we are currently performing double labelling experiments in living hyphae by following the time course of FM4-64 staining in which the green fluorescent protein has been targeted to specific organelles (e.g. Fernández-Ábalos *et al.*, 1998). This will need to be correlated with the localization of FM4-64 at the ultrastructural level as has been done for FM1-43 in nerve cells (Henkel *et al.*, 1996). The model in Fig. 12 is also being subjected to genetical analysis and in this respect our unpublished results have shown that FM4-64 is proving to be a very powerful tool for analysing growing hyphae of mutants compromised in vesicle trafficking.

Acknowledgements

We thank Charles Bracker, Rosamaría López-Franco and Bill Betz for extremely helpful advice and discussions. We are also grateful to all those providing cultures. The research was supported by an EC TMR Fellowship (to S.F.-P.), a BBSRC postdoctoral fellowship (to R.M.P.), a BBSRC studentship (to P.C.H.), a Leverhulme postdoctoral fellowship (to J.D.), and a BBSRC CASE studentship with AgrEvo UK Ltd (to H.A.A.).

References

Ashford, A.E. (1998) Dynamic pleiomorphic vacuole systems: are they endosomes and transport compartments in fungal hyphae? *Adv. Bot. Res.* **28**, 119–159.

Bartnicki-Garcia, S., Bartnicki, D.D., Gierz, G., Lopez-Franco, R. & Bracker, C.E. (1995) Evidence that Spitzenkörper behavior determines the shape of a fungal hypha – a test of the hyphoid model. *Exp. Mycol.* **19**, 153–159.

Bartnicki-Garcia, S., Hergert, F. & Gierz, G. (1989) Computer simulation of fungal morphogenesis and the mathematical basis for hyphal (tip) growth. *Protoplasma*, **153**, 46–57.

Betz, W.J. & Angleson, J.K. (1997) Now you see it, now you don't. *Nature*, **388**, 423–424.

Betz, W.J., Mao, F. & Smith, C.B. (1996) Imaging exocytosis and endocytosis. *Curr. Opin. Neurobiol.* **6**, 365–371.

Bölker, M. & Kahmann, R. (1993) Sexual pheromones and mating responses in fungi. *Plant Cell*, **5**, 1461–1469.

Bourett, T.M. & Howard, R.J. (1991) Ultrastructural immunolocalization of actin in a fungus. *Protoplasma*, **163**, 199–202.

Bracker, C.E. & Grove, S.N. (1971) Continuity between cytoplasmic endomembranes and outer mitochondrial membranes in fungi. *Protoplasma*, **73**, 15–34.

Caesar-Ton That, T.C., Hoangvan, K., Turian, G. & Hoch, H.C. (1987) Isolation and characterization of coated vesicles from filamentous fungi. *Eur. J. Cell Biol.* **43**, 189–194.

Chuang, J.S. & Schekman, R.W. (1996) Differential trafficking and timed localization of two chitin synthase proteins, Chs2p and Chs3p. *J. Cell Biol.* **135**, 597–610.

Cochilla, A.J., Angleson, J.K. & Betz, W.J. (1999) Monitoring secretory membrane with FM1-43 fluorescence. *Annu. Rev. Neurosci.* **22**, 1–10.

Cole, L., Hyde, G.J. & Ashford, A.E. (1997) Uptake and compartmentalisation of fluorescent probes by *Pisolithus tinctorius* hyphae: evidence for an anion transport mechanism at the tonoplast but not for fluid-phase endocytosis. *Protoplasma*, **199**, 18–29.

Cole, L., Orlovich, D.A. & Ashford, A.E. (1998) Structure, function,

and motility of vacuoles in filamentous fungi. *Fungal Genet. Biol.* **24**, 86–100.

Derksen, J., Rutten, T., Lichtscheidl, I.K., Dewin, A.H.N., Pierson, E.S. & Rongen, G. (1995) Quantitative analysis of the distribution of organelles in tobacco pollen tubes – implications for exocytosis and endocytosis. *Protoplasma*, **188**, 267–276.

Dulic, V., Egerton, M., Elgundi, I., Raths, S., Singer, B. & Riezman, H. (1991) Yeast endocytosis assays. *Meth. Enzymol.* **194**, 697–710.

Fernández-Ábalos, J.M., Fox, H., Pitt, C., Wells, B. & Doonan, J.H. (1998) Plant-adapted green fluorescent protein is a versatile vital reporter for gene expression, protein localization and mitosis in the filamentous fungus, *Aspergillus nidulans*. *Mol. Microbiol.* **27**, 121–130.

Fischer-Parton, S. (1999) Role of pH, calcium and vesicle trafficking in regulating hyphal tip growth of *Neurospora crassa*. PhD Thesis, University of Edinburgh.

Franke, W.W. & Kartenbeck, J. (1971) Outer mitochondrial membrane continuous with endoplasmic reticulum. *Protoplasma*, **73**, 35–41.

Gaynor, E.C., Chen, C.Y., Emr, S.D. & Graham, T.R. (1998) ARF is required for maintenance of yeast Golgi and endosome structure and function. *Mol. Biol. Cell*, **9**, 653–670.

Geli, M.I. & Riezman, H. (1998) Endocytic internalization in yeast and animal cells: similar and different. *J. Cell Sci.* **111**, 1031–1037.

Girbardt, M. (1957) Der Spitzenkörper von *Polystictus versicolor* (L.). *Planta*, **50**, 47–59.

Grove, S.N. & Bracker, C.E. (1970) Protoplasmic organization of hyphal tips among fungi: vesicles and Spitzenkörper. *J. Bacteriol.* **104**, 989–1009.

Gruenberg, J. & Clague, M.J. (1992) Regulation of intracellular membrane transport. *Curr. Opin. Cell Biol.* **4**, 593–599.

Haugland, R.P. (1996) *Molecular Probes: Handbook of Fluorescent Probes and Research Chemicals*. Molecular Probes, Inc., Eugene, Oregon.

Hawes, C., Crooks, K., Coleman, J. & Satiat-Jeunemaitre, B. (1995) Endocytosis in plants: fact or artifact? *Plant, Cell Environ.* **18**, 1245–1252.

Henkel, A.W., Lubke, J. & Betz, W.J. (1996) FM1-43 dye ultrastructural localisation in and release from frog motor nerve terminals. *Proc. Natl. Acad. Sci. USA*, **93**, 1918–1923.

Hoch, H.C. & Staples, R.C. (1983) Ultrastructural organization of the non-differentiated uredospore germling of *Uromyces phaseoli* variety *typica*. *Mycologia*, **75**, 795–824.

Hoffmann, J. & Mendgen, K. (1998) Endocytosis and membrane turnover in the germ tube of *Uromyces fabae*. *Fungal Genet. Biol.* **24**, 77–85.

Holthuis, J.C.M., Nichols, B.J. & Pelham, H.R.B. (1998) The syntaxin Tlg1p mediates trafficking of chitin synthase III to polarized growth sites in yeast. *Mol. Biol. Cell*, **9**, 3383–3397.

Howard, R.J. (1981) Ultrastructural analysis of hyphal tip cell growth in fungi: Spitzenkörper, cytoskeleton and endomembranes after freeze-substitution. *J. Cell Sci.* **48**, 89–103.

Howard, R.J. & Aist, J.R. (1980) Cytoplasmic microtubules and fungal morphogenesis: ultrastructural effects of methyl benzimidazole-2-ylcarbamate determined by freeze-substitution of hyphal tip cells. *J. Cell Biol.* **87**, 55–64.

Illinger, D. & Kuhry, J.G. (1994) The kinetic aspects of intracellular fluorescence labeling with TMA-DPH support the maturation model for endocytosis in L929 cells. *J. Cell Biol.* **125**, 783–794.

Jelitto, T.C., Page, H.A. & Read, N.D. (1994) Role of external signals in regulating the pre-penetration phase of infection by the rice blast fungus, *Magnaporthe grisea*. *Planta*, **194**, 471–477.

Kwon, Y.H., Hoch, H.C. & Aist, J.R. (1991) Initiation of appressorium formation in *Uromyces appendiculatus*: organization of the apex, and the responses involving microtubules and apical vesicles. *Can. J. Bot.* **69**, 2560–2573.

Littlefield, L.J. and Heath, M.C. (1979) *Ultrastructure of Rust Fungi*. Academic Press, New York.

López-Franco, R., Bartnicki-Garcia, S. & Bracker, C.E. (1994) Pulsed growth of fungal hyphal tips. *Proc. Natl. Acad. Sci. USA*, **91**, 12228–12232.

López-Franco, R. & Bracker, C.E. (1996) Diversity and dynamics of the Spitzenkörper in growing hyphal tips of higher fungi. *Protoplasma*, **195**, 90–111.

López-Franco, R., Howard, R.J. & Bracker, C.E. (1995) Satellite Spitzenkörper in growing hyphal tips. *Protoplasma*, **188**, 85–103.

Mellman, I. (1996) Endocytosis and molecular sorting. *Annu. Rev. Cell Dev. Biol.* **12**, 575–625.

Menon, A.K. (1995) Flippases. *Trends Cell Biol.* **5**, 355–360.

Miller, D.D., deRuijter, N.C.A. & Emons, A.M.C. (1997) From signal to form: aspects of the cytoskeleton-plasma membrane-cell wall continuum in root hair tips. *J. Exp. Bot.* **48**, 1881–1896.

Mukherjee, S., Soe, T.T. & Maxfield, F.R. (1999) Endocytic sorting of lipid analogues differing solely in the chemistry of their hydrophobic tails. *J. Cell Biol.* **144**, 1271–1284.

Parton, R.M., Fischer, S., Malhó, R., Papasouliotis, O., Jelitto, T.C., Leonard, T. & Read, N.D. (1997) Pronounced cytoplasmic pH gradients are not required for tip growth in plant and fungal cells. *J. Cell Sci.* **110**, 1187–1198.

Pelham, H.R.B. (1997) SNAREs and the organization of the secretory pathway. *Eur. J. Cell Biol.* **74**, 311–314.

Picton, J.M. & Steer, M.W. (1983) Membrane recycling and the control of secretory activity in pollen tubes. *J. Cell Sci.* **63**, 303–310.

Prescianotto-Baschong, C. & Riezman, H. (1998) Morphology of the yeast endocytic pathway. *Mol. Biol. Cell*, **9**, 173–189.

Read, N.D., Fischer, S. & Parton, R.M. (1998) Imaging Spitzenkörper, pH and calcium dynamics in growing fungal hyphae. *Pestic. Sci.* **54**, 179–181.

Read, N.D., Kellock, L.J., Collins, T.J. & Gundlach, A.M. (1997) Role of topography sensing for infection-structure differentiation in cereal rust fungi. *Planta*, **202**, 163–170.

Record, E., Asther, M., Moukha, S., Marion, D., Burlat, V. & Ruel, K. (1998) Localization of a phosphatidylglycerol/phosphatidylinositol transfer protein in *Aspergillus oryzae*. *Can. J. Microbiol.* **44**, 945–953.

Rieder, S.E., Banta, L.M., Kohrer, K., McCaffery, J.M. & Emr, S.D. (1996) Multilamellar endosome-like compartment accumulates in the yeast vps28 vacuolar protein sorting mutant. *Mol. Biol. Cell*, **7**, 985–999.

Riquelme, M., Reynaga-Peña, C.G., Gierz, G. & Bartnicki-Garcia, S. (1998) What determines growth direction in fungal hyphae? *Fungal Genet. Biol.* **24**, 101–109.

Roberson, R.W. (1992) The actin cytoskeleton in hyphal cells of *Sclerotium rolfsii*. *Mycologia*, **84**, 41–51.

Rothman, J.E. (1994) Mechanisms of intracellular protein transport. *Nature*, **372**, 55–63.

Seiler, S., Plamann, M. & Schliwa, M. (1999) Kinesin and dynein

mutants provide novel insights into the roles of vesicle trafficking during cell morphogenesis in *Neurospora*. *Curr. Biol.* **9**, 779–785.

Steer, M.W. (1988) Plasma membrane turnover in plant cells. *J. Exp. Bot.* **39**, 987–996.

Steer, M.W. & Steer, J.M. (1989) Pollen tube tip growth. *New Phytol.* **111**, 323–358.

Trinci, A.P.J. (1971) Influence of the width of the peripheral growth zone on the radial growth rate of fungal colonies on solid media. *J. Gen. Microbiol.* **67**, 325–344.

Vida, T.A. & Emr, S.D. (1995) A new vital stain for visualizing vacuolar membrane dynamics and endocytosis in yeast. *J. Cell Biol.* **128**, 779–792.

Vogel, H.J. (1956) A convenient growth medium for *Neurospora* (medium N). *Microbiol. Gen. Bull.* **13**, 42–43.

Wendland, B., Emr, S.D. & Riezman, H. (1998) Protein traffic in the yeast endocytic and vacuolar protein sorting pathways. *Curr. Opin. Cell Biol.* **10**, 513–522.

Wessels, J.G.H. (1993) Wall growth, protein excretion and morphogenesis in fungi. *New Phytol.* **123**, 397–413.

Wu, Q.D., Sandrock, T.M., Turgeon, B.G., Yoder, O.C., Wirsel, S.G. & Aist, J.R. (1998) A fungal kinesin required for organelle motility, hyphal growth, and morphogenesis. *Mol. Biol. Cell*, **9**, 89–101.

Zalokar, M. (1959) Growth and differentiation of *Neurospora* hyphae. *Am. J. Bot.* **46**, 602–610.

Ziman, M., Chuang, J.S. & Schekman, R.W. (1996) Chs1p and Chs3p, two proteins involved in chitin synthesis, populate a compartment of the *Saccharomyces cerevisiae* endocytic pathway. *Mol. Biol. Cell*, **7**, 1909–1919.

Ziman, M., Chuang, J.S., Tsung, M., Hamamoto, S. & Schekman, R. (1998) Chs6p-dependent anterograde transport of Chs3p from the chitosome to the plasma membrane in *Saccharomyces cerevisiae*. *Mol. Biol. Cell*, **9**, 1565–1576.